



저작자표시-비영리-변경금지 2.0 대한민국

이용자는 아래의 조건을 따르는 경우에 한하여 자유롭게

- 이 저작물을 복제, 배포, 전송, 전시, 공연 및 방송할 수 있습니다.

다음과 같은 조건을 따라야 합니다:



저작자표시. 귀하는 원저작자를 표시하여야 합니다.



비영리. 귀하는 이 저작물을 영리 목적으로 이용할 수 없습니다.



변경금지. 귀하는 이 저작물을 개작, 변형 또는 가공할 수 없습니다.

- 귀하는, 이 저작물의 재이용이나 배포의 경우, 이 저작물에 적용된 이용허락조건을 명확하게 나타내어야 합니다.
- 저작권자로부터 별도의 허가를 받으면 이러한 조건들은 적용되지 않습니다.

저작권법에 따른 이용자의 권리는 위의 내용에 의하여 영향을 받지 않습니다.

이것은 [이용허락규약\(Legal Code\)](#)을 이해하기 쉽게 요약한 것입니다.

[Disclaimer](#)

**A THESIS
FOR THE DEGREE OF DOCTOR OF PHILOSOPHY**

Transcriptome wide discovery of selected role players in acute phase response of black rockfish (*Sebastes schlegelii*) and antioxidative defense of rock bream (*Oplegnathus fasciatus*), revealing their putative significance in host immune responses.

Don Anushka Sandaruwan Elvitigala

Department of Marine Life Sciences

GRADUATE SCHOOL

JEJU NATIONAL UNIVERSITY

REPUBLIC OF KOREA

February 2016

Transcriptome wide discovery of selected role players in acute phase response of black rockfish (*Sebastes schlegelii*) and antioxidative defense of rock bream (*Oplegnathus fasciatus*), revealing their putative significance in host immune responses.

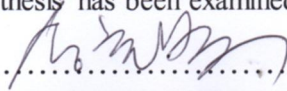

Don Anushka Sandaruwan Elvitigala
(Supervised by Professor Jehee Lee)

A thesis submitted in partial fulfillment of the requirement for the degree of

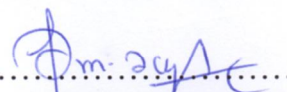

DOCTOR OF PHILOSOPHY

December, 2015

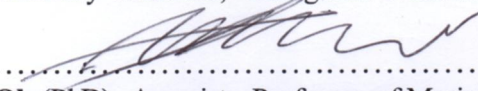

This thesis has been examined and approved by

..........

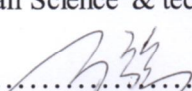

Thesis Director, **Choon Bok Song** (PhD), Professor of Marine Life Sciences
School of Marine Biomedical Sciences, Jeju National University

..........

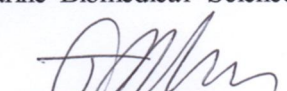

Mahanama De Zoysa (PhD), Associate Professor of Veterinary Medicine
College of Veterinary Medicine, Chungnam National University

..........

Chulhong Oh (PhD), Associate Professor of Marine Biology,
Korean Institute of Ocean Science & Technology, University of Science & Technology

..........

Qiang Wan (PhD), Research Professor of Marine life Sciences
School of Marine Biomedical Sciences, Jeju National University

..........

Jehee Lee (PhD), Professor of Marine Life Sciences
School of Marine Biomedical Sciences, Jeju National University

Date: 27.11.2015

Department of Marine Life Sciences
GRADUATE SCHOOL
JEJU NATIONAL UNIVERSITY
REPUBLIC OF KOREA

This thesis is based on the following peer reviewed international publications

- 1. Don Anushka Sandaruwan Elvitigala**, Qiang Wan, Hyun Chul Kim, Jehee Lee., (2015) Identification of a C-reactive protein like homologue from black rockfish (*Sebastes schlegelii*) evidencing its potent anti-microbial properties at molecular level. Dev. Comp. Immunol, 53, 169-178.
- 2. J.D.H.E. Jayasinghe, Don Anushka Sandaruwan Elvitigala**, Ilson Whang, Bo-Hye Nam, Jehee Lee., (2015) Molecular characterization of two immunity-related acute-phase proteins: Haptoglobin and serum amyloid A from black rockfish (*Sebastes schlegelii*). Fish & Shellfish Immunol, 45, 680-688.
- 3. Don Anushka Sandaruwan Elvitigala**, H.K.A Premachandra, Ilson Whang, Thantrige Thiunuwan Priyathilaka, Eunmi Kim, Bong-Soo Lim, Hyung-Bok Jung, Sang-Yeob Yeo, Hae-Chul Park, Jehee Lee. (2013) Marine teleost ortholog of catalase from rock bream (*Oplegnathus fasciatus*): Molecular perspectives from genomic organization to enzymatic behavior with respect to its potent antioxidant properties. Fish & Shellfish Immunol. 35, 1086-1096.
- 4. Don Anushka Sandaruwan Elvitigala**, Ilson Whang, Jehee Lee., (2015) Molecular profiling and functional insights of rock bream (*Oplegnathus fasciatus*) thioredoxin reductase 3-like molecule: investigation of its transcriptional modulation in response to live pathogen stress. Gene, 570, 122-131.
- 5. Don Anushka Sandaruwan Elvitigala**, Thantrige Thiunuwan priyathilaka, Bong-Soo Lim, Ilson Whang, Sang-Yeob Yeo, Cheol Young Choi, and Jehee Lee. (2014) Molecular profile and functional characterization of the ferritin H subunit from rock bream (*Oplegnathus fasciatus*), revealing its putative role in host antioxidant and immune defense. Dev. Comp. Immunol, 47, 104-114.
- 6. Don Anushka Sandaruwan Elvitigala**, H.K.A Premachandra, Ilson Whang, Myung-Joo Oh, Sung-Ju Jung, Choul-Ji Park, Jehee Lee. (2013) A teleostean counterpart of ferritin M subunit from rock bream (*Oplegnathus fasciatus*): An active constituent in iron chelation and DNA protection against oxidative damage, with a modulated expression upon pathogen stress. Fish & Shellfish Immunol, 35, 1455-1465.

ACKNOWLEDGMENTS

. ‘The impetus of life is dedication rather than fortune’. This is the conviction which always drives my life to the victories achieved to date and inspired me to stand on my feet in harsh circumstances. I am glade to have a supervisor in my graduate studies, who exactly follows this motto. I take this opportunity to award my sincere gratitude to Prof. Jehee Lee, my direct supervisor, for offering me an opportunity to study in Jeju National University and pursue my graduate studies under his kind guidance and encouragement in Marine Molecular Genetic laboratory. I found him as a grater character in my scientific life who has a remarkable capability of shaping up his students with tremendous productivity along with independent and innovative thinking. I am also indebted to my paraents for their unconditional love and care with the supporting hand in all my pursuits.

I am so much grateful to Dr. Ilson Whang for her valuable cooperation in my research work as well as in my publications. Moreover, I would like to express my honor to Prof. Ki-young Kim in Department of Marine Life Science for the facts on immunology taught in his course works, related to my research studies. I am also grateful to Prof. Choon Bok Song, Associate. Prof. Mahanama De Zoysa. Associate Prof. Chulhong Oh, and Research Prof. Qiang Wan for being members of my thesis committee. I also take this opportunity to pay my gratitude to Dr. Bong-Soo Lim and Dr. Hyung-Bok Jeong for their valuable support and kind guidance for my reseach studies.

My Special thanks go to one of the past members of our lab Mr. Ajith Premachandra, for his valuable cooperation and logical instructions for the progress of my research performance, even he is out of our lab todate. Further, I do not forget to acknowledge all of my former lab members, including Dr. Youngdeuk Lee, late Dr. Saranya Revathy, Dr. Niroshana

Wicramaaracchi, Dr. Umasuthan and Hyowan Kim as well as present ones, Sukkyoung Lee, Minyoung Oh, Yucheol Kim, Seoundo Lee, Eunyoung Oh, Jiyeon Kho, Dr. Qiang Wan, Handun Eranga, Lalinka Herath, Sachith Udara, Viraj Udayantha, Thiunuwan Priyathilaka, Gelshan Godahewa, Nadeeshani Perera, Kugapreethan, Thulasitha Williom, Sanjaya Bathige, Jeongin Ma and Sunhye Kan for their kind corporation to drive my research works to a success. I am also grateful to my other Sri Lankan colleagues in my department, Dr. Kalpa Samarakoon and Prasad Rajapaksha as well as other friends in Sri Lankan community in my university for sharing their experiences with me which in turn advanced my analytical thinking and cooperating with me as closer family members.

Finally, I gratefully mention the National Fisheries Research and Development Institute, and Brain Korea plus program which funded my research works.

CONTENTS

요약문	XII
Summary	XX
List of figures	XXVIII
List of tables	XXXV
Introduction	1
Chapter I. Identification and molecular characterization of three putative acute phase proteins from Black rock fish (<i>Sebastes schlegelii</i>) deciphering their roles in host acute phase response.	
Part A - Characterization of a C-reactive protein (CRP) homologue from Black rockfish	
1. Abstract	27
2. Materials and Methods	
2.1. cDNA database of black rockfish	28
2.2. <i>RfCRP</i> sequence identification and profiling	29
2.3. Preparation of the RfCRP recombinant plasmid construct	29
2.4. Overexpression and purification of recombinant RfCRP (rRfCRP)	31
2.5. Determination of bacterial agglutination activity and its inhibition	31
2.6. Antibacterial activity analysis	
2.6.1. Effect on growth of <i>E. coli</i> by overexpressing rRfCRP	32
2.6.2. Bacterial growth inhibition by purified rRfCRP	33
2.7. Fish husbandry and tissue collection	33

2.8. Immune stimulation	34
2.9. Total RNA isolation and cDNA synthesis	34
2. 10. Relative quantification of <i>RfCRP</i> mRNA expression	35
3. Results and Discussion	
3.1. Delineation of sequence features and homology	37
3.2. Phylogenetic reconstruction	41
3.3. Integrity of purified rRfCRP	43
3.4. Bacterial agglutination activity	44
3.5. Ligand binding ability	45
3.6. Bacterial growth inhibition	47
3.7. Tissue specific transcription of <i>RfCRP</i>	50
3.8. Transcriptional modulation of <i>RfCRP</i> upon immune stimulation	51
4. Conclusion	54
Part B - Characterization of serum amyloid A (SAA) counterpart from Black rockfish	
1. Abstract	56
2. Materials and Methods	
2.1. Identification, sequence analysis and comparison	57
2.2. Experimental fish, husbandry and tissue collection	57
2.3. Immune challenge experiments	58
2.4. RNA isolation and first-strand cDNA synthesis	58
2.5. Transcriptional analysis by Quantitative real-time PCR (qPCR) and statistical analysis	58
3. Results and Discussion	

3.1. Sequence characteristics and homology	60
3.2. Phylogenetic position of RfSAA	62
3.3. Protein folding prediction of RfSAA	63
3.4. Tissue-specific expression of <i>RfSAA</i>	65
3.5. Expressional modulation in response to challenge experiments	66
4. Conclusion	69
Part C - Characterization of haptoglobin (Hp) counterpart from Black rockfish	
1. Abstract	70
2. Materials and Methods	
2.1. Identification, sequence analysis and comparison of RfHp and RfSAA from the black rockfish	71
2.2. Experimental fish, husbandry and tissue collection	71
2.3. Immune challenge experiments	71
2.4. RNA isolation and first-strand cDNA synthesis	72
2.5. Transcriptional analysis by Quantitative real-time PCR (qPCR) and statistical analysis	72
3. Results and Discussion	
3.1. Sequence characterization of RfHp	74
3.2. Phylogenetic position of RfHp	77
3.3. Protein folding prediction of RfHp	77
3.4. Quantitative analysis of tissue-specific expression of <i>RfHp</i>	79
3.5. Quantitative analysis of expressional modulation in response to challenge experiments	80

4. Conclusion 83

Chapter 2. Identification and molecular characterization of selected role players in host antioxidative defense from Rock bream (*Oplegnathus fasciatus*) portraying their functional significances.

Part A - Characterization of a catalase homologue from Rock bream

1. Abstract 84

2. Materials and Methods

2.1. Construction of rock bream cDNA sequence database 86

2.2. Identification of the complete cDNA sequence of RbCat 86

2.3. Identification of the complete genomic sequence of RbCat 86

2.4. *In-silico* characterization of RbCat 87

2.5. Expression and purification of recombinant RbCat (rRbCat) 88

2.6. Analysis of antioxidant activity of rRbCat 90

2.7. Evaluation of the biochemical properties of rRbCat 90

2.8. Experimental fish and tissue collection 91

2.9. Immune challenge experiments 92

2.10. Total RNA extraction and cDNA synthesis 92

2.11. RbCat transcriptional analysis by reverse transcription PCR 93

followed by quantitative real time PCR

3. Results and Discussion

3.1. Sequence characterization and phylogenetic relationship of RbCat	94
3.2. Modeled tertiary structure of RbCat	99
3.3. Genomic architecture and predicted core promoter region of RbCat	100
3.4. Protein expression and purification of rRbCat	104
3.5. Antioxidant activity of rRbCat	105
3.6. Biochemical properties of rRbCat	106
3.7. Tissue-specific mRNA expression profile of RbCat	109
3.8. Transcriptional response of RbCat upon immune stimulation	111
4. Conclusion	114
 Part B - Characterization of a thioredoxin reductase 3 (TrxR3) homologue from Rock bream	
1. Abstract	116
2. Materials and Methods	
2.1. Identification of complete <i>RbTrxR-3</i> cDNA and genomic DNA Sequences	117
2.2. <i>RbTrxR-3</i> sequence profiles and phylogenetic analyses	118
2.3. Molecular cloning, over-expression, and purification of recombinant RbTrxR-3 (rRbTrxR-3)	119
2.4. rRbTrxR-3 thiol reductase activity analysis	120
2.5. Animal husbandry and tissue collection	120
2.6. Pathogen challenge experiments	121

2.7. Total RNA extraction and cDNA synthesis	122
2.8. Measurement of RbTrxR-3 and rock bream Trx-1 (RbTrx-1) mRNA expression levels in liver tissues by using quantitative PCR	122

3. Results and Discussion

3.1. Molecular properties and sequence similarity of RbTrxR-3	123
3.2. Comparative analysis of RbTrxR-3 gene architecture	128
3.3. Phylogenetic reconstruction of RbTrxR-3	129
3.4. Integrity of purified rRbTrxR-3	131
3.5. Thiol-reductase activity of RbTrxR-3	132
3.6. Distribution of RbTrxR-3 mRNA in rock bream tissues	133
3.7. Temporal transcriptional response of RbTrxR-3 to live pathogenic Stimuli	135

4. Conclusion 137

Part C - Characterization of ferritin H (FerH) subunit from rock bream

1. Abstract	139
2. Materials and Methods	
2.1. Identification and sequence analysis of <i>RbFerH</i>	140
2.2. Expression and purification of recombinant RbFerH fusion protein	141
2.3. Iron(II) depriving activity of rRbFerH	143
2.4. Antibacterial activity of rRbFerH	144

2.5. Determination of the effect of rRbFerH on oxidative damage of DNA	144
2.6. Experimental fish and tissue collection	145
2.7. Immune challenge experiments	146
2.8 Total RNA extraction and cDNA synthesis	146
2.9 <i>RbFerH</i> transcriptional analysis by quantitative real-time PCR	147
3. Results and Discussion	
3.1. Sequence profiles and homology	148
3.2. Phylogenetic relationship of RbFerH	154
3.3. Integrity, purity and degree of ferritin complex formation of rRbFerH	156
3.4. Iron(II) depriving activity of rRbFerH	157
3.5. Antibacterial activity of rRbFerH	159
3.6. Protective effect of rRbFerH in oxidative DNA damage	160
3.7. Spatial expression pattern of <i>RbFerH</i>	162
3.8. Transcriptional modulation of <i>RbFerH</i> expression upon immune stimulation	163
4. Conclusion	167
Part D - Characterization of ferritin M (FerM) subunit from rock bream	
1. Abstract	168

2. Materials and Methods

2.1 Identification and sequence profiling	169
2.2 Overexpression and purification of the recombinant RbFerM fusion Protein	169
2.3. Effect of rRbFerM protein concentration on the iron binding activity	172
2.4. Effect of temperature on the iron binding activity of rRbFerM	172
2.5. Determination of the DNA protection effect of rRbFerM under oxidative stress	173
2.6. Experimental fish and tissue collection	173
2.7. Immune challenge experiments	174
2.8 Total RNA extraction and cDNA synthesis	175
2.9 RbFerM transcriptional analysis by quantitative real time PCR	175

3. Results and Discussion

3.1. Sequence characterization of RbFerM	177
3.2. Evolutionary proximity of RbFerM with its orthologs	181
3.3. Integrity and purity of overexpressed recombinant RbFerM (rRbFerM)	182
3.4. Iron binding activity for different concentrations of rRbFerM	184
3.5. Iron binding activity of rRbFerM as a function of temperature	185
3.6. DNA protection effect of rRbFerM under oxidative stress	186
3.7. Transcriptional distribution of RbFerM in selected tissues	188

3.8. Transcriptional behavior of RbFerM upon immune stimulation	190
4. Conclusion	195
General Conclusion	196
References	198

요약문

돌돔 (*Oplegnathus fasciatus*)과 조피볼락 (*Sebastes schlegeli*)은 특히 한국과 일본 같은 아시아 태평양 지역의 대부분의 국가에서 매우 수요가 높은 어류이다. 하지만, 돌돔과 조피볼락 수산양식산업에서 다양한 세균, 바이러스 또는 기생충 더불어 다른 스트레스 요인들에 의한 병원체 감염의 유행은 상당한 폐사량을 야기하고 있고 이에 따라 적절한 질병 관리 전략의 필요성이 촉구되고 있다. 그래서, 이 어종에 대한 지속 가능한 수산양식을 보증할 수 있는 적절한 질병 또는 스트레스에 저항하는 기술을 개발하기 위해서 면역 방어와 산화 방어 기전에 대한 조사가 중요하다.

이 연구의 첫 장 (chapter 1)에서 우리는 조피볼락으로부터 C-reactive protein (CRP), serum amyloid A (SAA), haptoglobin (Hp)로 불리는 3 개의 acute phase proteins (APPs)를 동정하고 분자적 특성을 분석하였으며 병원체 스트레스 상태에서 이 유전자들의 전사적 조절을 판독하였다. C-reactive protein 은 pentraxin superfamily proteins 에 속하며 동물에서 pattern recognition receptor molecule 과 major positive APP 로써 그 기능이 알려져 있다. 첫번째 연구에서 CRP-like molecule 의 cDNA 서열을 이전에 구축한 조피볼락 cDNA database (RfCRP)로부터 동정하였고 그 뒤에 분자적 수준에서 특성을 분석하였다. RfCRP 의 전체 암호화 서열은 672bp 이고 예상 분자량이 25.19 kD 인 224 아미노산을 암호화하고 있었다. 아미노산서열 분석에서 RfCRP 는 pentraxin family signature 를 포함한 pentraxin family member 의 전형적인 특징이 확인되었다. Multiple sequence alignment 결과는 RfCRP 가 기능적으로 중요한 잔기가 보존된 것을 보여주었다. 다른 분류군으로부터 다른 pentraxin counterparts 를 사용하여 계통수를

재구축한 것에 따르면, RfCRP 는 일반적인 척추동물의 조상 기원을 공유하였고 대부분의 해양 어류의 CRP 와 균을 이루었다. 뿐만 아니라, 재조합 RfCRP 는 *Escherichia coli* 에 대응하여 Ca^{2+} -의존적 응집 활성을 보여주었는데 이것은 탄수화물을 기초로 한 ligand 의 존재를 완벽히 억제하였다. 게다가, 재조합 RfCRP 는 또한 *E. coli* 와 *Streptococcus iniae* 에 대하여 항균활성을 보여주었다. 또한, qPCR 분석은 RfCRP 가 생리적으로 중요한 조직에서 모두에서 발현하였으며 비장에서 확연하게 발현하였다. 건강한 어류에 polysaccharides 또는 살아있는 *S. iniae* 를 처리한 후에 RfCRP 의 발현은 비장과 두신조직에서 상당히 상향조절되었다. 종합하자면, 우리의 결과는 RfCRP 가 숙주의 항균방어에 중요하고 감염의 급성기에 참여하는 것으로 여겨진다.

우리의 두 번째 연구인 APPs 는 조피볼락으로부터 동정된 SAA counterpart 에 특히 패혈증상에서 발현 행동에 관하여 실질적 통찰을 얻는데 집중하였다. Serum amyloid A (SAA)는 감염이나 염증의 급성기에 관련된 중요한 단백질이다. SAAs 는 자기 파괴 메커니즘이나 병원균에 의해서 손상되는 건강한 세포를 보호하기 위하여 염증상태에서 간세포로부터 방출된다. 이 연구에서 이전에 구축한 조피볼락 cDNA library 는 SAA homolog (RfSAA)의 전체 cDNA 서열을 동정하고 분자적 수준에서 특성을 분석하는데 사용되었다. 예상대로, in silico analysis 에서 이 homolog 는 이전에 이 유전자의 알려진 counterparts 의 전형적인 도메인을 보여주었다. RfSAA 의 Open reading frame 은 313bp 의 DNA 서열로 구성되었다. RfSAA 의 파생된 폴리펩타이드는 121 개의 아미노산서열을 가지고 있었으며 분자량은 13kD 이다. 계통수 분석과 pairwise sequence alignment 의 결과는 RfSAA 가 *Epinephelus coioides* ortholog 와 가깝게

관련되어 있음을 보여주었다. 비록 RfSAA 가 분석한 모든 조직에서 발현되었지만, 간 조직에서 탁월하게 발현되었다. Quantitative real-time PCR 분석에서는 RfSAA 가 간조직에서 세균성과 바이러스성 자극에 의해서 상당히 상향 조절되었으며 이것은 1 차 숙주 면역 방어선의 급성기에서 중요성을 확인할 수 있다.

세 번째 연구에서, 우리는 조피볼락으로부터 Hp counterpart 를 동정하고 병원체 스트레스 상태에서 이 유전자의 발현 조절에 집중하여 분자적으로 특성을 분석하였다. Haptoglobin (Hp)는 간에서 합성되는 양성 급성 단백질이며, 감염의 급성기 동안 농도가 증가되었다. Hp 는 산화 손상을 포함한 자유 hemoglobin 에 의한 부정적인 효과를 막기위해서 용혈과정동안 hemoglobin (Hb)에 결합한다. 또한 여기에서 우리는 이전에 구축한 조피볼락의 cDNA library 는 Hp homolog (RfHp)의 전체 cDNA 서열을 동정하기 위하여 사용하였고 분자적 수준에서 특성을 분석하였다. 예상대로, in silico analysis 에서 RfHp 는 이전에 알려진 counterpart 의 전형적인 도메인을 포함하는 것을 보여주었다. RfHp 의 Open reading frame 은 942bp DNA 서열로 이루어져있었다. RfHp 의 파생된 아미노산 서열은 313 아미노산으로 구성되어 있었으며 예상되는 분자량은 34 kD 이다. 계통수 분석과 as pairwise sequence alignment 의 결과는 RfHp 가 진화적인 관점에서 *Oreochromis mossambicus* 의 counterpart 에 가장 가깝게 관련되어 있었다. 비록 RfHp 가 실험한 모든 조직에서 발현되었지만, 간조직에서 특히 발현되었으며 이 유전자의 기원이 간세포임을 시사한다. Quantitative real-time PCR 분석에서는 RfHp 가 간조직에서 세균성과 바이러스성 자극에 의해서 상당히 상향 조절되었으며 이것은 1 차 숙주 면역 방어선의 급성기에서 중요성을 확인할 수 있다.

이 연구의 두 번째 장 (chapter 2)에서 우리는 돌돔으로부터 4 개의 분별되는 항산화제를 동정과 특성 분석을 시도하였다. 이 중 2 개(catalase 와 thioredoxin reductase 3 (TrxR3))는 항산화 방어에 직접적으로 관여하는 것으로 알려져 있고, 다른 두 개 (ferritin H and M)는 ‘Fenton’ 유형의 반응과 같은 산화반응의 촉매(Fe^{2+})를 박탈하여 항산화 방어에 간접적으로 참여한다.

두 번째 장의 첫 번째 연구는 돌돔(*Oplegnathus fasciatus*)으로부터 catalase counterpart 동정하고 특성을 분석하였다. Catalases 는 산화스트레스를 방어하기 위하여 주로 과산화수소를 물과 산소로 불균등화 반응을 하는 항산화 효소로 알려져 있다. 돌돔 (*Oplegnathus fasciatus*)의 Catalase 의 전체 genomic DNA (gDNA) 서열은 our custom-constructed BAC genomic DNA library 으로부터 동정되었고, *RbCat* 로 명시하였다. *RbCat* 는 12 개의 intron 에 의하여 분리된 13 개의 exon 으로 13,722bp gDNA 서열로 이루어져있다. *RbCat* 의 전체 cDNA 서열(3,303bp)은 이론상의 등전점이 8.34 이고 분자량이 60 kD 인 길이가 527 개의 아미노산으로 된 펩타이드를 암호화한 1,581bp 의 코드영역으로 구성되었다. *RbCat* 의 참여된 프로모터 지역은 면역과 항산화 반응의 신호전달 분자에 결합되는 부위를 포함하여 여러 전자 인자 결합 부위를 포함하고 있으며 이것은 실질적인 전사 조절을 시사하고 있다. *RbCat* 는 전형적인 catalase family signature 와 유사하였고 즉, catalase proximal heme-ligand signature motif와 마찬가지로 catalase proximal active site motif로 구성되었으며 다른 어류들과 높은 상동성을 공유하였다. multiple sequence alignment 에 따르면, *RbCat* 에서 기능적으로 중요한 아미노산은 척추동물 사이에 완벽하게 보존되어 있었다. 계통수 분석에서는 *RbCat* 는 척추동물의 기원으로부터 진화되었고 그리고 더 나아가 어류의

분기군에 위치해 있었다. 재조합 RbCat 는 기질인 과산화수소에 대하여 농도-의존적 방법에 의하여 분명한 과산화 효소 활성을 가지고 있었다. 하지만, 이것은 pH 와 온도의 넓은 범위 내에서 상당한 과산화 효소 활성을 보여주었다. 조직에 따라서 각각 다른 양의 RbCat mRNA 발현을 확인할 수 있었고, 이것은 조직 종류에 따라서 생리적인 다양한 역할을 시사한다. 게다가, 살아있는 병원체인 *Edwardsiella tarda*, rock bream iridovirus (RBIV)와 유사체인 polyinosinic:polycytidylic acid, lipopolysaccharide 를 사용하여 면역 공격 실험하였을 때 면역 자극에 의하여 RbCat 의 전사가 조절되었다. 종합하자면, 이 연구에서 얻은 결과들은 RbCat 가 돌돔에서 강한 항산화 효소로서 기능을 하고, 과산화 효소 활성에 따라 면역 반응 후기에서 역할을 할 것이다.

이 장의 두 번째 연구는 돌돔의 TrxR3 counterpart 분자적인 특성을 분석하는데 전념하였다. Thioredoxin (Trx) 시스템은 활성산소종의 과잉을 불균등화반응에 의해 세포의 항산화 방어에 중요한 역할을 한다. 그래서, Trx enzyme cascade 의 개시에 관여하기 때문에 thioredoxin reductase (TrxR)의 역할을 무시할 수 없었다. 여기에, 우리는 다른 척추동물의 TrxR-3 isoforms 과 높은 유사성을 보여주는 teleostean TrxR (RbTrxR-3) ortholog 의 동정과 분자적 특성에 대하여 보고하고자 한다. 완전한 *RbTrxR-3* 암호화 서열은 예상 분자량이 66 kD 이상 되는 600 아미노산을 암호화하고 있는 1800 뉴클레오티드로 구성된다. *RbTrxR-3* 은 총 길이가 12658bp 가 되는 15 개의 intron 에 의해 나누어진 16 개의 exon 으로 구성되어 있다. RbTrxR-3 의 단백질 서열의 *In silico* analysis 에서는 전형적인 typical TrxR domain architecture 를 지니는 것으로 나타났다. 게다가, multiple sequence alignment 와 pairwise sequence alignment strategies 를 사용하였을 때, 우리는 RbTrxR-3 가 다른 어류의 TrxR-3 단백질과 매우 보존된 활성

부위 잔기를 포함하여 전체적으로 높은 서열 유사성을 가지고 있는 것을 보여주었다. RbTrxR-3 의 계통수에서는 어류의 TrxR-3 orthologs 와 같은 군으로 나타남으로써 가까운 진화적인 관계를 알 수 있었다. *RbTrxR-3* 전사적 분석은 quantitative polymerase chain reaction (qPCR)을 사용하여 실시하였고 *RbTrxR-3* 가 모든 조직에서 발현되고 가장 높게 발현하는 조직은 혈액이고 그 다음으로 아가미, 간이다. 살아있는 병원균과 바이러스 자극은 같은 병원성 스트레스에서 돌돔의 thioredoxin1 과 일시적으로 연관되어있는 간에서 *RbTrxR-3* 의 기본적인 전사의 변동을 촉발시켰다. 마지막으로, TrxR 단백질의 전형적인 기능부위를 재조합하고, 정제된 재조합 RbTrxR-3 가 5,5'-dithiobis (2-nitrobenzoic) acid 에 대하여 농도-의존적으로 반응하는 것을 확인할 수 있었다. 종합하자면, 이 결과들은 RbTrxR-3 가 산화와 병원성 스트레스에서 숙주의 Trx 시스템에서 역할을 맡고 있는 것을 시사하고 있다.

세 번째 연구로 우리는 ferritin complex 를 구성하는 중요한 요소로써 돌돔의 FerH like subunit 을 동정하였다. Ferritins 은 세포의 환경에서 물질대사나 철의 항상성 유지에 참여하는 24 subunit 로 만들어진 철 결합 단백질이다. 여기에서, 우리는 rock bream (*Oplegnathus fasciatus*; RbFerH) 으로부터 ferritin 의 subunits 중에 한 가지 타입(ferritin H-like subunit)의 특성을 분석하였다. *RbFerH* 의 완전한 암호화 서열은 예상되는 분자량이 20.8 kD 의 177 아미노산을 암호화하고 있는 길이가 531bp 인 서열이다. 추론되는 단백질 구조는 철 결합을 위한 metal ligand, ferroxidase center 와 두 개의 two iron-binding region signature 를 포함한 알려진 ferritin H subunit 의 특징적인 domain architecture 를 가지고 있었다. 예상대로 *RbFerH* cDNA 서열의 5' 비해석부위에는 전사에 관여하는 특징적인 조절 요소로 철 반응 요소 부위를 포함하고

있었다. *RbFerH* 유전자는 4195bp 로 구성된 4 개의 intron 과 5 개의 exon 으로 구성되어 있다. 과발현된 재조합 RbFerH 단백질은 산화된 이중나선 DNA 피해에 대응하여 보호하는 효과와 세균 발육 억제 특성, 현저한 Fe(II) 이온 박탈 활성을 보여주었다. quantitative polymerase chain reaction (qPCR) 사용하여, 우리는 돌돔에서 생리적으로 중요한 조직에서 모두 발현되는 것을 확인하였다. 높은 mRNA 전사는 혈액과 간 조직에서 확인되었다.

다른 미생물 병원체와 병원체에서 유래한 유사분열물질을 주입하였을 경우, *RbFerH* 전사는 현저하게 돌돔의 혈액에서 증가한다. 종합하자면, 우리가 찾아낸 것은 RbFerH 가 돌돔에서 강한 iron sequestrator 로서 역할을 하고, 항균성과 항산화 방어에 관여하여 활발히 관여할 것으로 생각된다.

두 번째 장의 마지막 연구로 우리는 돌돔으로부터 FerM like subunit 의 특성을 분석하였다. Ferritin “M” subunit 는 또한 H and L subunit 둘 다에서 특징적인 특성을 지니는 ferritin nano-cage (24 mer)를 형성하는데 기여하고 대부분의 어류는 하등 척추동물로부터 최근에 동정 된다. 이 연구에서, 돌돔 (*Oplegnathus fasciatus*)의 ferritin M-like subunit(RbFerM)은 분자적 수준에서 특성을 분석하였고 그리고 건강한 어류와 병원체와 유사체 자극을 받은 어류에서 이 전사적 분석을 실시하였다. 게다가. 이 유전자의 기능적인 특성을 재조합 단백질을 사용하여 평가하였다. RbFerM 의 완전한 암호화 서열은 계산된 분자량이 20 kD 인 176 개의 아미노산을 암호화하고있는 길이가 528bp 인 서열이다. RbFerM 의 *In silico* analysis 에서 다른 포유류의 ferritin subunits H 와 L 의 비슷한 특징을 가지고 있는 것으로 나타났다. 계통수 분석은 다른 어류들과 RbFerM 이 매우 진화적으로 가까운 것으로 확인되었다. Quantitative real time

polymerase chain reaction (PCR) 분석은 돌돔의 선택된 조직에서 RbFerM 이 전자적으로 모두 발현되었고 혈액과 간 조직에서 좀 더 확연한 발현을 관찰할 수 있었다. 시간 경과에 따른 면역 공격 실험에서 lipopolysaccharides (LPS), *Edwardsiella tarda*, *Streptococcus iniae*, rock bream irido virus (RBIV)에 노출되었을 때 간 조직에서 상당한 RbFerM 의 전자적 유도를 확인할 수 있었다. RbFerM 의 정제된 재조합 단백질은 온도에 의하여 변하는 철 결합 활성을 증명하였다. 게다가 재조합 RbFerM 은 iron (II)과 H₂O₂-mediated DNA damage 에 대응하여 확연한 보호 효과를 보여주었다.

종합하자면, 이 연구의 궁극적인 목적은 돌돔과 조피볼락에서 선택된 APP counterparts 와 antioxidants 를 각각 밝히고 더 나아가 병원체 스트레스에 반응하는 전사적 수준에서 발현의 조절을 판독하고자 한다. 게다가, 몇몇의 분자는 면역이나 어류 생리에서 기능적인 역할을 제시된 in-vitro 에서의 예상되는 기능을 보여주었다. 이런 우리의 공동연구의 결과는 병원체 감염이나 항산화 스트레스에 대응하여 어류의 생존을 높일 수 있는 점진적인 전략을 향상하는데 도움을 줄 것이다.

SUMMARY

Rock bream (*Oplegnathus fasciatus*) and black rockfish (*Sebastes schlegeli*) are highly demanded fish delicacies in most of the countries in Asia Pacific region, especially in Korea and Japan. However, prevalence of pathogenic infections caused by various bacterial, viral or parasitic agents along with other stress factors instigates considerable mortalities in rock bream and rockfish aquaculture industries, urging the need of proper disease management strategy. Thus, it is important to investigate on naturally existing host immune defense and oxidative defense mechanisms in those aqua-crops to develop proper disease or stress resistance strategies, assuring the sustainable aquaculture of these fish species.

In the first phase (chapter 1) of the studies we sought to identify and molecularly characterize three acute phase proteins (APPs), namely C-reactive protein (CRP), serum amyloid A (SAA) and haptoglobin (Hp) from black rockfish, deciphering their transcriptional modulation under induced pathogen stress. C-reactive protein is categorized under pentraxin superfamily proteins, and known to function as a pattern recognition receptor molecule and major positive APP in animals. In our first study, a cDNA sequence of a CRP-like molecule was identified from a previously constructed black rockfish cDNA database (RfCRP) and subsequently characterized at its molecular level. The complete coding region of RfCRP is 672 bp in length, and encodes a protein containing 224 amino acids with a predicted molecular mass of 25.19 kD. Analysis of its derived amino acid sequence enabled typical features of pentraxin family members to be identified, including the pentraxin family signature in RfCRP. Results from multiple sequence alignment suggest the conservation of functionally important residues in RfCRP. According to the phylogenetic reconstruction that was generated using different pentraxin counterparts from different taxa, RfCRP shares a common vertebrate ancestral origin and most closely clusters with marine teleostan CRP. Furthermore, recombinant

RfCRP demonstrated Ca^{2+} -dependent agglutination activity against *Escherichia coli*, which could be completely inhibited in the presence of carbohydrates based ligands. Moreover, recombinant RfCRP also exhibited anti-bacterial activity against both *E. coli* and *Streptococcus iniae*. In addition, qPCR analysis indicated that RfCRP is ubiquitously expressed in physiologically important tissues, with pronounced expression in the spleen. After healthy fish were treated with polysaccharides or live *S. iniae*, basal expression of RfCRP was significantly upregulated in spleen and head kidney tissues. Collectively, our results suggest that RfCRP may be important in host anti-bacterial defense, and it might potentially participate in the acute phase of an infection.

Our second study on APPs was centered on gaining substantial insights into a SAA counterpart identified from rockfish, especially regarding its expressional behavior under septic conditions. Serum amyloid A (SAA) is a vital protein involved in acute phase of an inflammation or infection. SAAs are released from hepatocytes under inflammatory conditions to protect healthy cells from being damaged by pathogens or from self-destructive mechanisms. In this study our previously constructed black rockfish (*Sebastes schlegeli*) cDNA library was used to identify the full-length cDNA sequence SAA homolog (RfSAA) and characterize at the molecular level. As expected, *in-silico* analysis of this homolog showed the typical domain architectures of their known counterparts. Open reading frame of *RfSAA* consisted of 313-bp DNA sequence. The derived polypeptide sequence of RfSAA had a 121-amino acid sequence with a molecular weight of 13 kD. Phylogenetic analysis as well as pairwise sequence alignment results showed that RfSAA was closely related to the *Epinephelus coioides* ortholog. Although *RfSAA* was expressed ubiquitously in the tissues analyzed, they were eminently expressed in liver tissue, suggesting their origin in hepatocytes. Quantitative real-time PCR analysis indicated that *RfSAA* can be significantly up-regulated by

both bacterial and viral stimulation in liver tissues, affirming its putative importance in the acute phase of first-line host immune defenses.

In our third study, we identified and molecularly characterize a Hp counterpart from black rockfish, focusing on its expressional modulation under pathogenic stress. Hp is a positive acute phase protein in most of the animals, synthesized in liver, and its concentration is elevated during the acute phase of an infection. Hp binds with hemoglobin (Hb) during the hemolysis process to prevent the negative effects exerted by free Hb, including oxidative damage. Also here in, our previously constructed black rockfish (*Sebastes schlegeli*) cDNA library was used to identify the full-length cDNA sequences of Hp homolog (RfHp) and it was molecularly characterized. As expected, *in silico* analysis showed that RfHp houses the typical domain architecture of its known counterparts. Open reading frames of *RfHp* consisted of 942 bp DNA sequence. The derived polypeptide sequence of RfHp was composed of 313 amino acids (aa) with a predicted molecular weight of 34 kD. Phylogenetic analysis as well as pairwise sequence alignment results showed that RfHp was more closely related to its counterpart of *Oreochromis mossambicus* from an evolutionary perspective. Although *RfHp* was expressed ubiquitously in the tissues analyzed, it was particularly expressed in liver tissue, suggesting their origin in hepatocytes. Quantitative real-time PCR analysis indicated that *RfHp* was significantly up-regulated by both bacterial and viral stimulation in liver tissue, affirming its putative importance in the acute phase of the first-line host immune defenses.

In the second phase of the studies (described in chapter 2) we attempted to identify and characterize four distinct antioxidants from rock bream, two of which (catalase and thioredoxin reductase 3 (TrxR3)) are known to directly partake in antioxidant defense and

other two (ferritin H and M) can indirectly participate in antioxidant defense by depriving the catalysts (Fe^{2+}) of oxidative reactions such as ‘Fenton’ type reactions.

In the first study under chapter 2 we identified and characterized a catalase counterpart from rock bream. Catalases are known to be antioxidant enzymes that can mainly dismutate hydrogen peroxide into water and oxygen in order to prevent oxidative stress. The complete genomic DNA (gDNA) sequence of the catalase gene from rock bream (*Oplegnathus fasciatus*) was identified from our custom-constructed BAC genomic DNA library and designated as *RbCat*. *RbCat* consists of 13 exons, separated by 12 introns, within a 13,722 bp gDNA sequence. The complete cDNA sequence (3,303 bp) of *RbCat* is comprised of a 1,581 bp coding region, encoding a peptide of 527 amino acids (aa) in length, with a predicted molecular mass of 60 kD and a theoretical isoelectric point of 8.34. The anticipated promoter region of *RbCat* contains several transcription factor binding sites, including sites that bind with immune- and antioxidant-responsive signaling molecules, suggesting its substantial transcriptional regulation. *RbCat* resembles the typical catalase family signature, i.e., it is composed of the catalase proximal active site motif along with a catalase proximal heme-ligand signature motif and shares great homology with its fish counterparts. According to multiple sequence alignment, functionally important aa present in *RbCat* were thoroughly conserved among its vertebrate counterparts. Phylogenetic analysis revealed that *RbCat* evolved from a vertebrate origin, and further positioned it in the fish clade. Recombinant *RbCat* had noticeable peroxidase activity against its substrate, hydrogen peroxide, in a dose-dependent manner. However, it demonstrated substantial peroxidase activity within a broad range of temperatures and pH values. Constitutive *RbCat* mRNA expression of different magnitudes was detected in a tissue-specific manner, suggesting its diverse role in physiology with respect to the tissue type. Moreover, immune challenge experiments using *Edwardsiella*

tarda and rock bream iridovirus (RBIV) as live pathogens and polyinosinic:polycytidylic acid and lipopolysaccharide as mitogens revealed that the transcription of *RbCat* can be modulated by immune stimulation. Collectively, the results obtained in this study suggest that RbCat can function as a potent antioxidant enzyme in rock bream and may play a role in post-immune responses with respect to its peroxidase activity.

Our second study in this chapter was devoted to molecularly characterize a TrxR3 counterpart from rock bream. The thioredoxin (Trx) system plays a significant role in cellular antioxidative defense by dismutating the surpluses of reactive oxygen species. Thus, the role of thioredoxin reductase (TrxR) cannot be ignored, owing to its participation in initiating the Trx enzyme cascade. Here, we report the identification and molecular characterization of a teleostean TrxR (RbTrxR-3) ortholog that showed high similarity with the TrxR-3 isoforms of other vertebrates. The complete *RbTrxR-3* coding sequence comprised 1800 nucleotides, encoding a 600-amino acid protein with a predicted molecular mass of ~ 66 kD. *RbTrxR-3* consisted of 16 exons separated by 15 introns and had a total length of 12658 bp. *In silico* analysis of the RbTrxR-3 protein sequence revealed that it possesses typical TrxR domain architecture. Moreover, using multiple sequence alignment and pairwise sequence alignment strategies we showed that RbTrxR-3 has high overall sequence similarity to other teleostean TrxR-3 proteins, including highly conserved active site residues. Phylogenetic reconstruction of RbTrxR-3 affirmed its close evolutionary relationship with fish TrxR-3 orthologs, as indicated by its clustering pattern. *RbTrxR-3* transcriptional analysis, performed using quantitative real time polymerase chain reaction (qPCR), showed that *RbTrxR-3* was ubiquitously distributed, with the highest level of mRNA expression in the blood, followed by the gill, and liver. Live bacterial and viral stimuli triggered the modulation of *RbTrxR-3* basal transcription in liver tissues that correlated temporally with that of its putative substrate,

rock bream thioredoxin1 under same conditions of pathogenic stress. Finally, resembling the typical function of TrxR protein, purified recombinant RbTrxR-3 showed detectable dose-dependent thiol reductase activity against 5,5'-dithiobis (2-nitrobenzoic) acid. Taken together, these results suggest that RbTrxR-3 plays a role in the host Trx system under conditions of oxidative and pathogenic stress.

As the third study, we could identify the rock bream FerH like subunit, as crucial component of make up the ferritin complex. Ferritins are iron binding proteins made out of 24 subunits, involved in iron homeostasis and metabolism in cellular environments. Here, we sought to characterize a one type of subunits of ferritin (ferritin H-like subunit) from rock bream (*Oplegnathus fasciatus*; RbFerH). The complete coding sequence of *RbFerH* was 531 bp in length, encoding a 177 amino acid protein with a predicted molecular mass of 20.8 kD. The deduced protein structure possessed the domain architecture characteristic of known ferritin H subunits, including metal ligands for iron binding, a ferroxidase center, and two iron-binding region signatures. As expected, the 5' untranslated region of the *RbFerH* cDNA sequence contained a putative iron response element region, a characteristic regulatory element involved in its translation. The *RbFerH* gene comprised 5 exons and 4 introns spanning a 4195 bp region. Overexpressed recombinant RbFerH protein demonstrated prominent Fe(II) ion depriving activity, bacteriostatic properties, and protective effects against oxidative double-stranded DNA damage. Using quantitative polymerase chain reaction (qPCR), we found that *RbFerH* was expressed ubiquitously in the majority of physiologically important tissues in rock bream. A greater abundance of the mRNA transcripts were detected in blood and liver tissues. Upon administering different microbial pathogens and pathogen-derived mitogens, *RbFerH* transcription was markedly elevated in the blood of rock bream. Taken together, our findings suggest that RbFerH acts as a potent

iron sequestrator in rock bream and may actively participate in antimicrobial as well as antioxidative defense.

In final study under chapter 2, we described the characterization of FerM like subunit from rock bream. ferritin “M” subunit also contributes to form the ferritin nano-cage (24 mer) which possesses characteristic features of both the H and L subunits and was recently identified from lower vertebrates, mostly in fish. In this study, a ferritin M-like subunit from rock bream (*Oplegnathus fasciatus*) (RbFerM) was characterized at the molecular level, and its transcriptional profile was analyzed in healthy fish, as well as in pathogen- and mitogen-stimulated fish. Furthermore, its functional properties were evaluated using a recombinant protein. The complete coding sequence of *RbFerM* was 528 bp in length, encoding a 176-amino acid peptide with a calculated molecular mass of 20 kD. *In silico* analysis of RbFerM revealed that it has features similar to both the mammalian ferritin subunits, H and L. Phylogenetic analysis depicted the higher evolutionary proximity of RbFerM with its fish counterparts. Quantitative real time polymerase chain reaction (PCR) analysis detected a ubiquitous transcriptional profile of *RbFerM* in selected tissues of rock bream, in which more pronounced expression was observed in blood and liver tissues. Significant transcriptional inductions of *RbFerM* were detected in liver tissues upon lipopolysaccharides (LPS), *Edwardsiella tarda*, *Streptococcus iniae*, and rock bream iridovirus (RBIV) exposures in time-course immune-challenge experiments. The purified recombinant protein of RbFerM demonstrated detectable iron binding activity that varied with the temperature. Moreover, the recombinant RbFerM rendered a detectable protection effect against iron (II) and H₂O₂-mediated DNA damage.

Collectively, this complete set of studies discovers selected putative APP counterparts and antioxidants exist in black rockfish and rock bream, respectively, further deciphering their

expressional modulation at transcriptional level in response to pathogen stress. Moreover, some of the molecules were demonstrated to exert their expected functions in-vitro, suggesting their functional roles in fish physiology or immunity. Hence, the findings of our collective studies may help to betterment the progressive strategies which can enhance the survival of these fish against pathogen infection or oxidative stress.

List of figures

- Fig. 1.** Schematic representation of typical APR occurs in animals (as depicted in (Cray et al., 2009)).
- Fig. 2.** Schematic depiction of functional roles of CRP in the APR (extracted from (Rhodes et al., 2011))
- Fig. 3.** Pentameric structure of CRP, harboring calcium and phosphocholine binding sites
- Fig. 4.** Schematic illustration of the Hp-Hb complex formation and its fate in macrophages (extracted from 1 (Dennis, 2001)).
- Fig. 5.** Schematic presentation of synthesis and metabolism of SAA in the APR (Yamada, 1999)
- Fig. 6.** Four conceptual domain arrangement of a catalase molecule depicted by a 3D model
- Fig 7.** Functional role of Trx system, as depicted in (Mustacich and Powis, 2000)
- Fig. 8.** Generalized Fenton type reactions generating ROS
- Fig.9.** Hollow spherical structure of ferritin made out of 24 ferritin subunits
- Fig. 10.** Appearance of matured (A). Black rock fish and (B) Rock bream fish.
- Fig. 11.** Multiple protein sequence alignment of vertebrate CRPs including black rockfish CRP (RfCRP)
- Fig. 12.** Phylogenetic reconstruction of RfCRP
- Fig. 13.** SDS-PAGE analysis of intermediate products and the final eluted recombinant RfCRP (rRfCRP) protein during the protein purification process.

- Fig. 14.** Bacterial agglutination activity of rRfCRP
- Fig. 15.** Inhibitory effect of LPS (0.25 $\mu\text{g/mL}$) or D-galactose (0.125 μM) on bacterial agglutination of rRfCRP (0.15 $\mu\text{g/mL}$) in the presence of Ca^{2+} in mildly acidic medium.
- Fig. 16.** Bacterial growth inhibition following overexpression of rRfCRP
- Fig. 17.** Bacteriostatic activity of rRfCRP on (A) *E. coli* or (B) *S. iniae* as detected by the variation of bacterial density over time at OD_{600}
- Fig. 18.** Tissue-specific distribution of *RfCRP* expression in black rockfish measured using quantitative real-time polymerase chain reaction (qPCR).
- Fig. 19.** Temporal modulation of mRNA expression in spleen and head kidney tissues upon immune stimulation with (A) LPS and (B) *S. iniae* as determined by qPCR
- Fig. 20.** Comparison of the derived amino acid sequences of RfSAA with other counterparts.
- Fig. 21.** Phylogenetic tree demonstrating the evolutionary relationship of RfSAA with counterparts of other organisms
- Fig. 22.** Graphical representation of FoldIndex[®]; (A) RfSAA, (B) Orange-spotted grouper SAA, (C) Barramundi SAA, (D) Human SAA
- Fig. 23.** Tissue specific transcriptional profile of *RfSAA*
- Fig. 24.** Expression analysis of *RfSAA* in different tissues after experimental infection with *S. iniae*, carried out by qPCR.
- Fig. 25.** Expression analysis of *RfSAA* in different tissues after the treatment of poly I:C, carried out by qPCR.
- Fig. 26.** Comparison of the derived amino acid sequence of RfHp with other organisms. RfHp – signal peptide is denoted in a black box while the Tryp_SPC domain is in a red color box.

- Fig. 27.** Phylogenetic tree demonstrating the evolutionary relationship of RfHp with amino acid sequences of other organisms. Accession numbers are indicated along with the species name.
- Fig. 28.** Graphical representation of FoldIndex®; (A) RfHp, (B) Nile tilapia Hp, (C) Channel catfish Hp, (D) Human Hp.
- Fig. 29.** Tissue specific transcriptional profile of *RfHp* detected in selected tissues by qPCR.
- Fig. 30.** Expression of *RfHp* after *S.iniae* challenge experiment, detected by qPCR.
- Fig. 31.** Expression of *RfHp* after poly I:C treatment, detected by qPCR.
- Fig. 32.** Multiple sequence alignment of rock bream catalase (RbCat) with its vertebrate counterparts.
- Fig. 33.** Phylogenetic tree construct generated on the basis of ClustalW alignment of the deduced amino acid sequences of various catalase protein sequences, estimated by using the neighbor-joining method in MEGA version 4.0.
- Fig. 34.** Tertiary structure of rock bream catalase (RbCat) modeled according to the ab-initio strategy.
- Fig. 35.** Genomic organization of the catalase gene from different species.
- Fig. 36.** Predicted promoter region of rock bream catalase (*RbCat*) with 5'-untranslated region (UTR) and start codon ATG (bold).
- Fig. 37.** Sodium dodecyl sulfate-polyacrylamide gel electrophoresis analysis of overexpressed and purified recombinant rock bream catalase (rRbCat) fusion protein.

Fig. 38. *In vitro* peroxidase activity of recombinant rock bream catalase (rRbCat) fusion protein against its substrate hydrogen peroxide at different concentrations.

Fig. 39. Variation of recombinant rock bream catalase (rRbCat) peroxidase activity as a function of temperature.

Fig. 40. Variation of recombinant rock bream catalase (rRbCat) peroxidase activity as a function of pH.

Fig. 41. Tissue-specific expression analysis of rock bream catalase mRNA, determined by quantitative real time-polymerase chain reaction.

Fig. 42. Expression profile of rock bream catalase mRNA in blood upon immune stimulation with (A) lipopolysaccharide or *Edwardsiella tarda* bacteria, (B) polyinosinic:polycytidylic acid or rock bream iridovirus, as determined by quantitative real time-polymerase chain reaction.

Fig. 43. Multiple-sequence alignment of RbTrxR-3 and its vertebrate orthologs.

Fig. 44. Genomic architecture of *RbTrxR-3* and its vertebrate orthologs.

Fig. 45. Phylogenetic reconstruction of RbTrxR-3.

Fig. 46. SDS-PAGE analysis of the rRbTrxR-3 fusion protein at different steps in the overexpression and purification process.

Fig. 47. *In vitro* DTNB-reducing activity of rRbTrxR-3.

Fig. 48. Tissue distribution of *RbTrxR-3* mRNA expression, analyzed using qPCR.

Fig. 49. Temporal mRNA expression of *RbTrxR-3* (A) and *RbTrx-1* (B) in the liver tissues of rock breams, under live pathogen stress induced by *Edwardsiella tarda*, *Streptococcus iniae*, and RBIV.

Fig. 50. Multiple sequence alignment of vertebrate ferritin H subunit orthologs including rock bream ferritin H (RbFerH).

Fig. 51. Exon-intron arrangement of the RbFerH gene and its orthologs from other vertebrate species.

Fig. 52. Phylogenetic reconstruction of RbFerH and its orthologs.

Fig. 53. (A), SDS-PAGE analysis of the purified recombinant RbFerH (rRbFerH)-maltose binding protein (MBP) fusion protein and its cleaved products after treatment with Factor Xa. ; (B), Non reducing, native PAGE analysis of Factor Xa cleaved rRbFerH.

Fig. 54. (A), *In vitro* iron(II) deprivation by rRbFerH. (B), The percentage Fe(II) deprivation for 0.2 g/ L of rRbFerH under reducing (with Tin(II) ions) and non-reducing (without Tin(II) ions) conditions. (C), The percentage Fe(II) deprivation for 0.2 g/ L of rRbFerH under reducing (with Tin(II) ions) and non-reducing (without Tin(II) ions) conditions.

Fig. 55. Bacteriostatic activity of rRbFerH, as measured by the effect of rRbFerH (50 µg/mL) on *E.coli* in LB medium.

Fig. 56. Protective effect of rRbFerH on oxidative damage to dsDNA.

- Fig. 57.** Tissue-specific distribution of *RbFerH* expression in rock bream measured using quantitative real-time polymerase chain reaction (qPCR).
- Fig. 58.** Temporal regulation of *RbFerH* transcription in blood tissue upon immune stimulation with (A) lipopolysaccharides (LPS) and *E. tarda*, and (B) polyinosinic:polycytidylic acid (poly I:C) and rock bream Iridovirus (RBIV), as measured using qPCR.
- Fig. 59.** Nucleotides and deduced amino acid sequence of RbFerM.
- Fig. 60.** Multiple sequence alignment of different vertebrate ferritin subunits.
- Fig. 61.** Phylogenetic relationship of RbFerM and its orthologs.
- Fig. 62.** SDS-PAGE analysis of the overexpressed and purified recombinant RbFerM fusion protein and cleaved products after treatment of the fusion protein with factor Xa
- Fig. 63.** *In vitro* iron binding activity at different concentrations of rRbFerM
- Fig. 64.** Variation of *in vitro* iron binding activity of rRbFerM with temperature
- Fig. 65.** The effect of rRbFerM on DNA cleavage by reaction of H₂O₂ with iron (II) ions, as analyzed using agarose gel electrophoresis
- Fig. 66.** The transcriptional distribution of RbFerM among different tissues of rock bream determined by qPCR
- Fig. 67.** Expression profile of RbFerM mRNA in liver tissues upon immune stimulation with (A) LPS, (B) *E. tarda*, as determined by qPCR

Fig. 68. Expression profile of RbFerM mRNA in liver tissues upon immune stimulation with *S.iniae*, as determined by qPCR

Fig. 69. Expression profile of RbFerM mRNA in liver tissues upon immune stimulation with RBIV, as determined by qPCR

List of tables

Table 1. Some of the identified positive and negative APPs from mammals, birds and fish species.

Table 2. Different APPs and their functional roles *in-vivo*, as reviewed in (Cray et al., 2009).

Table 3. Major diseases caused by pathogenic agents in Korean mariculture industry (Park, 2009).

Table 4. Primers used in the study on RfCRP

Table 5. Percentage similarity and identity values of RfCRP with different CRP homologues

Table 6. The primers used in the study on RfSAA

Table 7. Percentage of interspecies amino acid sequence identity and similarity with RfSAA

Table 8. FoldIndex® data summary of RfSAA with other selected counterparts.

Table 9. The primers used in the study on RfHp

Table 10. Percentage of interspecies amino acid sequence identity and similarity with RfHp

Table 11. FoldIndex® data summary of RfHp with other selected organisms

Table 12. Oligomers used in the study on RbCat

Table 13. Percentage similarity and identity values of RbCat with its orthologs.

Table 14. Primers used in the study on RbTrxR3

Table 15. Percent similarity and identity values of RbTrxR-3 and its homologs

Table 16. Oligomers used in the study on RbFerH

Table 17. Percentage similarity and identity values of RbFerH with its orthologs

Table 18. Oligomers used in the study on RbFerM

Table 19. Percentage similarity and identity values of RbFerM and its orthologs

INTRODUCTION

Acute phase response (APR) and host antioxidative defense are two major bio-machineries functioning in animals, which play crucial roles in their physical wellbeing. The studies described in this thesis were devoted to identify and molecularly characterize several putative role players in APR and antioxidative defense in two teleostan species; black rockfish (*Sebastes schlegelii*) and rock bream (*Oplegnathus fasciatus*), respectively; deciphering their significance in host innate immune responses.

Acute phase response as a host first line immune defense mechanism

Vertebrate immune system is divided into two basic arms, namely innate immune system and adaptive immune system, of which former is considered as less specific since it is unable to direct its responses against specific invaders. However, innate immunity is the first line of host defense system in vertebrates which is dedicated for the early detection and eradication of pathogenic invaders such as bacteria, virus or parasites, further triggering the adaptive immune responses. The innate immune system comprises of two parts; humoral immunity and cellular immunity. Humoral component is consisted of wide range of substances found in body fluids which can directly or in-directly involve in eradication of pathogens in the body, whereas various immune cells especially phagocytes make up the cellular component of innate immune system which basically eliminate the pathogens by ingesting and degrading them. Compared to higher vertebrates like mammals, lower vertebrates particularly fish are highly rely on the innate arm of the immunity, as they are free-living organism from the embryonic stage of life in their aquatic environment which makes them more vulnerable to different pathogenic encounters (Rombout et al., 2005).

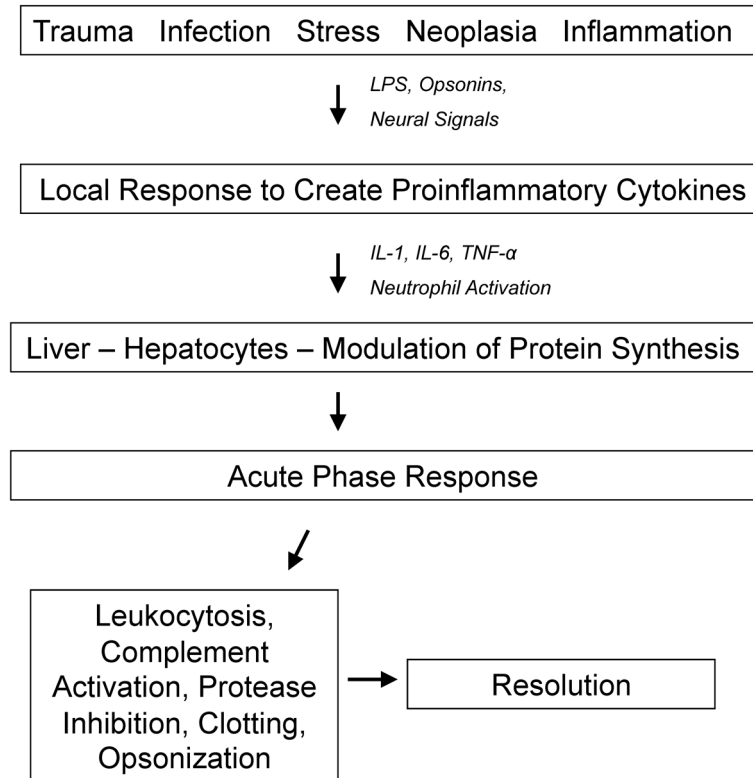


Fig. 1. Schematic representation of typical APR occurs in animals (as depicted in (Cray et al., 2009)).

Acute phase response is a complex systemic constituent of humoral part of innate immune system triggered by trauma, stress, neoplasia, inflammation or pathogen infections (Cray et al., 2009). Its crucial role in host immunity is represented by physical and molecular barriers along with responses urge to prevent infections, eliminate potential pathogens, and trigger inflammatory processes, direct resolution and healing process. The ultimate goal of this process is to reestablish the disturbed homeostasis in the body due to aforementioned stimuli. APR is known to be a universal innate immune mechanism in almost all the taxons in animal kingdom, which plays a profound role in invertebrates and fish compared to mammals, to counterbalance the less-evolved adaptive immunity (Armstrong and Quigley, 1999; Raida and Buchmann, 2009). APR is basically characterized by marked modulation of the concentrations of over 200 plasma proteins known as acute phase proteins (APP) (Gabay and

Kushner, 1999) including C-reactive proteins (CRPs), Serum amyloid A (SAA) and Haptoglobins (Hps), which are generally induced by toll like receptor (TLR) mediated production of pro-inflammatory cytokines, like interleukin (IL) 1, IL6 and tumor necrosis factor α (TNF α) under septic conditions (Cray et al., 2009). According to the elevation or reduction of their concentration in body fluids in response to a particular stimulus, APPs are categorized as either positive or negative responders (Kaneko, 1997). However, depending on the stimuli and host species, same APP can be elevated or decreased in animal body fluids (Table 1).

Table 1. Some of the identified positive and negative APPs from mammals, birds and fish species.

Taxonomic group	Positive APPs	Negative APPs
Mammals	SAA, CRP, Hp, AGP, Fibrinogen, Ceruloplasmin	TTR, RBP, Albumin, Transferrin
Birds	SAA, CRP, hemopexin, AGP, Transferrin, Ceruloplasmin	Hp, Albumin
Fish	SAA, CRP, Transferrin, C3	CRP, Apolipoprotein, Parvalbumin

AGP- α 1-acid glycoprotein; C3 – complement component 3; TTR – Transthyretin; RBP – Retinol binding protein. Ref (Uribe et al., 2011).

In general, APPs are mostly synthesized by hepatocytes, representing the initiation of APR. Positive APPs can be categorized into three main groups; namely, major, moderate and minor responders according to their fold increase during the APR. Major proteins are known to elevate its concentration from ~ 10 to 100 fold, whereas moderate ones indicate ~ 2 to 10 fold increase. However, concentration of minor APPs is slightly raised in an APR (Ceron et al., 2005). Major APPs were found to exhibit profound elevation in early phase (with in first

48 h) post triggering the APR by the respective stimulus, with a rapid decline owing to the very short half-life (Johnson et al., 1999). In contrast, moderate and minor APPs response gradually and increase slowly but within a prolonged duration according to the strength of the stimulus triggering the APR event. Thus, these APPs can be frequently observed to elevate in chronic inflammatory processes (Petersen et al., 2004; Ceron et al., 2005).

APPs exert wide range of biological roles in APR. Summary of some of those can be tabulated as follows.

Table 2. Different APPs and their functional roles *in-vivo*, as reviewed in (Cray et al., 2009).

APP	Biological functions
CRP	Opsonization of bacteria, fungi and parasites, in turn activating compliment system and phagocytosis
	Up regulation or down regulation of cytokine production and chemotaxis.
	Down-regulation of the inflammatory process
SAA	Chemotaxis of monocytes, polymorphonuclear cells and T-cells.
	Down-regulation of the inflammatory process
Hp	Reduction of oxidative damage associated with hemolysis, by binding free hemoglobin.
	Bacteriostatic and immunomodulatory function
α 1-acid glycoprotein	inhibition of LPS activity
	Down-regulation of neutrophils and complement
α 2-macroglobulin	Protease inhibition
	Removal of enzymes released during injury

Major acute phase protein (MAP) in pigs	Inhibition of trypsin
Ceruloplasmin	Free radical scavenging
Fibrinogen	Important in tissue repair by providing a substrate for fibrin formation

CRP, Hp and SAA as key role players in APR

Among the wide range of APPs identified to date, CRP, Hp and SAA are well known as potent positive APPs, concentration of which are profoundly elevated in an onset of a systemic inflammation or acute phase of an infection (Heinrich et al., 1990).

CRP

CRPs are phylogenetically conserved plasma proteins, classified under pentraxin superfamily as short pentraxins, under which serum amyloid P (SAP) was also categorized. Pentraxins including CRPs are considered as pattern recognition receptors which can recognize and bind conserved molecular patterns found on pathogenic microorganisms (Gordon, 2002) or typically exposed during cell death (Black et al., 2004). For instance, CRP can bind phosphocholine, phospholipids, carbohydrates and complement components (Chang et al., 2002; Szalai, 2002; Suresh et al., 2006) to facilitate the host immune defense mechanisms such as agglutination, phagocytosis and activation of complement system (Nauta et al., 2003; Pepys and Hirschfield, 2003). CRPs are known to increase rapidly to a highly significant level (~ 1000 fold or more) in human blood plasma upon an acute inflammatory signal via induced production in liver cells; hence were categorized as major positive APPs. Expression of CRP gene at transcriptional level is mainly regulated by IL-6 and IL-1 β through activation of transcriptional factors such as STAT3, C/EBP family members and NF- κ B (Agrawal and Volanakis, 1994).

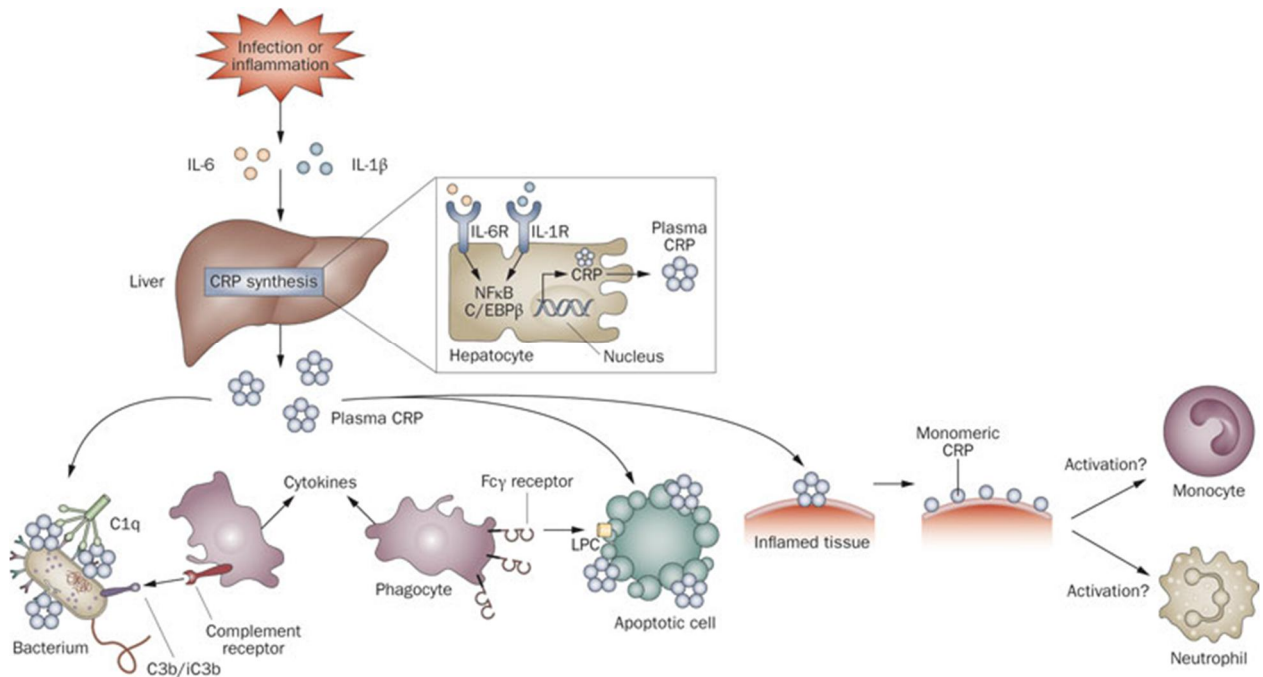


Fig. 2. Schematic depiction of functional roles of CRP in the APR (from (Rhodes et al., 2011))

CRPs are consisted of five non-covalently bound protomers forming a pentameric structure which symmetrically assemble to make a central pore. Resembling some lectins, each protomer was found to be folded into two antiparallel beta sheets bearing a jellyroll topology (Shrive et al., 1996). Each protomer harbors a recognition face with a phosphocholine binding site with two coordinated calcium ions next to a hydrophobic pocket. The opposite face of the pentameric assembly act as the effector face and binds complement C1q (Agrawal and Volanakis, 1994; Agrawal et al., 2001).

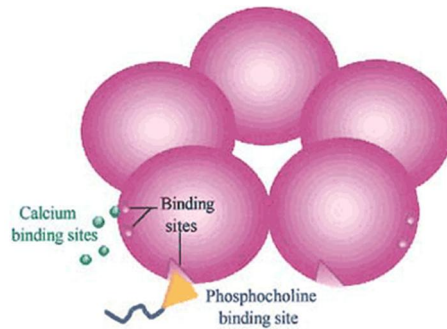


Fig. 3. Pentameric structure of CRP, harboring calcium and phosphocholine binding sites

HP

Hp is a positive APP which can be used as a valuable marker of an inflammation, as it augments its concentration by two to four folds during the acute phase of an infection (Kushner, 1982; Segawa et al., 2013). The central organ of Hp synthesis in animals is liver; however, it is also can be observed in organs such as lung, kidney, thymus, spleen and heart as well (Nielsen and Moestrup, 2009). Hp functions as a tetrachain ($\alpha_2\beta_2$) glycoprotein where the subunits are joined via inter-chain disulfide bonds (Adams and Weiss, 1969). Hp was recognized as a major receptor, locates on the cell membrane of the leukocytes and binds with hemoglobin (Hb) during the hemolysis process and prevent the possible damages which can be mounted by free Hb, including oxidative damages (Colon and Kelly, 1992; Lim et al., 2001; Tripathi, 2007; Polticelli et al., 2008). In addition, Hp also can mediate the leukocyte activation, recruitment and migration, further involving in the modulation of cytokine patterns and tissue repair (Wang et al., 2001). Collectively, Hp plays a major role in re-establishment of homeostasis after a local or systemic infection.

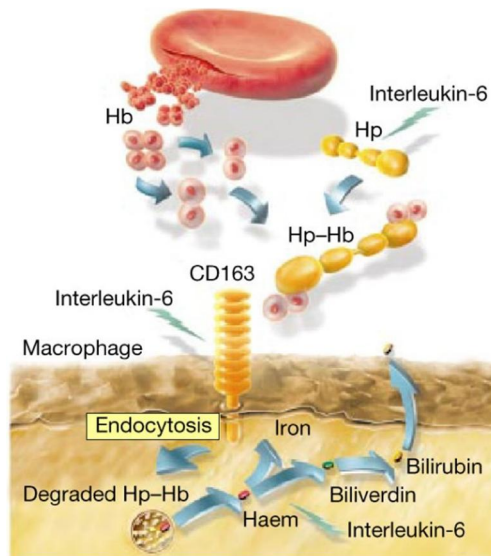


Fig. 4. Schematic illustration of the Hp-Hb complex formation and its fate in macrophages (from (Dennis, 2001)).

SAA

SAA is a major positive APP, concentration of which is elevated by several hundred folds during the acute phase of an infection under the regulation of TLR signaling cascade (Kushner, 1982). It is an apolipoprotein of high density lipoprotein (HDL), thus believed to modulate HDL-cholesterol transport in the APR (Earle et al., 1944; Nakayama et al., 1993). With respect to the immunity, two main functional roles of SAA have been identified; induction of extracellular matrix degrading enzymes such as, collagenase, stromelysin, matrix metalloproteinases which are indeed important for the tissue damage repair and chemo-attraction of the immune related cells such as monocytes, polymorphonuclear leukocytes and mast cells (Mitchell et al., 1991; Badolato et al., 1994; Strissel et al., 1997; Migita et al., 1998; Patel et al., 1998). Moreover, it was evidenced to bind LPS, compatible to LPS binding protein (LBP) (Schroedl et al., 2001).

In an APR, SAA are rapidly synthesized in liver and released. Immediately after the release, it binds with HDL and circulates in the body. Once it internalized into the phagocytes as

HDL-bound form, lysosomal proteases can degrade it leading to amyloidogenesis (Lavie et al., 1978; Bausserman et al., 1987; Yamada et al., 1995).

So far, several iso-types of SAA were identified from human, namely SAA1, SAA2 and SAA4, among them first two can act as positive APPs (Yamada, 1999). However, the gene coding SAA3 was found to be a pseudo gene. Apart from these, a negatively responding protein interacts with anti-SAA was also identified from a bovine origin (Yamamoto et al., 1998).

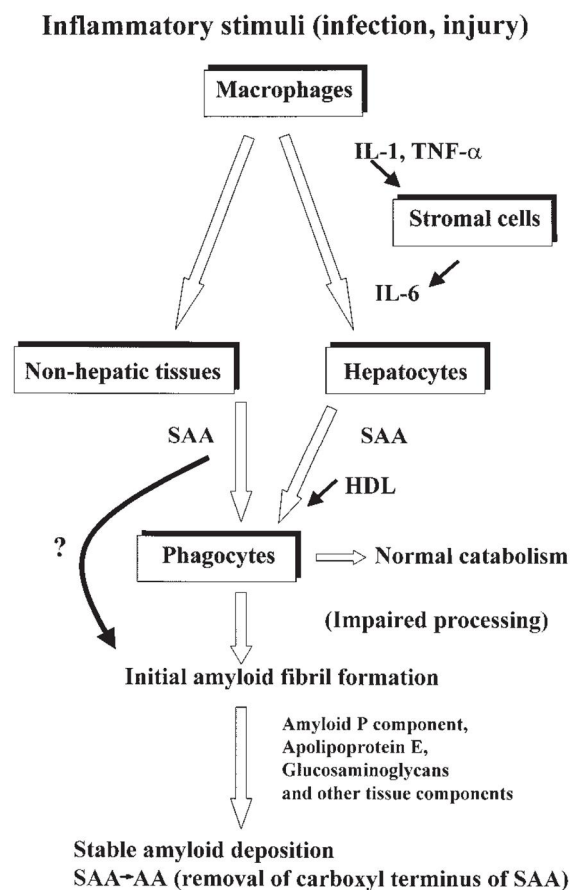


Fig. 5. Schematic presentation of synthesis and metabolism of SAA in the APR (Yamada, 1999).

APPs in fish

To date, substantial amount of studies on fish APPs have been carried out; mostly focusing on identification and evaluation of their expressional modulation in different tissues or dynamics of concentration in body fluids in response to different stimuli, mostly inflammatory stimuli (Bayne and Gerwick, 2001). Those studies evidence the existence of several APPs in both teleosts and elasmobranchs including pentraxins, especially CRPs and serum amyloid P (SAP), SAA, Transferins, complement component C3, and Lysozymes (Bayne and Gerwick, 2001).

CRP was the first APP identified from plaice in 1973 (Baldo and Fletcher, 1973) which could bind and form precipitates with extracts of various microbes, including fungi and nematodes, demonstrating broad specificity against pathogenic encounters. Thereafter, CRP like molecules were reported from different teleostan species, such as tilapia (Ramos and Smith, 1978), catfish (Szalai et al., 1992), Japanese eel (Nunomura, 1991), Atlantic salmon (Lund and Olafsen, 1999) and rainbow trout (Winkelhake and Chang, 1982; Kodama et al., 1989; Murata et al., 1995). Those studies evidence for the concentration dynamics or expressional inductions of CRPs against different stimuli including tissue injury, thermal stress, chemical stress and pathogenic stress along with for their functional properties like agglutination, opsonization and bacteriocidal activity. Intriguingly, CRP counterpart of trout was shown to enhance phagocytosis and chemokinetic activities of fish head kidney cells (Kodama et al., 1999). Moreover, another similitude of trout CRP was also found to serve as a surface receptor on cytotoxic cells (Edagawa et al., 1993).

SAA was also reported from several fish species, including Arctic char (Jensen et al., 1997), Common carp (Fujiki et al., 2000), Atlantic salmon (Jorgensen et al., 2000), and rock bream

(Saranya Revathy et al., 2012). According the studies, expression of SAA was found to be up-regulated by live pathogens such as bacteria and virus, chemical stress, cytokines and pathogen associated molecular patterns (PAMPs) like poly I:C and LPS.

Transferrin was found to behave as a positive APP in rainbow trout (Bayne et al., 2001) which likely bind free iron in plasma under septic conditions. Lysozyme are known to damage bacterial cell walls, rendering bactericidal effects, being a component of blood plasma and mucus secretions (Ellison and Giehl, 1991). Lysozyme homologs of Atlantic salmon (Engstad et al., 1992), rainbow trout (Jorgensen et al., 1993), yellow tail (Matsuyama et al., 1992) and turbot (Santarem et al., 1997) was found to elevate their concentration by the treatment of different glucans.

Reactive oxygen species (ROS), oxidative stress and antioxidant defense in animals

Aerobic respiration is a key metabolic mechanism to gain chemical energy in biological systems, which directly contributes to the cellular functions and survival of organisms. However, as a result of this biological process, toxic molecules, known as reactive oxygen species (ROS), are released as byproducts, which represent a risk to the cellular environments leading to grievous consequences. ROS is a collective term used to designate both oxygen radicals and certain oxidizing agents that are easily converted into radicals, including singlet oxygens ($^1\text{O}_2$), superoxide anions (O_2^-), hydrogen peroxides (H_2O_2), and hydroxyl radicals ($\cdot\text{OH}$) (Nordberg and Arner, 2001; Buonocore et al., 2010). ROS generation is known to be stimulated under pathogenic conditions upon microbial invasions, through identification of different molecular patterns of these invaders by pathogen recognition receptors such as NLRX1 (Moore et al., 2008; Arnoult et al., 2009; Groeger et al., 2009). Therefore, production

of ROS is considered as one of the early responses in host innate immunity that is highly toxic to the invaded pathogens. As a consequence of pathogenic infection, phagocytosis in the host organism is activated, consuming excessive amounts of oxygen to facilitate changes in cellular environments, leading to respiratory burst. The major result of this process is the generation of ROS under the catalysis of NADPH oxidase complexes (Groeger et al., 2009; Leto et al., 2009). In addition to the direct harm to the invading pathogens, it can act as a secondary signaling molecule to induce host inflammatory and immune responses. According to previous literature, ROS are able to induce a wide array of signaling networks, including innate immune pathways, enhancing the expression levels of nuclear factor kappa B and mitogen-activated protein kinase, further mediating cell growth and apoptosis (Morey et al., 2001; Nakano et al., 2006; Circu and Aw, 2010).

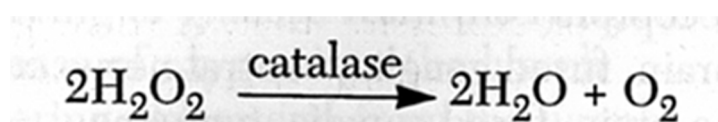
The extreme condition of ROS accumulation is known as 'oxidative stress'. This condition may potentiate cellular responses such as apoptosis, tumorigenesis, and immune responses (Kowaltowski et al., 2009; Circu and Aw, 2010; Forman et al., 2010). On one hand, exerting immune responses against invaders are considered as desirable features of ROS. On the other hand, damages to the cell membranes due to lipid peroxidation, oxidative damage to proteins, generation of mutations in the DNA, and activation of pro-cell death factors are considered as major deleterious effects of the generated ROS in cellular environments, rendering them as double-edged swords (Buonocore et al., 2010). Moreover, accumulation of ROS surpluses in cellular environment is also known to evoke immune dysfunction (Wang et al., 2013).

In general, potent players in counterbalancing the produced ROS, mostly through converting them to less toxic products or controlling the ROS formation in cellular environments are termed as antioxidants, which in turn protect the cells from the grievous effects of oxidative stress. These molecules bear either exogenous or endogenous origin and synergistically

function to build up the antioxidant system of an organism (Jacob, 1995). This system harbors nutrient-derived antioxidants such as some vitamins like vitamin C and E and carotenoids etc., antioxidant enzymes including superoxide dismutase, glutathione reductase, thioredoxin, catalase and peroxiredoxins etc. and metal binding proteins which can sequester free iron ions or copper ions involving in catalysis of oxidative reactions, such as ferritins, albumin and ceruloplasmin etc.

Catalase as a peroxidase in host antioxidant system

Among enzymatic components in antioxidant system, catalase plays an indispensable role in detoxifying hydrogen peroxide to form the nontoxic end-products; water and oxygen (Nordberg and Arner, 2001). Generally two types of catalases could be identified in organisms, namely classical Fe heme enzymes and catalase-peroxidases. The former belongs to the small group of manganese enzymes whereas latter contain a covalent triplet of distal side chains, which catalyze peroxidatic and catalytic reactions following a different mechanism compared to the classical heme enzymes. In addition to hydrogen peroxide, catalase can also breakdown several other substrates including phenol, methanol, ethanol and nitrites (Oshino et al., 1973). Interestingly, catalase is one of the efficient enzymes in cells with eminent turn-over rate; each second, one catalase molecule can dismutate millions of peroxide molecules into water and oxygen (Nicholls et al., 2000).



Catalase is ubiquitously distributed enzyme in prokaryotes as well as in eukaryotes consisting four identical subunits of 50 – 60 kD (9467862 (Kashiwagi et al., 1997; Klotz et

al., 1997). Each of this monomeric subunit comprises a single heme group and NADPH molecule on its surface (Putnam et al., 2000; Yamamoto et al., 2005). This NADPH prevents the enzyme from oxidation by its own substrate. Much of the information on catalase, especially regarding its structure and expressional regulation has been reported in mammals (Mackay and Bewley, 1989; Bryant and Wilson, 1995), plants (McClung, 1997) and bacteria (Storz and Tartaglia, 1992). Human catalase is known to be a member of peroxisomal glycoprotein family (Ken et al., 2000; Tavares-Sanchez et al., 2004) with four subunits, each harboring four conceptual domains, namely β -barrel, N-terminal threading arm, wrapping loop and C-terminal helices (Goyal and Basak, 2010).

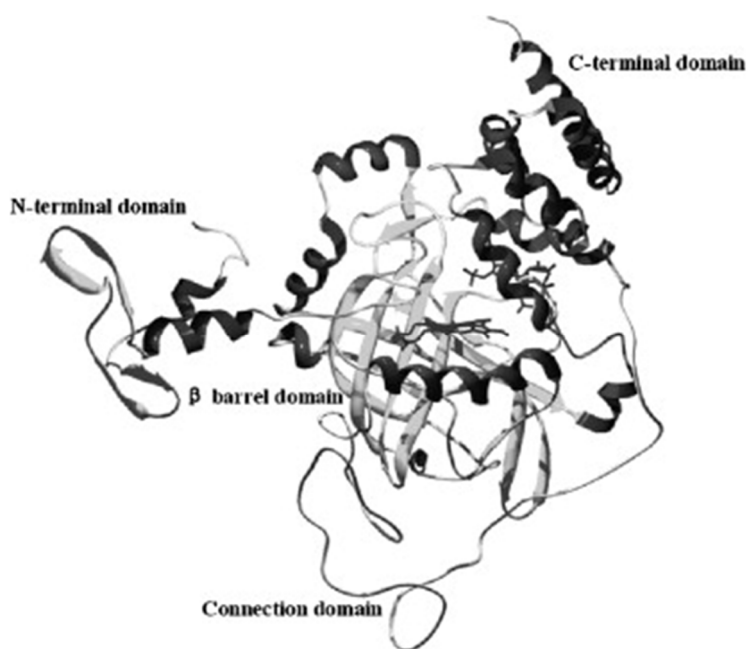


Fig. 6. Four conceptual domain arrangement of a catalase molecule depicted by a 3D model.

There are some credible evidences which hint that catalase can mediate the host immune responses besides its main ROS scavenging role in cells. For instance, *Caenorhabditis elegans* catalase was found to act as a cell stimulus for the induction of innate immune gene response (Vigneshkumar et al., 2013) and catalase was shown to mediate a main host defense

system required in host-microbe interactions in the gastrointestinal tract of fruit fly (Ha et al., 2005)). Moreover, catalase activity or expression was shown to be altered by virus infections in crustaceans (Mohankumar and Ramasamy, 2006; Mathew et al., 2007; Zhang et al., 2008; Arockiaraj et al., 2012), and positive transcriptional response of *catalase* was detected in mollusks upon bacterial infection (Li et al., 2008; Guo et al., 2011). Hence, gaining insights into different counterparts of catalase in different taxons is essentially important to complete our knowledge on its potential but unrevealed roles in organisms.

Catalases from teleostan origin

Information on lower vertebrate catalase homologues, especially on teleost origin is relatively scarce. Characterization studies on fish catalases reported exclusively from rock bream (*Oplegnathus fasciatus*) (Elvitigala et al., 2013) Black rockfish (Elvitigala et al., 2015) and zebrafish (*Danio rerio*) (Gerhard et al., 2000; Ken et al., 2000) to date clearly affirm this fact. According to these reports, teleostan catalases can demonstrate a strong peroxidase activity at broad spectrum of temperatures and pH conditions along with oxidative DNA or cellular damage protection activity and its expression can be modulated by pathogen invasions. In addition, another study showed that catalase gene expression can be temporary induced by food starvation in rock breams (Nam et al., 2005).

Thioredoxin system and its components

In general animal thioredoxin system is consisted of three main molecular components, namely, nicotinamide adenine dinucleotide phosphate (NADP), thioredoxin reductase (TrxR), and thioredoxin (Trx) and has an indispensable role in controlling oxidative stress and regulating apoptosis (Lu and Holmgren, 2012). Trxs are known to involve in wide range of functions in its reduced form, providing reducing equivalents to enzymes such as ribonucleotide reductase (Laurent et al., 1964) and thioredoxin peroxidase (Chae et al., 1994), to facilitate the DNA synthesis via reducing ribonucleotides to deoxy ribonucleotides and antioxidant defense through breaking down of hydrogen peroxide, respectively. Moreover, extracellular Trx and its truncated form, Trx80 was also found to take part in inflammatory responses by acting as cytokines and co-cytokines (Nordberg and Arner, 2001). In addition, mediation of cell growth (Gasdaska et al., 1995) and inhibition of apoptosis (Baker et al., 1997) are two subsidiary functions which were encountered to be exerted by reduced Trxs. However, in order to play most of these vital functions, oxidized form of Trx should undergo reduction under the catalysis of TrxR in the presence of NADH or NADPH as the donor of reducing power. Moreover, TrxR is the only known enzyme involve in reduction of Trxs to date, furnishing its essential role in thioredoxin system.

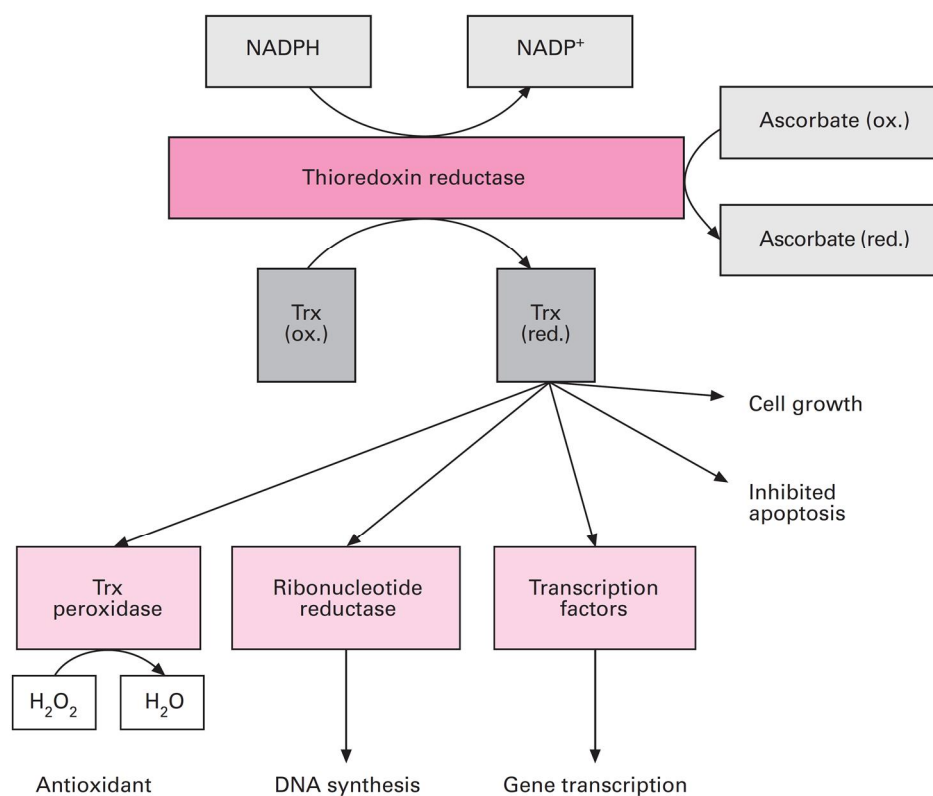


Fig 7. Functional role of Trx system as depicted in (Mustacich and Powis, 2000)

TrxR in Trx system

TrxRs belong to the flavoprotein family of pyridine nucleotide-disulfide oxidoreductases, which also includes several enzymes involved in cellular oxidation and reduction, such as lipoamide dehydrogenase, glutathione reductase, and mercuric ion reductase (Mustacich and Powis, 2000). Members of this family are homodimeric proteins formed from monomers, that contain a flavin adenine dinucleotide (FAD) prosthetic group, an NADPH-binding site, and a redox-active disulfide located in the active site. Besides Trx, TrxR can also act upon some other substrates, including lipoic acid (Arner et al., 1996), lipid hydroperoxides (Bjornstedt et al., 1995), NK-lysin (Andersson et al., 1996), vitamin K3 (Holmgren, 1979), dehydroascorbic acid (May et al., 1997), ascorbyl free radical (May et al., 1998) and tumor

suppressor protein p53 (Casso and Beach, 1996). In the case of NK lysine, which is a prominent antibacterial cytotoxic compound of T lymphocytes, TrxR is important for its inactivation after completing its defense role, which in turn convinces the importance of TrxR for the post immune functions.

Three isoforms of TrxR were identified from mammals, designated as TrxR1, TrxR2 and TrxR3, from which first two are located in cytosol and mitochondria, respectively, whereas the last was found to be exclusively expressed in testis as thiol regulator (Urig and Becker, 2006). Furthermore, mammalian TrxR sequence exhibits higher sequence homology with glutathione reductase, especially containing conserved -Cys-Val-Asn-Val-Gly-Cys- redox catalytic site. Almost all of the functions of TrxR are gathered around its basic role of reduction of Trx using NADH or NADPH, which is indirectly important in recycling of thioredoxin (Mustacich and Powis, 2000). Hence, TrxR is apparently important in cell growth and regulation of apoptosis as well as antioxidative defense in organisms. In addition, its role in cellular environment is also important in recycling ascorbate through ascorbyl free radical, which is used as a potent marker of oxidative stress (Buettner and Jurkiewicz, 1993), in turn trimming down the risk of triggering oxidative stress in cells.

TrxRs are widely distributed among eukaryotic and prokaryotic taxa; however, those found in prokaryotes and in some eukaryotes are rather different from mammalian TrxRs with respect to their molecular structure and substrate specificity. Low molecular weight TrxR variants (~35–37 kD per monomer) are found commonly in Archaea, Bacteria, Fungi, and in some eukaryotes including plants and intracellular parasites (Ellis et al., 1994; Bruchhaus and Tannich, 1995; Brown et al., 1996; Dai et al., 1996), whereas high molecular weight variants (~55–56 kD per monomer), which are analogous to glutathione reductases, are found prominently in mammals. However, to our knowledge, fish TrxR was exclusively reported

from rainbow trout (*Oncorhynchus mykiss*) (Pacitti et al., 2014) representing a teleost origin, in which two isoforms were identified and characterized.

Iron, oxidative stress and ferritin

Iron, a vital element found abundantly in living organisms has indispensable roles in an array of biological events including metabolic redox processes. However, excessive levels of reduced or free iron in cells can lead to detrimental toxic effects. Fenton-type reactions involving the catalysis of free Fe(II) ions in cellular environments induces reactive oxygen species (ROS)-mediated oxidative stress. Therefore, proper *in vivo* regulation of free iron availability is required for the survival of living cells. This is facilitated by balancing the uptake of iron through increasing the efficacy of iron transport and storage. Ferritins play a major role in iron storage by binding excessive free Fe(II) ions in cellular environments, releasing them only in times of iron shortage (Watt, 2011). Thus, ferritin is involved in iron detoxification through its iron binding property, maintaining iron homeostasis and limiting iron bioavailability to nontoxic levels.

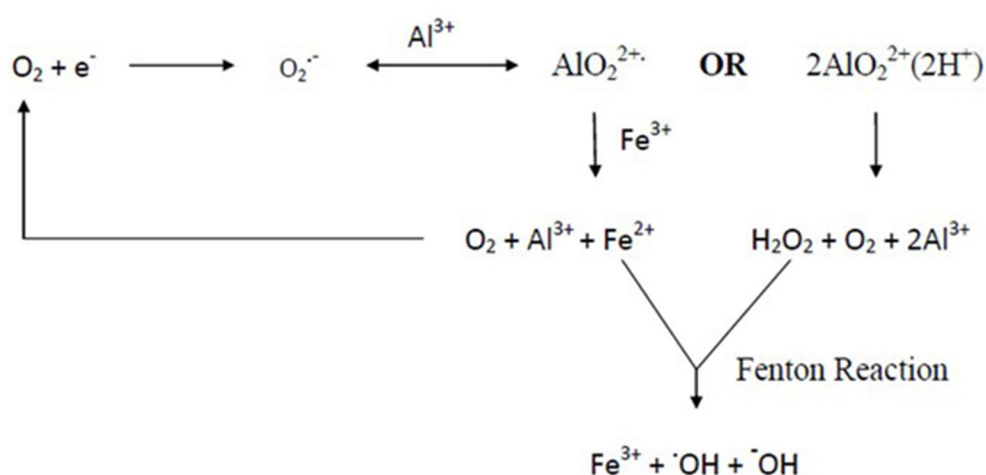


Fig. 8. Generalized Fenton type reactions which generates ROS

Ferritin at a glance

Ferritins are ubiquitously distributed proteins, both in prokaryotes and eukaryotes. According to the molecular distribution in three dimensional space, eukaryotic ferritin is known to be a hollow spherical protein complex consisted of 24 subunits, which can mineralize around 4,500 iron atoms inside its thick protein shell (Crichton and Declercq, 2010). In vertebrate linages, basically two types of ferritin chain subunits could be identified as heavy (H) subunits and light (L) subunits (Arosio et al., 2009), from which H subunits were characterized by their unique ferroxidase center involve in Fe (II) ion binding (Lawson et al., 1991) whereas L subunits were signified by their iron nucleation sites which provide ligands to bind Fe (III) ions, with different molecular masses ranging between 18 to 28 kD. Moreover, these two subunits were found to be encoded by two distinct genes (Caskey et al., 1983; Worwood et al., 1985).

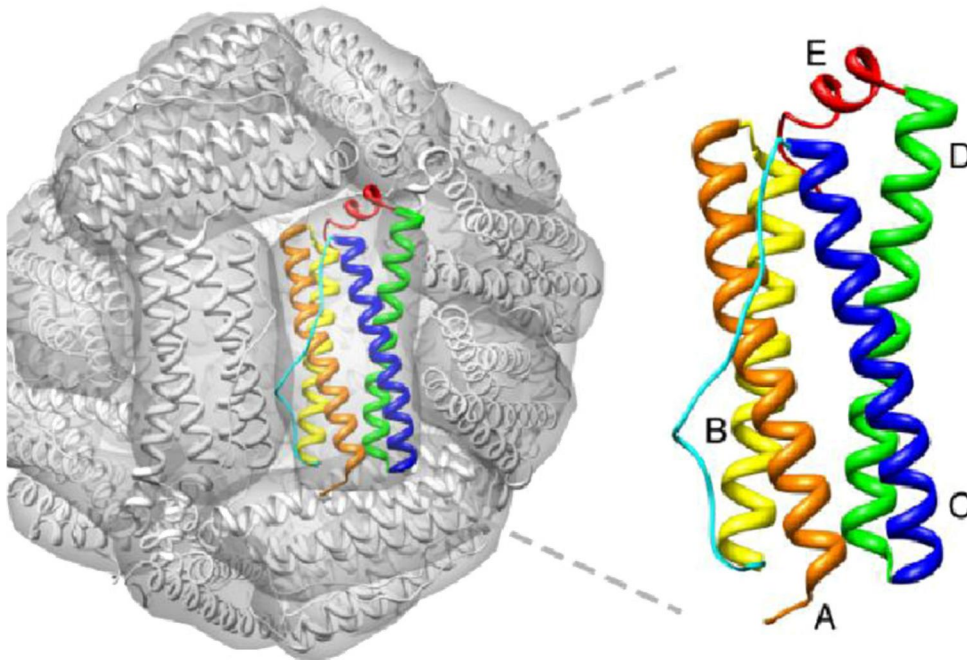


Fig.9. Hollow spherical structure of ferritin made out of 24 ferritin subunits

Ferritins can recognize and bind Fe (II) ions in the ferroxidase, center, in which those get oxidized by di-oxygen to Fe (III) ions (Lawson et al., 1989) and then which are bound to the nucleation sites for mineralization process (Santambrogio et al., 1996). The composition ratio of H and L subunits in ferritin can be widely varied depending on the tissue type and physiological status of different cells. For instance, H rich ferritins can be prominently identified in heart and kidney tissues whereas L rich ferritins are more abundant in liver or spleen tissues (Arosio et al., 1976). Apart from the two main subunit chains of ferritin, another variant, known as middle (M) subunit was also identified especially from lower vertebrate counterparts of ferritins which shows characteristic features and functions of both H and L subunits (Dickey et al., 1987; Andersen et al., 1995; Arosio et al., 2009; Zheng et al., 2010a).

Ferritins have been identified in a diverse group of living organisms including microorganisms, plants, and most vertebrate and invertebrate species examined (Theil, 1987). The ferritins from different species share common features. Ferritins are predominantly cytosolic proteins; however, they are also present in the mitochondria in some insects (Missirlis et al., 2006) and both mitochondria and nuclei of several mammalian cell types, protecting these organelles from iron toxicity and oxidative damage. Ferritins are also found in the plastids of plant cells and secreted forms have been identified in insects (Andrews et al., 1992; Arosio et al., 2009). Further, regarding their function in iron metabolism, ferritins reportedly play a significant role in other biological processes including cell activation, development, immune defense, and angiogenesis (Coffman et al., 2008; Alkhateeb and Connor, 2010; Wang et al., 2010)(Alkhateeb et al., 2010; Coffman et al., 2008; Parthasarathy et al., 2002; Wang et al., 2010). Expression of the ferritin subunits is tightly regulated at the transcriptional and post-transcriptional levels. Iron responsive element binding proteins have

a major role in their transcriptional regulation (Outten and Theil, 2009; Theil, 2007; Torti and Torti, 2002). These regulatory mechanisms cooperatively control the pathogen infection (Zheng et al., 2010a), xenobiotic stress (Torti and Torti, 2002), iron load (Wu et al., 2010), temperature stress (Salinas-Clarot et al., 2011), pH stress (Zhou et al., 2008), and endogenous factors like oxidative stress (Zheng et al., 2010a), and inflammatory cytokines (Torti and Torti, 2002) also regulate the expression of ferritin subunit genes at the transcriptional level.

Marine aquaculture industry and its challenges

Aquaculture is a worldwide rapidly developing industry, which is an optimal alternative for the ‘capture fishery’, especially regarding edible aquatic species categorized as endangered or about to be extinct. Moreover, it in turn helps to save the natural population of fish or shellfish species, without been significantly decimated by human activities. As an extension of inland aquaculture or brine water farming, marine aquaculture, also known as ‘Mariculture’ was begun few decades ago in several countries in the world, but now highly expanded almost all over the world, prominently in Asia-Pacific region. In mariculture, marine organisms including marine finfish, shellfish such as prawns and oysters along with plant species such as algae are cultured in open ocean or an enclosed section of the ocean or sea water filled tanks, ponds and raceways under controlled environmental conditions. Mainly these aqua-crops are consumed for food and subsidiarily for other products. Thus, mariculture has become one of the economically profitable industries in most of areas in the world through international trade. In addition, domestically it could ensure the food security and provide better solution for unemployment in most of the countries in the world. Nevertheless, due to the intensive culture conditions with high density of aquacrops, farming of marine organisms is plagued with stress related detrimental conditions, including

pathogenic infections. In addition, oxidative stress conditions in the aquacrops can suppress their immunity, in turn making them more vulnerable to infections (Tort, 2011). Particularly, fish mariculture is threatened by infections caused by different viruses, bacteria and parasites (Stewart et al., 2004; Toranzo et al., 2005; Rismstad, 2011). The total annual fish production in South Korea is around 91,123 tons, accounting for 15.2 % of its total marine production. However, red sea bream iridovirus (Rockbream iridovirus), bacterial species including *Edwardsiella tarda* along with some *Vibrio* and *Streptococcus* species and parasitic species like scuticociliatida play an important role as causative agents for lethal fish diseases in Korean aqua farms, resulting in mass mortalities and low quality mariculture production (Park, 2009).

Antibiotic usage is wildly applied method of disease management in mariculture industry, especially in Asian countries. However, it becomes hazardous to the environment, consumers and in turn to the aqua-crops them self in several aspects. Treating the fish or water bodies with different antibiotics frequently, with high doses was found to raise antibiotic resistance in bacteria which in turn can increase the long term pathogenic threat on aquacrops (Alderman and Hastings, 1998). On the other hand, consumption of antibiotic treated farmed fish or shellfish lead to the non-intentional up-take of antibiotics by consumers, ultimately accumulating them in humans in high concentrations. Consequently, due to the serious damages to the beneficial microbiome in the body and development of antibiotic resistance in bacteria, susceptibility for the infections can be increased, challenging the human health (Anderson et al., 2003).

The aforementioned background prompts the necessity of unraveling the fish host pathogen interactions, potential immune responses urging against invaders and stress defense mechanisms functioning under septic conditions. This knowledge can essentially be used to develop successful fish disease management schemes using modern molecular techniques,

especially increasing the disease resistance in aquacrops, further identifying suitable molecular targets for potential therapeutics.

Table 3. Major diseases caused by pathogenic agents in Korean mariculture industry (Park, 2009).

Group	Disease	Causative agent	Affected species*
Viral disease	Lymphocystis disease	Lymphocystis disease virus (LDV)	Many fishes
	Red seabream iridoviral disease (RSIVD)	Red sea bream iridovirus (RSIV)	Red sea bream, Rock bream
	Rhabdoviral infection	Hirame rhabdovirus (HIRRV)	Olive flounder
	Birnavirus infection	Yellowtail ascites virus (YTAV)	Olive flounder
	Viral nervous necrosis (VNN)	Piscine nodavirus	Several fishes
	Viral ascites	Yellowtail ascites virus (YTAV)	Yellowtail
	Viral hemorrhagic septicemia (VHS)	Viral hemorrhagic septicemia virus (VHSV)	Olive flounder
	Viral epidermal hyperplasia	Flounder herpesvirus (FHV)	Olive flounder
Bacterial disease	Vibriosis	<i>Vibrio anguillarum</i> (<i>Listonella anguillara</i>), <i>Vibrio harveyi</i>	Several fishes
	Bacterial enteritis	<i>Vibrio ichthyoenteri</i>	Larvae of olive flounder
	Photobacterium infection	<i>Photobacterium damsela</i> subsp. <i>damseke</i>	Several fishes
	Pseudomonas infection	<i>Pseudomonas</i> sp.	Several fishes
	Edwardsiellosis	<i>Edwardsiella tarda</i>	Several fishes
	Gliding bacterial disease	<i>Tenacibaculum maritimum</i>	Several fishes
	Streptococciosis	<i>Streptococcus iniae</i> , <i>S. parauberis</i> , <i>Lactococcus garvieae</i> , etc.	Several fishes
Parasitic disease	Scuticociliatidosis	Scuticociliatida	Several fishes
	Trichodinosis	<i>Trichodina</i> spp.	Several fishes
	Monogenean infestation	<i>Microcotyle sebastis</i> , <i>Bivagina tai</i>	Black rockfish
	Crustacean infestation	<i>Dactylogyrus</i> spp., <i>Gyrodactylus</i> spp., <i>Allela macrotrachelus</i>	Other fishes

* Red sea bream, *Pagrus major*; Rock bream, *Oplegnathus fasciatus*; Olive flounder, *Paralichthys olivaceus*; Yellowtail, *Seriola quinqueradiata*; Black rockfish, *Sebastes schlegelii*.

Black rockfish and rock bream as aqua crops.

Black rockfish (*Sebastes schlegelii*) and rock bream (*Oplegnathus fasciatus*) are economically important fish delicacies in Asia pacific region of the world and cultured in large quantity in mariculture farms. Seeds of black rock fish are produced in open field in ocean and subsequently raise them to 500 g to 1 Kg of weight in embankments and cages. Initial culture density is around 700-1000 fish at the size of 4 cm to 5 cm, but the density is

reduced with the time due to the increasing size. Rock breams are basically cultured in tanks or cages with seed density in a cage of $\sim 5 - 10 \text{ Kg/m}^3$.

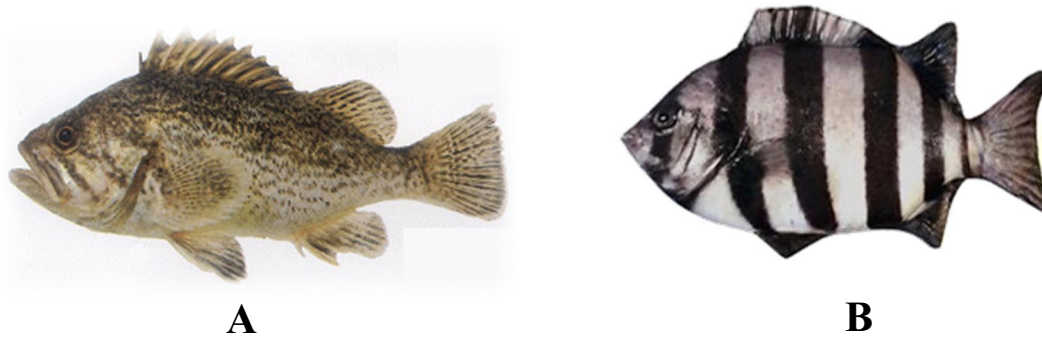


Fig. 10. Appearance of matured (A). Black rock fish and (B) Rock bream fish.

As other maricultured fish, rock bream and black rockfish are challenged by the pathogenic threat. As reported Rock breams are mainly infected by bacterial such as *Edwardsiella tarda*, *Sterptococcus iniae* and virus like red sea bream iridovirus (Rock bream iridovirus) (Park, 2009). Black rock fish are highly susceptible for the infections caused by bacteria such as *Sterptococcus* species and *Aeromonas salmonocida* (Han et al., 2011), virus such as hiram rhabdovirus (Kimura et al., 1989) and parasitic species like *Microcotyle sebastis* and *Bivagina tai* (Park, 2009).

Aims and objectives of the studies

The overall goal of these studies was to gain substantial insights into selected players in rock bream antioxidant defense at molecular level, deciphering their relevance in host immune responses and to molecularly evidence the existence of selected and conserved acute phase proteins in black rockfish, investigating their putative significance in host immune defense mechanisms. This thesis will concern on following undertakings.

- Molecular characterization of selected molecular antioxidants (ferritin H, ferritin M, catalase, thioredoxin reductase 3 like homologues) from rock bream and putative acute phase proteins (haptoglobin, serum amyloid A and C-reactive protein like counterparts) from black rockfish.
- Analysis of expressional modulation of above molecules upon experimental pathogen infections or the treatment with PAMPs.
- Demonstration of the biological activities of aforementioned molecules, deciphering their *in-vivo* functionality.

CHAPTER 1

Identification and molecular characterization of three putative acute phase proteins from Black rock fish (*Sebastes schlegelii*) deciphering their roles in host acute phase response.

This chapter presents the three separate studies of identification and molecular characterization of C-reactive protein (CRP), serum amyloid A (SAA) and haptoglobin (Hp) homologues from black rockfish respectively, demonstrating basal expression along with its transient modulation, in response to pathogen stress in selected tissues. Additionally, CRP counterpart was further characterized at functional level using its recombinant protein to decipher its significance in host immune defense.

PART A

Characterization of a C-reactive protein (CRP) homologue from Black rockfish

1. ABSTRACT

Pentraxins are a family of evolutionary conserved proteins that contains two main members, namely c-reactive proteins (CRPs) and serum amyloid P (SAP), which are involved in acute phase responses in animals. In this study, a cDNA sequence of a CRP-like molecule was identified from a previously constructed black rockfish cDNA database (RfCRP) and subsequently characterized at its molecular level. The complete coding region of RfCRP is 672 bp in length, and encodes a protein containing 224 amino acids with a predicted molecular mass of 25.19 kD. Analysis of its derived amino acid sequence enabled typical features of pentraxin family members to be identified, including the pentraxin family signature in RfCRP. Results from multiple sequence alignment suggest the conservation of

functionally important residues in RfCRP. According to the phylogenetic reconstruction that was generated using different pentraxin counterparts from different taxa, RfCRP shares a common vertebrate ancestral origin and most closely clusters with marine teleostan CRP. Furthermore, recombinant RfCRP demonstrated Ca^{2+} -dependent agglutination activity against *Escherichia coli*, which could be completely inhibited in the presence of carbohydrate based ligands. Moreover, recombinant RfCRP also exhibited anti-bacterial activity against both *E. coli* and *Streptococcus iniae*. In addition, qPCR analysis indicated that RfCRP is ubiquitously expressed in physiologically important tissues, with pronounced expression in the spleen. After healthy fish were treated with polysaccharides or live *S. iniae*, basal expression of RfCRP was significantly upregulated in spleen and head kidney tissues. Collectively, our results suggest that RfCRP may be important in host anti-bacterial defense, and it might potentially participate in the acute phase of infection.

2. MATERIALS AND METHODS

2.1. cDNA database of black rockfish

A cDNA database of black rockfish was established using the GS-FLXTM sequencing platform (18616967 (Droege and Hill, 2008)). Briefly, total RNA was isolated from blood, liver, head kidney, gill, intestine, and spleen tissues of three fish (~100 g) challenged with immune stimulants, including *Edwardsiella tarda* (10^7 CFU/fish), *Streptococcus iniae* (10^7 CFU/fish), lipopolysaccharide (1.5 mg/fish), polyinosinic:polycytidylic acid (poly I:C; 1.5 mg/fish) using TRIzol reagent (TaKaRa, Japan) according to the manufacturer's instructions. Next, extracted RNA was further purified using an RNeasy Mini kit (Qiagen, USA), according to the manufacturer's instructions. Thereafter, the quality and quantity of purified RNA were assessed using an Agilent 2100 Bio-analyzer (Agilent Technologies, Canada), resulting in an RNA integration score (RIN) of 7.1. Then, the GS-FLXTM 454 shotgun library

was constructed, and a cDNA database was established using fragmented RNA (average size of 1147 bp) from the aforementioned samples (Macrogen, Korea).

2.2 *RfCRP* sequence identification and profiling

Analysis of contig sequences in our black rockfish sequence database using Basic Local Alignment Search Tool (BLAST) algorithm (<http://blast.ncbi.nlm.nih.gov/Blast.cgi>) led us to identify a homologous sequence to known CRPs, which was designated *RfCRP*. Thereafter, the cDNA sequence was characterized using different bioinformatic tools. The putative complete coding sequence of *RfCRP* was identified using DNAsist 2.2 software from which its amino acid sequence was derived. The amino acid sequence was then used to predict the typical domain structure and functionally important residues of RfCRP using the SMART online server (<http://smart.embl-heidelberg.de/>) and NCBI-CDD tool (<http://www.ncbi.nlm.nih.gov/Structure/cdd/wrpsb.cgi>). Some of the physicochemical properties of RfCRP were predicted by ExPASy ProtParam tool (<http://web.expasy.org/protparam>). Comparative protein sequence analysis of RfCRP was carried out through pairwise and multiple sequence alignment approaches, using Matgat software (Campanella et al., 2003) and ClustalW2 (<http://www.Ebi.ac.uk/Tools/clustalw2>) servers, respectively. The phylogeny of RfCRP was investigated through the construction of a phylogenetic tree diagram under the neighbor-joining strategy using Molecular Evolutionary Genetics Analysis (version 4.0) software (MEGA 4.0) (Tamura et al., 2007) with the support of 5000 bootstrap replications.

2.3. Preparation of the RfCRP recombinant plasmid construct

The coding sequence of RfCRP, excluding the coding segment for the putative signal peptide, was PCR-amplified and cloned into the pMAL-c5X vector, as instructed in the

pMALTM Protein Fusion and Purification protocol (New England Biolabs, Ipswich, MA, USA). Briefly, the corresponding coding region of RfCRP was amplified using the sequence specific primer pair, RfCRP-F and RfCRP-R, which harbored restriction enzyme sites for *EcoRI* and *HindIII*, respectively (Table 4). PCR was employed in a TaKaRa thermal cycler in a total volume of 50 μ L with 5 U of Ex TaqTM Polymerase (TaKaRa, Japan), 5 μ L of Ex TaqTM Buffer, 4 μ L of 2.5 mM dNTPs, 100 ng of template DNA, and 40 pmol of each primer. The reaction was completed in 35 cycles under the following conditions: 94°C for 30 s, 57°C for 30 s, and 72°C for 1 min, along with a final extension at 72°C for 5 min. The resultant amplicon (630 bp) and pMAL-c5X plasmid were then double digested with *EcoRI* and *HindIII* enzymes, resolved on a 1% agarose gel, excised, and purified using an AccuprepTM gel purification kit (Bioneer Co. Korea), according to the manufacturer's instructions. Thereafter, the purified pMAL-c5X vector (100 ng) and PCR product (33 ng) were ligated using Mighty mix (5 μ L, TaKaRa, Japan) at 4°C overnight. Subsequently, the ligation mixture was transformed into *E. coli* DH5 α competent cells and the construct was sequenced. The sequence verified construct was then transformed into *E. coli* ER2523 cells for subsequent protein expression.

Table 4. Primers used in the study on RfCRP

Name	Purpose	Sequence (5' →3')
RfCRP-qF	qPCR of <i>RfCRP</i>	CACTCCATTTGTACCACATGGGACTCTAC
RfCRP-qR	qPCR of <i>RfCRP</i>	ATCCTGCTCCTGTCCCAAGACAAT
RfCRP-F	Amplification of coding region (<i>EcoRI</i>)	GAGAGAgaaattcACTCCTCAAGATCTGTCAGGTAAAATGTTTAC
RfCRP-R	Amplification of coding region (<i>HindIII</i>)	GAGAGAAagettTTAGACACAGGACTCGTGTATTATCTTCTATCAGC
RfEFA-F	qPCR for black rockfish EFA	AACCTGACCACTGAGGTGAAGTCTG
RfEFA-R	qPCR for black rockfish EFA	TCCTTGACGGACACGTTCTTGATGTT

2.4. Overexpression and purification of recombinant RfCRP (rRfCRP)

Recombinant RfCRP was expressed in *E. coli* ER2523, as a fusion protein of maltose binding protein (MBP), as described in the pMALTM Protein Fusion and Purification protocol (New England Biolabs, Ipswich, MA, USA) with some modifications. Briefly, *E. coli* ER2523 cells harboring a sequence confirmed RfCat/pMAL-c5X construct were grown in 500 mL Luria broth (LB) supplemented with ampicillin (100 µg/mL) and glucose (0.2%) at 20°C for 8 h under the induction of isopropyl-β-D-galactopyranoside (IPTG, 0.5 mM). Induced cells were then chilled on ice for 30 min and harvested by centrifugation at 2500 x g for 30 min at 4°C. Harvested cells were resuspended in 20 mL of column buffer (20 mM Tris-HCL pH 7.4 and 200 mM NaCl) and were stored at -20°C. The following day, *E. coli* cells were thawed and lysed in column buffer by cold sonication. Thereafter, the recombinant protein was purified using the pMALTM Protein Fusion and Purification System (New England BioLabs, Ipswich, MA, USA). The purified protein was eluted using an elution buffer (10 mM maltose in column buffer) and the concentration was determined by the Bradford method using bovine serum albumin as the standard (Bradford, 1976). The antimicrobial functions of the purified fusion protein (rRfCat) were then assayed. Samples collected at different steps of the rRfCat purification were analyzed by 12% sodium dodecyl sulfate polyacrylamide gel electrophoresis (SDS-PAGE) using standard protein size markers (Enzyomics, Korea) under reducing conditions. The gel was stained with 0.05% Coomassie blue R-250 and observed, followed by a standard destaining procedure.

2.5. Determination of bacterial agglutination activity and its inhibition

In order to evaluate the potential bacterial agglutination activity of rRfCRP, *E. coli* and *Streptococcus iniae* were used as Gram negative and Gram positive bacterial species,

respectively. *E. coli* and *S. iniae* were grown in LB and Brain Heart Infusion (BHI) media, respectively and harvested by centrifugation. Subsequently, bacteria were washed and resuspended in column buffer to obtain an optical density (OD) of 0.3 at 600 nm. Thereafter, 25 μ L of these bacterial mixtures was incubated with different concentrations of rRfCRP or MBP (control) in the presence or absence of 10 mM CaCl_2 at 25°C for 2 h. Bacterial suspensions similarly treated with column buffer, with or without 10mM CaCl_2 served as negative controls. Agglutination was observed using light microscopy.

To decipher the potential ligand binding property of RfCRP through the inhibition of bacterial agglutination, the above assay was repeated using lipopolysaccharide (LPS) and D-galactose as ligands in slightly acidic medium, and *E. coli* as the model bacterium. Briefly, 25 μ L of LPS or D-galactose was dissolved in acetate buffer (pH = 5) containing 10 mM CaCl_2 to obtain the relevant concentrations and was incubated with rRfCRP (0.15 μ g/mL) at 25°C for 40 min. Thereafter, the mixtures were treated with 25 μ L of *E. coli* suspension in column buffer (OD₆₀₀ = 0.3). Finally, the mixtures were incubated at 25°C for 2 h and agglutination was observed by microscopy. Each assay was carried out in triplicate to increase the credibility of the results.

2.6. Antibacterial activity analysis

2.6.1. Effect on growth of *E. coli* by overexpressing rRfCRP

The effect of recombinant rRfCRP on bacterial growth was determined by overexpressing rRfCRP in *E. coli* and evaluating the bacterial cell density. Briefly, the recombinant pMAL-c5x/RfCRP vector construct and the empty vector (control) were separately transformed into *E. coli* ER2523 cells and the transformed cells were subsequently induced with 0.5 mM IPTG to overexpress rRfCRP or MBP, respectively, in LB medium,

supplemented with ampicillin (100 µg/mL) and glucose (0.2%), for 12 h with shaking, as described in section 2.4. Subsequently, the bacterial cultures were serially diluted in sterilized column buffer, then spread onto LB-ampicillin agar plates and incubated overnight at 37°C. The following day, colonies on each corresponding plate were counted and the number of colony forming units (CFU) in 1 mL of induced *E. coli* culture was calculated (*E. coli* harbored pMAL-c5x and pMAL-c5x/RfCRP, respectively). The results are presented as the mean value of triplicated assays.

2.6.2. Bacterial growth inhibition by purified rRfCRP

In order to determine the effect of purified rRfCRP on bacterial growth, cell densities of *E. coli* (Gram negative) and *S. iniae* (Gram positive) in liquid culture medium treated with rRfCRP were monitored by determining the OD at 600 nm over time. *E. coli* (DH5α) and *S. iniae* were cultured in LB and BHI media at 37°C and 28°C, respectively until the exponential phase was reached. Cultures were then diluted to ~10⁴ CFU/mL using the relevant fresh liquid media and were then each aliquoted (150 µL) into three sets of vials. Each set of vials was treated with rRfCRP (300 µg/mL), MBP (300 µg/mL), or column buffer (control). Subsequently, 50 µL of each treated culture was seeded into two 96-well cell culture plates. Cultures containing *S. iniae* and *E. coli* were then incubated at 37°C and 28°C, respectively, in rocking incubators and the OD₆₀₀ was determined at different time points, post incubation. The assays were performed in triplicate and the mean OD₆₀₀ was reported corresponding to each time point.

2.7. Fish husbandry and tissue collection

Healthy rockfish that were acclimatized to laboratory conditions after being obtained from the aquariums at the Marine Science Institute of Jeju National University, Jeju Self

Governing Province, Republic of Korea, and were maintained in 400 L laboratory aquarium tanks filled with aerated seawater at $22 \pm 1^\circ\text{C}$. Five healthy fish, with an average body weight of 200 g, were sacrificed for tissue collection. Before the fish were sacrificed, approximately 1 mL blood was collected from each fish using sterile syringes coated with 0.2% heparin sodium salt (USB, USA), and the peripheral blood cells were separated by immediate centrifugation at $3,000 \times g$ for 10 min at 4°C . Other tissues, including head kidneys, spleen, liver, gills, intestines, kidney, brain, muscle, skin, heart, and stomach were excised, snap-frozen in liquid nitrogen, and stored at -80°C .

2.8. Immune stimulation

Healthy rockfish with an average body weight of 200 g were used in an immune challenge time course experiment to determine the transcriptional response of *RfCRP* under pathogenic stress. Viable Gram positive *S. iniae* (10^5 CFU/ L), Gram negative bacterial endotoxin, LPS (*E. coli* 055:B5, Sigma) and polyinosinic:polycytidylic acid (1.5 g/ L; Poly I:C; Sigma, St. Louis, MO, USA), which resembles the double stranded viral RNA, were used as immune stimulants after resuspending or dissolving in PBS. Fish were intraperitoneally injected with each stimulant in a total volume of 200 L. For the control group, fish were injected with 200 L PBS. Spleen and head kidney tissues were sampled from five individuals in each group at 3, 6, 12, 24, 48, and 72 h post-injection, as described in section 2.7.

2.9. Total RNA isolation and cDNA synthesis

Total RNA was extracted from a pool of tissue samples (~40 mg from each fish) from five individual fish (both un-injected and injected) using QIAzol[®] (Qiagen), according to the manufacturer's instructions. RNA samples from the liver of healthy fish were further purified

using an RNeasy Mini Kit (Qiagen). RNA quality was examined using 1.5% agarose gel electrophoresis, and the concentration was determined at 260 nm using a μ Drop Plate (Thermo Scientific). First strand cDNA was synthesized in a 20 μ L reaction mixture using 2.5 μ g of RNA from each sample as a template with the PrimeScriptTM II 1st strand cDNA Synthesis Kit (TaKaRa). The synthesized cDNA was diluted 40-fold in RNase free water and stored in a freezer at -80°C until use.

2. 10. Relative quantification of *RfCRP* mRNA expression

Basal expression levels of *RfCRP* in tissues (section 2.8) obtained from healthy fish, along with the modulated expression over time in the head kidney and spleen of immune challenged animals following immune stimulations were quantified by qPCR using diluted cDNA samples as the templates (section 2.9). qPCR was performed using the DiceTM Real time system thermal cycler (TP800; TaKaRa, Japan) in a 10 μ L reaction volume, containing 3 μ L of diluted cDNA from each tissue, 5 μ L of $2\times$ TaKaRa ExTaqTM SYBR premix, 0.4 μ L of each primer (*RfCRP*-qF and *RfCRP*-qR; Table 4), and 1.2 μ L of ddH₂O, as per the essential MIQE guidelines (Bustin et al., 2009). PCR conditions were as follows: 95°C for 10 s; 35 cycles of 95°C for 5 s, 58°C for 10 s, and 72°C for 20 s; and a final cycle of 95°C for 15 s, 60°C for 30 s, and 95°C for 15 s. Each assay was conducted in triplicates. The baseline was set automatically by the DiceTM Real Time System software (version 2.00). The relative *RfCRP* expression was determined using the Livak ($2^{-\Delta\Delta\text{CT}}$) method (Livak and Schmittgen, 2001). The black rockfish elongation factor 1 α (*RfEF1A*) gene was used as an internal reference (GenBank ID: KF430623), because it was previously validated as an appropriate internal control for qPCR in black rockfish gene expression studies (Liman et al., 2013). The primers used for the internal reference are listed in Table 4. Data are presented as the mean \pm standard deviation (SD) of the relative mRNA expression from three experiments. In the

immune challenge experiments, the level of *RfCRP* mRNA was calculated relative to that of *RfEF1A*. The expression values were further normalized to the corresponding PBS-injected controls at each time point. The relative expression level in the un-injected control at 0 h was used as the baseline reference. To determine the statistical significance ($p < 0.05$) between the experimental and un-injected control groups, a two-tailed un-paired Student's *t*-test was applied.

3. RESULTS AND DISCUSSION

3.1. Delineation of sequence features and homology

According to our *in-silico* study, the identified cDNA sequence (1020 bp) of RfCRP harbors a 672-bp coding region, which encodes a protein consisting of 224 amino acids with a predicted molecular mass of 25.19 kD and a theoretical isoelectric point of 6.29. These sequence data were deposited in NCBI-GenBank database (Accession number–KP728999). This protein sequence was further analyzed using bioinformatic tools to determine the characteristic features that are commonly shared with known pentraxin family proteins, including an N-terminal signal peptide sequence (residues 1-15) and a pentraxin family signature (residues 17-222) (Fig.11). The presence of a signal peptide infers the secretory properties of RfCRP. Furthermore, data derived from multiple sequence alignment showed that Ca²⁺-mediated ligand binding sites, residues involved in the formation of intra-molecular salt bridges, and cysteine residues that are potentially important in di-sulfide bond formation are well conserved in RfCRP (Fig.11).

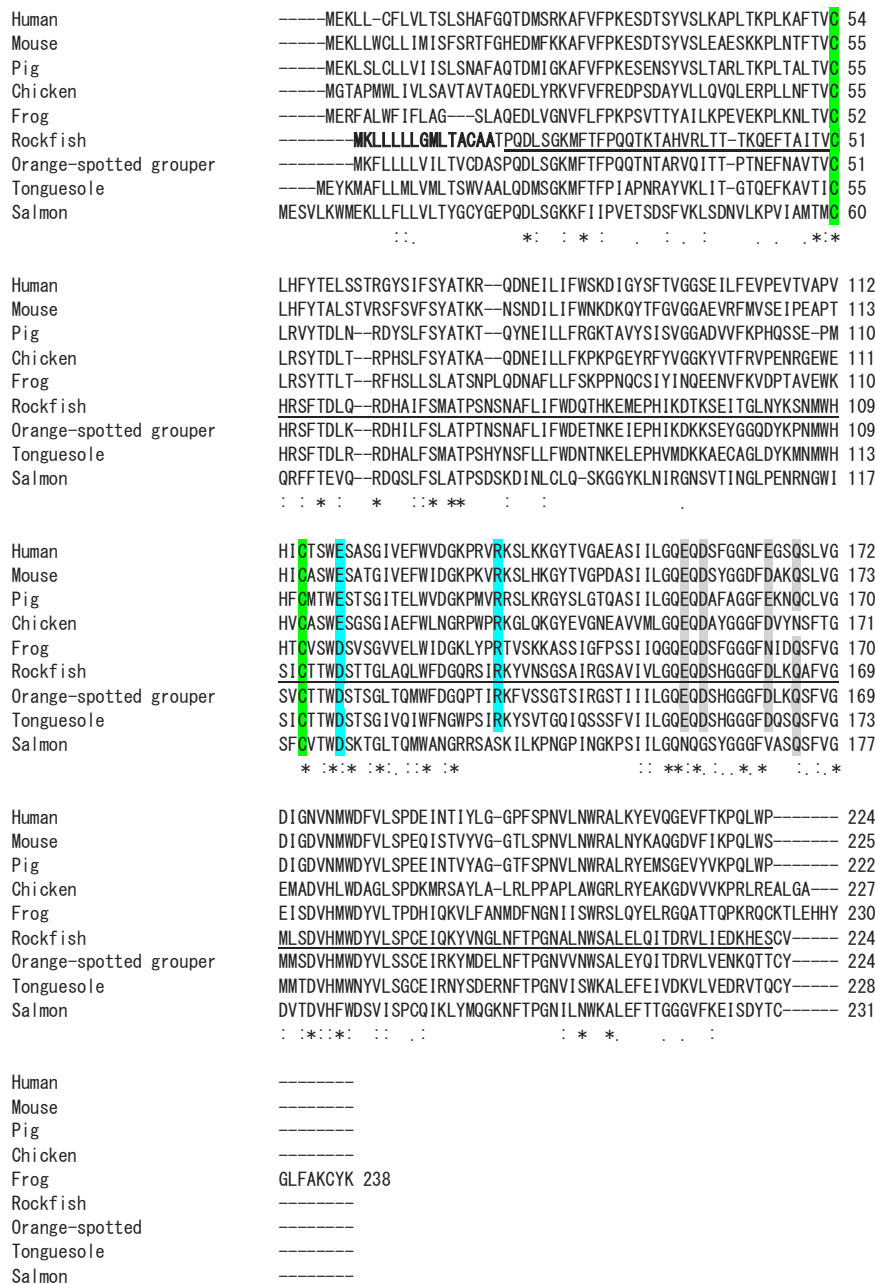


Fig. 11. Multiple protein sequence alignment of vertebrate CRPs including black rockfish CRP (RfCRP). Completely or partially conserved residues, putatively involved in intermolecular salt bridge formation and Ca^{2+} mediated ligand binding are shaded in a pale blue or gray color and conserved cysteine residues are denoted by green color shading. The predicted signal peptide

sequence and putative pentraxin family signature of RfCRP are indicated by bold phase letters and are underlined, respectively on the corresponding sequence.

As revealed by pairwise sequence alignment with different CRP homologues, RfCRP shared significant sequence identity with its marine teleostan counterparts, with marked similarity (89.3%) and identity (74.1%) with CRP from *Epinephelus coioides* (Table 5). However, comparatively low sequence identity was shared with its freshwater teleostan, mammalian, and amphibian counterparts that were used in this comparison. Collectively, outcomes of bioinformatic analyses suggest that RfCRP is a member of the pentraxin superfamily.

Table 5. Percentage similarity and identity values of RfCRP with different CRP homologues

Species name	NCBI-GenBank accession number	Amino acids	Identity (%)	Similarity (%)
1. <i>Epinephelus coioides</i> (Orange-spotted grouper)	ADC92292	224	74.1	89.3
2. <i>Cynoglossus semilaevis</i> (Tongue sole)	NP001281151	228	61.4	78.1
3. <i>Salmo salar</i> (Atlantic salmon)	NP001134140	231	42.9	59.7
4. <i>Sus scrofa</i> (Pig)	ACF28537	222	37.7	60.3
5. <i>Homo sapiens</i> (Human)	NP000558	224	37	57.1
6. <i>Bos taurus</i> (Bovine)	NP001137569	224	36.5	57.8
7. <i>Mus musculus</i> (Mouse)	NP031794	225	36.5	57.8
8. <i>Cyprinus carpio carpio</i> (Common carp)	AEU04519	227	33.5	55.9
9. <i>Xenopus laevis</i> (Frog)	NP001165686	238	32.8	55.9
10. <i>Gallus gallus</i> (Chicken)	NP001034653	227	31.6	54.2
11. <i>Danio rerio</i> (Zebrafish)	AGB69036	223	31.3	53.6
12. <i>Lates calcarifer</i> (Barramundi perch)	ADX06859	223	28.3	51.3
13. <i>Limulus polyphemus</i> (Horseshoe crab)	AAA28270	242	25.2	46.3

3.2. Phylogenetic reconstruction

In order to decipher the evolutionary relationship between RfCRP and its homologues, a phylogenetic reconstruction was generated using different short pentraxin (Ptx) counterparts. As shown in the tree diagram, marine teleostan Ptx (represented by SAPs, CRPs, and Ptxs) and non-teleostan vertebrate Ptxs (SAPs and CRPs) clustered closely and independently while sharing common ancestors, respectively (Fig. 12). However, both of these ancestors possess a single common vertebrate ancestral origin. As expected, the single cluster formed by mammalian and avian pentraxin counterparts was split into two clades represented by their SAPs and CRPs. Interestingly; frog SAP exhibited an evolutionary distant relationship with mammalian SAP counterparts, which in turn showed a closer relationship with its own CRP counterpart. Moreover, chicken CRP shared a more recent common ancestor with mammalian SAP, showing that there was more evolutionary proximity with SAPs than with the CRP counterparts. Confirming the expected prominent phylogenetic relationship with teleostan counterparts, RfCRP was clustered with a sub-clade made by ‘grouper’ CRP and ‘sea bass’ Ptx with substantial bootstrap support (97) within the separate cluster consisting of marine teleostan Prxs. Intriguingly, CRP similitudes of fresh water teleosts (Perch, carp, and zebrafish) formed a separate cluster that deviated from the main cluster of vertebrate Ptxs, confirming their evolutionary distance from other vertebrate Ptxs, including marine teleostan CRPs. As expected, the invertebrate Ptx represented by crab CRP in the reconstruction served as the out-group. Taken together, our phylogenetic analyses provide evidence for a common vertebrate ancestral origin of RfCRP, further reinforcing its homology to the marine teleostan CRPs.

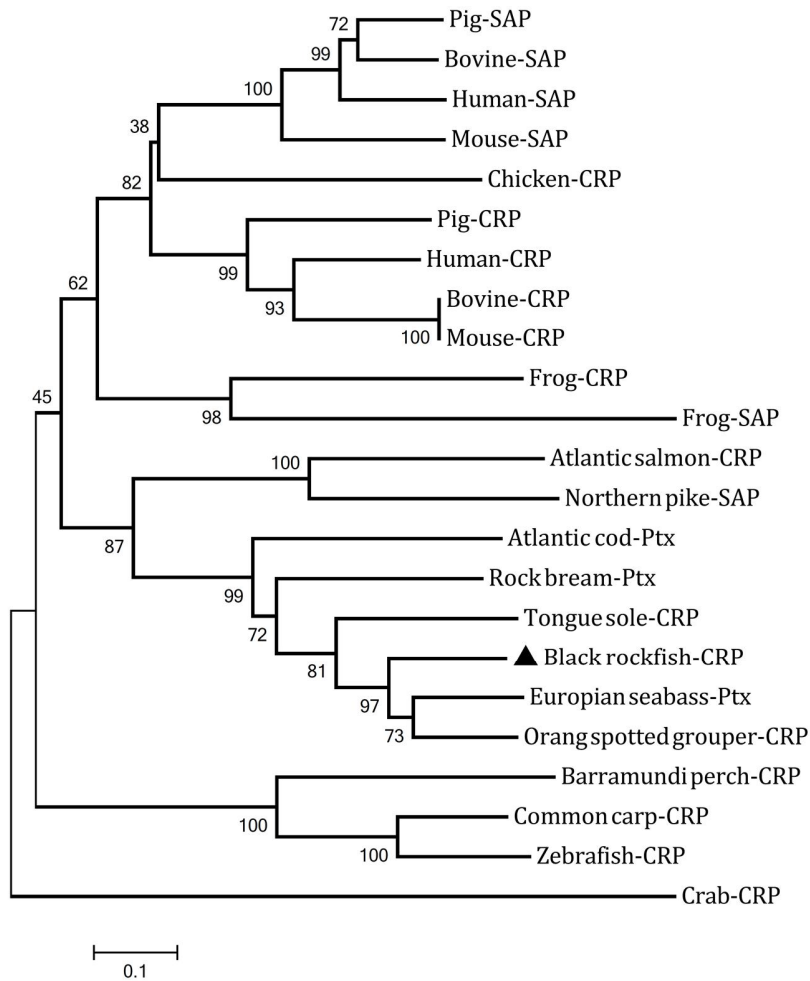


Fig. 12. Phylogenetic reconstruction of RfCRP based on ClustalW multiple sequence alignment of different vertebrates and invertebrates under the neighbor-joining platform using MEGA version 4.0. Bootstrap supporting values are denoted at the tree branches and NCBI-GenBank accession numbers of used pentraxin homologues are mentioned in Table 5, except, Pig-SAP: BAA21474, Bovine-SAP: AAI02624, Human-SAP: BAA00060, Mouse-SAP: NP035448, Frog-SAP: NP001092180, Northern pike-SAP: ACO14371, Atlantic cod-Ptx: ACZ06557, Rock bream-Ptx: BAM36372, and European seabass-Ptx: ACF77002.

3.3. Integrity of purified rRfCRP

Samples collected at different steps of the rRfCRP purification process were analyzed using SDS-PAGE. According to the bands on the gel that corresponded to the crude extract (Fig. 13, lane 3), there was clear overexpression of rRfCRP under IPTG induction, and an intense band was resolved that corresponded to the rRfCRP-MBP fusion protein (~67.7 kD; fusion of rRfCRP = 25.19 kD and MBP = 42.5 kD). In the next lane (lane-4), a single band was resolved, which corresponded to the size of the fusion rRfCRP, suggesting substantial purity and integrity of the eluted rRfCRP after the protein purification process.

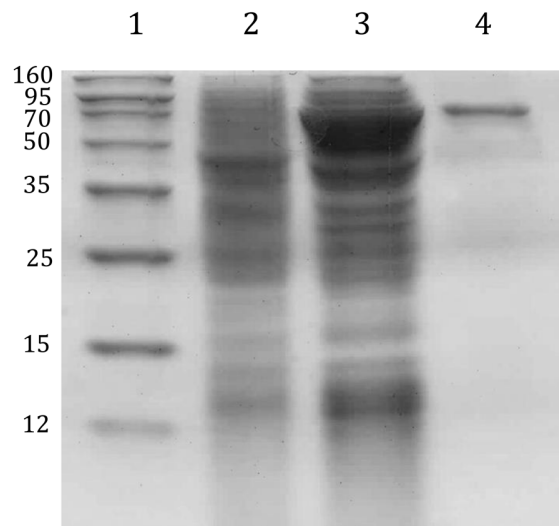


Fig. 13. SDS-PAGE analysis of intermediate products and the final eluted recombinant RfCRP (rRfCRP) protein during the protein purification process. Lane 1, protein size marker (Enzymomics-Korea); Lane 2, total soluble cellular extract from *E. coli* ER2523 harbors a rRfCRP-MBP fusion vector construct prior to IPTG induction; lane 3, crude extract of rRfCRP following IPTG induction; lane 4, purified rRfCRP

3.4. Bacterial agglutination activity

The *in-vitro* agglutination activity of RfCRP against *E. coli* and *S. iniae* was investigated using serial 2-fold dilutions of rRfCRP, with or without the addition of Ca^{2+} in the medium. According to the microscopic observations after treatment of the corresponding bacterial cultures with decreasing concentrations of rRfCRP, rRfCRP could agglutinate *E. coli* exclusively in the presence of Ca^{2+} in a concentration dependent manner (Fig. 14). However, the degree of agglutination decreased from the highest (0.6 $\mu\text{g/mL}$) to the lowest concentration (0.02 $\mu\text{g/mL}$) of protein used in the experiment. Nevertheless, no detectable agglutination against *S. iniae* could be detected that corresponded to any of the concentrations of rRfCRP used in the presence or absence of the Ca^{2+} with respect to the negative controls (data not shown). As expected, MBP (0.6 $\mu\text{g/mL}$) treated bacterial cultures did not show any microscopically detectable agglutination, even with the addition of Ca^{2+} to the medium, inferring that the MBP in the rRfCRP fusion protein has a negligible effect on bacterial agglutination (Fig. 14). These results clearly suggest that RfCRP can involve Ca^{2+} dependent bacterial agglutination events in a dose-dependent manner. Moreover, the dependence of RfCRP agglutination activity on Ca^{2+} further validates the conservation of a Ca^{2+} mediated ligand binding site in the RfCRP protein sequence, as detected by *in-silico* analysis. The bacterial agglutination property of rRfCRP supports the notion that pentraxins including CRPs may have a potential role in host defense against pathogens (Agrawal et al., 2009). Similar to the outcomes of this experimental approach, two short pentraxins identified from *Pangasius hypophthalmus*, CRP and SAP was shown to agglutinate pathogenic bacteria such as *Edwardsiella ictaluri* and *Aeromonas hydrophila*, which can be inhibited by galactose (Huong Giang et al., 2010). However, those proteins could not agglutinate *E.coli* or *Micrococcus lysodeikticu*, reflecting a selective agglutination activity against deferent bacterial

species. Moreover, recombinantly expressed CRP counterpart was also reported from horseshoe crab, which shows detectable agglutination activity against *Pseudomonas aeruginosa* (Tan et al., 2005).

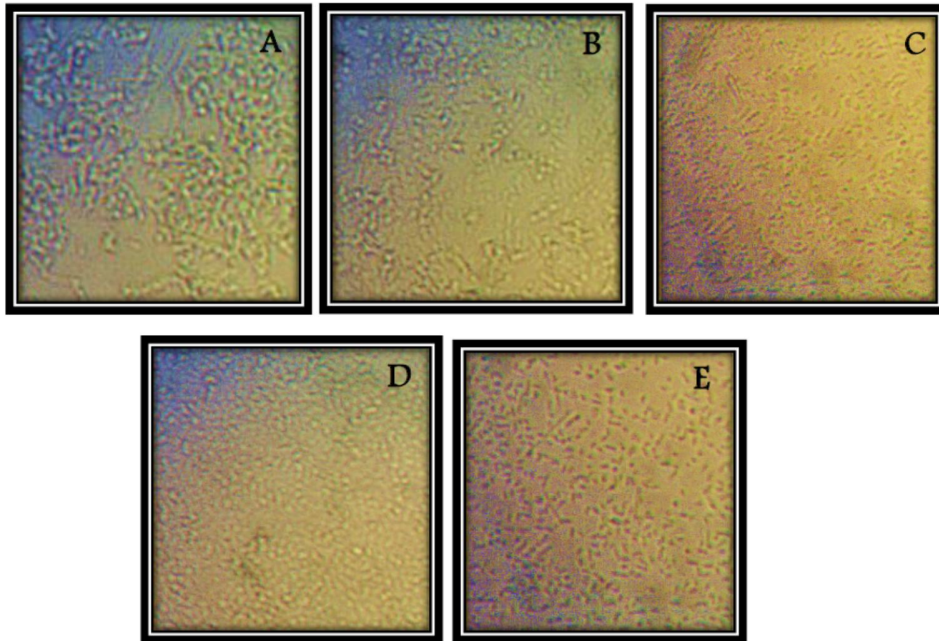


Fig. 14. Bacterial agglutination activity of rRfCRP. Agglutination of *E. coli* by rRfCRP (A-0.6 $\mu\text{g/mL}$ or B-0.02 $\mu\text{g/mL}$ final concentration) in the presence or absence (C-0.6 $\mu\text{g/mL}$ final concentration of rRfCRP) of 10 mM Ca^{2+} , and by MBP (D-0.6 $\mu\text{g/mL}$ final concentration) or column buffer (E) in the presence of Ca^{2+} .

3.5. Ligand binding ability

We have determined the binding ability of two carbohydrate based ligands by rRfCRP, that are known to bind short pentraxins; LPS and D-galactose (Agrawal et al., 2009), through inhibition of *E. coli* agglutination. As observed by light microscopy, incubation of rRfCRP with

LPS or D-galactose in slightly acidic media (pH = 5) led to detectable inhibition of *E. coli* agglutination in the presence of Ca^{2+} , which corresponded to the concentration of each ligand used in the experiment (1, 0.5, and 0.25 $\mu\text{g}/\text{mL}$ with respect to LPS, and 0.5 M, 0.25 M and 0.125 M with respect to D-galactose) (Fig. 15). This observation suggests that RfCRP may function as a PRR, which is a common characteristic feature of pentraxins (Agrawal et al., 2009). Consistent with our observations, short pentraxins such as SAPs or CRPs have been reported to interact with carbohydrates under mildly acidic conditions (Kottgen et al., 1992; Danielsen et al., 1997). The Ca^{2+} dependent LPS binding ability of rRfCRP hints of a possible mechanism of agglutination of gram negative bacteria like *E. coli*, since LPS is a prominent endotoxin on Gram negative bacterial cell walls.

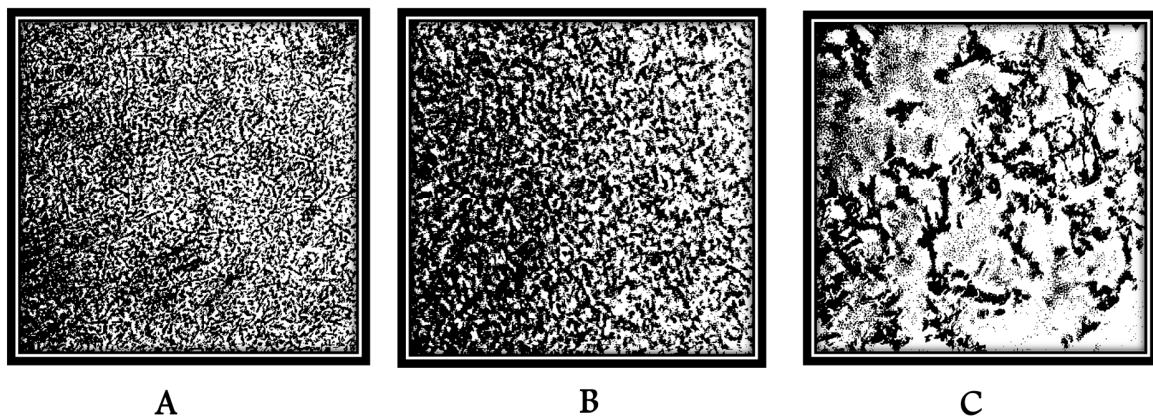


Fig. 15. Inhibitory effect of LPS (0.25 $\mu\text{g}/\text{mL}$) or D-galactose (0.125 μM) on bacterial agglutination of rRfCRP (0.15 $\mu\text{g}/\text{mL}$) in the presence of Ca^{2+} in mildly acidic medium. Agglutination of *E. coli* by rRfCRP in the presence of (A) LPS or (B) D-galactose and in the absence of any ligand (C).

3.6. Bacterial growth inhibition

Potent antibacterial properties of short pentraxins, especially CRPs identified from teleosts have been reported previously. For instance, Tongue sole CRP was found to increase respiratory burst and phagocytic activity of peripheral blood leukocytes infected by bacteria (Li et al., 2013). On the other hand, horseshoe crab CRP was reported to exhibit potent bacteriocidal as well as bacteriostatic activities against Gram negative bacteria (Tan et al., 2005). Thus, in order to investigate the effect of bacterial rRfCRP overexpression on growth, *E. coli* (ER2523) harboring a pMAL-c5X vector ligated with the *RfCRP* coding region and an empty pMAL-c5X vector (control) were separately cultured in LB medium under IPTG induction. According to the calculated CFU of each culture after 12 h of bacterial growth, *E. coli* harboring the recombinant construct (pMAL-c5X/*RfCRP*) was found to have a significantly lower CFU level, compared to that observed in *E. coli* cultured with an empty vector (Fig. 16). This observation is consistent with the overexpression of rRfCRP in *E. coli*, which leads to their growth suppression, suggesting that RfCRP has potent antibacterial activity. Moreover, this evidence further infers that RfCRP in the infected bacterial cells can potentially induce growth inhibition through an effect on cell division.

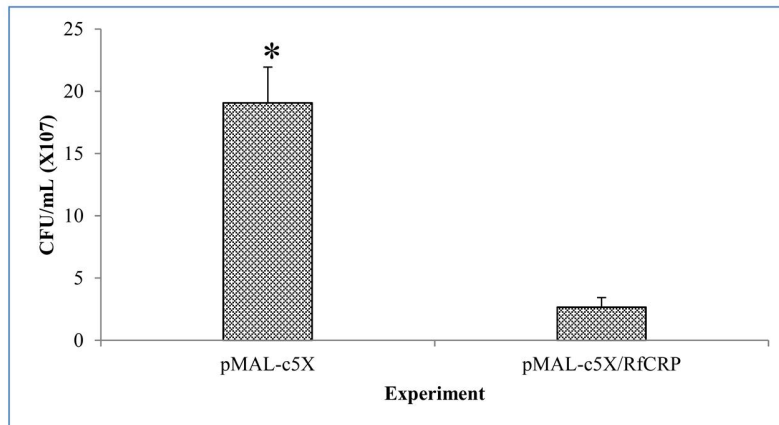


Fig. 16. Bacterial growth inhibition following overexpression of rRfCRP. *E. coli* (ER2523) harboring the pMAL-c5X or pMAL-c5X-RfCRP recombinant vectors were overexpressed by IPTG induction for 12 h at 20°C. The bacterial density of the final culture is presented as CFU/mL. Error bars represent SD (n = 3); * $p < 0.05$.

In addition, rRfCRP led to detectable growth retardation of both *E. coli* and *S. iniae* over time, as evidenced by the notably low OD₆₀₀ at each time point from 8 h or 4 h post incubation in *E. coli* or *S. iniae* cultures treated with rRfCRP compared to the MBP or column buffer treated controls (Fig. 17A and 17B). Similar to our observation, recombinant *Lates calcarifer* CRP also demonstrated significant antibacterial activity against *E. coli*, even though it did not show any effect on the Gram positive bacterium, *Streptococcus aureus* (Mohomad-Jawad et al., 2012). However, the compatible pattern of OD₆₀₀ elevation in MBP treated and control cultures infers that MBP had a negligible effect on the bacteriostatic activity of the rRfCRP fusion protein. Collectively, the results observed in both experimental approaches clearly suggest that RfCRP may play an indispensable role in host antibacterial defense against both gram positive and negative bacteria.

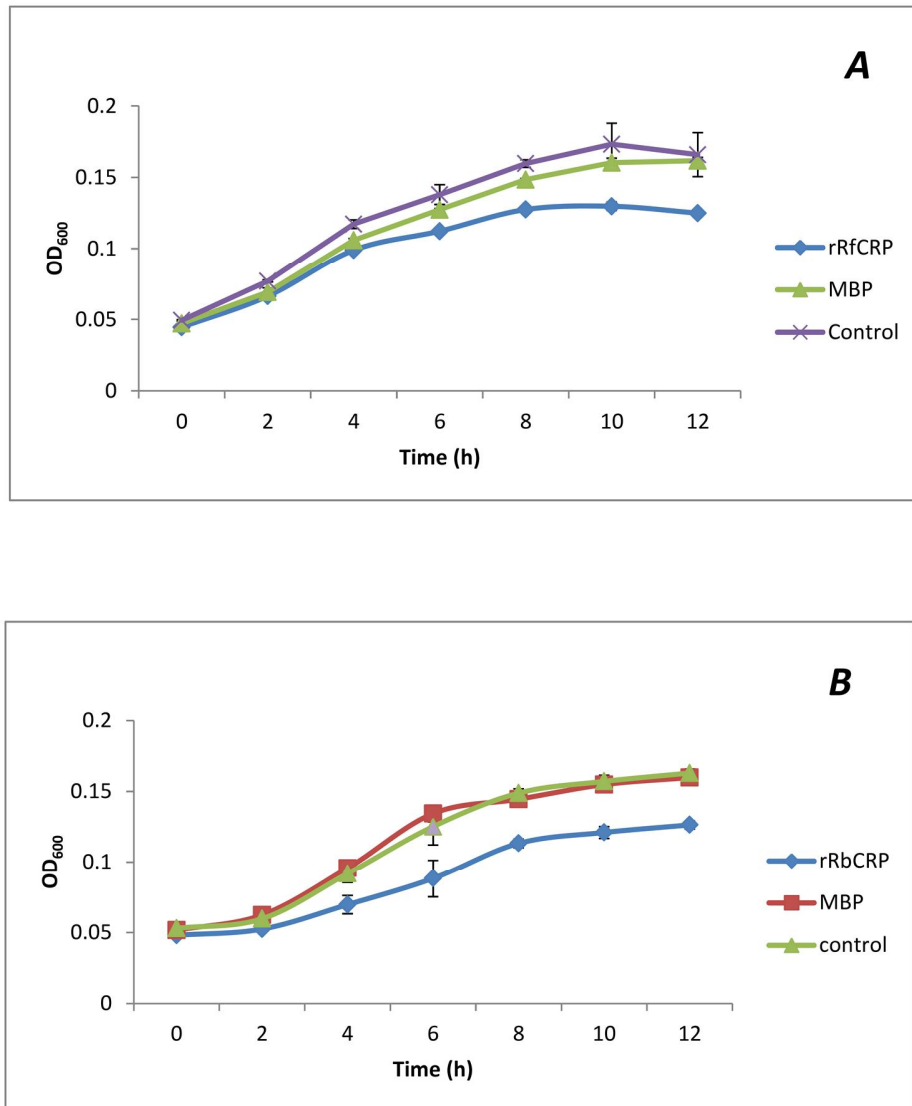


Fig. 17. Bacteriostatic activity of rRfCRP on (A) *E. coli* or (B) *S. iniae* as detected by the variation of bacterial density over time at OD₆₀₀. MBP or column buffer treated cultures were used as controls in both assays. Error bars represent SD (n = 3).

3.7. Tissue specific transcription of RfCRP

Transcript levels of RfCRP in physiologically important healthy black rockfish tissues, as detected by qPCR, confirmed its ubiquitous expression, albeit with different magnitudes (Fig. 18). According to the results, RfCRP expression was more pronounced in the spleen, followed by the head kidney, although the fold difference between expressions in the two tissues was ~ 4.8 . The spleen is an organ that links innate and adaptive immunity while promoting innate immune responses against microbial invasions (Tiron and Vasilescu, 2008). The head kidney is known to be an important immune organ in teleosts, which harbors different cellular components that belong to both innate and adaptive immune systems (Press and Evensen, 1999). Therefore, it is not unexpected to detect the prominent expression of RfCRP in spleen and head kidney tissues of black rockfish, since CRPs are reported to be involved in host anti-microbial defense strategies including agglutination, phagocytosis, and complement activation (Nauta et al., 2003; Pepys and Hirschfield, 2003). Similar to our observation, the CRP counterparts in tongue sole (Li et al., 2013) and common carp (Falco et al., 2012) were also reported to be constitutively expressed in tissues examined under physiological conditions, where tongue sole CRP was markedly expressed in spleen.

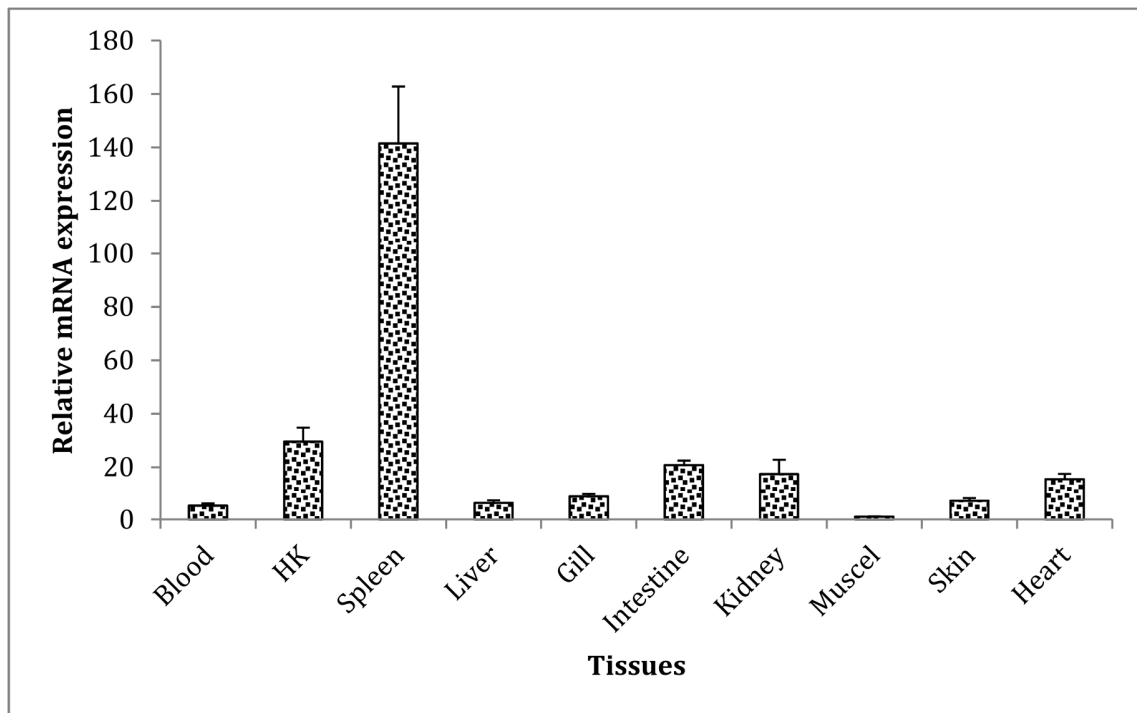


Fig. 18. Tissue-specific distribution of *RfCRP* expression in black rockfish measured using quantitative real-time polymerase chain reaction (qPCR). Fold-changes in expression are shown relative to the level of mRNA expression 1 in muscle tissue. HK– head kidney. Error bars represent SD (n = 3).

3.8. Transcriptional modulation of *RfCRP* upon immune stimulation

Basal mRNA expression of *RfCRP* in spleen and head kidney tissues was modulated under pathogenic stress elicited by LPS and *S. iniae*. According to the quantified transcript levels in spleen, LPS significantly ($P < 0.05$) induced the expression of *RfCRP* in both the early [6 h post stimulation (p.s.)] and late phase (72 h p.s.) of the experiment with a significant ($P < 0.05$) down-regulation at 12 h p.s (Fig. 19A). In contrast, *RfCRP* expression in the head kidney showed significant ($P < 0.05$) up-regulation exclusively at 24 h p.s. with a low fold change (Fig. 19A)

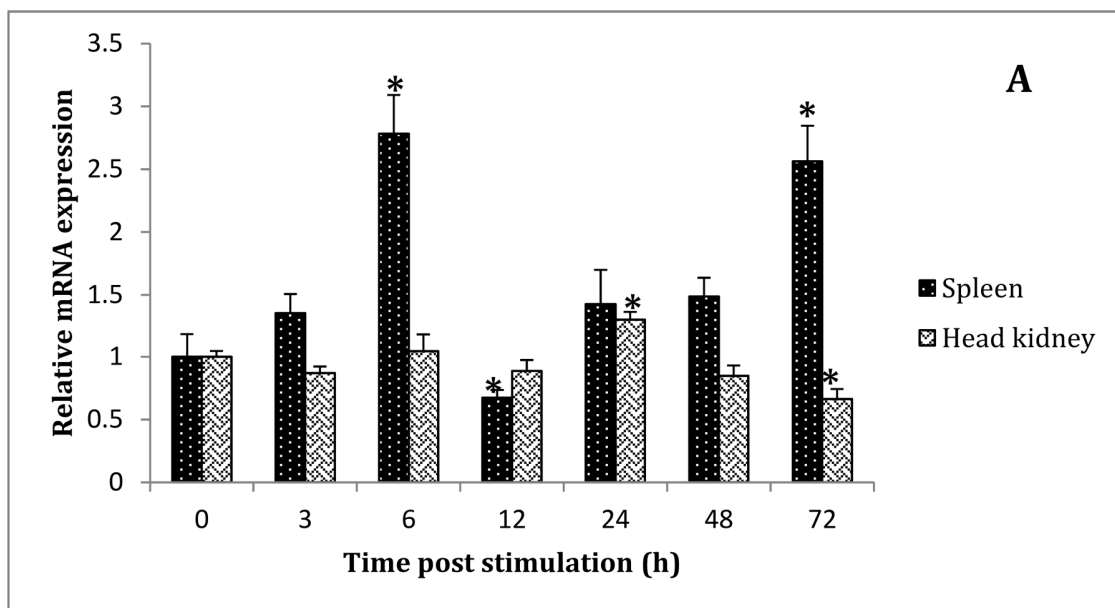
compared to the expression detected in the spleen. However, the expression of *RfCRP* in the head kidney was significantly ($P < 0.05$) down-regulated in response to LPS stimulation at 72 h p.s. These different *RfCRP* transcriptional responses in the head kidney and spleen may reflect distinct efficacies of pro-inflammatory cytokine release by phagocytes in the two different tissues under infectious conditions, which in turn triggers the induction of acute phase proteins including CRPs in fish (Whyte, 2007). Furthermore, a tissue specific transcriptional response may be due to the efficiency of LPS recognition by TLRs which possibly triggers the induction of pro-inflammatory cytokines in two distinct tissues (Cray et al., 2009) or to the cumulative effect of both. However, early and late phase down-regulation of *RfCRP* in the spleen and head kidney, respectively, might be suggestive of mRNA turn over (Mitchell and Tollervey, 2001) or of endotoxin tolerance (Fan and Cook, 2004).

Treatment with live *S. iniae* bacteria evoked the transcriptional up-regulation of *RfCRP* at 24 and 72 h p.s. in spleen tissues with a ~ 4- and 2 fold increase, respectively, although at 12 and 24 h p.s. in head kidney with ~ 3.5- and 2-fold increase, respectively, relative to baseline (Fig. 19B). The earlier induction in the head kidney (12 h p.s.) upon *S. iniae* stimulation than in the spleen might indicate that the head kidney possesses a more efficient Gram negative bacterial PAMP recognition mechanism and subsequent cytokine induction compared to that in the spleen, which in turn may lead to augment APP expression such as CRPs.

As previously reported, expression of tongue sole CRP was also found to be induced exclusively in the spleen during the early phase of treatment with *Vibrio anguillarum*. This observation is compatible with the transcriptional profile reported here in the head kidney after *S. iniae*

treatment. However, tongue sole CRP was continuously upregulated until 48 h post treatment in blood, liver, and kidney tissues in response to the same stimulus.

Collectively, the transcriptional regulation of *RfCRP* in response to live pathogens and treatments using pathogen associated molecules in both spleen and head kidney tissues, along with its anti-microbial properties detected using recombinant proteins suggest that RfCRP might play an indispensable role in antimicrobial defense in black rockfish. However, the magnitude of change detected as the transcriptional up regulation, and significant ($P < 0.05$) down regulation in response to immune stimulants suggests that RfCRP is a moderate or minor responder during the APR in black rockfish (Eckersall and Bell, 2010), especially during live bacterial infection.



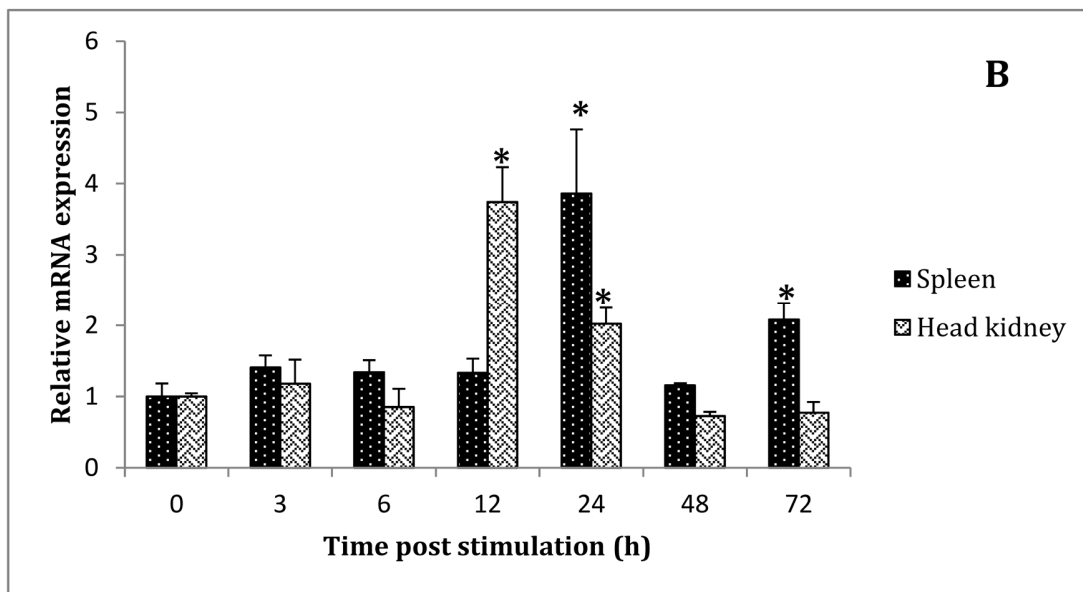


Fig. 19. Temporal modulation of mRNA expression in spleen and head kidney tissues upon immune stimulation with (A) LPS and (B) *S. iniae* as determined by qPCR. The relative expression was calculated using the $2^{-\Delta\Delta CT}$ method. The black rockfish EF1A gene was used as the internal reference gene and mRNA expression was further normalized to the corresponding PBS-injected controls at each time point. The relative fold-change in expression at 0 h post-injection (un-injected control) was used as the baseline. Error bars represent SD (n = 3); * $p < 0.05$.

4. CONCLUSION

The current study focused on the identification and molecular characterization of a CRP homologue in black rockfish. According to the sequence profile obtained by bioinformatic tools, the structural domains of RfCRP were arranged in an analogous manner to those of known pentraxin family members, especially the CRPs. Our phylogenetic analysis and multiple

sequence alignment provide evidence for its homology with the known teleostan CRPs. Recombinant RfCRP demonstrated detectable Ca^{2+} -dependent agglutination activity against *E. coli*, which could be inhibited by LPS and D-galactose, confirming its prominent affinity to carbohydrate based ligands. Moreover, recombinant RfCRP could inhibit the growth of both *E. coli* and *S. iniae* bacteria. Basal expression of RfCRP was ubiquitously detected in physiologically important tissues, and the most pronounced expression was observed in the spleen. In addition, there was significant induction of RfCRP expression upon *S. iniae* and LPS treatment. Taken together, these results suggest the role of RfCRP in black rockfish immune defense against bacterial pathogens.

PART B

Characterization of serum amyloid A (SAA) counterpart from Black rockfish

1. ABSTRACT

Serum amyloid A (SAA) is a vital protein involved in acute phase of an inflammation or infection. SAAs are released from hepatocytes under inflammatory conditions to protect healthy cells from being damaged by pathogens or from self-destructive mechanisms. In this study, a previously constructed black rockfish (*Sebastes schlegeli*) cDNA library was used to identify the full-length cDNA sequence SAA homolog (RfSAA) and characterize at the molecular level. As expected, *in silico* analysis of this homolog showed the typical domain architectures of their known counterparts. Open reading frame of RfSAA consisted of 313-bp DNA sequence. The derived polypeptide sequence of RfSAA had a 121-amino acid sequence with a molecular weight of 13 kD. Phylogenetic analysis as well as pairwise sequence alignment results showed that RfSAA was closely related to the *Epinephelus coioides* ortholog. Although *RfSAA* was expressed ubiquitously in the tissues analyzed, they were eminently expressed in liver tissue, suggesting their origin in hepatocytes. Quantitative real-time PCR analysis indicated that *RfSAA* can be significantly up-regulated by both bacterial and viral stimulation in liver tissues, affirming its putative importance in the acute phase of first-line host immune defenses.

2. MATERIALS AND METHODS

2.1 Identification, sequence analysis and comparison

The full-length cDNA sequences of RfSAA was identified from our previously constructed Black rockfish cDNA sequence database (section 2.1 in Chapter I- part A) using the Basic Local Alignment Tool (BLAST) in the National Center for Biotechnology Information (NCBI) web-based query system (<http://www.ncbi.nlm.nih.gov/BLAST>) with the default algorithm parameters, and *in silico* analysis was conducted using web-based software and servers.

2.2 Experimental fish, husbandry and tissue collection

Pre-acclimatized healthy black rockfish (~200 g) obtained from the aquaria at the Marine Science Institute of Jeju National University, Jeju Self Governing Province, Republic of Korea, were maintained in 400 L laboratory aquarium tanks filled with aerated water at 22 ± 1 °C. Peripheral blood cells were collected from caudal fins of five healthy unchallenged fish (~200 g) using sterile syringes coated with 0.2% heparin sodium salt (USB, USA). The harvested blood cells were immediately centrifuged at $3000 \times g$ in 4 °C for 10 minutes. Other than blood cells, 13 tissues were excised from five healthy fish (~200 g): head kidney, spleen, liver, gill, intestine, posterior kidney, brain, muscle, skin, heart, stomach, and male and female gonads. All the harvested tissues and peripheral blood cells were snap-frozen and stored at -80 °C until further use.

2.3. Immune challenge experiments

The transcriptional response of *RfSAA* to immune challenge with *Streptococcus iniae* (1×10^5 CFU/ μ L) and 1.5 μ g/ μ L polyinosinic:polycytidylic acid (poly I:C) was determined after resuspending or dissolving in $1 \times$ phosphate-buffered saline (PBS). Fish were intraperitoneally (i.p.) injected with each stimulant in a total volume of 200 μ L. A group of fish challenged with 200 μ l PBS alone served as controls. Thereafter, spleen, liver, and peripheral blood cells were collected at 3, 6, 12, 24, 48, and 72 h post-injection from each challenged group as described above.

2.4. RNA isolation and first-strand cDNA synthesis

QIAzol® (Qiagen) reagent was used to extract total RNA from the tissue samples (both challenged and healthy fish) weighing ~ 40 mg each from five individual fish following the manufacturer's protocol. RNA quality was examined by 1.5% agarose gel electrophoresis and the concentration was determined at 260 nm in Drop Plate (Thermo Scientific). The 1st-strand cDNA synthesis was carried out using the PrimeScript™ II 1st strand cDNA Synthesis Kit (TaKaRa, Japan) following the manufacturer's protocol, using 2.5 μ g of RNA as templates. The synthesized cDNA was then diluted 40 fold in nuclease-free water and stored at -80 °C for further use.

2.5. Transcriptional analysis by Quantitative real-time PCR (qPCR) and statistical analysis

To determine the basal transcript levels of *RfSAA* in collected tissues of healthy unchallenged fish and to analyze their transcriptional modulation in blood, liver, and spleen tissues of injected fish, quantitative real-time PCR (qPCR) assays were performed using gene-

specific primers, designed as follows: amplicon size ~150 bp, GC content ~50%, and T_m of 60°C (Table 6) using synthesized cDNA as templates. Assays were performed using the Dice™ Real Time System Thermal Cycler (TP800; TaKaRa, Japan) in a 10 μ L reaction volume containing 3 μ L of diluted cDNA from each tissue, 5 μ L of 2 \times TaKaRa ExTaq™ SYBR premix, 0.4 μ L of each primer, and 1.2 μ L of ddH₂O. The thermal cycling conditions were as follows: one cycle of 95°C for 10 s, followed by 45 cycles of 95°C for 5 s, 58°C for 20 s, 72°C for 20 s, and final single cycles of 95°C for 15 s, 60°C for 30 s and 95°C for 15 s. Each assay was conducted in triplicate and the baseline was set automatically by the Dice™ Real Time System Software (version 2.00). The results were analyzed using the $2^{-\Delta\Delta CT}$ method (Livak and Schmittgen, 2001) to quantify the mRNA expression level. Elongation factor -1-alpha (EF1A) of black rockfish (KF430623) (Liman et al., 2013) was used to normalize the *RfSAA* transcripts in each tissue using the same PCR cycling conditions applied to amplify *RfSAA*. Moreover, the expression values with respect to the immune challenge experiments were further normalized to the corresponding PBS-injected controls at each time point. The relative expression level in the un-injected controls (healthy fish) at the 0 h time point was used as the basal level reference. All the expression data were presented as mean relative mRNA expression \pm standard deviation (SD). To determine statistical significance between experimental and un-injected controls, data were analyzed using a two-tailed unpaired *t*-test considering the significance level at $p < 0.05$.

Table 6. The primers used in the study on RfSAA

Primer Name	Sequence of Primer (5'-3')
RfSAA, qPCR Forward	AGATATGAGGGACGCCAACTGGAAAG
RfSAA, qPCR Reverse	CACCATGACCCGTTCTCTCCTGTATC
RfEF1A, qPCR Forward	AACCTGACCACTGAGGTGAAGTCTG
RfEF1A, qPCR Reverse	TCCTTGACGGACACGTTCTTGATGTT

3. RESULTS AND DISCUSSION

3.1 Sequence characteristics and homology

RfSAA (GenBank accession No: KP842831) had a 366 bp ORF that encoded for a protein of 121 aa. The putative molecular weight of RfSAA was ~13 kD and its theoretical isoelectric point was ~5.9. According to our pairwise sequence alignment, *Epinephelus coioides* ortholog showed the highest identity and similarity with RfSAA, with 85.1% identity and 91.7% similarity (Table 7).). This molecular evidence partially validates the homology of RfSAA with their corresponding counterparts in other fish

Table 7. Percentage of interspecies amino acid sequence identity and similarity with RfSAA counterparts .

Species	Common name	Accession No.	Amino acids	Identity %	Similarity %
<i>Epinephelus coioides</i>	Orange-spotted grouper	AFQ00087	121	85.1	91.7
<i>Lates calcarifer</i>	Barramundi perch	ADE05545	121	76.9	86.0
<i>Oncorhynchus mykiss</i>	Rainbow trout	CAM12348	121	74.4	81.8
<i>Salmo salar</i>	Atlantic salmon	ACM09349	121	74.4	81.8
<i>Apostichopus japonicus</i>	Japanese sea cucumber	ABX55830	121	74.4	81.8
<i>Danio rerio</i>	Zebrafish	NP_001005599	121	66.9	78.5
<i>Homo sapiens</i>	Human	AAB24060	130	43.5	65.4
<i>Mus musculus</i>	House mouse	AAG24633	122	60.7	73.0
<i>Tursiops truncatus</i>	Bottlenosed dolphin	AAB21386	130	59.2	68.5
<i>Gallus gallus</i>	Chicken	AAM46103	127	54.3	70.1

The aa sequence of SAA is known to have a common signature pattern “A-R-G-N-Y-[ED]-A-x-[QKR]-R-G-x-G-G-x-W-A,” which is also found in RfSAA with one amino acid substitution where “Y” is replaced by “A” (Fig. 20) (Malle et al., 1993). Even though the SAA-specific putative calcium binding site “GPGG” is conserved among most of the homologs, RfSAA and some other teleost counterparts, including *E. coioides* and *Lates calcarifer*, were found to have “GAGG” in place of “GPGG,” suggesting that RfSAA may not be involved in amyloidogenesis, which takes place via a calcium-dependent protein-binding interaction (Pepys et al., 1979; Turnell et al., 1986). RfSAA had a signal peptide of 18 amino acid residues reflecting its

secretory property. Moreover, it harbored the SAA domain lies in between 20 and 121 aa, and it is highly conserved in other SAA counterparts, particularly in the teleost counterparts analyzed in this study (Fig. 20).

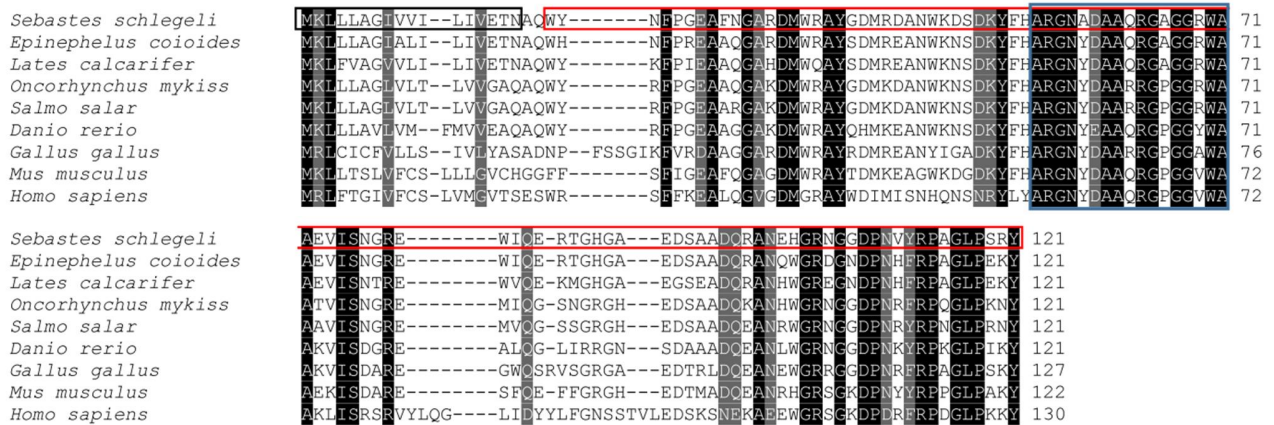


Fig. 20. Comparison of the derived amino acid sequences of RfSAA with other counterparts. signal peptide is represented in a black color box while the SAA domain is in a red color box. The common signature pattern is denoted in a blue color box.

3.2 Phylogenetic position of RfSAA

Phylogenetic analysis of RfSAA resulted in a poorly supported topology (Fig. 21). However, fish along with RfSAA formed a distinct clade. Interestingly, *M. musculus* SAA showed a close evolutionary relationship with non-mammalian counterparts than mammals, clustering with non-mammalian counterparts as an out-group, while *H. sapiens* SAA was isolated as an outlier of whole reconstruction. RfSAA was in a clade with *E. coioides* and *L. calcarifer* counterparts with a bootstrap support of 92. This phylogenetic relationship and our

identity/similarity analysis (Table 4) supported to the closer consistency between RfSAA and its counterpart of *E. coioides*.

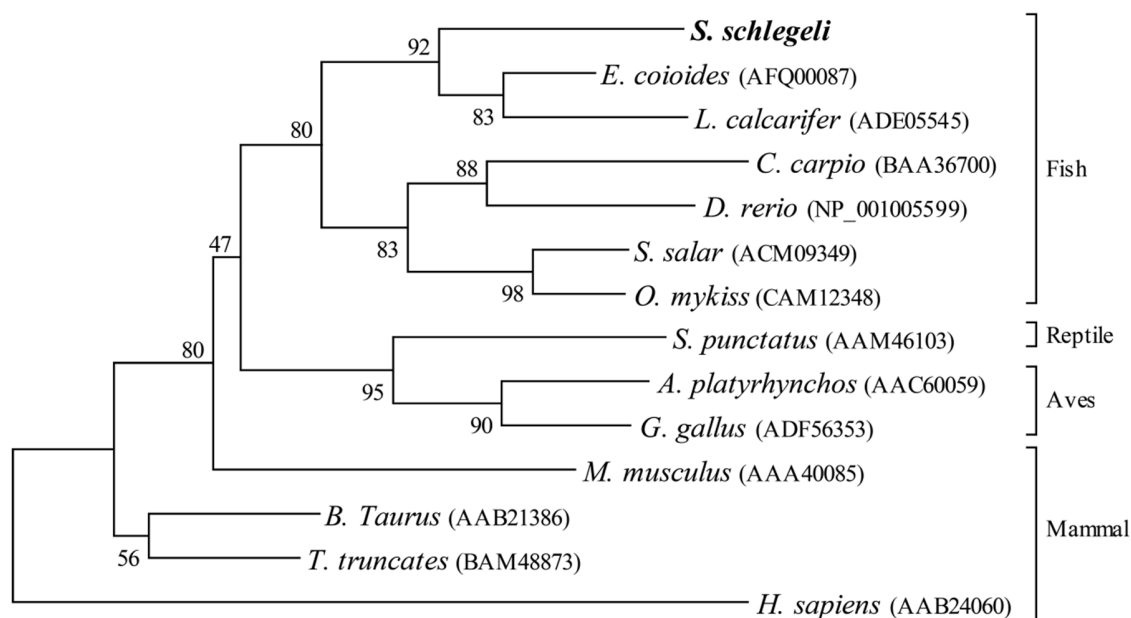


Fig. 21. Phylogenetic tree demonstrating the evolutionary relationship of RfSAA with counterparts of other organisms. Accession numbers are indicated along with the species name.

3.3 Protein folding prediction of RfSAA

FoldIndex® analyzes the average hydrophobicity of aa and the absolute net charge of aa to predict the foldability of a given aa sequence (Prilusky et al., 2005). According to the prediction, RfSAA is a highly intrinsically disordered molecule with 88 disordered residues accounting for 72.72% of the total residues, affirming its instability and substantial reactivity (Table 8). Interestingly, the *H. sapiens* counterpart, which contains three disordered regions but no additional domains, showed different conformation from that of fish counterparts with 40.77% disordered residues (Fig. 22). Intrinsically unfolded proteins function by undergoing disorder-to-

order transition; hence, they have the ability to exert the activity whenever needed, saving the entropic cost for protein ordering to and fro than intrinsically folded proteins (Bracken, 2001). Therefore, it can be stated that the FoldIndex© results further reinforce the high reactivity of fish APPs considered in our study.

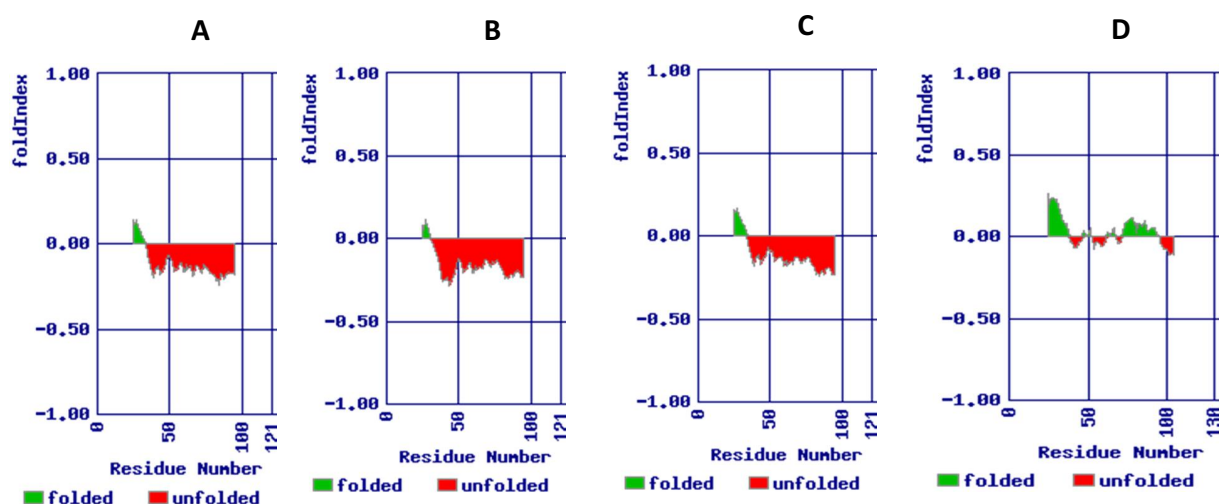


Fig. 22. Graphical representation of FoldIndex®.; (A) RfSAA, (B) Orange-spotted grouper SAA, (C) Barramundi SAA, (D) Human SAA

Table 8. FoldIndex® data summary of RfSAA with other selected counterparts.

	No. of disordered regions	Longest disordered region	No. of Disordered residues	Disordered residues as a percentage (%)
RfSAA	1	88	88	72.72
Orange-spotted grouper	1	92	92	76.03
Barramundi perch	1	88	88	72.72
Human	3	36	53	40.77

3.4 Tissue-specific expression of *RfSAA*

As detected by our qPCR assay, RfSAA had universal spatial expression in tissues examined albeit in different magnitudes. During the acute phase of inflammation, many acute-phase proteins are secreted from liver tissue in which they are produced (Kushner, 1982). Our results also showed notable mRNA expression level of *RfSAA* in liver tissue. RfSAA was expressed in liver tissue with a 38,214-fold difference compared to that in head kidney tissue. Next to liver, a higher expression level of RfSAA was detected in blood followed by skin and spleen (Fig. 23).

Blood functions as a circulatory medium in animals including teleosts and harbors a pool of wide array of immune cells; hence can prominently mediate the inflammatory reactions. On the other hand, SAA like major APPs (phase III) should be readily available in a transportable module in cells rapidly involved in inflammations, such as blood cells. Thus, it is not unlike to observe markedly high expression level of RfSAA in blood.

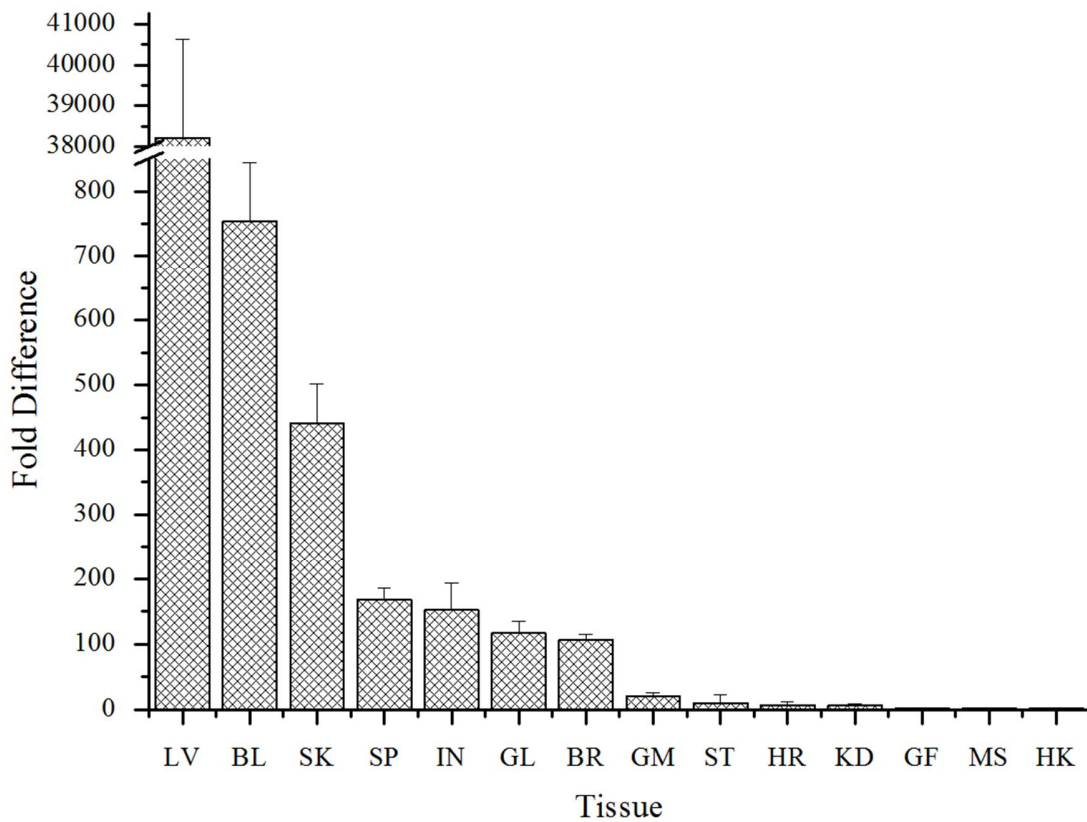


Fig. 23. Tissue specific transcriptional profile of *RfSAA*; BL, blood; GL, gill; LV, liver; SP, spleen; HK, head kidney; KD, kidney; SK, skin; MS, muscle; HR, heart; BR, brain; IN, intestine; ST, stomach; GM, testis; GF, ovary. Data are presented as mean ($n = 3$) \pm SD. *RfSAA* - mRNA detected in each tissue by qPCR was normalized to *RfSAA* mRNA detected in HK.

3.5 Expressional modulation in response to challenge experiments

The mRNA expression levels of *RfSAA* in liver, spleen, and peripheral blood cells in response to the *S. iniae* and poly I:C treatments were investigated to ascertain their expressional modulation in the acute phase of an infection. In liver tissue, with *S. iniae* challenge, *RfSAA* was up-regulated at all the time points relative to the controls (0 h) ($P < 0.05$), and the highest expression level was detected at 48 h (197 fold) post stimulation (p.s.) (Fig. 24). *RfSAA* showed its highest expression

at 12 h p.s. (2.5 fold) in response to *S.iniae* infection in spleen tissue. Interestingly, in the spleen tissue, significant downregulation was observed at 3 h p.s.. This may be due to the mRNA turnover event that occurred in the spleen tissue during the pathogenic stress (Mitchell and Tollervey, 2001). However, in peripheral blood cells, *RfSAA* showed comparatively less strong transcriptional modulation after *S. iniae* invasion, although it showed detectable positive modulation at 12 h and 48 h p.s. (1.7 fold and 1.9 fold, respectively). Collectively, these observed transcriptional responses show that *RfSAA* is positively modulated at a significant level in some of the immune-relevant tissues in the acute phase of a live bacterial infection.

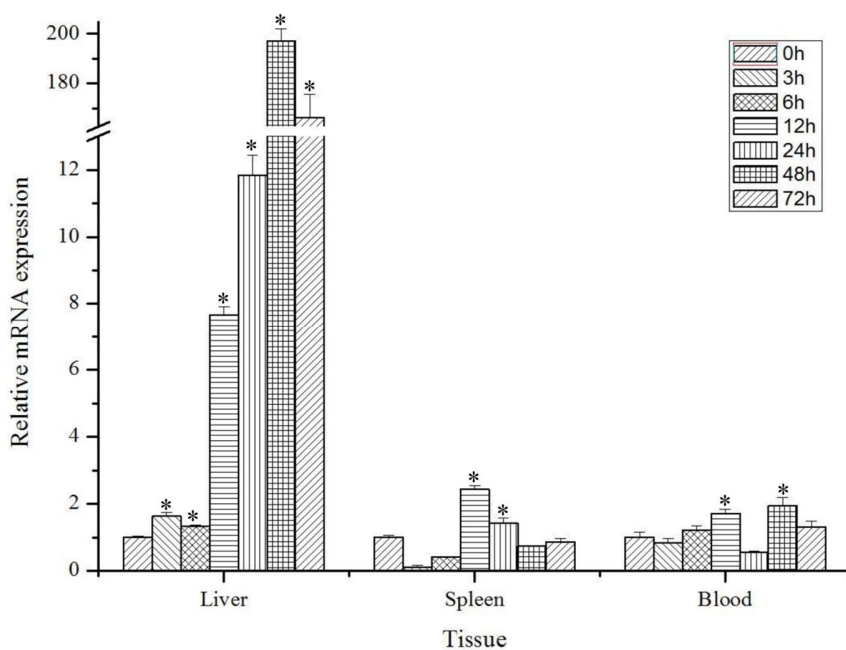


Fig. 24. Expression analysis of *RfSAA* in different tissues after experimental infection with *S.iniae*, carried out by qPCR. Data are expressed as mean fold-induction (n = 3) relative to the PBS control \pm SD. * t-test, $p < 0.05$ vs. unchallenged control at 0 h.

Upon stimulation by poly I:C, the liver tissue showed comparatively higher up-regulation of RfSAA than in spleen and peripheral blood cells (Fig. 25). The highest transcriptional inductive response in liver tissue following poly I:C treatment was obtained at 72 h p.s. (34 fold). In spleen *RfSAA* did not show any significant up-regulation. However, the same initial downregulation pattern detected in *S. iniae* challenge was also observed here, with additional downregulations at the later time points. In peripheral blood cells, *RfSAA* showed up-regulated expression at both 6 h and 12 h p.s. time points (1.5 fold and 3.2 fold respectively) upon poly I:C treatment. Interestingly, the qPCR results for the challenge experiment with poly I:C also suggested that expression of *RfSAA* genes can be induced by viral infections.

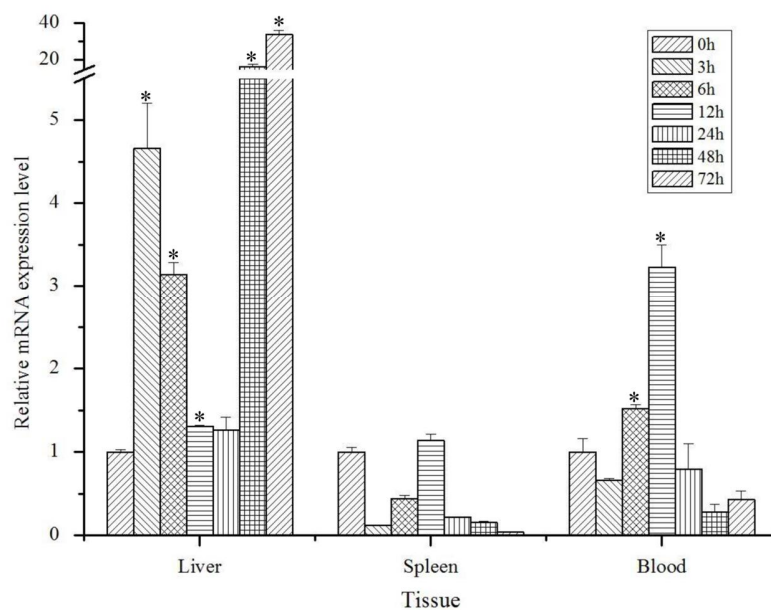


Fig. 25. Expression analysis of *RfSAA* in different tissues after the treatment of poly I:C, carried out by qPCR. Data are expressed as mean fold-induction (n = 3) relative to the PBS control \pm SD.

* t-test, $p < 0.05$ vs. unchallenged control at 0 h.

SAA like group III acute phase proteins increase their concentrations at the early phase of an infection; for instance substantial expressional induction at 4 h from the initiation of the pathogenic invasion and the highest elevated concentration level is known to reach about 24–72 h after an infection (Kushner and Mackiewicz, 1993). Our observation on expressional modulation of *RfSAA* in liver upon *S. iniae* and poly (I:C) treatment reinforces this finding.

4. CONCLUSION

In conclusion, full-length cDNA sequences encoding SAA homolog was identified from black rockfish and characterized molecularly. RfSAA was predicted to be an intrinsically highly disordered protein. At mRNA level RfSAA gene is highly expressed in the liver tissue. The qPCR analysis of mRNA expression in tissues of immune-challenged animals revealed that RfSAA is up-regulated in response to bacterial and poly (I:C) treatment. According to the results, it can be suggested that RfSAA may act as positive APPs in black rockfish. However, further studies are needed, particularly focusing on the tentative functionality of RfSAA in host immune defenses.

PART C

Characterization of haptoglobin (Hp) counterpart from Black rockfish

1. ABSTRACT

Haptoglobin (Hp) is a positive acute phase protein synthesized in liver, and its concentration is elevated during the acute phase of an infection. Hp binds with hemoglobin (Hb) during the hemolysis process to prevent the negative effects exerted by free Hb, including oxidative damage. In this study, a previously constructed black rockfish (*Sebastes schlegeli*) cDNA library was used to identify the full-length cDNA sequences of Hp homolog (RfHp) and molecularly characterized. As expected, *in silico* analysis showed that RfHp houses the typical domain architecture of its known counterparts. Open reading frames of RfHp consisted of 942-bp DNA sequence. The derived polypeptide sequence of RfHp was composed of 313 amino acids (aa) with a predicted molecular weight of 34 kD. Phylogenetic analysis as well as pairwise sequence alignment results showed that RfHp was more closely related to its counterpart of *Oreochromis mossambicus* from an evolutionary perspective. Although *RfHp* was expressed ubiquitously in the tissues analyzed, it was particularly expressed in liver tissue, suggesting their origin in hepatocytes. Quantitative real-time PCR analysis indicated that *RfHp* was significantly up-regulated by both bacterial and viral stimulation in liver tissue, affirming its putative importance in the acute phase of first-line host immune defenses.

2. MATERIALS AND METHODS

2.1. Identification, sequence analysis and comparison of RfHp and RfSAA from the black rockfish

The full-length cDNA sequences of RfHp was identified from our previously constructed Black rockfish cDNA sequence database (section 2.1 in Chapter I- part A) using the Basic Local Alignment Tool (BLAST) in the National Center for Biotechnology Information (NCBI) web-based query system (<http://www.ncbi.nlm.nih.gov/BLAST>) using the default algorithm parameters, and *in silico* analysis was conducted using web-based software and servers.

2.2. Experimental fish, husbandry and tissue collection

Pre-acclimatized healthy black rockfish (~200 g) obtained from the aquaria at the Marine Science Institute of Jeju National University, Jeju Self Governing Province, Republic of Korea, were maintained in 400 L laboratory aquarium tanks filled with aerated water at 22 ± 1 °C. Peripheral blood cells were collected from caudal fins of five healthy unchallenged fish (~200 g) using sterile syringes coated with 0.2% heparin sodium salt (USB, USA). The harvested blood cells were immediately centrifuged at $3000 \times g$ in 4 °C for 10 minutes. Other than blood cells, 13 tissues were excised from five healthy fish (~200 g): head kidney, spleen, liver, gill, intestine, posterior kidney, brain, muscle, skin, heart, stomach, and male and female gonads. All the harvested tissues and peripheral blood cells were snap-frozen and stored at -80 °C until further use.

2.3 Immune challenge experiments

The transcriptional response of RfHp and RfSAA to immune challenge with *Streptococcus iniae* (1×10^5 CFU/ μ L) and 1.5 μ g/ μ L polyinosinic:polycytidylic acid (poly I:C)

was determined after resuspending or dissolving in 1× phosphate-buffered saline (PBS). Fish were intraperitoneally (i.p.) injected with each stimulant in a total volume of 200 μL. A group of fish challenged with 200 μl PBS alone served as controls. Thereafter, spleen, liver, and peripheral blood cells were collected at 3, 6, 12, 24, 48, and 72 h post-injection from each challenged group as described above.

2.4. RNA isolation and first-strand cDNA synthesis

QIAzol® (Qiagen) reagent was used to extract total RNA from the tissue samples (both challenged and healthy fish) weighing ~ 40 mg each from five individual fish following the manufacturer's protocol. RNA quality was examined by 1.5% agarose gel electrophoresis and the concentration was determined at 260 nm in Drop Plate (Thermo Scientific). The 1st-strand cDNA synthesis was carried out using the PrimeScript™ II 1st strand cDNA Synthesis Kit (TaKaRa, Japan) following the manufacturer's protocol, using 2.5 μg of RNA as templates. The synthesized cDNA was then diluted 40 fold in nuclease-free water and stored at -80 °C for further use.

2.5 Transcriptional analysis by Quantitative real-time PCR (qPCR) and statistical analysis

To determine the basal transcript levels of *RfHp* in collected tissues of healthy unchallenged fish and to analyze their transcriptional modulation in blood, liver, and spleen tissues of injected fish, quantitative real-time PCR (qPCR) assays were performed using gene-specific primers, designed as follows: amplicon size ~150 bp, GC content ~50%, and T_m of 60°C (Table 9) using synthesized cDNA as templates. Assays were performed using the Dice™ Real Time System Thermal Cycler (TP800; TaKaRa, Japan) in a 10 μL reaction volume containing 3 μL of diluted cDNA from each tissue, 5 μL of 2× TaKaRa ExTaq™ SYBR premix,

0.4 μ L of each primer, and 1.2 μ L of ddH₂O. The thermal cycling conditions were as follows: one cycle of 95°C for 10 s, followed by 45 cycles of 95°C for 5 s, 58°C for 20 s, 72°C for 20 s, and final single cycles of 95°C for 15 s, 60°C for 30 s and 95°C for 15 s. Each assay was conducted in triplicate and the baseline was set automatically by the Dice™ Real Time System Software (version 2.00). The results were analyzed using the $2^{-\Delta\Delta CT}$ method (Livak and Schmittgen, 2001) to quantify the mRNA expression level. Elongation factor -1- α (EF1A) of black rockfish (KF430623) (Liman et al., 2013) was used to normalize the *RfHp* transcripts in each tissue using the same PCR cycling conditions applied to amplify *RfHp*. Moreover, the expression values with respect to the immune challenge experiments were further normalized to the corresponding PBS-injected controls at each time point. The relative expression level in the un-injected controls (healthy fish) at the 0 h time point was used as the basal level reference. All the expression data were presented as mean relative mRNA expression \pm standard deviation (SD). To determine statistical significance between experimental and un-injected controls, data were analyzed using a two-tailed unpaired t-test considering the significance level at $p < 0.05$.

Table 9. The primers used in the study on RfHp

Primer Name	Sequence of Primer (5'-3')
RfHp, qPCR Forward	ACCTGGGAATCACTGAACGATCACAAG
RfHp, qPCR Reverse	TAACCACAGGCACCTCCAGTTTGA
RfEF1A, qPCR Forward	AACCTGACCACTGAGGTGAAGTCTG
RfEF1A, qPCR Reverse	TCCTTGACGGACACGTTCTTGATGTT

3. RESULTS AND DISCUSSION

3.1 Sequence characterization of RfHp

The RfHp cDNA sequence (GenBank accession No: KP842830) consisted of an open reading frame (ORF) of 942 bp that encoded a 313 amino acid (aa) sequence. The predicted molecular weight of this sequence was around 34 kD and the theoretical isoelectric point was 8.0. As detected by our pairwise sequence alignment, the *Oreochromis mossambicus* ortholog showed the highest identity (71.5%) and similarity (84%) with RfHp (Table 10). This molecular evidence partially validates the homology of black rockfish Hp with its corresponding counterparts in other fish.

Table 10. Percentage of interspecies amino acid sequence identity and similarity with RfHp

Species	Common name	Accession No.	Amino acids	Identity %	Similarity %
<i>Oreochromis mossambicus</i>	Mozambique tilapia	CBH32482	312	71.5	84.0
<i>Ictalurus punctatus</i>	Channel catfish	AHH39487	298	50.6	67.7
<i>Leucoraja erinacea</i>	Little skate	AFN85000	417	22.4	35.7
<i>Ginglymostoma cirratum</i>	Nurse shark	AEB61473	429	23.1	36.6
<i>Homo sapiens</i>	Human	AAA88080	406	23.7	41.6
<i>Mus musculus</i>	House mouse	AAA37779	347	27.4	48.7
<i>Sus scrofa</i>	Pig	ACD93463	347	27.9	50.1
<i>Tursiops truncatus</i>	Bottlenosed dolphin	BAN62638	345	27.7	49.0

When compared with human Hp (HsHp), RfHp shows higher identity and similarity with the β -chain of HsHp (27.2% identity and 42.8% similarity) than with that of α -chain (5.0% identity and 7.3% similarity), suggesting that RfHp shares more homology with HsHp β -chain (Fig. 26).

Four N-glycosylated sites were found at the 94–96, 120–122, 138–140, and 204–206 amino acid positions of RfHp (Fig. 26). However, other teleost counterparts from *O. mossambicus* and *Ictalurus punctatus* had only two and one N-glycosylated sites, respectively. Interestingly, mammalian Hps, including HsHp, also consist of four N-glycosylated sites, suggesting that RfHp in black rockfish has a higher possibility of glycosylation compared to that of other teleosts considered here. According to our *in silico* study, RfHp had two disulfide bonds between the 208–227 and 238–268 residues (Fig. 26). However, the mammalian counterparts considered here had three to four disulfide bonds, while RfHp and other teleost counterparts had only one to two disulfide bonds. This observation implies that mammalian Hp counterparts are more likely to be highly folded than those of teleosts. RfHp also harbored a 23-aa residue signal peptide (aa 1–23) suggesting its secretory nature.

RfHp had a trypsin-like serine peptidase (Tryp_SPC) domain between 46 and 286 aa (Fig. 1A), suggesting that RfHp belongs to the chymotrypsin (S1) family involved in digestive and degradative processes in cellular and humoral immunity (Rawlings and Barrett, 1993; Krem and Di Cera, 2002). Interestingly, the complement control protein (CCP) domain that is important in forming the functional Hp-Hb complex is missing in teleost counterparts. The *H. sapiens* ortholog has two dimerized CCP domains, whereas other mammals have only one CCP domain (Vinayagam et al., 2004). This comparative observation indicates that fish Hps may bind Hp by a different mechanism compared to that in mammals or fish Hps may not bind Hp at all, as reported in some other fish species (Massad et al., 1992).

<i>Sebastes schlegeli</i>	-----	0
<i>Oreochromis mossambicus</i>	-----	0
<i>Ictalurus punctatus</i>	-----	0
<i>Tursiops truncatus</i>	--MSALQAVVALLCG--	28
<i>Mus musculus</i>	--MRALGAVTLLWG--	29
<i>Homo sapiens</i>	--MSALGAVIALLLWG--	29
<hr/>		
<i>Sebastes schlegeli</i>	-----	0
<i>Oreochromis mossambicus</i>	-----	0
<i>Ictalurus punctatus</i>	-----	0
<i>Tursiops truncatus</i>	-----DDSLCKPPEIAN--	40
<i>Mus musculus</i>	-----DDSCPKEPEIAN--	41
<i>Homo sapiens</i>	-----DDGCPKPEPEIAHGVEHSVRYQCKNYKLRTEGDGVYTLNDKKQWINKAVGDKLPECEADDG	91
<hr/>		
<i>Sebastes schlegeli</i>	-----MNIINNMWFSLTLLAALACLAD-VTBERVKRSV-SASGLASL---RSHRMVGGTLAP-	54
<i>Oreochromis mossambicus</i>	-----MWFSTVLLAACACLADEVLTTEMNQPL-SASRLASP---RSRERMVGGTLAP-	49
<i>Ictalurus punctatus</i>	-----MKWFSVAVFLVGLMICLSESRVVDGIKEHT-EANTDAAL---RTRERMVGGLLTPG	51
<i>Tursiops truncatus</i>	-----GYLEHLVRYRCKTYKLRGT-DGYTINTEKOWINKDLGQVPECE-AVCGKPKHPAVOVORIIIGSSLDAK	109
<i>Mus musculus</i>	-----GYVEHLVRYRCQFYRLRAEGDGYTINDEKQWVNTVAGDKLPECE-AVCGKPKHPVDQVORIIIGSSMDAK	111
<i>Homo sapiens</i>	CPKPEPEIAHGVEHSVRYQCKNYKLRTEGDGVYTLNNEKQWINKAVGDKLPECE-AVCGKPKHPANVORIIIGGHLDAK	170
<hr/>		
<i>Sebastes schlegeli</i>	-HVPWQALVYISDNVLDGSHGGCALISERWLLTAGRNLFVNRSS-OPAGKEGIVIPKYYLGIITERSQANPKEVAWVKVFL	132
<i>Oreochromis mossambicus</i>	-HVPWQAMVYIADKVVDCGSAGCALISDRWLLTAGRNLFVNRSSROHTQKDPVIKVVYLGIHGRPQAVASKEVAWVKVFL	128
<i>Ictalurus punctatus</i>	-HVPWQALVYLSDSKLDGIGGGCALIAPWLLTAGRNLFVNRSTQKDTRGKEPLIPKVVYLGIVRRAKADSASEVAWVKVFL	130
<i>Tursiops truncatus</i>	GSEFWQAKMVSRRNLTSG---ATLINEQWLLTAKNLFVNRSDNTTKAKDIAPTLRLIYVGRK-----OLVETEKVFL	177
<i>Mus musculus</i>	GSEFWQAKMISRHLTTC---ATLISDOWLLTAKNLFVNRSENTAKDIAPTLRLIYVGRK-----OLVETEKVFL	179
<i>Homo sapiens</i>	GSEFWQAKMVSHHLLTTC---ATLINEQWLLTAKNLFVNRSENTAKDIAPTLRLIYVGRK-----OLVETEKVFL	238
<hr/>		
<i>Sebastes schlegeli</i>	HPHFQNRKRW--DNDLALIKLEVPVITDKVTPTELPER---CODTMCSTGVITGCGWGI--LLTPSKSLKHVLPVLANH	205
<i>Oreochromis mossambicus</i>	HPGFQNGSDW--ENDLALIKLKEPVLMSNKVTPTELPERGHDLADTLGGTGVITGCGWGI--HFTLATSLKHVLPVLANH	204
<i>Ictalurus punctatus</i>	HPAFQNASDV--DNDLALIKLKEPVSYTDHFPTELPERDDNLEESERQGVVAGWGWGP--LLTFSESLKFLSLVPIPG	206
<i>Tursiops truncatus</i>	HPDYS---EVDIGLILKLRKVPIDETVMPICLPSKD--YVEAQRVGYNSGWGRNA--NLVFTHEHLYIMLPVADQ	245
<i>Mus musculus</i>	HPNHS---VVDIGLILKLRKRVLVTETVMPICLPSKD--YIAPQRVGYNSGWGRNA--NFRFTDRLRYVMLPVADQ	247
<i>Homo sapiens</i>	HPNYS---QVDIGLILKLRKQVSVNERVMPICLPSKD--YAEVQRVGYNSGWGRNA--NFKFTDHLRYVMLPVADQ	306
<hr/>		
<i>Sebastes schlegeli</i>	SYOKAEYERNPF-----TPAWDQNMHCSTGTRKYDENVCFGDAGSABAVHDAETGDIYAAGILSPDKSIVSHKY	273
<i>Oreochromis mossambicus</i>	TEOKAEYDLTEL-----TPAWDQHMFCSTGTRKYDENVCFGDAGSABAVHDAATGDIYAAGILSPDKSIVSHKY	272
<i>Ictalurus punctatus</i>	-----NVKGGKIVTIRTEFOENVCYGDAGSABAVHNPVTKKVVYAAGILSPDKSIVSHKY	260
<i>Tursiops truncatus</i>	DKCVQHYEGSTVPEKKTTPKSPVGVQPIINBHTHCAGLSKYQEDICYGDAQSABAVHDEADDTWYAAGILSPDKSIVSHKY	325
<i>Mus musculus</i>	DKCVVHYENSTVPEKKNLTPKSPVGVQPIINBHTHCAGLSKYQEDICYGDAQSABAVHDEEDTWYAAGILSPDKSIVSHKY	327
<i>Homo sapiens</i>	DCQIRHYEGSTVPEKKTTPKSPVGVQPIINBHTHCAAGMSKYQEDICYGDAQSABAVHLEEDTWYAAGILSPDKSIVSHKY	386
<hr/>		
<i>Sebastes schlegeli</i>	GVMKICSYLFWIHSVIRGDTDKSPALRADAMSKMYLWOO	313
<i>Oreochromis mossambicus</i>	GVMKICSSYLFWIHSVIRGDEKSSALRSDAMSKMYLWOO	312
<i>Ictalurus punctatus</i>	AVFMKICSTYLFWIHSVMRAPSDFRSLRTSISIMNDLLSK--	298
<i>Tursiops truncatus</i>	GVMKICSYLFWIHSVIRGDTDKSPALRADAMSKMYLWOO	345
<i>Mus musculus</i>	GVMKICSYLFWIHSVIRGDTDKSPALRADAMSKMYLWOO	347
<i>Homo sapiens</i>	GVMKICSYLFWIHSVIRGDTDKSPALRADAMSKMYLWOO	406

Fig. 26. Comparison of the derived amino acid sequence of RfHp with other organisms. RfHp – signal peptide is denoted in a black box while the Tryp_SPc domain is in a red color box. The Cysteine residues for disulfide bonds are denoted in blue color boxes. N-glycosylation sites are denoted in green color boxes. The α -chain and β - chain of Human Hp are underlined in blue and yellow respectively.

3.2 Phylogenetic position of RfHp

Phylogenetic analysis of RfHp and other Hp counterparts showed two distinct clades; fish and RfHp were clustered in one clade and mammalian Hp counterparts formed the other clade (Fig. 27). Furthermore, in the fish clade, bony fish and cartilage fish formed two sister clades. RfHp was placed in a clade with *O. mossambicus* with a bootstrap support value of 99. The identity similarity values (Table 7) and phylogenetic analyses suggest that RfHp shows a closer evolutionary relationship with its homologue of *O. mossambicus*.

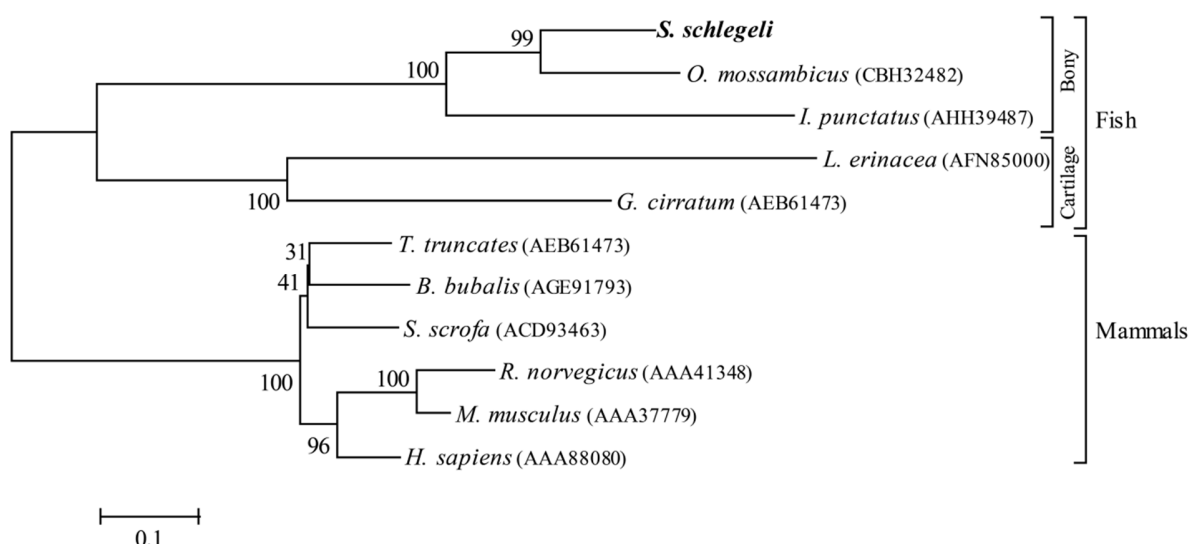


Fig. 27. Phylogenetic tree demonstrating the evolutionary relationship of RfHp with amino acid sequences of other organisms. Accession numbers are indicated along with the species name.

3.3 Protein folding prediction of RfHp and RfSAA

FoldIndex® analyzes the average hydrophobicity of aa and the absolute net charge of aa to predict the foldability of a given aa sequence (Prilusky et al., 2005). Here, RfHp had one disordered region composed of nine amino acid residues, which is only 2.88% of the total residue number. This implies that RfHp is intrinsically a highly folded molecule (Table 11) as

shown by the presence of a high number of N-glycosylation sites and disulfide bonds, in accordance with our *in silico* predictions (Fig. 28).

Table 11 . FoldIndex® data summary of RfHp with other selected organisms

	No. of disordered regions	Longest disordered region	No. of Disordered residues	Disordered residues as a percentage (%)
RfHp	1	9	9	2.88
Mozambique tilapia	0	-	-	-
Channel catfish	2	15	21	7.05
Human	4	106	130	32.02

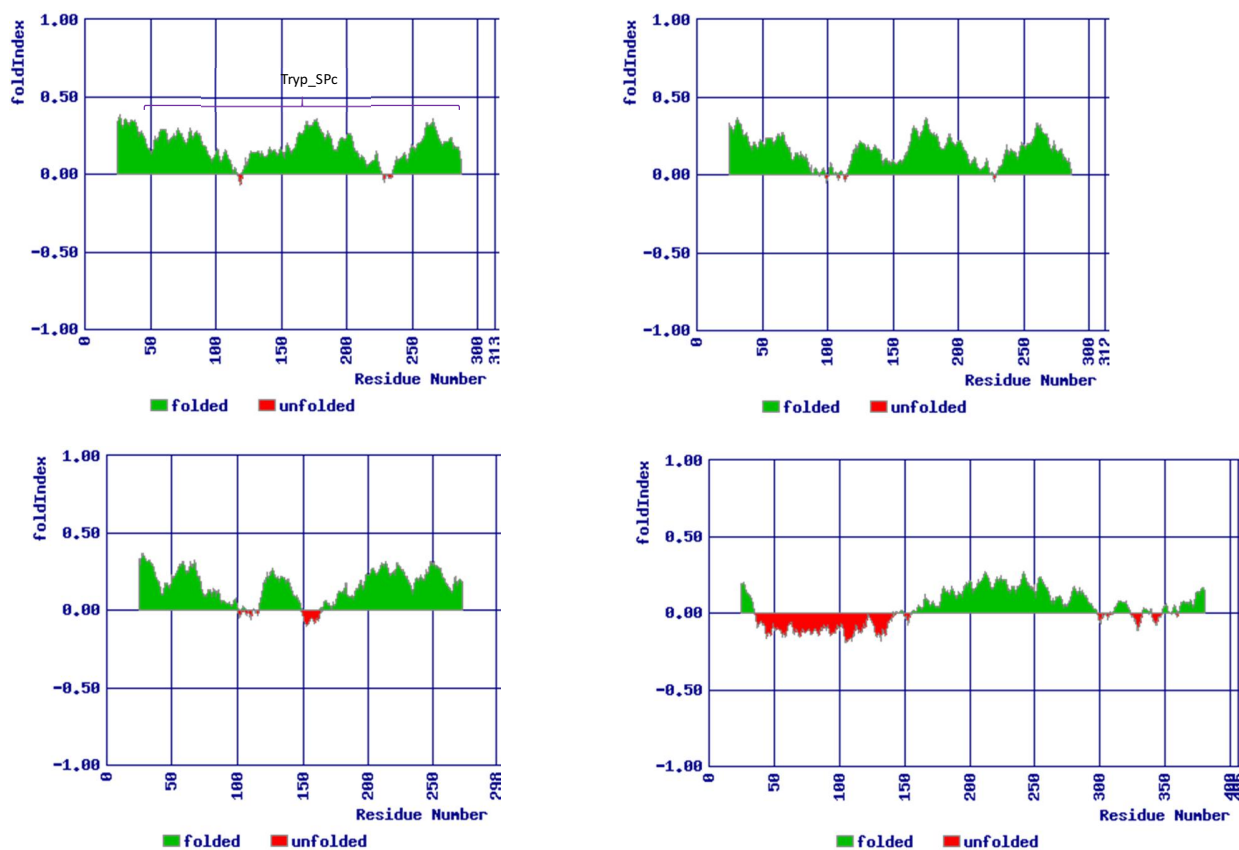


Fig. 28. Graphical representation of FoldIndex®.; (A) RfHp, (B) Nile tilapia Hp, (C) Channel catfish Hp, (D) Human Hp,

Intrinsically unfolded proteins function by undergoing disorder-to-order transition; hence, they have the ability to exert the activity whenever needed, saving the entropic cost for protein ordering to and fro than intrinsically folded proteins (Bracken, 2001). Hence, relatively less disordered nature of the teleostan counterparts compared to human Hp suggests that teleostan Hps may exert relatively less reactivity in their acute phase responses. Moreover, in the case of *H. sapiens*, CCP domains are in the disordered regions reflecting their potential involvement in protein-protein interactions, in which these regions acquire different conformations (Govind et al., 2014).

3.4 Quantitative analysis of tissue-specific expression of *RfHp*

As detected by our qPCR assay, *RfHp* showed universal spatial expression in tissues examined albeit in different magnitudes. During the acute phase of inflammation, many acute-phase proteins are secreted from liver tissue in which they are produced (Kushner, 1982). Showing an agreement with this notion, notable mRNA expression level of *RfHp* was observed in liver tissue. In liver tissue, *RfHp* had an approximate 288,000-fold expression level compared to that in heart tissue. Next to liver, *RfHp* had a higher expression level in testis and gills, exceeding 100 fold, compared to that in heart (Fig.29). Hp was expressed with a minute magnitude in blood. The same expression pattern was reported with mice where Hp was expressed splendidly in liver, but no expression was detected in blood (D'Armiento et al., 1997).

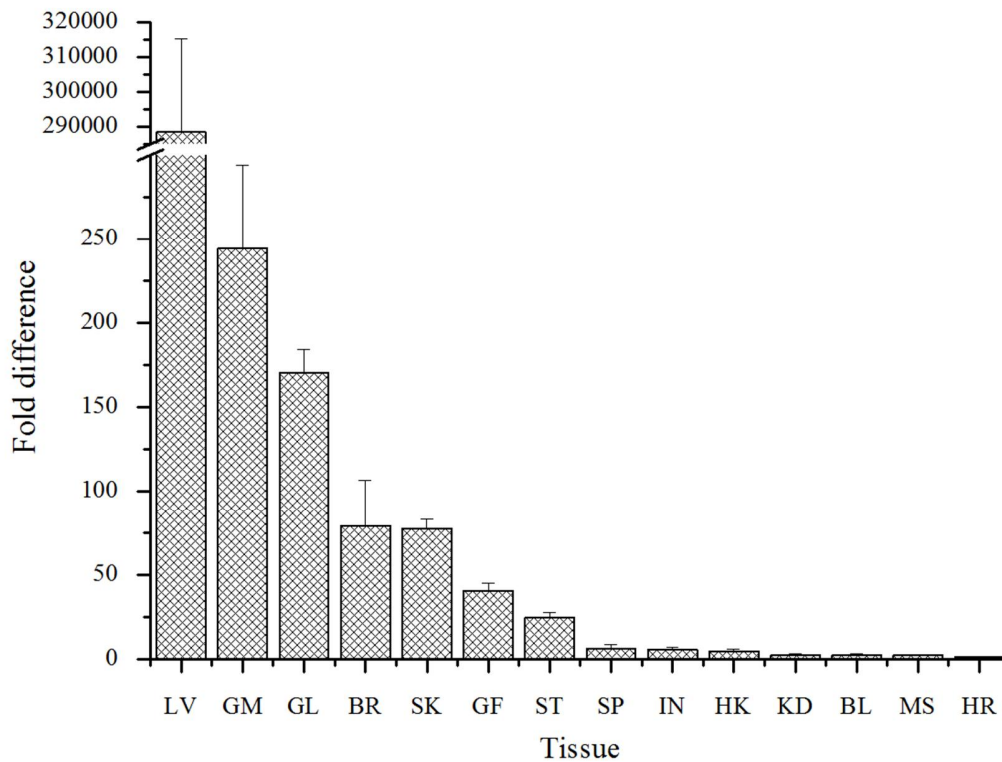


Fig. 29. Tissue specific transcriptional profile of *RfHp* detected in selected tissues by qPCR. BL, blood; GL, gill; LV, liver; SP, spleen; HK, head kidney; KD, kidney; SK, skin; MS, muscle; HR, heart; BR, brain; IN, intestine; ST, stomach; GM, testis; GF, ovary. Data are presented as mean ($n = 3$) \pm SD. *RfHp* - mRNA detected in each tissue by qPCR was normalized to *RfHp* mRNA detected in HR.

3.5. Quantitative analysis of expressional modulation in response to challenge experiments

The mRNA expression level of *RfHp* in liver, spleen, and peripheral blood cells in response to the *S. iniae* and poly I:C treatments were investigated to ascertain their expressional modulation in the acute phase of an infection. In liver tissue, with *S. iniae* challenge, *RfHp* was up-regulated at all the time points relative to the controls (0 h) ($P < 0.05$), and the highest

expression level was detected at 48 h (25 fold) post stimulation (p.s.) (Fig. 30). Interestingly, the up-regulation pattern of *RfHp* appeared to be similar. *RfHp* showed the highest mRNA expression (six fold) in spleen tissue at 48 h after treatment with *S. iniae* (Fig. 30). Interestingly, in the spleen tissue, *RfHp* transcription showed significant downregulation at 3 h p.s. This may be due to the mRNA turnover event that occurred in the spleen tissue during the pathogenic stress (Mitchell and Tollervey, 2001). However, in peripheral blood cells, it showed comparatively less strong transcriptional modulation after *S. iniae* invasion with a slight up-regulation at 12 h p.s. (1.6-fold). Collectively, these observed transcriptional responses show that *RfHp* are positively modulated at a significant level in some of the immune-relevant tissues in the acute phase of a live bacterial infection.

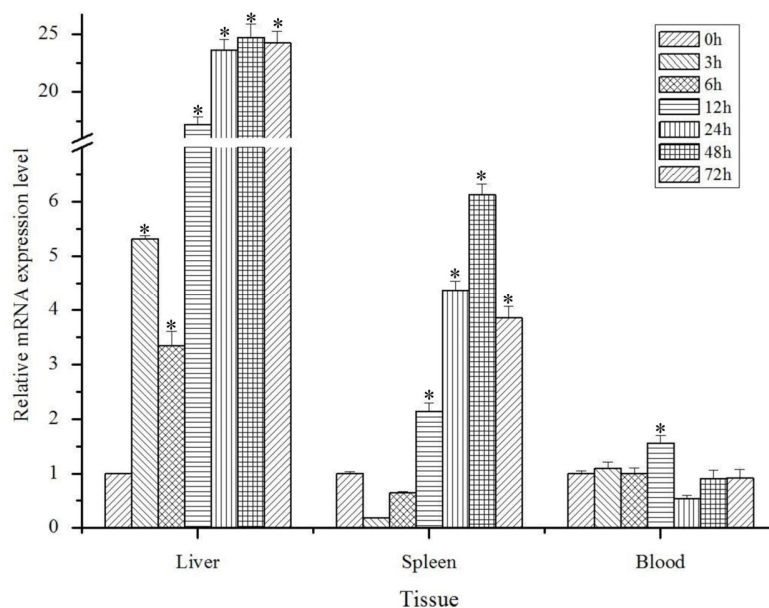


Fig. 30. Expression of *RfHp* after *S.iniae* challenge experiment, detected by qPCR. Data are expressed as mean fold-induction (n = 3) relative to the PBS control \pm SD. * t-test, $p < 0.05$ vs. unchallenged control at 0 h.

Upon stimulation by poly I:C, the liver tissue showed comparatively higher up-regulation of *RfHp* than in spleen and peripheral blood cells (Fig 31). The highest transcriptional inductive response in liver tissue following poly I:C treatment was obtained at 24 h p.s. with respect to (10 fold). In spleen tissue, only *RfHp* showed a slight up-regulation at 6 h p.s. (1.5 fold). However, an initial downregulation was detected after *S. iniae* challenge. In peripheral blood cells, *RfHp* showed a slight up-regulation at 6 h p.s. (1.6 fold) upon poly I:C treatment. Interestingly, the qPCR results for the challenge experiment with poly I:C also suggested that expression of *RfHp* gene can be induced by viral infections.

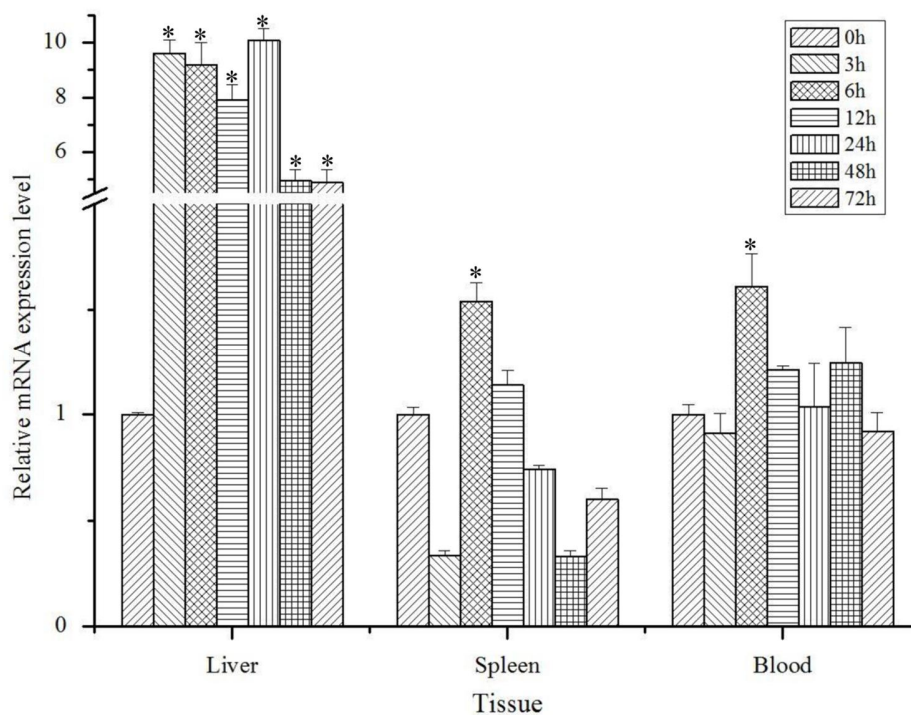


Fig. 31. Expression of *RfHp* after poly I:C treatment, detected by qPCR. Data are expressed as mean fold-induction (n = 3) relative to the PBS control \pm SD. * t-test, $p < 0.05$ vs. unchallenged control at 0 h.

In general, group II acute-phase proteins that carry Hp start to increase in concentration between 24 and 48 h from the beginning of an infection and reach their maximum around 7–10 days (Kushner, 1982; Dancygier, 2010). This is in accordance with the observation that *RfHp* expression is elevated significantly from 3 h onwards in liver tissue by both immune stimuli used in our study. RfHp mRNA expression in liver tissue was elevated by 20 to 25 fold at the late phase after *S. iniae* treatment. Its mRNA expression level in liver tissue was elevated by 10-fold compared to the basal expression following poly I:C challenge. However, *RfHp* has a slightly different transcriptional modulation after an infection than that in mammals, suggesting there are mechanistic differences in triggering the acute phase response in teleosts as compared with mammals subjected to a pathogenic stress.

4. CONCLUSION

In conclusion, full-length cDNA sequence encoding RfHp was identified from black rockfish and molecularly characterized. RfHp was an intrinsically highly folded protein reflecting its relatively less reactivity. The mRNA levels of both genes were highly expressed in the liver tissue. The qPCR analysis of mRNA expression in tissues of immune-challenged animals revealed that both genes are up-regulated in bacterial and poly (I:C) treatment. According to the results, we can suggest that RfHp may act as positive APP in black rockfish. However, further studies are needed, particularly focusing on the tentative functionality of RfHp in host immune defenses.

CHAPTER 2

Identification and molecular characterization of selected role players in host antioxidative defense from Rock bream (*Oplegnathus fasciatus*) portraying their functional significances.

This chapter presents the four separate studies of identification and molecular characterization of Ferritin H subunit, Ferritin M subunit, catalase and thioredoxin reductase 3 homologues from rock bream respectively, demonstrating their functional properties using recombinant proteins and basal expression along with its transient modulation, in response to pathogen stress in selected tissues.

PART A

Characterization of a catalase homologue from Rock bream

1. ABSTRACT

Catalases are known to be antioxidant enzymes that can mainly dismutate hydrogen peroxide into water and oxygen in order to prevent oxidative stress. The complete genomic DNA (gDNA) sequence of the catalase gene from rock bream (*Oplegnathus fasciatus*) was identified from our custom-constructed BAC genomic DNA library and designated as *RbCat*. *RbCat* consists of 13 exons, separated by 12 introns, within a 13,722-bp gDNA sequence. The complete cDNA sequence (3,303 bp) of *RbCat* is comprised of a 1,581-bp coding region, encoding a peptide of

527 amino acids (aa) in length, with a predicted molecular mass of 60 kD and a theoretical isoelectric point of 8.34. The anticipated promoter region of *RbCat* contains several transcription factor binding sites, including sites that bind with immune- and antioxidant-responsive signaling molecules, suggesting its substantial transcriptional regulation. RbCat resembles the typical catalase family signature, i.e., it is composed of the catalase proximal active site motif along with a catalase proximal heme-ligand signature motif and shares great homology with its fish counterparts. According to multiple sequence alignment, functionally important aa present in RbCat were thoroughly conserved among its vertebrate counterparts. Phylogenetic analysis revealed that RbCat evolved from a vertebrate origin, and further positioned it in the fish clade. Recombinant RbCat had noticeable peroxidase activity against its substrate, hydrogen peroxide, in a dose-dependent manner. However, it demonstrated substantial peroxidase activity within a broad range of temperatures and pH values. Constitutive RbCat mRNA expression of different magnitudes was detected in a tissue-specific manner, suggesting its diverse role in physiology with respect to the tissue type. Moreover, immune challenge experiments using *Edwardsiella tarda* and rock bream iridovirus (RBIV) as live pathogens and polyinosinic:polycytidylic acid and lipopolysaccharide as mitogens revealed that the transcription of RbCat can be modulated by immune stimulation. Collectively, the results obtained in this study suggest that RbCat can function as a potent antioxidant enzyme in rock bream and may play a role in post-immune responses with respect to its peroxidase activity.

2. MATERIALS AND METHODS

2.1. Construction of rock bream cDNA sequence database

A rock bream cDNA sequence database was established by using the Roche 454 Genome Sequencer FLX System (GS-FLX™), a next-generation DNA sequencing technology using the GS-FLX Titanium instrument (Droege and Hill, 2008). Briefly, total RNA was isolated from pooled tissues (pituitary gland, brain, gill, blood, liver, spleen, head kidney and posterior kidney) of three healthy rock breams by using the Tri Reagent™ (Sigma, USA). Then, the mRNA was purified using an mRNA isolation kit (FastTrack® 2.0; Invitrogen, USA). The first strand cDNA synthesis and normalization were carried out, respectively, with the Creator™ SMART™ cDNA library construction kit (Clontech, USA) and Trimmer cDNA normalization kit (Evrogen, Russia). Thereafter, the sequencing of rock bream cDNA was performed by the Roche GS-FLX™ system (DNA Link, Inc.).

2.2. Identification of the complete cDNA sequence of *RbCat*

The complete cDNA sequence of the catalase gene (*RbCat* - Contig number – 02273) of rock bream was identified using the Basic Local Alignment Search Tool (BLAST) algorithm (<http://blast.ncbi.nlm.nih.gov/Blast.cgi>) from the aforementioned cDNA sequence database.

2.3. Identification of the complete genomic sequence of *RbCat*

A random-shear bacterial artificial chromosome (BAC) library of rock bream genomic DNA was custom-constructed (Lucigen, USA) and used to screen the *RbCat* gene, according to pooling and super pooling strategies, implemented through polymerase chain reaction (PCR), using a sequence-specific primer pair, RbCat-qF and RbCat-qR (Table 12), as described previously (Quiniou et al., 2003). The primers were designed according to the previously

identified *RbCat* (section 2.1) cDNA sequence. The PCR was conducted in a TaKaRa thermal cycler in a total volume of 20 μ L with 0.5 U of Ex Taq polymerase (TaKaRa, Japan), 2 μ L of 10 \times Ex Taq buffer, 1.6 μ L of 2.5 mM dNTPs, 75 ng of template, and 10 pmol of each primer. The reaction was carried out with an initial incubation at 94 $^{\circ}$ C, followed by 35 cycles of 94 $^{\circ}$ C for 30 s, 58 $^{\circ}$ C for 30 s, and 72 $^{\circ}$ C for 30 s. The PCR products were analyzed on a 1.5% agarose gel and the correct location of the BAC clone was detected according to the appearance of the corresponding band. Subsequently, the detected clone was sequenced (GS-FLXTM) in order to obtain the genomic DNA sequence of the *RbCat* gene. The open reading frame of *RbCat* was identified by using a NCBI-BLAST algorithm (<http://www.ncbi.nlm.nih.gov/BLAST>) from the above-confirmed genomic DNA sequence. The nucleotide sequence of the *RbCat* gene was deposited in GenBank under the accession number KC201280.

Table 12. Oligomers used in the study on RbCat

Name	Purpose	Sequence (5' \rightarrow 3')
RbCat-qF	BAC library screening and qRT-PCR of <i>RbCat</i>	TGG CAGGTTACATGGTACGTTTAATGC T
RbCat-qR	BAC library screening and qRT-PCR of <i>RbCat</i>	TTGTGGGCGTCTGCATATCATGAAGA
RbCat-F	ORF amplification (<i>Eco</i> RI)	GAGAGAGaattcATGGCTGACAACAGAGGCAAAGCTAC
RbCat-R	ORF amplification (<i>Hind</i> III)	GAGAGAAagcttTCACAT CTTGGAGGACGCAGCG
Rb- β F	qRT-PCR for rock bream β -actin gene	TCATCACCATCGGCAATGAGAGGT
Rb- β R	qRT-PCR for rock bream β -actin gene	TGATGCTGTTGTAGGTGGTCTCGT

2.4. *In silico* characterization of RbCat

Orthologous sequences of RbCat were compared by using the BLAST search program. Pairwise sequence alignment (<http://www.Ebi.ac.uk/Tools/emboss/align>) and multiple sequence alignment (<http://www.Ebi.ac.uk/Tools/clustalw2>) were performed using the EMBOSS Needle

and ClustalW2 programs, respectively. The phylogenetic relationship of RbCat was determined by using the neighbor-joining method and Molecular Evolutionary Genetics Analysis (MEGA) software version 4 (Tamura et al., 2007). Protein domains were predicted by using the ExPASy prosite database (<http://prosite.expasy.org>), MotifScan scanning algorithm (http://myhits.isb-sib.ch/cgi-bin/motif_scan), and the NCBI-CDS server (Marchler-Bauer et al., 2009). Some properties of RbCat were determined by using the ExPASy ProtParam tool (<http://web.expasy.org/protparam>). Moreover, the tertiary structure of RbCat was predicted on the basis of the iterative assembly simulation strategy using the I-TASSER online server (Zhang, 2008; Roy et al., 2010) and three-dimensional (3D) images were generated using RasMol 2.7.5.2 software (Goodsell, 2005).

The genomic sequence of RbCat, identified from the BAC clone, was used to identify the genomic architecture revealing the exon-intron arrangement and tentatively derive the promoter region, along with potential transcriptional factor-binding sites. The transcription initiation site (TIS) was predicted using the neural network promoter prediction tool from the Berkeley Drosophila Genome Project (Reese, 2001), and potential *cis*-acting elements around 1 kb upstream of TIS was detected using TFSEARCH ver.1.3 and Alibaba 2.1 software.

2.5. Expression and purification of recombinant RbCat (rRbCat)

Recombinant RbCat was expressed as a fusion protein with the maltose binding protein (MBP) and purified using the pMAL protein fusion and purification system (New England Biolabs, USA) according to the vendor's protocol. Briefly, the open reading frame of the *RbCat* gene was amplified using the sequence-specific primers RbCat-F and RbCat-R with restriction enzyme sites for *Eco*RI and *Hind*III, respectively (Table 12). The PCR was performed in a

TaKaRa thermal cycler in a total volume of 50 μ L with 5 U of ExTaq polymerase (TaKaRa, Japan), 5 μ L of 10 \times Ex Taq buffer, 8 μ L of 2.5 mM dNTPs, 80 ng of template, and 20 pmol of each primer. The reaction was carried out at 94 $^{\circ}$ C for 30 s, 58 $^{\circ}$ C for 30 s, and 72 $^{\circ}$ C for 1 min, followed by a final extension step at 72 $^{\circ}$ C for 5 min. The PCR product (\sim 1.6 kbp) was resolved on a 1% agarose gel, excised, and purified using the AccuprepTM gel purification kit (Bioneer Co., Korea). The digested pMAL-c2X vector (150 ng) and PCR product (180 ng) were ligated using Mighty Mix (7.5 μ L; TaKaRa) at 4 $^{\circ}$ C overnight. The ligated pMAL-c2X/RbCat product was transformed into DH5 α cells and sequenced. The Sequence-confirmed recombinant expression plasmid was transformed into *Escherichia coli* BL21 (DE3) competent cells. The rRbCat protein was overexpressed using isopropyl- β -galactopyranoside (IPTG, 1 mM final concentration) at 20 $^{\circ}$ C for 8 h. Induced *E. coli* BL21 (DE3) cells were then cooled on ice for 30 min and harvested by centrifugation at 3500 rpm for 30 min at 4 $^{\circ}$ C. Harvested cells were resuspended in 20 mL of column buffer (20 mM Tris-HCl pH 7.4 and 200 mM NaCl) and stored at -20 $^{\circ}$ C. *E. coli* cells were thawed and lysed in column buffer using cold sonication. The protein was then purified using the pMALTM Protein Fusion and Purification System (New England BioLabs, Beverly, MA, USA). The purified protein was eluted using an elution buffer (10 mM maltose in column buffer). Subsequently the concentration of the eluted protein was determined by the 'Bradford method' using bovine serum albumin as a standard (Bradford, 1976). The purified fusion protein (rRfCat) was then assayed for peroxidase activity and the ability to inhibit oxidative DNA damage. Samples collected at different steps of the rRfCat purification were analyzed by 12% sodium dodecyl sulfate polyacrylamide gel electrophoresis (SDS-PAGE) using standard protein size markers (Enzymomics, Korea) under reducing conditions. The gel was

stained with 0.05% Coomassie blue R-250 and observed followed by a standard destaining procedure.

2.6. Analysis of antioxidant activity of rRbCat

In order to functionally characterize rRbCat, the peroxidase activity of rRbCat fusion protein was analyzed using a gradient of different concentrations of the protein, according to a previous report, with some modifications (Muller, 1985). Briefly, 50 μL rRbCat (containing different amounts of protein at each time) was dissolved in 70 μL of phosphate buffer (0.05 M, pH 5) with 20 μL of 10 mM H_2O_2 in a 96-microwell plate and incubated at 37 $^\circ\text{C}$ for 5 min. Subsequently, 30 μL of 1.25 mM 2,2-Azino-bis (ABTS; 3-ethylbenzthiazolin-6-sulfonic acid) and 30 μL of peroxidase (1 U/mL) were added to the mixture and the mixture was again incubated at 37 $^\circ\text{C}$ for 10 min. As a result of the incubation of ABTS with peroxidase, a blue-green colored cationic radical of ABTS is produced, which can be spectrophotometrically detected at 405 nm. The enzyme assay was performed in triplicates and the mean values were considered for the final calculation. One unit of catalase activity was defined as the amount of catalase required to decompose 1.0 μmol of H_2O_2 per min under the applied assay conditions. In each assay, MBP was used as positive control to determine the effect of fusion on the activity of rRbCat. Blanks were prepared in a similar manner without adding the protein, while a constant volume was maintained by increasing the volume of phosphate buffer accordingly.

2.7. Evaluation of the biochemical properties of rRbCat

To characterize the enzymatic activity of rRbCat with respect to the reaction temperature and pH, an antioxidant assay for RbCat, described in the above section, was carried out using 25

μg of protein under different temperature and pH conditions. The activity was calculated as percentage activity, considering the difference in the optical density (OD) at 405 nm of the corresponding reaction mixtures of sample and negative control (without protein), relative to the OD₄₀₅ of the negative control. In order to analyze the temperature dependency, the reaction was performed at temperatures ranging from 10 °C to 80 °C in 10 °C intervals. However, instead of 40 °C, 37 °C was used, since it was the previously mentioned optimal temperature for the reaction in the standard procedure. Similarly, the standard peroxidase reaction catalyzed by rRbCat was employed under different pH conditions. A pH gradient was obtained using acetate, phosphate, and glycine-NaOH buffers of different pH values, ranging from pH 4.5 to 9.5 in 0.5 pH intervals.

2.8. Experimental fish and tissue collection

Rock breams, with an average body weight of 30 g, were obtained from the Jeju Special Self-Governing Province Ocean and Fisheries Research Institute (Jeju, Republic of Korea). The fish were maintained in a controlled environment at 22–24 °C and acclimatized for 1 week prior to experimentation. During this period fish were daily fed with commercially available feed. Whole blood (~1 mL/fish) was collected from the caudal fin using a sterilized syringe, and the sample was immediately centrifuged at $3,000 \times g$ for 10 min at 4 °C to separate the blood cells from the plasma. The collected cells were snap-frozen in liquid nitrogen. Meanwhile, the sampled fish was dissected and gill, liver, skin, spleen, head kidney, kidney, skin, muscle, brain, intestine, and heart were excised, immediately snap-frozen in liquid nitrogen, and stored at -80 °C until use for total RNA extraction.

2.9. Immune challenge experiments

In order to determine the changes in the transcription of *RbCat* upon live pathogen infection and pathogen derived mitogen stimulation, *E. tarda* and RBIV along with LPS, and poly I:C were employed as immune stimulants in time-course immune challenge experiments, respectively. Blood cells were collected as described in section 2.7. For chemical challenge, each rock bream was administered a single intraperitoneal (i.p.) injection of 100 μ L LPS in phosphate buffered saline (PBS) suspension (1.25 μ g/ μ L, *E. coli* 055:B5; Sigma) or 100 μ L poly I:C in PBS suspension (1.5 μ g/ μ L; Sigma). For the bacterial-challenge experiment, *E. tarda* was obtained from the Department of Aqualife Medicine, Chonnam National University, Korea. The bacteria were incubated at 25 $^{\circ}$ C for 12 h using a brain heart infusion (BHI) broth (Eiken Chemical Co., Japan) supplemented with 1% sodium chloride. The cultures were resuspended in sterile PBS, and then diluted to a desired concentration. Each rock bream was i.p. injected with 100 μ L live *E. tarda* in PBS (5×10^3 CFU/ μ L) or 100 μ L live *S. iniae* in PBS (1×10^5 CFU/ μ L). For the virus challenge experiment, kidney tissue specimens obtained from the moribund rock bream infected with rock bream iridovirus (RBIV) were homogenized in 20 volumes of PBS. The tissue homogenate was centrifuged at $3000 \times g$ for 10 min at 4 $^{\circ}$ C, and the supernatant of a RBIV sample was filtered through a 0.45 μ m membrane. Each rock bream was then infected with a single i.p. injection of 100 μ L RBIV in PBS. A control group was injected with an equal volume (100 μ L) of PBS. Rock bream blood samples were collected at 3, 6, 12, 24 and 48 h post-injection (p.i.) from LPS-, poly I:C-, *E. tarda*, or RBIV-infected rock breams. PBS-injected control samples were isolated at 3 h and 48 h p.i. Three replicate rock breams were obtained for each time point and the pooled tissues from each group were subjected to total RNA extraction and cDNA synthesis according to the procedure described in Section 2.10.

2.10. Total RNA extraction and cDNA synthesis

Total RNA was extracted by using Tri ReagentTM (Sigma) from blood, gill, liver, spleen, head kidney, kidney, skin, muscle, brain, intestine, and heart from healthy rock breams along with blood cells from immune-challenged animals. Subsequently, cDNA was synthesized from each set of RNA as described previously (Whang et al., 2011a) according to the manufacturer's protocols.

2.11. *RbCat* transcriptional analysis by reverse transcription PCR followed by quantitative real time PCR

qPCR was used to analyze the expression levels of *RbCat* in all tissues mentioned in section 2.9, collected from healthy animals and the temporal expression of *RbCat* in blood. Subsequent to the cDNA synthesis using the total RNA extracted from each tissue, qRT-PCR was carried out using the thermal cycler DiceTM Real Time System (TP800; TaKaRa, Japan). The reaction was conducted in a 15 μ L reaction volume containing 4 μ L of diluted cDNA from each tissue, 7.5 μ L of $2 \times$ TaKaRa Ex TaqTM, SYBR premix, 0.6 μ L of each primer (*RbCat*-qF and *RbCat*-qR; Table 12), and 2.3 μ L of ddH₂O. The qPCR was performed under the following conditions: 95 °C for 10 s, followed by 35 cycles of 95 °C for 5 s, 58 °C for 10 s, and 72 °C for 20 s, and a final cycle of 95 °C for 15 s, 60 °C for 30 s, and 95 °C for 15 s. The base line was set automatically by the DiceTM Real Time System software (version 2.00). *RbCat* expression was determined by applying the Livak ($2^{-\Delta\Delta CT}$) method (Livak and Schmittgen, 2001). The same qPCR cycle profile was used for the internal control gene, rock bream β -actin (GenBank ID:FJ975145), using respective oligomers (Table 12). All data are presented as mean \pm standard deviation (SD) of the relative mRNA expression of 3 replicates. To determine statistical

significance ($P < 0.05$) between the experimental and control groups, a two-tailed paired t-test was carried out.

3. RESULTS AND DISCUSSION

3.1 Sequence characterization and phylogenetic relationship of RbCat

The complete cDNA sequence of *RbCat* consists of 3,303 bp nucleotides, which comprises a 1,581-bp coding sequence, encoding a peptide of 527 amino acids, a 293-bp 5'-untranslated region (5'-UTR), and a 1,429-bp 3'-UTR. The predicted molecular mass of RbCat was around 60 kD, complying with that of other known catalases (Scibior and Czczot, 2006), and the theoretical isoelectric point was 8.34. According to the *in-silico* predictions, RbCat resembled the typical catalase family signature, containing catalase proximal active site motif (64–81) and catalase proximal heme-ligand signature motif (354–361) (Fig. 32), which are known to be highly conserved motifs in most catalases (Moreira et al., 2004). In addition, well conserved potential heme-binding sites (H₇₅, F₁₁₃, N₁₄₈, F₁₅₃, F₁₆₁, R₃₅₄, Y₃₅₈) and NADPH-binding residues (P₁₅₁, H₁₉₄, F₁₉₈, S₂₀₁, R₂₀₃, N₂₁₃, H₂₃₅, K₂₃₇, W₃₀₃, H₃₀₅) were also present in the derived amino acid sequence of RbCat, as anticipated by NCBI-CDS server (Fig. 32). These binding sites render antioxidant protection from its substrate, H₂O₂, on the surface and within the enzyme (Chelikani et al., 2004).

Chicken MADGRDVAEQLKRWQSQRGSKPDAITTGAGNPIGDKLNITVGPGRGILLVQDVVFTDE 60
 Lizard MAGGRDYADDQMRWQDQRGSKADALITGAGLPVGGDKLNLITVGPGRGILLVQDVVFTDE 60
 Frog MADKRDMAADQMKLWNGRGSQRDPVLTITGGGNPISDKLNIMLTAGSRGILLVQDVVFTDE 60
 Mouse MSDSRDPSADQMKWKEQRASQRDPVLTITGGGNPISDKLNIMLTAGSRGILLVQDVVFTDE 60
 Human MADSRDPSADQMKWKEQRASQRDPVLTITGAGNPIGDKLNITVGPGRGILLVQDVVFTDE 60
Rock bream MADNRCKATDMQKTWKENRSQRDPVLTITGAGHVPQDKLNITVGPGRGILLVQDVVFTDE 60
 Cobia MADNRDKTDMQKLWKEQRASQRDPVLTITGAGHVPQDKLNITVGPGRGILLVQDVVFTDE 60
 Mefugu MADKRDKATDMQKLWKEGRGYPDIITGGGHPISDKLNITVGPGRGILLVQDVVFTDE 59
 Zebrafish MADDRKSTDMQKLWKEGRGSRDPVLTITGAGVPIGDKNAMTAPGRGILLVQDVVFTDE 60
 Atlantic salmon MDEDRKATDMQKLWKENRRAQRDPVLTITGAGHPISDKLNITVGPGRGILLVQDVVFTDE 60

Chicken MAHFDREIRIPERVVHAKGAGAFGYFEVTHDITRYCKAKVFEHIGKRTPIAVRESTVAGES 120
 Lizard MAHFDREIRIPERVVHAKGAGAFGYFEVTHDITRYCKAKVFEHIGKRTPIAVRESTVAGEA 120
 Frog MAHFDREIRIPERVVHAKGAGAFGYFEVTHDITRYCKAKVFEHIGKRTPIAVRESTVAGEA 120
 Mouse MAHFDREIRIPERVVHAKGAGAFGYFEVTHDITRYCKAKVFEHIGKRTPIAVRESTVAGES 120
 Human MAHFDREIRIPERVVHAKGAGAFGYFEVTHDITRYCKAKVFEHIGKRTPIAVRESTVAGES 120
Rock bream MAHFDREIRIPERVVHAKGAGAFGYFEVTHDITRYCKAKVFEHIGKRTPIAVRESTVAGES 120
 Cobia MAHFDREIRIPERVVHAKGAGAFGYFEVTHDITRYCKAKVFEHIGKRTPIAVRESTVAGES 120
 Mefugu MAHFDREIRIPERVVHAKGAGAFGYFEVTHDITRYCKAKVFEHIGKRTPIAVRESTVAGES 119
 Zebrafish MAHFDREIRIPERVVHAKGAGAFGYFEVTHDITRYCKAKVFEHIGKRTPIAVRESTVAGEA 120
 Atlantic salmon MAHFDREIRIPERVVHAKGAGAFGYFEVTHDITRYCKAKVFEHIGKRTPIAVRESTVAGES 120

Chicken GSADTVRDPGFAMKYFTTEGNWDLGNNTHIEFIRDALMPEPSFHSQKRNPTHLKDDP 180
 Lizard GSADTVRDPGFAMKYFTTEGNWDLGNNTHIEFIRDALMPEPSFHSQKRNPTHLKDDP 180
 Frog GSSDTRVDRP GFAMKYFTTEGNWDLGNNTHIEFIRDALMPEPSFHSQKRNPTHLKDDP 180
 Mouse GSADTVRDPGFAMKYFTTEGNWDLGNNTHIEFIRDALMPEPSFHSQKRNPTHLKDDP 180
 Human GSADTVRDPGFAMKYFTTEGNWDLGNNTHIEFIRDALMPEPSFHSQKRNPTHLKDDP 180
Rock bream GSADTVRDPGFAMKYFTTEGNWDLGNNTHIEFIRDALMPEPSFHSQKRNPTHLKDDP 180
 Cobia GSADTVRDPGFAMKYFTTEGNWDLGNNTHIEFIRDALMPEPSFHSQKRNPTHLKDDP 180
 Mefugu GSADTVRDPGFAMKYFTTEGNWDLGNNTHIEFIRDALMPEPSFHSQKRNPTHLKDDP 179
 Zebrafish GSSDTRVDRP GFAMKYFTTEGNWDLGNNTHIEFIRDALMPEPSFHSQKRNPTHLKDDP 180
 Atlantic salmon GSADTVRDPGFAMKYFTTEGNWDLGNNTHIEFIRDALMPEPSFHSQKRNPTHLKDDP 180

Chicken MVWDFSLRPESLHOVSFLESIDRGLDPGHRMNYGSHTFKLVNAGGAVYCKEFLRQDQ 240
 Lizard MVWDFSLRPESLHOVSFLESIDRGLDPGHRMNYGSHTFKLVNAGGAVYCKEFLRQDQ 240
 Frog MVWDFSLRPESLHOVSFLESIDRGLDPGHRMNYGSHTFKLVNAGGAVYCKEFLRQDQ 240
 Mouse MVWDFSLRPESLHOVSFLESIDRGLDPGHRMNYGSHTFKLVNAGGAVYCKEFLRQDQ 240
 Human MVWDFSLRPESLHOVSFLESIDRGLDPGHRMNYGSHTFKLVNAGGAVYCKEFLRQDQ 240
Rock bream MVWDFSLRPESLHOVSFLESIDRGLDPGHRMNYGSHTFKLVNAGGAVYCKEFLRQDQ 240
 Cobia MVWDFSLRPESLHOVSFLESIDRGLDPGHRMNYGSHTFKLVNAGGAVYCKEFLRQDQ 240
 Mefugu MVWDFSLRPESLHOVSFLESIDRGLDPGHRMNYGSHTFKLVNAGGAVYCKEFLRQDQ 239
 Zebrafish MVWDFSLRPESLHOVSFLESIDRGLDPGHRMNYGSHTFKLVNAGGAVYCKEFLRQDQ 240
 Atlantic salmon MVWDFSLRPESLHOVSFLESIDRGLDPGHRMNYGSHTFKLVNAGGAVYCKEFLRQDQ 240

Chicken GIKNLSVEEAARLASTDPDYGIRDLNLIANGNYPSSWFYIQVMTFQAEKRFENFDLIT 300
 Lizard GIKNLSVEEAARLASTDPDYGIRDLNLIANGNYPSSWFYIQVMTFQAEKRFENFDLIT 300
 Frog CIQNLTVDEANRLASDDPDYGIHDLIYAITTNYPSSWFYIQVMTFQAEKRFENFDLIT 300
 Mouse GIKNLPVGEAARLAQEDPDYGIHDLIYAITTNYPSSWFYIQVMTFQAEKRFENFDLIT 300
 Human GIKNLSVEEAARLASTDPDYGIRDLNLIANGNYPSSWFYIQVMTFQAEKRFENFDLIT 300
Rock bream GIKNLSVEEAARLASTDPDYGIRDLNLIANGNYPSSWFYIQVMTFQAEKRFENFDLIT 300
 Cobia GIKNLSVEEAARLASTDPDYGIRDLNLIANGNYPSSWFYIQVMTFQAEKRFENFDLIT 300
 Mefugu GIKNLSVEEAARLASTDPDYGIRDLNLIANGNYPSSWFYIQVMTFQAEKRFENFDLIT 299
 Zebrafish GIKNLSVEEAARLASTDPDYGIRDLNLIANGNYPSSWFYIQVMTFQAEKRFENFDLIT 300
 Atlantic salmon GIKNLPEDAARLASTDPDYGIRDLNLIANGNYPSSWFYIQVMTFQAEKRFENFDLIT 300

Chicken KIPVPEADYPLIPVGVKIVLNRRPNVYFAEVGLAEDFDSNMPGGIPEPDRMKLQGLFLAPD 360
 Lizard KIPVPEADYPLIPVGVKIVLNRRPNVYFAEVGLAEDFDSNMPGGIPEPDRMKLQGLFLAPD 360
 Frog KIPVPEADYPLIPVGVKIVLNRRPNVYFAEVGLAEDFDSNMPGGIPEPDRMKLQGLFLAPD 360
 Mouse KIPVPEADYPLIPVGVKIVLNRRPNVYFAEVGLAEDFDSNMPGGIPEPDRMKLQGLFLAPD 360
 Human KIPVPEADYPLIPVGVKIVLNRRPNVYFAEVGLAEDFDSNMPGGIPEPDRMKLQGLFLAPD 360
Rock bream KIPVPEADYPLIPVGVKIVLNRRPNVYFAEVGLAEDFDSNMPGGIPEPDRMKLQGLFLAPD 360
 Cobia KIPVPEADYPLIPVGVKIVLNRRPNVYFAEVGLAEDFDSNMPGGIPEPDRMKLQGLFLAPD 360
 Mefugu KIPVPEADYPLIPVGVKIVLNRRPNVYFAEVGLAEDFDSNMPGGIPEPDRMKLQGLFLAPD 359
 Zebrafish KIPVPEADYPLIPVGVKIVLNRRPNVYFAEVGLAEDFDSNMPGGIPEPDRMKLQGLFLAPD 360
 Atlantic salmon KIPVPEADYPLIPVGVKIVLNRRPNVYFAEVGLAEDFDSNMPGGIPEPDRMKLQGLFLAPD 360

Chicken THIRRLGPNYLQIPVNCPRRVRVANYQRDPMCSVNDQGGAPNYNSFTGPEQPVLE 420
 Lizard THIRRLGPNYLQIPVNCPRRVRVANYQRDPMCSVNDQGGAPNYNSFTGPEQPVLE 420
 Frog THIRRLGPNYLQIPVNCPRRVRVANYQRDPMCSVNDQGGAPNYNSFTGPEQPVLE 420
 Mouse THIRRLGPNYLQIPVNCPRRVRVANYQRDPMCSVNDQGGAPNYNSFTGPEQPVLE 420
 Human THIRRLGPNYLQIPVNCPRRVRVANYQRDPMCSVNDQGGAPNYNSFTGPEQPVLE 420
Rock bream THIRRLGPNYLQIPVNCPRRVRVANYQRDPMCSVNDQGGAPNYNSFTGPEQPVLE 420
 Cobia THIRRLGPNYLQIPVNCPRRVRVANYQRDPMCSVNDQGGAPNYNSFTGPEQPVLE 420
 Mefugu THIRRLGPNYLQIPVNCPRRVRVANYQRDPMCSVNDQGGAPNYNSFTGPEQPVLE 419
 Zebrafish THIRRLGPNYLQIPVNCPRRVRVANYQRDPMCSVNDQGGAPNYNSFTGPEQPVLE 420
 Atlantic salmon THIRRLGPNYLQIPVNCPRRVRVANYQRDPMCSVNDQGGAPNYNSFTGPEQPVLE 420

Chicken SRMSVSGDVQRESSANEDVSVQRDFYLKVLKEDERQRLCNIADHLKDAQLFIQKRRAV 480
 Lizard TRANIISGVQRESANEDVSVQRDFYLKVLKEDERQRLCNIADHLKDAQLFIQKRRAV 480
 Frog HRFQVSADVARYNSDEENVTVQRTFVYVNLSEQRIRLCENIAGHLKDAQLFIQKRRAV 480
 Mouse HSVQCAVDVARYNSDEENVTVQRTFVYVNLSEQRIRLCENIAGHLKDAQLFIQKRRAV 480
 Human HSIQSGVRRRENTANDDNVTVQRTFVYVNLSEQRIRLCENIAGHLKDAQLFIQKRRAV 480
Rock bream SKFKVSPDVARYNSDEENVTVQRTFVYVNLSEQRIRLCENIAGHLKDAQLFIQKRRAV 480
 Cobia SKFKVSPDVARYNSDEENVTVQRTFVYVNLSEQRIRLCENIAGHLKDAQLFIQKRRAV 480
 Mefugu SKFKVSPDVARYNSDEENVTVQRTFVYVNLSEQRIRLCENIAGHLKDAQLFIQKRRAV 479
 Zebrafish SKFKVSPDVARYNSDEENVTVQRTFVYVNLSEQRIRLCENIAGHLKDAQLFIQKRRAV 480
 Atlantic salmon TRFKVSPDVARYNSDEENVTVQRTFVYVNLSEQRIRLCENIAGHLKDAQLFIQKRRAV 480

Chicken NFDVHPDYGARIQALLDKYNAEAGKKVIRTYYTQATSRVSAKERSNL 528
 Lizard NFDVHPDYGARIQALLDKYNAEAGKKVIRTYYTQATSRVSAKERSNL 527
 Frog NFDVHPDYGARIQALLDKYNAEAGKKVIRTYYTQATSRVSAKERSNL 528
 Mouse NFDVHPDYGARIQALLDKYNAEAGKKVIRTYYTQATSRVSAKERSNL 527
 Human NFDVHPDYGARIQALLDKYNAEAGKKVIRTYYTQATSRVSAKERSNL 527
Rock bream NLKAIHPDYGNRVQTLNKNYNAEAKSSTVRRVYRPGASATAAASKM 527
 Cobia NLKAIHPDYGNRVQTLNKNYNAEAKSSTVRRVYRPGASATAAASKM 527
 Mefugu NLKAIHPDYGNRVQTLNKNYNAEAKSSTVRRVYRPGASATAAASKM 526
 Zebrafish NLMAVHSYGNRVQTLNKNYNAEAKSSTVRRVYRPGASATAAASKM 526
 Atlantic salmon NLMAVHSYGNRVQTLNKNYNAEAKSSTVRRVYRPGASATAAASKM 524

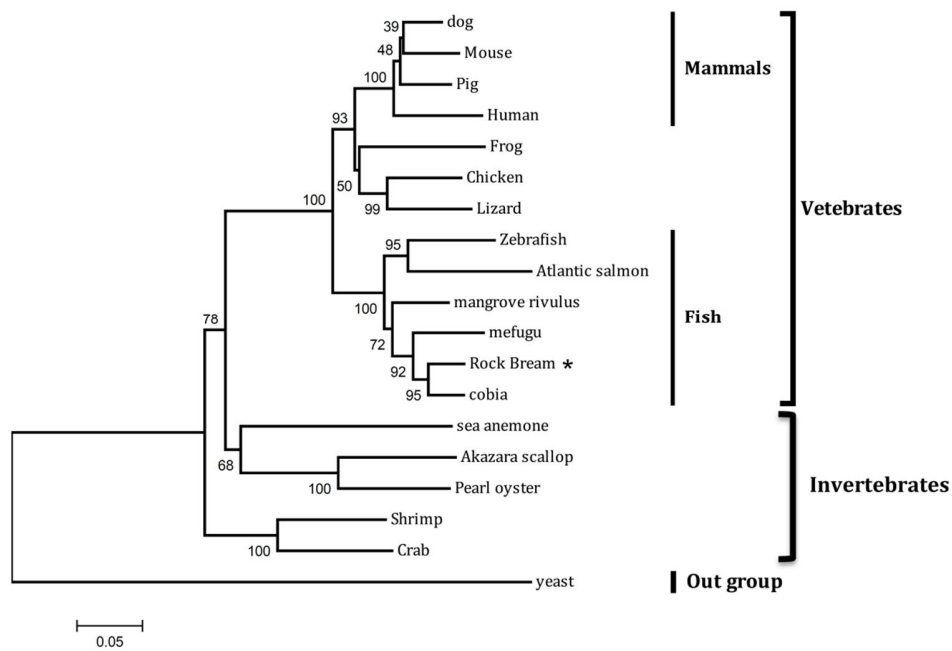
Fig. 32. Multiple sequence alignment of rock bream catalase (RbCat) with its vertebrate counterparts. Sequence alignment was obtained using Clustal-W method. The conserved catalase proximal active site motifs (64–81) and proximal heme-ligand signature motifs (354–361) among the species were denoted by red color boxes, while the corresponding sequence in RbCat is indicated using double underlining and pattern underlining, respectively. Conserved heme-binding sites were shaded in gray color and NADPH-binding sites were boxed separately.

According to the results from pair wise sequence alignment, RbCat shared greatest identity (94.1%) and similarity (97.2%) with its vertebrate counterpart from *Rachycentron canadum* (Cobia), whereas the lowest identity value (66%) and similarity value (77.4%) was shown with its invertebrate counterpart from *Eisenia fetida* (worm) (Table 13), validating RbCat as a vertebrate ortholog of catalases.

- 1 **Table 13.** Percentage similarity and identity values of RbCat with its orthologs. Accession numbers of chicken and anole lizard
- 2 catalases protein sequences were obtained from Ensemble and EMBL databases, respectively, and the remaining ones were extracted
- 3 from NCBI-GenBank sequence database.

Species	Accession Number	Amino acids	Identity (%)	Similarity (%)
1. <i>Rachycentron canadum</i> (Cobia)	ACO07305	527	94.1	97.2
2. <i>Takifugu obscurus</i> (Mefugu)	ABV24056	526	89.4	93.7
3. <i>Kryptolebias marmoratus</i> (Mangrove rivulus)	ABW88893	514	88.2	93.4
4. <i>Danio rerio</i> (Zebrafish)	AAF89686	526	86.3	93.5
5. <i>Salmo salar</i> (Atlantic salmon)	ACN11170	524	83.9	92.6
6. <i>Mus musculus</i> (Mouse)	AAA66054	527	80.3	88.7
7. <i>Canis lupus familiaris</i> (Dog)	BAB20764	527	80.3	88.5
8. <i>Sus scrofa</i> (Pig)	NP999466	527	80.5	87.9
9. <i>Homo sapiens</i> (Human)	AAK29181	527	77.3	86.7
10. <i>Xenopus laevis</i> (Frog)	ABK62836	528	77.5	86.6
11. <i>Gallus gallus</i> (Chicken)	ENSGALP00000023319	528	78.1	87.7
12. <i>Anolis carolinensis</i> (Anole lizard)	ENSACAP00000013065	527	77.8	86.7
13. <i>Chlamys farreri</i> (<i>Akazara scallop</i>)	ABI64115	507	66.2	78.6
14. <i>Fenneropenaeus chinensis</i> (Shrimp)	ABW82155	520	67.0	78.1
15. <i>Pinctada fucata</i> (Pearl oyster)	ADW08700	512	67.0	78.7
16. <i>Scylla paramamosain</i> (Crab)	ACX46120	517	67.3	78.8
17. <i>Anemonia viridis</i> (Sea anemone)	AAZ50618	509	67.9	78.0
18. <i>Eisenia fetida</i> (worm)	AEO50756	505	66.0	77.4

4 In order to evaluate the evolutionary relationship of RbCat with its vertebrate and invertebrate
 5 counterparts, a phylogenetic analysis was carried out. As depicted in Fig. 33, there were 2 main
 6 independent clusters in the generated tree diagram as expected, vertebrates and invertebrates.
 7 Interestingly, RbCat was grouped in the vertebrate cluster, further subclustered into the fish
 8 showing a close evolutionary proximity with the catalase counterpart of cobia fish, exhibiting a
 9 prominent bootstrap value (95). This pattern of clustering indicates that RbCat evolved from a
 10 common vertebrate ancestral origin of catalases, further affirming its diversification from
 11 mammalian, avian, and amphibian counterparts.



12

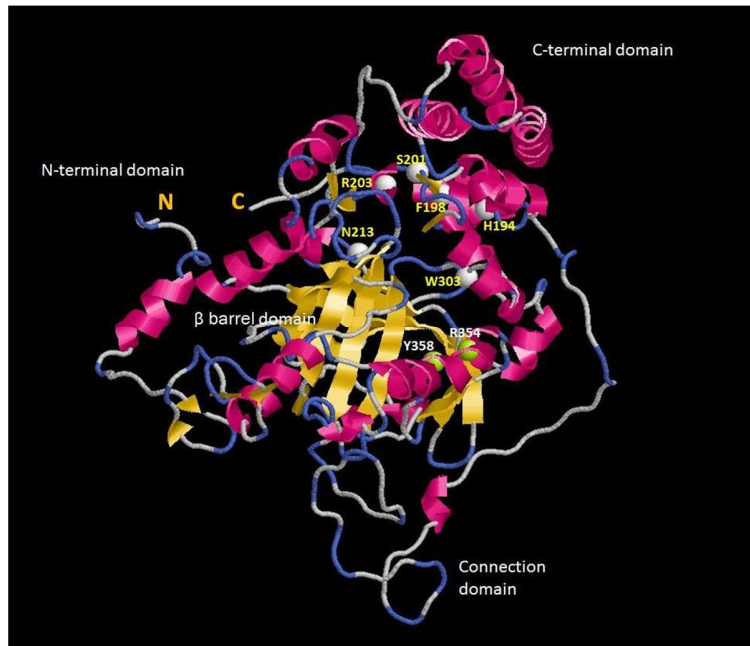
13 **Fig. 33.** Phylogenetic tree construct generated on the basis of ClustalW alignment of the deduced
 14 amino acid sequences of various catalase protein sequences, estimated by using the neighbor-
 15 joining method in MEGA version 4.0. Bootstrap values are shown on the lineages of the tree and
 16 NCBI and Ensemble accession numbers of the respective sequences are given in Table 13.

17 3.2. Modeled tertiary structure of RbCat

18 In order to correlate the function of RbCat with its structural properties, the 3D structure
19 of RbCat was modeled using the ab-initio protein prediction strategy. The model represented
20 valuable information on the arrangement of its functionally important residues in 3D space. The
21 top ten catalase template structures obtained from the Research Collaboratory for Structural
22 Bioinformatics (RCSB) protein data bank exhibited 42% to 78% identity with the query
23 sequences, while normalized Z-scores of the threading alignment of each sequence exceeded 1
24 (3.39–4.47). These parameters, calculated by the server program, substantially affirm the
25 reliability of the predicted model.

26 Resembling the tertiary structure of human catalase, four conceptual domains were identified in
27 the generated model of RbCat. They were designated as N-terminal domain that forms an
28 extended non-globular amino-terminal arm, C-terminal domain that bears four α -helices, anti-
29 parallel octa-stranded β -barrel domain, and connection domain forming a folding loop (Fig. 34),
30 validating RbCat as a novel counterpart of the human catalase enzyme (Putnam et al., 2000).
31 Moreover, some of the amino acid residues present in the heme-binding sites (R₃₅₄ and Y₃₅₈) and
32 important in the NADPH-binding sites (H₁₉₄, F₁₉₈, S₂₀₁, R₂₀₃, N₂₁₃, W₃₀₃) and noticed in our
33 generated model structure were compatible with those of the human catalase tertiary structure.
34 This finding affirms the correct orientation of the 3D globular arrangement of RbCat with respect
35 to its functional properties.

36



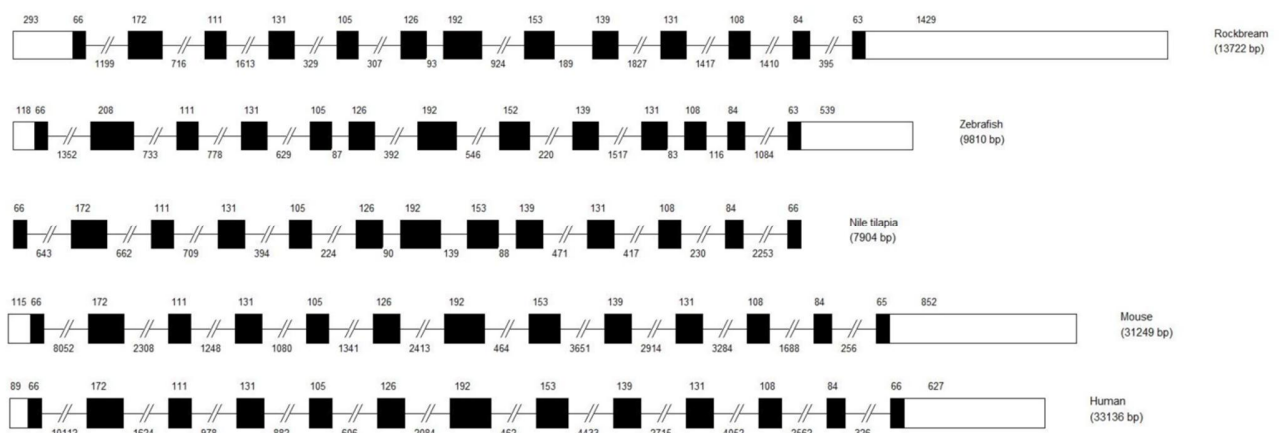
37

38 **Fig. 34.** Tertiary structure of rock bream catalase (RbCat) modeled according to the ab-initio
 39 strategy. Four conceptual domains of RbCat were labeled in the model. α -Helixes and β -strands
 40 are depicted in pink color and yellow color, respectively. Ash color spherical bulges represent
 41 some of the amino acid residues important in NADPH binding, whereas green color bulges
 42 represent the residues important in heme binding. N and C letters were used to indicate the
 43 amino and carboxyl terminal, respectively.

44 3.3. Genomic architecture and predicted core promoter region of RbCat

45 According to the canonical AG/exon/GT rule, the exon-intron organization of the *RbCat*
 46 gene in the identified BAC gDNA sequence was analyzed and compared with the derived
 47 complete cDNA sequence. The genomic structure revealed that RbCat consists of 13 exons,
 48 separated by 12 introns, with a genome length of 13,722 bp (Fig. 35). According to the
 49 comparison with its orthologs, the number and size of the exons (from the 3rd to 12th) of RbCat
 50 were found to be well conserved among all vertebrate species. The second exon is conserved

51 among the majority, including the mammals considered in the comparison, rendering a greater
 52 potential of evolution through mechanisms such as alternative splicing (Black, 2000; Modrek
 53 and Lee, 2002), which further supports the potential existence of different isoforms. Moreover,
 54 among the 3 fish species considered, rock bream exhibited eminent genomic length, possessing
 55 large exons at the beginning and end of the sequence.



56

57 **Fig. 35.** Genomic organization of the catalase gene from different species. The exons and introns
 58 are indicated by boxes and solid lines, respectively. The sizes of exons are indicated above the
 59 exons and sizes of introns are indicated below the introns. Black regions represent the coding
 60 sequences whereas white regions represent untranslated regions. When representing introns,
 61 sequence regions larger than 100 bp are truncated by 2 inclined lines. NCBI-Gen Bank accession
 62 numbers of the genomic sequences of organisms used in the comparison are as follows:
 63 Zebrafish-NC007136, Nile tilapia-NT167433, Mouse-NC000068, Human-NG013339.

64

65 According to the promoter prediction, the approximate 1-Kbp region upstream from TIS
66 consisted of several transcriptional factor binding sites, including a TATA box and a CAAT box,
67 reflecting the tight regulation of its transcription (Fig. 36). Most of the predicted *cis*-active sites
68 coincided with the previously characterized promoters of different catalases from vertebrates,
69 especially from mammals. Factors recognizing Sp1 and CCAAT sites were found to be strong
70 regulators of catalase expression at the transcriptional level (Nenoi et al., 2001); C/EBP- β was
71 reported as a potent transcriptional regulator that can interact with corresponding binding regions
72 of catalase promoters (Taniguchi et al., 2005). Catalase gene expression can also be regulated by
73 the OCT-1 transcriptional factor, which is also present in the predicted RbCat promoter region.
74 OCT-1 has been shown to induce the catalase transcription in human hepatocellular carcinoma
75 cells (Quan et al., 2011). On the other hand, the presence of binding sites for the transcriptional
76 factors Sp1, AP1, and nuclear factor kappa B in our promoter prediction indicates the potential
77 transcriptional modulation of RbCat upon exposure to immune signals (Parrott et al., 1991;
78 Lacroix et al., 2002; Tian and Brasier, 2003; Hess et al., 2004).

79

80

GCATATTTCAACC**CAAT**CCAGTG**AAAAATAAGC**AACTGAATGCACATACAAAGAATTGCA -945
OCT-1

AAAATGATGAAATTTAGCTCTGAGGGCCAAACFTCAAAA**ATTCATAACT**AAAAAAGTATT -885
GCN4

TGTAGTAGAGCTGTAGGATTTTGCAAGGTCCCATGAATTTAATAAGAAGTTTTCACATGAA -825

TGTTTT**CAAGAAAATCCATGACATGAA**CTGGGAG**GTCTGGGTGTGT**TGGTATGGAATGA -765
NF- κ B CREB-2 SP1

CCCAAAATAGCAATTAGAAAA**GAGGAAGAA**ATGTGCAATTTAT**GTAGAAGTCA**GTATTTGA -705
C/EBP- β AP1

AATGATGTAGAGTAAGAATTACTTTTGAAAACCTTCATTTTATTACTGAATAGGCCTAT -645

GCTGTATTTTGCAAAT**AAAGATAATG**TAGTCTAAAGTCTGACTTTACCACAAACTTATA -585
GATA-1

TTG**GTGACTGTAC**TTTCACTGCATCAGTTTAATCATTTAAAAATACAGGAAGCTACAGTAAT -525
ARE

AATATAATGCTAGAAAAGCATATGGCAGTAAACATAATTTCCACTATTGTAACAGACACT -465

AATTACACTGTGACATTTGTGACATTTTCTTT**CCGCTACTGC**CATACATTAGAAAGCCAT -405
SP1

ACATTTGAAATGGA**GCAGTGGTGG**TGACGTAATCAGTAATAATTAGTGTATGTTGCAATG -345
SP1

CTGCTCCGGTAATGTTGCTCAAAATAAGG**AGAAATGTCT**GCACACTCATGTTGCATTGATT -285
C/EBP- β

CAGTGATCTGTATGTGTAGTATCCTGACCATTTGATTC AACGTGTTGCACTTTAAGGACA -225

GCAATTTCTATGGGGCTGTTATTGTAGCAGAACTATTTACAAAATGTGAGTGGAGAGTTG -165

TTTAACTGTGTCACAATCCATGTGTGCATAATCAGATTTGTAAATGTGTAAAAGAATAGC -105

AATAAACATAGTAAGTAGAAATTATAAGAAAAGGTGTTCAAAAGCAATACTGCGAGTCAG -45

AAGCATAGATTAGA**TATAAAA**CAGACA**CAAT**AAAAATGAAAAAAT**A**ATTCTAAAAATAAGA 16
TATA-Box CAAT-Box

TATAGACAATATGAACAATATGACTGTTATTTAAATGAAAGAACAGTACAAACATACTAT 76
ATTATGTAAGACAACAATGATTTCTAGTGTGGTTCTCCTCTTGTGTCGAAAGTAGGTC 136
AGTTTCCTCCTTTCAGCCAATCAGAGGAGAGGGGCACAGGAGGGGGCGGGCCACATTGA 196
GCAAAGTCCAGGAACAATTTTGAGGCATCGGGTTAAATAGATAACGCCTTTTCTCCGCTA 256
CATCTCCCGAGTAGTGTGTTGGTCTAAGCGTCTGTCGA**GATG** 307

81

82 **Fig. 36.** Predicted promoter region of rock bream catalase (*RbCat*) with 5'-untranslated region
83 (UTR) and start codon ATG (bold). The transcription initiation site (+1) is denoted by a curved
84 arrow from which 5'-UTR starts. Anticipated transcription factor binding sites are indicated by
85 bold and underlined letters with their corresponding identity. To distinguish the closely
86 positioned binding sites of nuclear factor kappa B and cAMP-response element binding protein 2,
87 the binding site of cAMP-response element binding protein 2 is additionally shaded in gray color.

88 **3.4. Protein expression and purification of rRbCat**

89 After cloning the coding sequence of RbCat into the pMAL-c2X vector, RbCat was
90 overexpressed as a fusion protein of MBP and purified as described in the materials and method
91 section. Fractions collected at different stages during the purification steps were visualized by
92 SDS-PAGE (Fig. 37). The purified fusion rRbCat appeared as 2 bands, from which one (102.5
93 kD) was detected to be compatible with the predicted size of RbCat (60 kD) with MBP, since the
94 molecular mass of MBP is 42.5 kD. However, another band was also appeared below the
95 expected size of the fusion product, probably due to degradation of rRbCat, since vertebrate
96 catalases are known to undergo epigenetic modifications such as proteolysis and form truncated
97 products of the original enzyme (Crane et al., 1982; Sun, 1997). This observation is similar to
98 previous reports on the characterization of catalases from invertebrates such as disk abalone,
99 where multiple bands were detected in addition to the expected purified catalase protein band at
100 the respective SDS-PAGE analysis (Ekanayake et al., 2008).

101

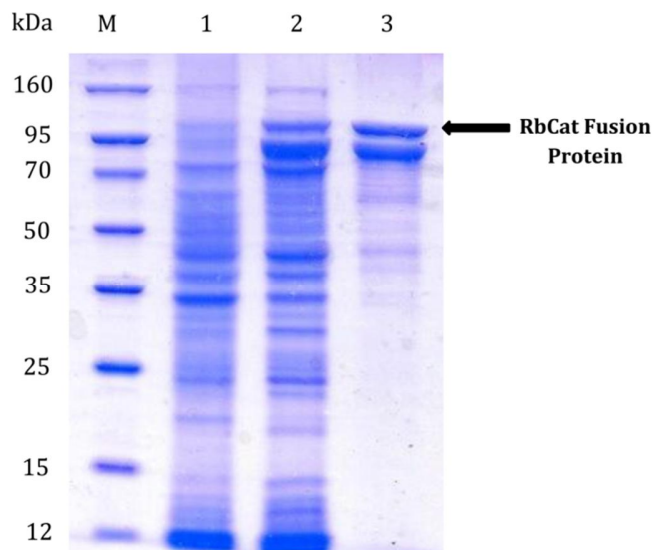
102

103

104

105

106



107 **Fig. 37.** Sodium dodecyl sulfate-polyacrylamide gel electrophoresis analysis of overexpressed
108 and purified recombinant rock bream catalase (rRbCat) fusion protein. Lane 1, total cellular
109 extract from *Escherichia coli* BL21 (DE3) carrying the rRbCat-MBP expression vector prior to
110 isopropyl- β -galactopyranoside (IPTG) induction; 2, crude extract of rRbCat fusion; 3, purified
111 recombinant fusion protein (rRbCat-MBP) after IPTG induction (1 mM); 4, protein marker
112 (Enzynomics-Korea).

113 **3.5. Antioxidant activity of rRbCat**

114 Subsequent to the purification step, peroxidase activity of rRbCat against H_2O_2 was
115 evaluated as a function of its concentration. The percent peroxidase activity was plotted against
116 the different rRbCat concentrations used in the experiment (Fig. 38). As expected, the peroxidase
117 activity increased with increasing concentrations of rRbCat, until it reached to a certain threshold
118 level (178.57 $\mu\text{g/mL}$), exhibiting the optimum peroxidase activity ($\sim 94\%$). This threshold level
119 of rRbCat indicates its optimal concentration for the catalysis of the peroxidase reaction under
120 the provided conditions. Thereafter, the activity of rRbCat was detected to be almost stable with
121 increasing concentration, as evidenced by a plateau shape of the graph. However, the percent
122 peroxidase activity exhibited by MBP against the same substrate, H_2O_2 , was found to be
123 negligible compared to the reported activity of the rRbCat fusion protein, especially with
124 increased concentrations of the fusion protein, affirming that the MBP portion of the fusion
125 product did not noticeably affect the overall peroxidase activity. The estimated specific activity
126 of rRbCat using the detected optimal concentration of the enzyme was around 2,320 U/mg,
127 which is more or less compatible with the specific activity value obtained for the recombinant
128 catalase enzyme of zebrafish (3,160 U/mg) (Ken et al., 2000).

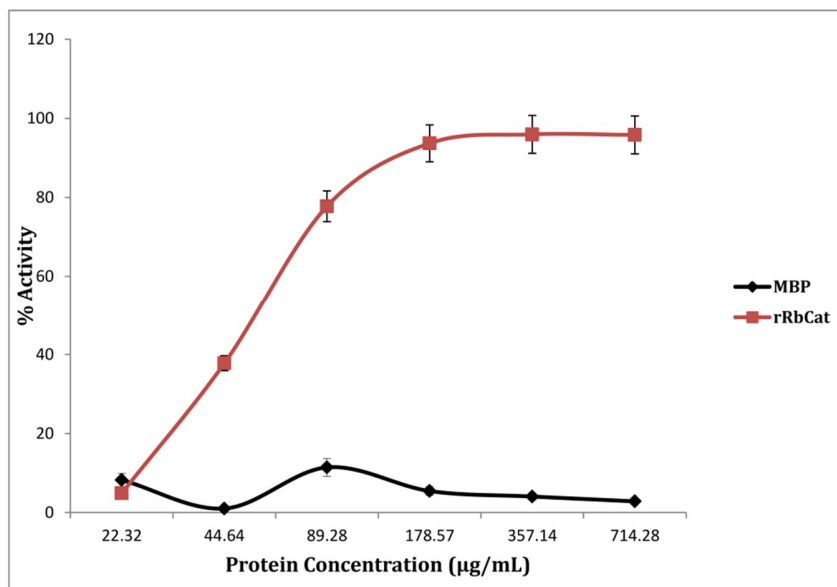


Fig. 38. *In vitro* peroxidase activity of recombinant rock bream catalase (rRbCat) fusion protein against its substrate hydrogen peroxide at different concentrations. Error bars represent the SD (n = 3).

3.6. Biochemical properties of rRbCat

In order to understand the favorable reaction conditions for rRbCat catalysis, its relative activity was evaluated over a range of different pH and temperature conditions. As shown in Fig. 39, rRbCat showed a substantial percent activity, (over 80 %) under a wide range of temperatures. The relative enzymatic activity from 10 °C to 37 °C varied slightly. Subsequently, the activity was found to decrease slightly from 37 °C to 60 °C and came to a plateau at 70 °C and 80 °C. Altogether, overall percent activity of RbCat was maintained almost constantly, without any considerable variation within the experimental range of temperatures. This observation was not unlike with our previous observation of abalone catalase, in which activity was found to be constant from 30 °C to 70 °C (Ekanayake et al., 2008). Our observation of

prominent activity of RbCat maintained at even higher temperatures may be attributed with its specific arrangement of β -barrel domain with anti-parallel β sheets, which was already known to support for the higher activity of catalase at increased temperatures, as reported previously (Murthy et al., 1981). However, MBP alone did not show any significant activity compared to rRbCat under any temperature condition provided, suggesting its inert behavior in the rRbCat fusion protein.

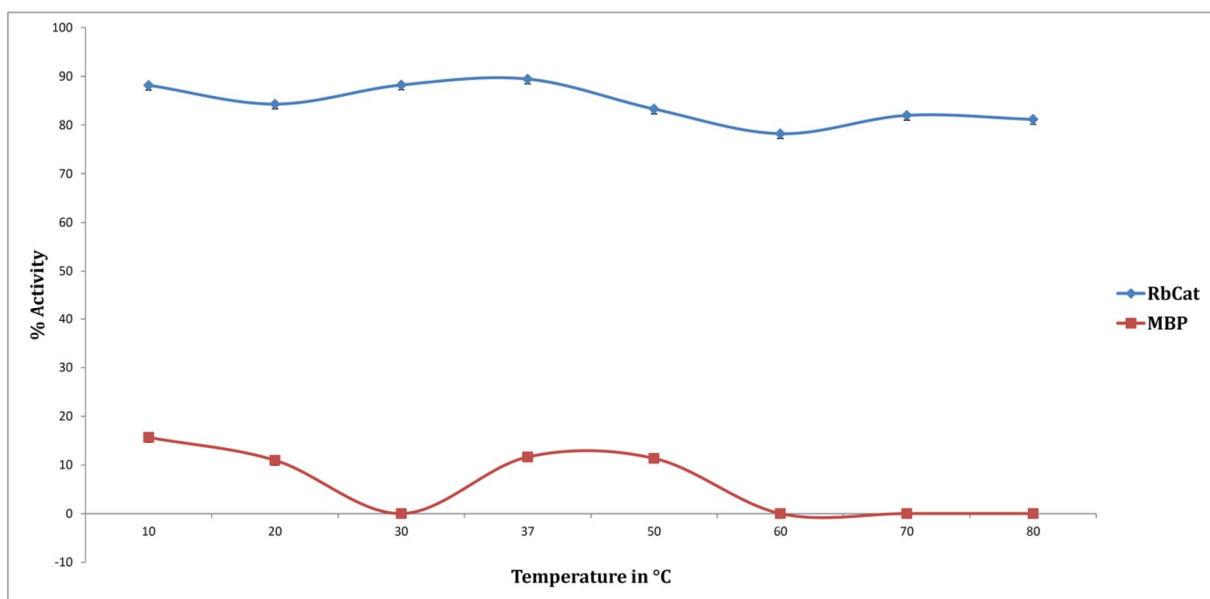


Fig. 39. Variation of recombinant rock bream catalase (rRbCat) peroxidase activity as a function of temperature. Relative enzyme activity percentage (%) was determined at different temperatures ranging from 10 to 80 °C. Error bars represent the SD (n = 3).

Recombinant RbCat catalyzed the substrate H_2O_2 efficiently, showing a relative activity within the range of 80% to 100% over a broad pH spectrum, as shown in the plotted graph of its relative activity under different pH conditions; however, a small but noticeable decrease in its activity was observed at pH 5.5 (~86% activity) (Fig. 40). The maximum percent activity (~96%–97%)

laid at pH 6.5–pH 7.5, suggesting that this is the optimal pH for the catalytic reaction under provided conditions. Nevertheless, from pH 7.5 to 8.5, a slight decrease in the RbCat activity was observed. Similarly, chicken catalase also exerted substantial activity within a broad pH range (4–10) (Aydemir and Kuru, 2003). Furthermore, the detected optimal pH range for human catalase (6.8–7.5) (Aebi, 1984) and chicken catalase (6–8) (Aydemir and Kuru, 2003) is similar to the optimal pH range of rRbCat, further lying within the acceptable pH range (4–11) of various catalases from different species, as retrieved from the “BRENDA” enzyme information system (Scheer et al., 2011). Nonetheless, similar to the temperature dependency, MBP did not show any detectable activity within the applied pH range, rendering its dormant behavior in the fusion product.

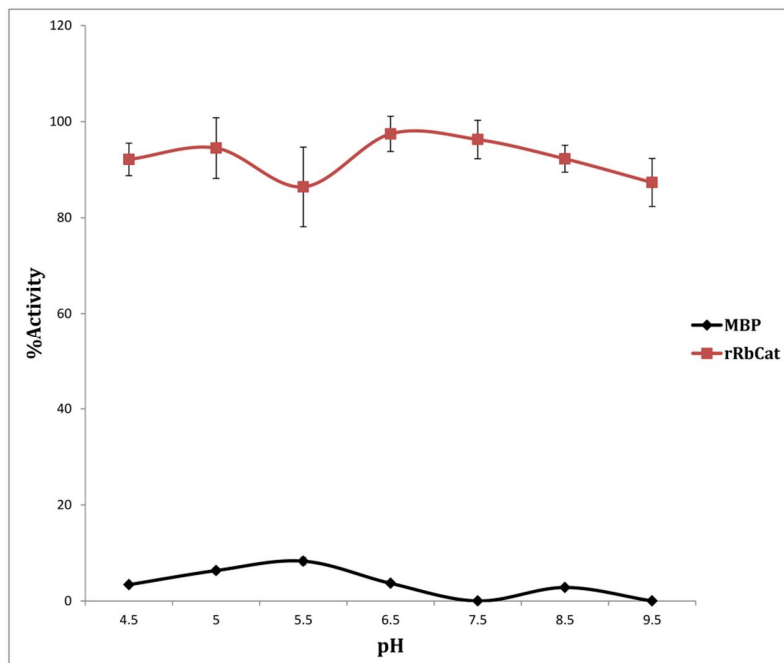


Fig. 40. Variation of recombinant rock bream catalase (rRbCat) peroxidase activity as a function of pH. Relative enzyme activity percentage (%) was determined at different pH conditions, ranging from 4.5 to 9.5. Error bars represent the SD (n = 3).

3.7 Tissue-specific mRNA expression profile of RbCat

According to the tissue-specific mRNA expression in selected tissues of rock bream, RbCat was found to be ubiquitously expressed in tissues examined with the highest transcript level in blood and a moderately high level in liver, compared to the expression level in muscle, which showed the lowest expression level among all tissues used in this comparison (Fig. 41). The detected variable transcript profile in different tissues of rock bream reflects the differential metabolic activity in those tissues with respect to the production of ROS and different environmental conditions. In this regard, ROS production plays a key role as an innate immune response during pathogen infections while evacuating foreign invaders by activating immune signaling pathways (Kohchi et al., 2009). On the other hand, for immune reactions such as phagocytosis, blood cells consume high amounts of oxygen for their metabolic functions, which may in turn contribute to the increase of ROS production. Therefore, it is logical to correlate the high levels of catalase-like antioxidant enzyme expression in blood with their antioxidant properties to counterbalance the highly potential overproduction of ROS as a quick response to pathogenic invasion. Furthermore, liver cells frequently undergo oxidative stress, which affects the liver function and induces apoptosis (Kamata et al., 2005). Therefore, ROS production should be tightly regulated in the liver. Interestingly, our observation of substantial expression of RbCat in liver tissues supports to this fact.

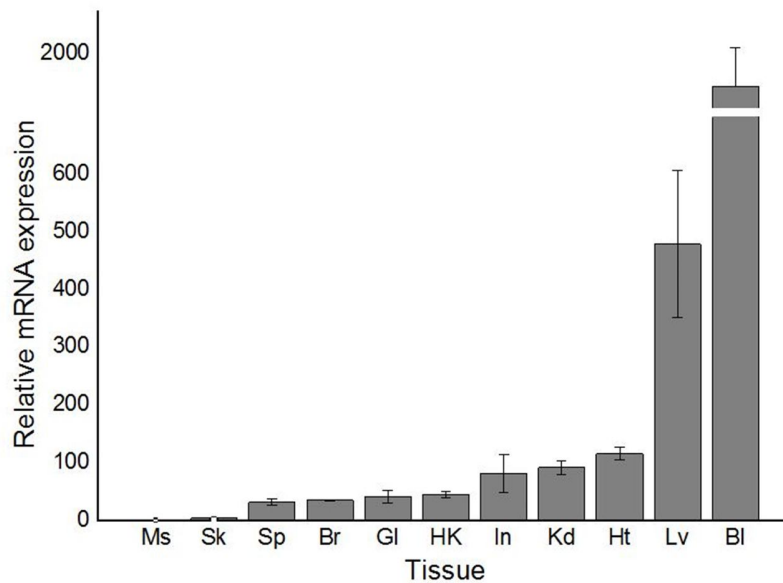


Fig. 41. Tissue-specific expression analysis of rock bream catalase mRNA, determined by quantitative real time-polymerase chain reaction. Expression fold changes are shown relative to the mRNA expression level in muscle tissue. Error bars represent the SD (n = 3). Ms-muscle, Sk-skin, Sp-spleen, Br-brain, Gl-gill, HK-head kidney, In-intestine, Kd-kidney, Ht-heart, Lv-liver, and Bl-blood.

Complying with the pronounced expression of RbCat in liver tissue, catalase transcription was found to be prominent in liver tissues of mefugu (*Takifugu obscurus*) in a previous report (Kim et al., 2010). On the other hand, both substantial mRNA and protein expression of zebrafish catalase were detected in its abdominal section. Catalases from Chinese shrimp, *Fenneropenaeus chinensis* (Zhang et al., 2008) and pearl oyster (*Pinctada fucata*) (Guo et al., 2011) showed their highest expression levels in their intestines, whereas moderately high transcript levels in hemocytes and hepatopancreas with respect to shrimp and in gonad, gill, and mantle regarding oyster.

3.8 Transcriptional response of *RbCat* upon immune stimulation

With the objective of evaluating the role of *RbCat* in the regulation of the cellular redox balance in rock bream upon pathogen infection, its temporal transcriptional variation in blood was investigated under pathological conditions, using two live pathogens, *E. tarda* and RBIV, along with the well-characterized mitogens LPS and poly I:C for immune stimulation. Transcript levels of *RbCat* at each time point after the respective immune stimulation were detected using qPCR. In all qPCR analyses, mRNA expression levels of *RbCat* were detected relative to the corresponding expression of the rock bream β -actin gene and further normalized to the corresponding PBS-injected controls at each time point. The relative expression level at the 0 h time point (un-injected control) was used as basal level.

In accordance with graph A in Fig. 42, *RbCat* expression following exposure to *E. tarda* was significantly ($P < 0.05$) elevated at 12 h post injection (p.i.), although the fold induction (1.2) was relatively low compared to the un-injected control. However, upon LPS stimulation, the *RbCat* transcript level was significantly ($P < 0.05$) up-regulated with a higher inductive fold change (~2) also at 12 h p.i. (Fig. 42A). The induction at the same time point suggests that LPS may act as a pathogen-associated molecular pattern (PAMP) on *E. tarda*, which triggers the immune response in rock bream, stimulating the production of ROS such as H_2O_2 , since LPS is a well-characterized endotoxin of Gram-negative bacteria such as *E. tarda*. Similarly, upon RBIV injection, *RbCat* transcription was significantly ($P < 0.05$) increased at 12 h p.i., exhibiting a low induction fold (1.4) compared to the basal level (Fig. 42B). Further, a significant down regulation ($P < 0.05$) was also noted at 6 h p.i, under the stress of RBIV. The mitogen poly I:C, which mimics viral dsRNA, boosted its expression by almost 2-fold at 12 h p.i. (Fig. 42B).

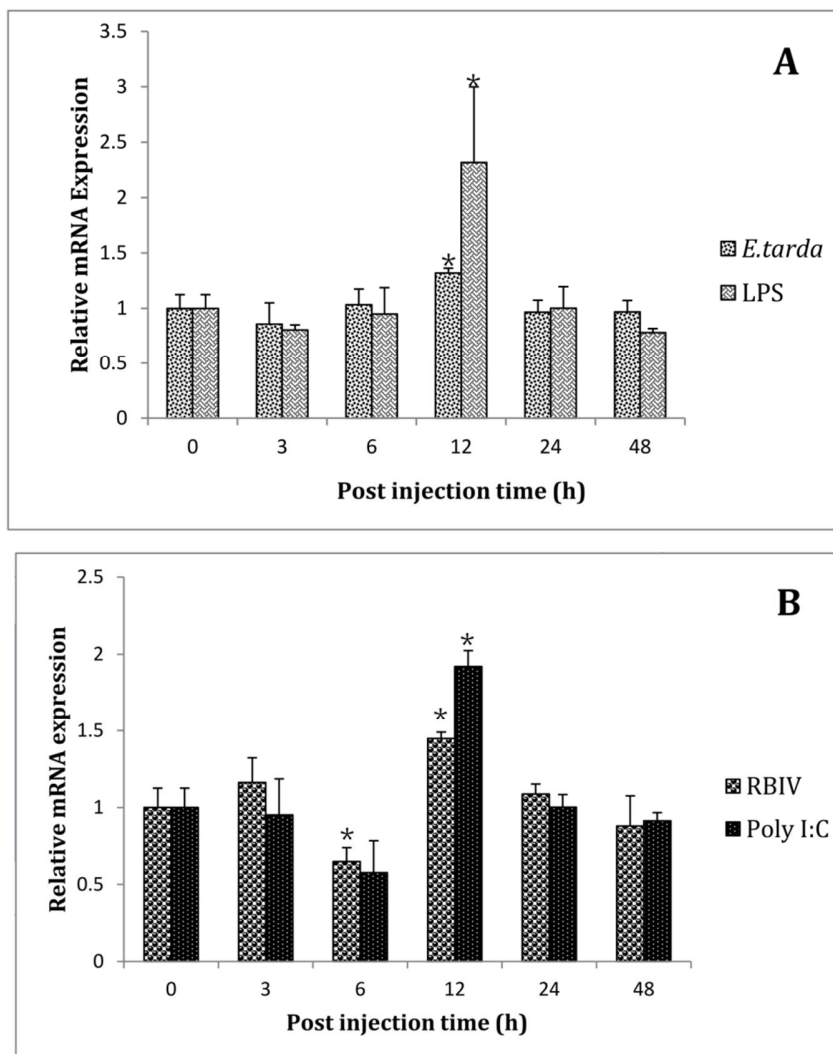


Fig. 42. Expression profile of rock bream catalase mRNA in blood upon immune stimulation with (A) lipopolysaccharide or *Edwardsiella tarda* bacteria, (B) polyinosinic:polycytidylic acid or rock bream iridovirus, as determined by quantitative real time-polymerase chain reaction. The relative expression was calculated by applying the $2^{-\Delta\Delta CT}$ method using rock bream β -actin as reference gene with respect to corresponding phosphate-buffered saline-injected controls at each time point. The relative expression fold change at 0 h post-injection was used as the basal line. Error bars represent the SD (n = 3); * $P < 0.05$.

According to the overall insights into the immune inductions, mitogen stimulation induced the *RbCat* expression with a higher fold change compared to live pathogen exposure. This observation can be attributed to the immune evasion mechanisms orchestrated by pathogenic organisms, especially bacteria and virus, against the host immune responses, including ROS production (Borjesson et al., 2005). In this regard, intracellular bacteria such as *E. tarda* (Ling et al., 2000) and some viruses can alter the ROS production; particularly bacteria can reduce ROS production. Therefore, the expression levels of antioxidant enzymes such as catalase may not be dramatically induced upon infection with these bacteria. On the other hand, some viruses such as Japanese encephalitis virus can down-regulate antioxidant enzymes to induce ROS production in host cells and, in turn, induce cell apoptosis, in order to spread the infection to other cells (Borjesson et al., 2005; Yang et al., 2010). This mechanism used by the virus can be correlated with our observation of down-regulated *RbCat* transcript levels at the early phase of RBIV exposure, where catalase expression may be suppressed by RBIV. Nevertheless, subsequent up-regulation of *RbCat* transcription may be triggered by other immune responses elicited by host cells to control the viral population.

Regarding the antioxidant system in animals, thioredoxin peroxidase and glutathione peroxidase are known to be the predominant antioxidant enzymes involved in the efficient detoxification of H_2O_2 with a higher affinity than catalases, even at a very low concentration of H_2O_2 in cells (Jang et al., 2004; Kang et al., 2005). Moreover, due to the narrow distribution within the cell, and restricted to the peroxisomes, catalases can only act on H_2O_2 after H_2O_2 diffused into peroxisomes and when its concentration reached a substantial level. Therefore, ROS production at the early stage of pathogen infection may be counterbalanced by thioredoxin

peroxidase and glutathione peroxidase, instead of catalase, which is reflected through the detected transcriptional variation of RbCat under pathological conditions.

The temporal transcription pattern of RbCat upon RBIV exposure does not show any significant variation from the overall transcriptional response of its invertebrate counterpart of *Fenneropenaeus chinensis*, upon white spot syndrome virus stimulation. That is, transcriptional down-regulation was observed at the early phase while significant ($P < 0.05$) up-regulation was observed in the later phase, both in hemocytes and hepatopancreas (Zhang et al., 2008). Moreover, temporal transcriptional induction of RbCat under *E. tarda* and LPS exposure can be correlated with the mRNA expression pattern of *Chlamys farreri* in hemocytes after *Vibrio anguillarum* infection, showing up-regulated transcript levels at 12 h p.i. (Li et al., 2008). This is in contrast with the changes in the mRNA expression pattern of its invertebrate counterpart of pearl oyster in intestine following challenge with *V. alginolyticus*, where transcription was up-regulated at the early phase as well as at the late phase of the experiment (Guo et al., 2011).

4. CONCLUSION

In conclusion, a novel catalase from rock bream was identified and characterized at genomic, transcriptional, and protein levels, and its biochemical properties were analyzed as a function of different environmental factors. According to genomic sequence studies, *RbCat* was found to be a multi-exonic gene, in which most of the exons are highly conserved among vertebrates. The *in-silico* predicted core promoter region of *RbCat* reflected its significant regulation at the transcriptional level, especially upon exposure to immune signals and signals generated by oxidative agents. With respect to molecular characterization and phylogenetic analysis, RbCat was positioned with known counterparts of other vertebrates, particularly with teleosts.

Constitutive *RbCat* mRNA expression was detected in a tissue-specific manner, suggesting its diverse importance in the physiology with respect to the tissue type. Moreover, *RbCat* transcription was differently modulated upon exposure to four different immune stimulants, suggesting its potential role as an antioxidative enzyme in post-immune responses at the protein level. Recombinant RbCat demonstrated detectable peroxidase activity against H₂O₂ in a dose-dependent manner, affirming its functional viability, while it exhibited substantial activity under a broad range of temperatures and pH conditions. However, this study can be further extended to examine RbCat with respect to its potential functional properties in fish physiology.

PART B

Characterization of a thioredoxin reductase 3 (TrxR3) homologue from Rock bream

1. ABSTRACT

The thioredoxin (Trx) system plays a significant role in cellular antioxidative defense by dismutating the surpluses of reactive oxygen species. Thus, the role of thioredoxin reductase (TrxR) cannot be ignored, owing to its participation in initiating the Trx enzyme cascade. Here, we report the identification and molecular characterization of a teleostean TrxR (RbTrxR-3) ortholog that showed high similarity with the TrxR-3 isoforms of other vertebrates. The complete *RbTrxR-3* coding sequence comprised 1800 nucleotides, encoding a 600-amino acid protein with a predicted molecular mass of ~66 kD. *RbTrxR-3* consisted of 16 exons separated by 15 introns and had a total length of 12658 bp. *In silico* analysis of the RbTrxR-3 protein sequence revealed that it possesses typical TrxR domain architecture. Moreover, using multiple sequence alignment and pairwise sequence alignment strategies, we showed that RbTrxR-3 has high overall sequence similarity to other teleostean TrxR-3 proteins, including highly conserved active site residues. Phylogenetic reconstruction of RbTrxR-3 affirmed its close evolutionary relationship with fish TrxR-3 orthologs, as indicated by its clustering pattern. *RbTrxR-3* transcriptional analysis, performed using quantitative polymerase chain reaction (qPCR), showed that *RbTrxR-3* was ubiquitously distributed, with the highest level of mRNA expression in the blood, followed by the gill, and liver. Live bacterial and viral stimuli triggered the modulation of *RbTrxR-3* basal transcription in liver tissues that correlated temporally with that of its putative substrate, rock bream thioredoxin1 under same conditions of pathogenic stress. Finally, resembling the typical

function of TrxR protein, purified recombinant RbTrxR-3 showed detectable dose-dependent thiol reductase activity against 5,5'-dithiobis (2-nitrobenzoic) acid. Taken together, these results suggest that RbTrxR-3 plays a role in the host Trx system under conditions of oxidative and pathogenic stress.

2. MATERIALS AND METHODS

2.1. Identification of complete *RbTrxR-3* cDNA and genomic DNA sequences

A rock bream cDNA shotgun sequence database was established based on sequence data from a cDNA library constructed previously by using a next-generation sequencing technology, the GS-FLX titanium system (section 2.1 in part A, chapter 2). A complete cDNA sequence with high sequence similarity to known TrxR-3 orthologs from other organisms was identified using NCBI BLAST. The complete *RbTrxR-3* genomic DNA (gDNA) sequence was obtained from a custom-constructed random-sheared BAC gDNA library (Lucigen®, USA). The library was screened to identify a putative BAC clone that contained *RbTrxR-3* by a polymerase chain reaction (PCR)-based approach using gene-specific primers: RbTrxR-3-qF and RbTrxR-3-qR (Table 14). *RbTrxR-3* was sequenced using the GS-FLX™ system (Macrogen, Korea).

Table 14. Primers used in the study on RbTrxR3

Name	Purpose	Sequence (5' →3')
RbTrxR-3_qF	BAC gDNA library screening and qPCR amplification of <i>RbTrxR-3</i>	AGGGTGGCACTGAGAGACAAGAA
RbTrxR-3_qR	BAC gDNA library screening and qPCR amplification of <i>RbTrxR-3</i>	AGGTCGTCCTGGTGATGCAGTA
RbTrx_qF	qPCR amplification of <i>RbTrx-1</i>	GGCTGGTGGTGGTGGACTT
RbTrx_qR	qPCR amplification of <i>RbTrx-1</i>	ACTCGGACACCTTCGCTTCATTCT
RbTrxR-3-F	amplification of coding region (<i>EcoR</i> I)	GAGAGAgattcATGCCTCCCATCGAAAGTGACAC
RbTrxR-3-R	amplification of coding region (<i>Sal</i> I)	GAGAGAgtcgacTTAACCTCAGCAGCCGGCCTG
Rb-βF	qPCR amplification of rock bream β-actin gene	TCATCACCATCGGCAATGAGAGGT
Rb-βR	qPCR amplification of rock bream β-actin gene	TGATGCTGTTGTAGGTGGTCTCGT

2.2. *RbTrxR-3* sequence profiles and phylogenetic analyses

The complete cDNA sequence and corresponding amino acid sequence of RbTrxR-3 were derived using DNAsist 2.2 software, and the putative TrxR domain architecture was predicted using ExPASy-prosite (<http://prosite.expasy.org/>), NCBI-CDS (<http://www.ncbi.nlm.nih.gov/Structure/cdd/wrpsb.cgi>), and SMART (<http://smart.embl-heidelberg.de/>) online servers. Putative SECIS elements were predicted using SECISearch online server (<http://genome.unl.edu/SECISearch.html>). Several important physicochemical properties of RbTrxR-3 were determined using the ExPASy ProtParam tool (<http://web.expasy.org/protparam>). The derived RbTrxR-3 sequence was compared with those of its homologs by performing pairwise sequence alignment and multiple-sequence alignment strategies, using EMBOSS Needle (<http://www.Ebi.ac.uk/Tools/emboss/align>) and ClustalW2 (<http://www.Ebi.ac.uk/Tools/clustalw2>) programs, respectively. The phylogenetic relationship of RbTrxR-3 with its vertebrate orthologs (including isoforms) was determined using MEGA software version 4 (Tamura et al., 2007), by the neighbor-joining method, supported by 1000

bootstrapped replicates. The exon-intron arrangement of the identified *RbTrxR-3* sequence was annotated using the NCBI-Spidey online server (<http://www.ncbi.nlm.nih.gov/spidey>) based on its complete cDNA sequence that has been identified previously.

2.3. Molecular cloning, over-expression, and purification of recombinant RbTrxR-3 (rRbTrxR-3)

The complete *RbTrxR-3* coding sequence was amplified by PCR using gene-specific cloning oligomers (Table 14) containing *EcoRI* and *SalI* restriction sites. PCR amplification was performed in a TaKaRa thermal cycler (TaKaRa Korea Biomedical Inc, Korea) in a 50 μ L reaction volume that contained 5 U of ExTaq polymerase (TaKaRa), 5 μ L of 10 \times ExTaq buffer, and 4 μ L of 2.5 mM dNTPs, 80 ng of DNA template, and 20 pmol of each oligomer. The following cycling conditions were used: an initial incubation at 94 $^{\circ}$ C for 3min followed by 35 cycles of 94 $^{\circ}$ C for 30 sec, 57 $^{\circ}$ C for 30 s, 72 $^{\circ}$ C for 2 min, and a final extension at 72 $^{\circ}$ C for 5 min. The resultant PCR product was ligated into pMAL-c2X vector, and the recombinant vector was transformed into *Escherichia coli* DH5 α cells. The identity of the insert was confirmed by sequencing. Next, the recombinant vector was transformed into *E. coli* BL21 (DE3) cells, and selected putative transformants were grown overnight in 500 mL of Luria-Bertani broth, supplemented with 100 μ g/mL of ampicillin and 0.5 mg/mL of glucose, at 37 $^{\circ}$ C with shaking (200 rpm). Once the OD₆₀₀ of the culture reached 0.5, isopropyl- β -D-1-thiogalactopyranoside (IPTG) was added to a final concentration of 1 mM and the mixture was then incubated for 3 h at 37 $^{\circ}$ C to induce protein expression. Cells were subsequently chilled on ice for 30 min and harvested by cold centrifugation. The obtained pellets were resuspended in column buffer (20 mM Tris-HCl pH 7.4 and 200 mM NaCl) and stored at -20 $^{\circ}$ C overnight. Frozen cells were thawed on ice, lysed, and ruptured using cold sonication in the presence of lysozyme (1 mg/mL).

The resultant whole cell lysate was centrifuged ($9000 \times g$ for 30 min at 4 °C) and the supernatant (crude extract) was then purified to obtain rRbTrxR-3 by using the pMAL protein fusion and purification technique (New England Biolabs, USA). Finally, the concentration of the purified recombinant protein was determined using the Bradford method, and its integrity and purity were analyzed using 12% sodium dodecyl sulfate polyacrylamide gel electrophoresis (SDS-PAGE) under reducing as well as non-reducing conditions.

2.4. rRbTrxR-3 thiol reductase activity analysis

Reducing activity of rRbTrxR-3 against thiol groups in 5,5'-dithiobis(2-nitrobenzoic acid) (DTNB) was analyzed using a commercially available colorimetric assay kit (BioVision, USA) according to the manufacturer's instructions, with some minor modifications. Briefly, rRbTrxR-3 was diluted to different concentrations with the assay buffer (final volume of 50 μ L) provided with the kit, and then combined with a reaction solution containing 30 μ L of assay buffer, 8 μ L of DTNB solution, and 2 μ L of NADPH in 96-well microtiter plates. The samples were immediately incubated at 25 °C for 20 min, and the OD₄₁₂ of each reaction was measured. The same procedure was performed using maltose-binding protein (MBP) and 50 μ L of assay buffer in place of RbTrxR-3 as controls. OD₄₁₂ values were calculated by subtracting the mean OD₄₁₂ value of three replicates of the negative control (assay buffer) from that of each experimental sample.

2.5. Animal husbandry and tissue collection

Healthy rock breams, which were obtained from the Jeju Special Self-Governing Province Ocean and Fisheries Research Institute (Jeju, Republic of Korea), with an average body weight of 30 g were reared in a controlled environment (salinity 34 ± 1 ‰, pH 7.6 ± 0.5 , and 22–24 °C). The

animals were acclimatized for one week prior to experimentation. Within the acclimatization period, fish were fed with a commercially available fish feed. Whole blood (1 mL/fish) was collected from the caudal fin by using a sterilized syringe and the samples were centrifuged immediately at $3000 \times g$ for 10 min at 4 °C to separate the blood cells from the plasma. Collected cells were snap-frozen in liquid nitrogen. The gill, liver, skin, spleen, head kidney, muscle, brain, heart, kidney and intestine were excised from three animals and immediately snap-frozen in liquid nitrogen. Tissue samples were stored at -80 °C until total RNA was extracted.

2.6. Pathogen challenge experiments

To gain insights into the modulatory effects of common and potentially infectious pathogens on *RbTrxR-3* mRNA expression, two live bacterial pathogens, *Edwardsiella tarda* (*E. tarda*) and *Streptococcus iniae* (*S. iniae*) as well as a well-known fish viral pathogen, rock bream iridovirus (RBIV) were used to stimulate healthy rock breams, reared as described previously (section 2.5), in a time-course immune challenge experiment. The complete experiment was performed as described in our previous study on RbCat (section 2.9 in part A, chapter 2). Liver tissues of the experimental animals were collected as described in section 2.5. At least three animals from each challenge group were sacrificed at each time point.

2.7. Total RNA extraction and cDNA synthesis

Total RNA was extracted from each of the tissues collected from healthy fish, as well as from the liver tissues from the immune-challenged group by using Tri ReagentTM (Sigma-Aldrich, USA) according to the vendor's protocol. The concentration of each extracted RNA sample was measured at 260 nm in a UV-spectrophotometer (Bio-Rad, USA) and diluted to 1 µg/µL. RNA (2.5 µg) from each tissue was used to synthesize cDNA by reverse transcription using a cDNA synthesis kit (TaKaRa, Japan) according to the manufacturer's instructions. Synthesized cDNAs were diluted 40-fold (total volume of 800 µL) and stored at -20 °C for future analysis.

2.8. Measurement of *RbTrxR-3* and rock bream *Trx-1* (*RbTrx-1*) mRNA expression levels in liver tissues by using quantitative PCR.

RbTrxR-3 and *RbTrx-1* transcripts levels were measured in the liver tissues of infected fish as well as in the selected tissues of healthy fish (section 2.5) by performing qPCR using the synthesized cDNAs as templates (section 2.7). qPCR was performed using a DiceTM Real-time System (TP800; TaKaRa, Japan). Each 15 µL reaction contained 4 µL of diluted cDNA, 7.5 µL of 2× TaKaRa Ex TaqTM, SYBR premix, 0.6 µL of each primer (*RbTrxR-3*_qF and *RbTrxR-3*_qR or *RbTrx*_qF and *RbTrx*_qR; Table 14), and 2.3 µL of ddH₂O, following essential MIQE guidelines (Bustin et al., 2009). The full-length *RbTrx-1* coding sequence was obtained from the NCBI-GenBank database (accession no. AB603653) and used to design qPCR oligomers. The following qPCR conditions were used: an initial denaturation at 95 °C for 10 s; followed by 35 cycles of 95 °C for 5 s, 58 °C for 10 s, and 72 °C for 20 s; and a final cycle of 95 °C for 15 s, 60 °C for 30 s, and 95 °C for 15 s. The base line was set automatically by the DiceTM Real Time

System software (version 2.00). *RbTrxR-3* mRNA expression levels were determined using the Livak ($2^{-\Delta\Delta CT}$) method (Livak and Schmittgen, 2001). The same qPCR cycling conditions were used to amplify the internal reference gene, rock bream β -actin (GeneBank ID: FJ975146), using gene-specific primers (Table 14). All data are represented as the mean \pm standard deviation (SD) of experiments performed in triplicate. Gene expression levels were compared to that of the rock bream β actin gene to obtain relative gene expression values at mRNA levels. The relative changes in *RbTrxR-3* and *RbTrx-1* expression (Hatfield and Gladyshev, 2002) at mRNA level were determined for the immune-challenged groups at various time points by normalizing the mRNA expression levels to those of the corresponding phosphate-buffered saline (PBS)-injected control, to eliminate the effect of the injection. Transcripts levels in the uninjected control (0 h) were considered as baseline. The statistical difference between the experimental and uninjected control groups were analyzed using two tailed unpaired Student's *t*-tests. $P < 0.05$ was considered statistically significant.

3. RESULTS AND DISCUSSION

3.1. Molecular properties and sequence similarity of RbTrxR-3

The full-length cDNA sequence of *RbTrxR-3* comprised 3247 nucleotides, consisting of an 1806-bp open reading frame (ORF) as well as 5' and 3' untranslated regions (UTRs) that were 256 bp and 1182 bp, respectively. As expected, we could identify an in-frame opal codon ($^{1798}\text{TGA}^{1800}$) in *RbTrxR-3* ORF which probably code for a selenocysteine amino acid (U in Fig.33), positioned one amino acid before the termination codon of RbTrxR-3, confirming the characteristic feature of selenoproteins, including thioredoxin reductases. Moreover, we could decipher the loose SECIS element pattern in 3' UTR ($^{2450}\text{GTGAC}^{2455}$, $^{2468}\text{AA}^{2469}$ and $^{2497}\text{CGAT}^{2500}$) which is known

to direct the insertion mechanism of selenocystein residue at the position of TGA codon, using SECISearch server, based on non-canonical A-G pairs of human TrxR-3 (Hatfield and Gladyshev, 2002). This evidence further validates that aforementioned opal codon likely encodes a U residue in RbTrxR-3. Based on our *in silico* analysis, we determined that the identified ORF encoded a 602-amino acid protein with a molecular mass of ~66 kD and theoretical isoelectric point of 5.8. Protein and cDNA sequence information for RbTrxR-3 was deposited in the NCBI-GenBank database under the accession number KF742679. Our computational domain analysis showed that RbTrxR-3 possesses typical TrxR features including a proximal glutaredoxin domain (residues 14–114), glutaredoxin active site (residues 28–43), pyridine nucleotide-disulfide oxidoreductase class-1 active site (PYRIDINE REDOX_1; residues 159–169), putative FAD-binding domain (residues 117–193), and pyridine nucleotide-disulfide oxidoreductase dimerization domain (residues 473–586) (Fig. 43). Multiple-sequence alignments showed that cysteine residues in the RbTrxR-3 active site (residues 34 and 37) were completely or partially conserved, while the PYRIDINE REDOX_1 site was conserved in all sequences examined. The predicted glutathione binding sites in RbTrxR-3 (residues 77, 78, 79, 89, 90, 91, and 92) also showed good conservation. Pairwise sequence alignments of RbTrxR-3 and its orthologs confirmed that it was a TrxR homolog, sharing prominent percent identity and similarity values to other teleostean TrxRs, especially to that of *Dicentrarchus labrax* (Table 15).

Human MERSPP-----QSPGPGKAGDAPNRRSGHVRGARVLSPPGRRARLSSPGPSR--SSEA 51
 Dog -----MNF PENSAMALKAP-----SNEA 18
 Mouse MEKPPSPPPPRAQT SPGLGKVGVL PNRRLGAVRGLMSSPPGRRARLASPGTSRPSSEA 60
 Zebra finch -----MP PPGQTRLPDWDGLKLRVRT 22
 Chicken -----MPP-PGQTQLPDWDGLKLRVRT 21
 Frog -----MEPTGRDLLQAR-----VKE 15
Rock bream -----MEPIESDTGKNE--LKSRIQQ 19
 Seabass -----MPPINDTGKNE--LKSRIQL 19
 Zebrafish -----MEPIENDAGREQ--IRSKIKE 19

Human REELRRLVGLIERSRVVIFSKSYCPHSTRVKELFSSLGVEC NVLELDQVDDGARVQEV L 111
 Dog LMDQLD-----VKEFSSLGVACNILELDQVDDGANVQEV L 54
 Mouse REELRRLRLDIEGNRVMIFSKSYCPHSTRVKELFSSLGVVYNIILELDQVDDGASVQEV L 120
 Zebra finch LIASHR-----VMIFSKSYCPYCNKVKELFNSLHVEYYALELDV IDDGASIQV L 72
 Chicken LIATHR-----VMIFSKSYCPYCHRVKELFSSLGVQYYALELDV TDDGPSIQV L 71
 Frog LIDSNR-----VMVFSKSEFCPYCDR VKDLFSSLGAEYHSELEDE CDDGSDIQEAL 65
Rock bream LIDSNQ-----VVVFSKSYCPYCDR VKDLFSELKLVECNVVLELDLIEDGTNYQEM L 69
 Seabass LIDSNQ-----VLVFSKSYCPYCDR VKDLFSELKLVECNVVLELDLIEDGTNYQEM L 69
 Zebrafish LIDSSA-----VVVFSKSEFCPYCDR VKDLFSELKLVKYNTILELDMEDGTNYQD L L 69
 * : * * * * * : * * * * * : * * * * * : * * * * *

Human SEITNQKTVPNIFVNVKHVGGCDOTFOAYQSGLLQKLLQE---DLAYDYDLII IGGSGG 168
 Dog SEITNQRTVPNIFVNVKHMGGCDRTFOAHQSGLLQKLLQE---DSAYDYDLI IGGSGG 111
 Mouse TEISNQKTVPNIFVNVKHVGGCDRTFOAHQSGLLQKLLQD---DSAHDYDLII IGGSGG 177
 Zebra finch AELTNQRTVPNVNFVNGTHIGGCDATFOAYKDGSLQKLLGDNQITEPYEYDLII IGGSGG 132
 Chicken AELTNQRTVPNVNFVNGKHI GGCDATYKAYENGTQRI LGDVKDAETDYDLI IGGSGG 131
 Frog QELTGQKTVPNVNFVNGKHI GGCDKTLQAHKDGSLQKLLGDN---SVTYDYDLI IGGSGG 123
Rock bream LEMTGQKTVPNVNFVNGKHI GGCDKTLQAHKDGSLQKLLSGE---NEAYDYDLI IGGSGG 127
 Seabass LEMTGQKTVPNVNFVNGKHI GGCDKTLQAHKDGSLQKLLTGD---NEAYDYDLI IGGSGG 127
 Zebrafish HEMTGQKTVPNVNFVNGKHI GGCDNTMKAHKDGV LQKLLGEG---SEVYDYDLI IGGSGG 127
 * : * * * * * : * * * * * : * * * * * : * * * * *

Human LSCAKEAAILGKKVMVLDVFPVSPQGT SWGLGGTCVNVGCI PKKLMHQ AALLGQALCDSR 228
 Dog LACAQEAAILGKKVMVLDVFPVSPQGT SWGLGGTCVNVGCI PKKLMHQ AALLGQALRDAR 171
 Mouse LSCAKEAAILGKKVMVLDVFPVSPQGT TWGLGGTCVNVGCI PKKLMHQ AALLGHALQDAK 237
 Zebra finch LACSKEAAILGKKVMVLDYVVP TPLGTSWGLGGTCVNVGCI PKKLMHQ AALLGQALQDSR 192
 Chicken LACSKEAATL GKKVMVLDYVVP TPLGTSWGLGGTCVNVGCI PKKLMHQ AALLGQALKDSR 191
 Frog LACSKEAASF GKKVMVLDVFPVSPQGT SWGLGGTCVNVGCI PKKLMHQ AAILGQSLKDSR 183
Rock bream LACSKEAALGKKAMVLDYVVP TPKGTTWGLGGTCVNVGCI PKKLMHQ TALLGTAMQDAR 187
 Seabass LACSKEAAMLGKKVMVLDYVVP TPKGTSWGLGGTCVNVGCI PKKLMHQ TALLGTAMQDAR 187
 Zebrafish LACSKEAATL GKKVMVLDYVVP TPOGTAWGLGGTCVNVGCI PKKLMHQ TALLGTAMEDAR 187
 * : * * * * * : * * * * * : * * * * * : * * * * *

Human KFGWEYNQQVRHNWETMTKAIQNHISSLNWGYRLS LREKAVAYVNSYGEFVEHHKIKATN 288
 Dog KFGWEYSQQVKHTWETMTEAIQNHI GSNLWGYRLS LREKAVAYVNSYGEFVEHHKIKATN 231
 Mouse KYGWQYEEQVKHNWETMTEAIQNYI GSNLWGYRVT LREKGVTVYVNSYGEFVDLHKIKATN 297
 Zebra finch KYGWQYEEQVKHNWETMVEAIQNYI GSNLWGYRVS LREKSVTYLNSYGEFVEPHKIKATN 252
 Chicken AYGWQYDEQVKHNWETMVEAVQNYI GSNLWGYRLS LREKSVTYQNSYGEFVEPHKIKATN 251
 Frog KFGWEYEEQVKHNWETMREAIQNYI GSNLWGYRVALRDKQVRYENAYGEFVESHKIKATN 243
Rock bream KFGWEYDETVKHNWETMKMAVNNYI GSNLWGYRVALRDKNVNYVNAVAYAEFIEPHKIKATN 247
 Seabass KFGWEFEETVKHNWETMKTA VNNYI GSNLWGYRVALRDKNVNYVNAVAYAEFIEPHKIKATN 247
 Zebrafish KFGWEFAEQVTHNWETMKTA VNNYI GSNLWGYRVS LRDKNVNYVNAVAYAEFVEPHKIKATN 247
 * : * * * * * : * * * * * : * * * * * : * * * * *

Human KKGQETYYTAAQFVIATGERPRYLGIQGDKEYCITSDDLFS LPHYCPGKTLVVGASYVALE 348
 Dog RKGQETCYTAAKFVLATGQRPRYLGIQGDKEYCITSDDLFS LPHYCPGKTLVVGASYVALE 291
 Mouse KKGQETFYTASKFVIATGERPRYLGIQGDKEYCITSDDLFS LPHYCPGKTLVVGASYVGL 357
 Zebra finch RKGQVTYHTAETFV VATGERPRYLGI PGDKEFCITSDDLFS LPHYCPGKTLVVGASYVALE 312
 Chicken RKGQVTYHTAETFV VATGERPRYLGI PGDKEYCITSDDLFS LPHYCPGKTLVVGASYVALE 311
 Frog KKGKESFFTA EK FV VATGERPRYLNI PGDKEYCITSDDLFS LPHYCPGKTLVVGASYVALE 303
Rock bream KRKGETFYTAAKFVLATGERPRYLGI PGDKEYCITSDDLFS LPHYCPGKTLVIGASYVALE 307
 seabass KRKGETLYTAAKFVLATGERPRYLGI PGDKEYCITSDDLFS LPHYCPGKTLVIGASYVALE 307
 Zebrafish KRKGETFYTAAQFVIATGERPRYLGI PGDKEFCITSDDLFS LPHYCPGKTLVVGASYVALE 307
 * : * * * * * : * * * * * : * * * * * : * * * * *

Human	CAGFLAGFGLDVTVMVRSILLRGFDQEMAEKVGSYMEQHGVKFLRKFI PVMVQQLEKGSF	408
Dog	CAGFLAGLGLDVTIMVRSILLRGFDQEMAEKVGSYMEQHGVKFLRKFPVPLVQQLEKGSF	351
Mouse	CAGFLAGLGLDVTVMVRSVLLRGFDQEMAEKVGSYLEQQGVKFKRKFPIILVQQLEKGLF	417
Zebra finch	CAGFLAGLGLDVTVMVRSILLRGFDQEMAEKVGAYMETHGVKFIKRFVPPVQVEQLEQQMF	372
Chicken	CAGFLAGLGLDVTVMVRSILLRGFDQEMAEKIGAHMETHGVTFIRKFPVPTQVERLEDGTF	371
Frog	CAGFLAGLGLDVTVMVRSIFLRGFDQEMANRAGAYMETHGVKFIKQFVPIKVELLEEGTF	363
Rock bream	CGGFLAGLGLDVTVMVRSILLRGFDQDMANRAGEHMEEHGVKFLRKVYPVKVEE LEAGTF	367
Seabass	CGGFLAGLGLDVTVMVRSILLRGFDQDMANRAGEHMEEHGVKFLRKVYPVKVEE LEAGTF	367
Zebrafish	CGGFLAGLGLDVTIMVRSILLRGFDQDMADRAGEYMETHGVKFLRKFPVPTKIEQLEAGTF	367
	*.****.***.*:****.:*****.***: * :.* :*. * :.: * :. : * * *	
Human	GKLVVAKSTEGTETIEGYNTVLLAIGRDSCTRKIGLEKIGVKINEKSGKIPVNDVEQT	468
Dog	GKLVVAKSTEGPETIEEYNTVLLAIGRDSCTRKIGLEKIGVKINEKSGKIPVNDVEQT	411
Mouse	GKLVVAKSTEGPETVEGIYNTVLLAIGRDSCTRKIGLEKIGVKINEKNGKIPVNDVEQT	477
Zebra finch	GRLKVTAKSTEGPETLEEYNTVLLAVGRDACTRNIGLQTIKVKINEKNGKVPVNDDEERT	432
Chicken	GRLKVTAKSTEGPEFEEGEYNTVLLAIGRDACTRNIGLQTIKVKINEKNGKVPVNDDEERT	431
Frog	GRIKVTAKSTQGDQIEEYNTVLLAVGRDACTRNIGLEKIGVKINEKNGKIPVNDDEERT	423
Rock bream	GRLKVTAKSTETDEIEEYNTVLLAVGRDACTDKIGLDKAGVKVNPKNKIPVNDDEERT	427
Seabass	GRLKVTAKSTESDEIEEYNTVLLAVGRDACTDKIGLDKAGVKVNPKNKIPVNDDEERT	427
Zebrafish	GRIKVTAKSTESEEVFEGEYNTVLLAVGRDACTGKIGLDKAGVKINEKNGKVPVNDDEERT	427
	*.:** ****. : . * *****:*.***.* :***. . ****. * :.**:** * * :	
Human	NVPVYAVGDILEDKPELTPVAIQSGKLLAQRLLFGASLEKCDYINVPTTVFTPLEYGCCG	528
Dog	NVPVYAVGDILEGKLELTPVAIQAGKLLARRLFAGRLEKCDYVNVPTTVFTPLEYGCCG	471
Mouse	NVPVYAVGDILEGKPELTPVAIQAGKLLARRLFVGSLEKCDYINIPPTTVFTPLEYGCCG	537
Zebra finch	NVPVYAVGDILEGKLELTPVAIQAGRLLAQRLLYGGSSKCDYINVPTTVFTPLEYGSCG	492
Chicken	NVPVYAVGDILEGKLELTPVAIQAGKLLARRLYGGSSKCDYINVPTTVFTPLEYGSCG	491
Frog	SVPHVYAVGDILEGKLELTPVAIQAGRLLARRLYRGSVKCDYINVPTTVFTPLEYGCCG	483
Rock bream	NVPVYAVGDILEGKLELTPVAIQAGKLLARRLYGGSKLCDYVNVPTTVFTPLEYGACG	487
Seabass	NVPVYAVGDILEGKLELTPVAIQAGKLLARRLYGGSKLCDYINVPTTVFTPLEYGACG	487
Zebrafish	NVPVYAVGDILEGKLELTPVAIQAGKLLARLYAGATMKCDYVNVPTTVFTPMEYGSCG	487
	.**.:** ****. * *****:*.***.* :***. . ****. * :.**:** * * :	
Human	LSEKAIEVYKKNLEIYHTLFWPLEWTVAGRENNTCYAKIICNKFDHDRVIGFHVLGPN	588
Dog	LSEKAIEVYKKNLEVYHTLFWPLEWTVAGRDNNTCYAKIICNKLDNRYVIGFHVLGPN	531
Mouse	LSEKAIEVYKKNLEVYHTLFWPLEWTVAGRDNNTCYAKIICNKFDNERVVGFLHLLGPN	597
Zebra finch	YPEEKAISEYGEQNLVYHTLFWPLEWTVVGRDNNTCYAKIICNKQDNNRVIGLHVLGPN	552
Chicken	LAEEKAIEEYKQNLVYHSLFWPLEWTVVGRDNNTCYAKIICNKLDGNNRVVGFHVLGPN	551
Frog	YAEKAIEIYGEENLEVYHTLFWPLEWTVPSRDNNTCFAKIICNKQDNNRVIGFHVLGPN	543
Rock bream	<u>LSEERATELYGKDNIEVFHSLFWPLEFTVVPNRDNNKCYGKIICNKLSDRVIGFHVLGPN</u>	547
Seabass	LSEERATELYGQENIEVYHSLFWPLEFTVVPGRDNNRCYSKIICNKLDNDRVIGFHVLGPN	547
Zebrafish	HPEEKAIQMYGQENIEVYHSLFWPLEFTVVPGRDNNKCYAKIICNKLDNLRVIGFHVLGPN	547
	.**.* . * :.**:*.***.* :***. . ****. * :.**:** * * *	
Human	AGEVTQGF ^{AA} AMKCGLTKQLLDDTI GIHPTCGEVFTTLEITKSSGLDITQKCGG	643
Dog	AGEVTQGF ^{AA} AMKCGLTKQLLDDTI GIHPTCGEVFTTLEITKSSGLDITQKCGG	586
Mouse	AGEITQGF ^{AA} AMKCGLTKQLLDDTI GIHPTCGEVFTTLEITKSSGLDITQKCGG	652
Zebra finch	AGEVTQGF ^{AA} AIKCGLTKELLDDETI GIHPTCAEVFTTMDITKSSGQDITQKCGG	607
Chicken	AGEVTQGF ^{AA} AIKCGLTKELLDDETI GIHPTCAEVFTTMDITKSSGQDITQKCGG	606
Frog	AGEITQGF ^{AA} AMKCGLTKELLDDETI GIHPTCAEIFTTMDITKSSGGDISQKGC--	596
Rock bream	<u>AGEVTQGF^{AA}AMKCGATKEQLDSTIGIHPTCAEIFTTLEVTKSSGGDITQAGCG</u>	602
Seabass	AGEVTQGF ^{AA} AMKCGATKEQLDNTIGIHPTCAEIFTTLEVTKSSGGDIAQSGC--	600
Zebrafish	AGEVTQGF ^{AA} AMKCGITKDQLDNTIGIHPTCAEIFTTMEVTKSSGGDITQSGCG	602
	.:*. .*:*** ** :.**:*****.***: .****. **:* **	

Fig. 43. Multiple-sequence alignment of RbTrxR-3 and its vertebrate orthologs. Sequence alignments were obtained using ClustalW server. Conserved residues are shaded in gray. The predicted glutaredoxin domain profile, glutaredoxin active site signature, and pyridine nucleotide-disulfide oxidoreductase class-I active site signature are indicated on the RbTrxR-3 sequence by a box, wavy underline, and normal underline, respectively. The putative FAD-

binding signature is denoted in bold fonts and predicted pyridine nucleotide-disulfide oxidoreductase dimerization domain is represented by red color letters. The selenocystein residues positioned at the 3' of the sequences were denoted by 'U' and shaded in green color. Residues that form GSH-binding sites that are conserved in all the homologs are indicated by bold fonts (TVP and GGCD), and completely or partially conserved catalytic residues are indicated by vertical boxes.

Table 15. Percent similarity and identity values of RbTrxR-3 and its homologs

Organism	Common Name	Protein	Accession number	Identity (%)	Similarity (%)	Length in amino acids
1. <i>Dicentrarchus labrax</i>	European seabass	Thioredoxin reductase 3	CBN80599	95.2	98.2	600
2. <i>Danio rerio</i>	Zebrafish	Thioredoxin reductase 3	NP898895	84.4	93.4	602
3. <i>Xenopus laevis</i>	African clawed frog	Thioredoxin reductase 3	NP001087660	75.8	89.0	596
4. <i>Taeniopygia guttata</i>	Zebra finch	Thioredoxin reductase 3	NP001245307	72.9	85.5	607
5. <i>Gallus gallus</i>	Chicken	Thioredoxin reductase 3	NP001116249	72.5	84.6	606
6. <i>Canis lupus familiaris</i>	Dog	Thioredoxin reductase 3	NP001116250	70.5	83.1	586
7. <i>Pteropus alecto</i>	Black flying fox	Thioredoxin reductase 3	ELK13077	68.1	81.2	636
8. <i>Myotis brandtii</i>	Bat	Thioredoxin reductase 3	EPQ08225	66.2	79.6	647
9. <i>Mus musculus</i>	Mouse	Thioredoxin reductase 3	NP001171529	64.5	78.0	652
10. <i>Homo sapiens</i>	Human	Thioredoxin reductase 1	NP001087240	64.5	77.0	649
11. <i>Xenopus tropicalis</i>	Western clawed frog	Thioredoxin reductase 1	NP001243400	62.1	74.1	653
12. <i>Mus musculus</i>	Mouse	Thioredoxin reductase 1	NP001035978	61.4	71.8	499
13. <i>Homo sapiens</i>	Human	Thioredoxin reductase 3	NP443115	55.0	66.5	643
14. <i>Homo sapiens</i>	Human	Thioredoxin reductase 2	NP006431	45.5	59.3	524
15. <i>Mus musculus</i>	Mouse	Thioredoxin reductase 2	NP038739	44.6	57.9	527

3.2. Comparative analysis of *RbTrxR-3* gene architecture

Using the Spidey server, we determined that *RbTrxR-3* consists of 16 exons and 15 introns spread along a 12658 bp sequence, according to the canonical AG-GT splicing rule (Fig. 44). To gain a better understanding of the molecular evolution and genomic diversity of TrxR-3, we compared the gDNA sequences TrxR-3 genes from a number of vertebrate taxa (Fig. 44). With the exception of the lengths of exons 4 and 9, the architecture of the internal exons those flanked by the first and last exons—were conserved among the different taxonomic groups, which included teleosts, mammals, and birds. Interestingly, the size of each exon was found to be conserved among teleosts; further teleosts and mammals shared 13 exons with equal length (exon 2 to 15, except exon 4). Notably, the number of exons (16) in lower vertebrates (i.e., teleosts) and higher vertebrates (i.e., mammals and birds) were highly conserved, confirming that no gain or loss of introns had occurred during the molecular evolution of vertebrate TrxR-3s. Moreover, the splitting of the *TrxR-3* into a relatively high number of exons could indicate the existence of *TrxR-3* splice variants in teleosts and other vertebrates (Keren et al., 2010) and tightly regulated gene expression, a process in which introns are known to be involved (Rose, 2008). However, these predictions warrant further investigation. The overall comparison of TrxR-3 gene architecture in vertebrates suggests that the gene has a slow rate in genomic evolution and a greater potency of eliciting significant diversity at protein level through formation of spliced variants.

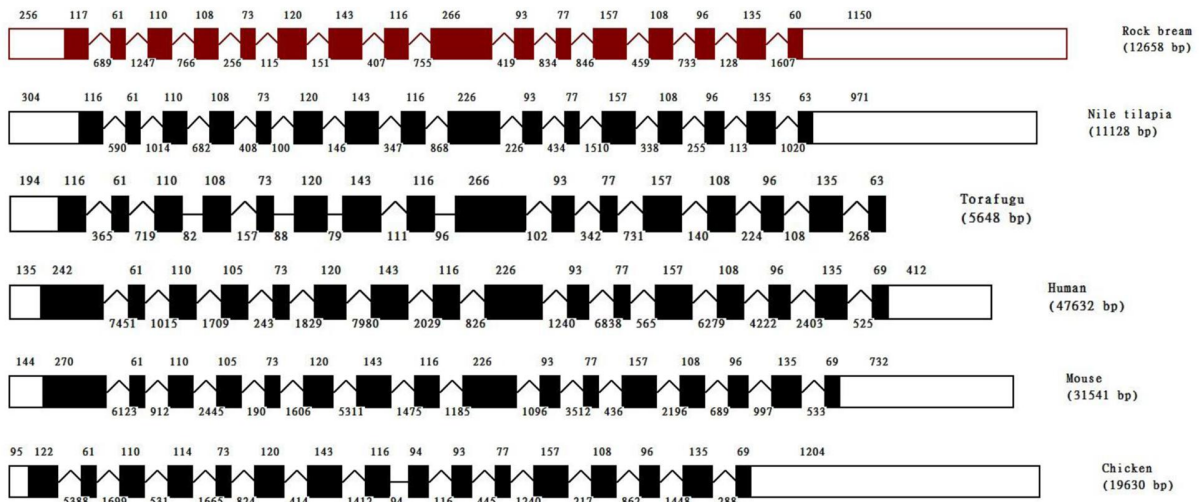


Fig. 44. Genomic architecture of *RbTrxR-3* and its vertebrate orthologs. UTR and coding regions are represented by empty and filled boxes, respectively. Introns less than 100 bp are denoted using black lines and those >100 bp are depicted as Λ -shaped lines. The intron and exon lengths are indicated at the top and bottom of each structure, respectively. The genomic DNA sequence information for each ortholog was obtained from the NCBI-GenBank database: Nile tilapia, 100702976; Torafugu, 101068545; mouse, 232223; human, 114112; and chicken, 416031.

3.3. Phylogenetic reconstruction of RbTrxR-3

As expected, our phylogenetic reconstruction clearly separated the different vertebrate TrxR orthologs into three main clusters according to the basic isoforms: TrxR-1, TrxR-2, and TrxR-3. Within the TrxR-3 cluster, mammalian, bird, amphibian, and fish orthologs clustered closely and independently in which RbTrxR-3 clustered within the fish (piscine) clade (Fig. 45). RbTrxR-3 subclustered with sea bass TrxR-3 within the fish clade, with a supporting bootstrap value of 100. However, zebrafish TrxR-3 showed a relatively distant evolutionary relationship

with the other two marine teleost homologs. Taken together, our phylogenetic analysis, based on the TrxR protein sequences of different species, confirmed that RbTrxR-3 is a vertebrate TrxR-3 isoform that has evolved from a common ancestral piscine gene.

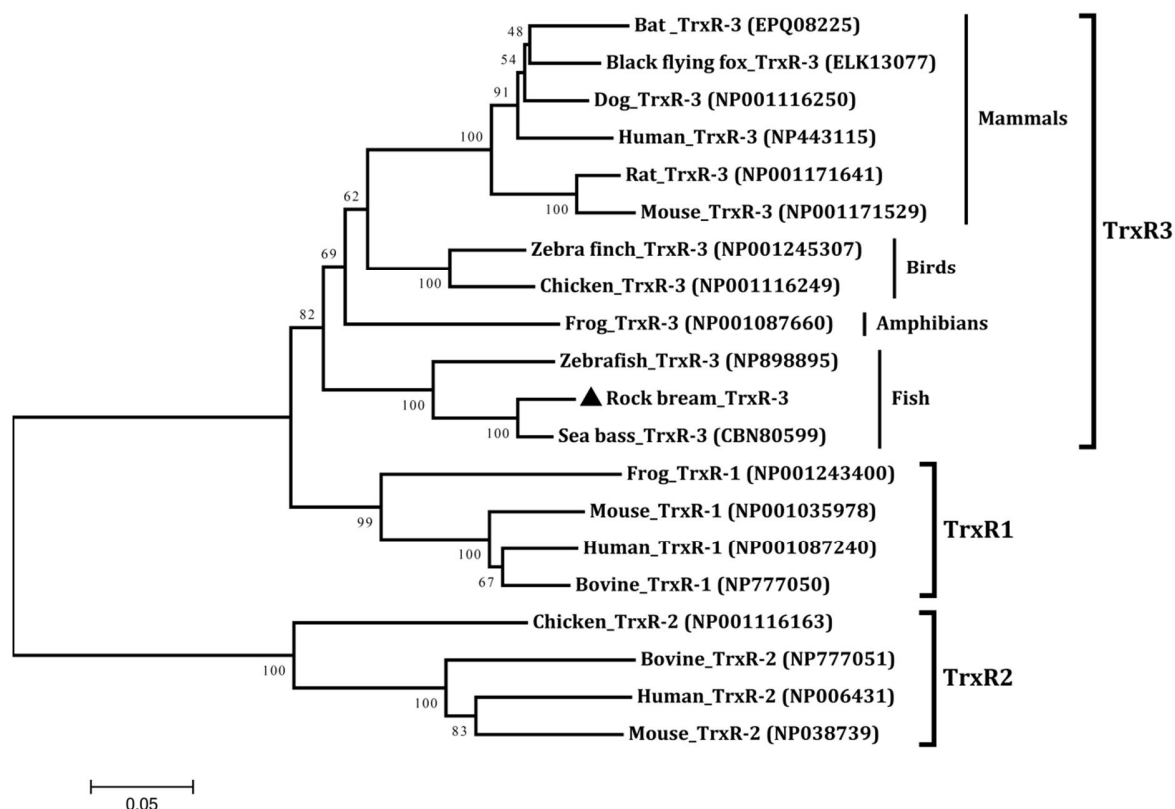


Fig. 45. Phylogenetic reconstruction of RbTrxR-3. The evolutionary development of RbTrxR-3 was analyzed with its different homologous (including the isoforms of TrxRs) categorized under different taxonomic groups based on the multiple alignment profile of the protein sequences generated by the neighbor-joining method using MEGA 5.0 software. Bootstrap support values corresponding to the each branch are indicated. The NCBI-GenBank accession numbers of each TrxR ortholog is listed in Table 15.

3.4. Integrity of purified rRbTrxR-3

We performed SDS-PAGE analysis on samples collected at different steps in the overexpression and purification procedure of rRbTrxR-3. The recombinant RbTrxR-3-MBP fusion protein was successfully expressed in *E. coli* BL21 cells and purified (Fig. 46). A single band (Fig. 46, lane 2) was observed at ~102.5 kD, consistent with predicted molecular mass of reduced RbTrxR-3 (~66 kD; mass of MBP is ~42.5 kD), confirming the purity and integrity of the recombinant protein. Interestingly, two bands were resolved for the eluted fusion protein when the polyacrylamide gel was run under non-reducing conditions (Fig. 46, lane 5) suggesting that rRbTrxR-3 formed dimers. Because homodimerization is a characteristic of TrxRs, these data further support to our prediction on rRbTrxR-3's homology to known TrxR-3s.

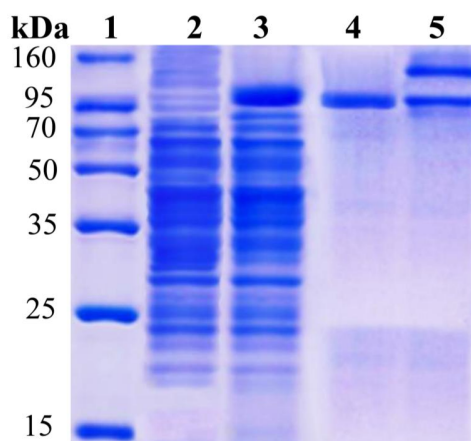


Fig. 46. SDS-PAGE analysis of the rRbTrxR-3 fusion protein at different steps in the overexpression and purification process. Lane 1, protein size marker (Enzygnomics, Korea); lane 2, total cellular extract from *Escherichia coli* BL21 (DE3) carrying the rRbTrxR-3-MBP expression vector prior to the IPTG induction; lane 3, crude rRbTrxR-3 fusion protein extract; lane 4, purified recombinant fusion protein (rRbTrxR-33-MBP) under reducing conditions; and lane 5, purified recombinant fusion protein (rRbTrxR-3-MBP) under non-reducing conditions

3.5. Thiol-reductase activity of RbTrxR-3

In the presence of NADPH, rRbTrxR-3 reduced the thiol groups of DTNB, producing 5'-thiol-2-nitrobenzoic acid (TNB²⁻), which generates a strong yellow color with an absorption maximum (λ_{\max}) of 412 nm (Fig. 47). OD₄₁₂ values increased with increasing rRbTrxR-3 concentration. Thus, RbTrxR-3 possesses a typical functional property of TrxR family members, suggesting their functional homology. Compared to rRbTrxR-3, MBP had negligible reducing activity against DTNB, as indicated by significantly lower OD₄₁₂ values, suggesting that MBP did not affect the function of the rRbTrxR-3 fusion protein. Consistent with the dose-dependent thiol-reducing activity of RbTrxR-3 observed in this study, *Entamoeba histolytica* (Arias et al., 2012) and *Caenorhabditis elegans* (Lacey and Hondal, 2006) TrxR proteins also demonstrated marked concentration- and NADPH-dependent thiol reductase activities against DTNB.

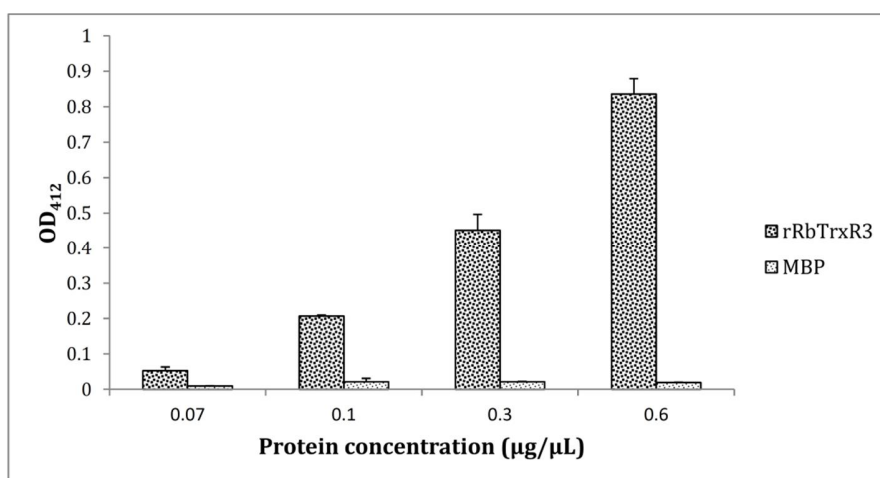


Fig. 47. *In vitro* DTNB-reducing activity of rRbTrxR-3. Reducing activities of rRbTrxR-3 and MBP towards DTNB were measured using a colorimetric assay. The yellow-colored reduction product produced in each sample was quantified using OD₄₁₂ measurements. Error bars represent SD (n = 3).

3.6. Distribution of *RbTrxR-3* mRNA in rock bream tissues

RbTrxR-3 was ubiquitously distributed in rock bream tissues, with blood tissue showing the highest mRNA expression level (Fig. 48). Gill and liver tissues had moderately high *RbTrxR-3* transcript levels. The differential levels of *RbTrxR-3* mRNA expression detected in the different tissue types examined may reflect distinct levels of metabolic activity in those tissues, which may in turn reflect differences in ROS levels, because TrxR has a known function in balancing ROS levels.

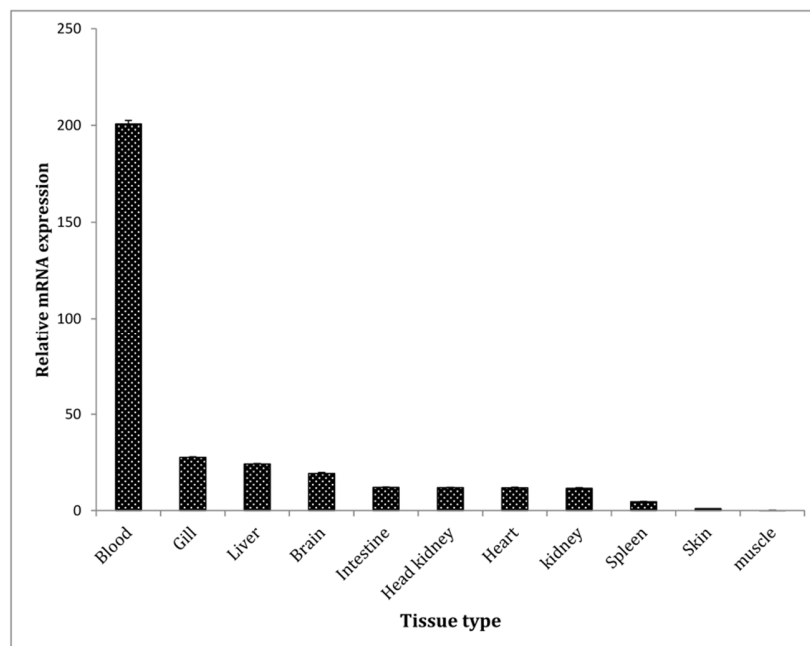


Fig. 48. Tissue distribution of *RbTrxR-3* mRNA expression, analyzed using qPCR. Relative expression values were determined by comparing the expression in each tissue to that in the skin. Error bars represent SD (n = 3).

Blood cells, especially phagocytic cells, can produce excessive amounts of ROS in response to invading pathogens as a first-line host defense mechanism, eventually activating immune signaling pathways (Kohchi et al., 2009). Moreover, blood cells have a higher level of oxygen consumption, which in turn potentiates ROS formation. Therefore, we speculate that TrxRs are expressed at high levels in certain tissues, such as in rock bream blood cells, to maintain an optimum redox balance. TrxR can also directly act upon NK-lysin-like cytotoxic compounds produced by T-lymphocytes to deactivate them after they have completed their function (Andersson et al., 1996). This may also explain the pronounced *RbTrxR-3* mRNA expression in blood cells. Similarly, one isoform of rainbow trout TrxR-3 (TrxR-3a) showed its highest basal expression in blood cells whereas the other (TrxR-3b) also found to be pronouncedly expressed in blood (Pacitti et al., 2014). The gills of fish are continuously exposed to the aquatic environment, increasing the risk of frequent microbial infections. As mentioned above, ROS are formed in response to invading pathogenic microorganisms as a primitive immune defence strategy that is executed by immune cells in tissues including the gills (Kohchi et al., 2009). Therefore, to prevent the harmful effects of oxidative stress in these cells, antioxidative defense mechanisms must be activated in host organisms, in which the thioredoxin system plays an indispensable role. Therefore, pronounced TrxR expression would be expected in gill tissues of teleost fish, consistent with our findings. Moreover, the high levels of *RbTrxR-3* in liver tissues can be attributed to the prominent metabolic activity of liver cells, which contributes to ROS production (Martin et al., 2002). In response to oxidative stress, liver cells can undergo apoptosis (Kamata et al., 2005); thus, the abundant mRNA expression of *RbTrxR-3* in liver tissues may relate to the known anti-apoptotic function of TrxRs. Although, pronounced expression of other

fish TrxRs in liver have not been reported to date, it is not uncommon to find abundant TrxR expression in the livers of higher vertebrates such as rats (Lee et al., 1999).

3.7. Temporal transcriptional response of *RbTrxR-3* to live pathogenic stimuli

Liver tissues are known to play an important role in host immunity (Sheth and Bankey, 2001); thus, we examined the transcriptional response of *RbTrxR-3* in the livers of rock breams exposed to live bacterial and viral pathogenic stimuli. Moreover, parallelly we investigated the transcriptional responses of the putative substrate *RbTrx-1* to the same stimuli, in order to compare those with corresponding expressional modulation of *RbTrxR-3*, deciphering the expressional behavior of thioredoxin system under pathogen stress. Both stimuli significantly increased *RbTrxR-3* mRNA expression ($P < 0.05$) during the middle (6 h and 12 h post-injection [p.i.]) and late phases (48 h p.i.) of the experimental period (Fig. 49A). Interestingly, transcript levels of the putative *RbTrxR-3* substrate in rock breams, *RbTrx-1*, were also elevated significantly ($P < 0.05$) during the middle (12 h p.i.) and late phase (24 h, and 48 h p.i.) in response to the live pathogens RBIV and *E. tarda*, while live *S.iniae* treatment was inducing its basal transcription throughout the whole period of post immune challenge. In contrast, *RbTrx-1* transcript levels were found to be significantly ($P < 0.05$) down-regulated at 6 h p.i. following RBIV challenge (Fig. 49B). Some viruses are known to diminish the expression of antioxidant enzymes to induce ROS formation in host cells in order to induce apoptosis and spread the infection to uninfected cell population (Borjesson et al., 2005; Yang et al., 2010). Thus, the initial down-regulation of *RbTrx-1* transcript may be part of the mechanism of RBIV infection

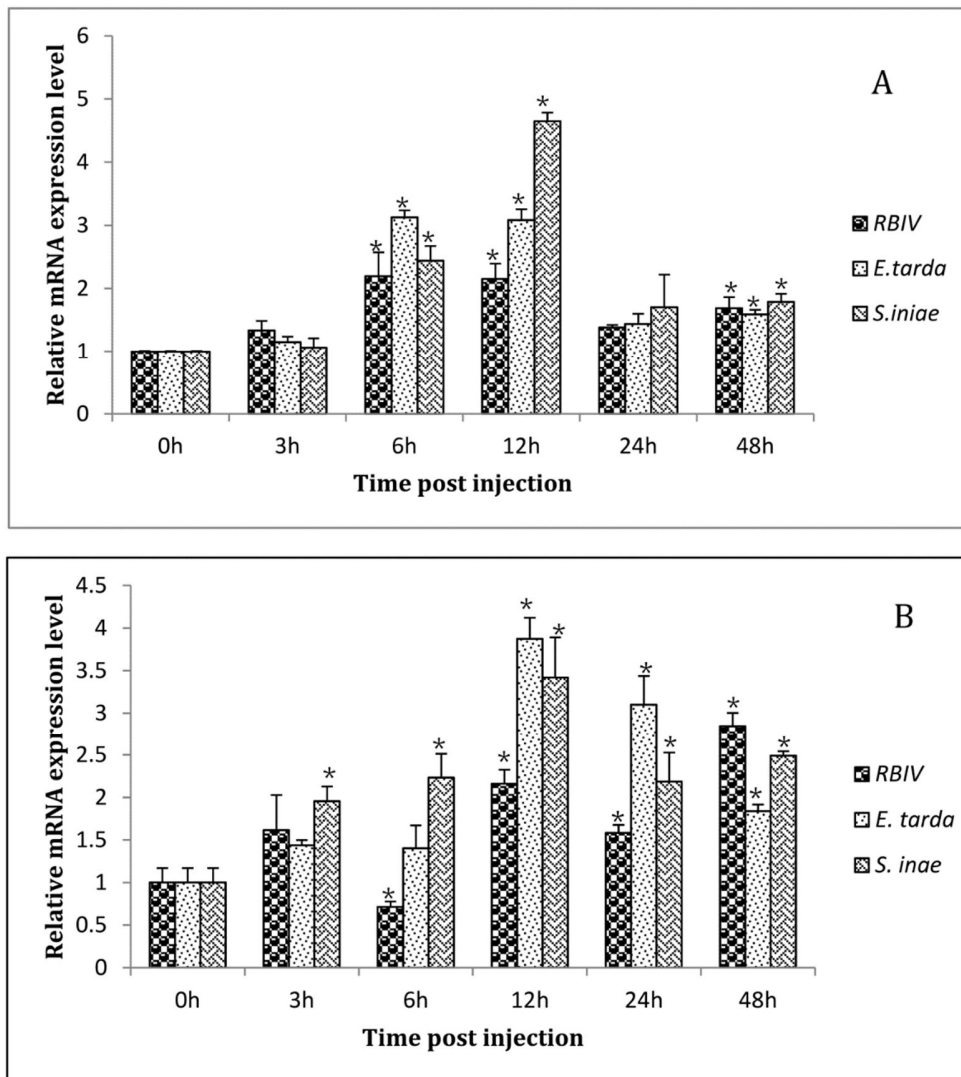


Fig. 49. Temporal mRNA expression of *RbTrxR-3* (A) and *RbTrx-1* (B) in the liver tissues of rock breams, under live pathogen stress induced by *Edwardsiella tarda*, *Streptococcus iniae*, and RBIV. The relative expression levels were calculated using the $2^{-\Delta\Delta CT}$ method, using rock bream β -actin as a reference gene. Expression levels were further normalized to the corresponding expression levels in PBS-injected controls at each time point. The relative expression at 0 h post-stimulation (uninjected control) was set as the baseline. Error bars represents SD (n = 3); * $P < 0.05$.

Phagocytosis, a process associated with the innate immune system, can efficiently mediate the recognition and elimination of pathogenic invaders (Vatansever et al., 2013). In this complex process, phagocytic cells, such as macrophages and neutrophils in different immune defense-related tissues including the liver, engulf invading microbial pathogens and destroy them using numerous chemical species, including ROS. Therefore, immediately after microbial infection, ROS production is expected to increase, leading to oxidative burst (Forman et al., 2010). As a consequence, endogenous antioxidative defense mechanisms (Nordberg and Arner, 2001) are activated to counterbalance the ROS surplus. In this regard, it is not unexpected to observe the activation of Trx system, especially in liver cells. Thus, the marked increase we observed in *RbTrxR-3* expression at mRNA level most likely occurred in response to live pathogenic stress. Consistent with these findings, *RbTrx-1* transcript levels were elevated in response to the same stimuli. The reduced form of Trx, which is produced as a result of TrxR catalytic activity, was found to activate several transcriptional factors, including NF- κ B (Nishiyama et al., 2001), that are known to induce the expression of cytokines and antimicrobial effectors (Hayden et al., 2006). Moreover, TrxRs can act upon antimicrobial compounds such as NK-lysin to inactivate them upon completion of their antimicrobial function (Andersson et al., 1996). These facts may also explain the elevated levels of *RbTrxR-3* transcript in liver tissue in rock breams exposed to live bacterial and viral stimuli.

4. CONCLUSION

Here, we characterized a rock bream TrxR and investigated its transcriptional response to the pathogen invasion, along with functional properties that are important in host antioxidant defense. The results of our *in silico* homology analysis and phylogenetic construction showed

that RbTrxR-3 is a TrxR family ortholog. The genomic architecture of *RbTrxR-3* convinced its potency to be contributed in diversity at protein level, probably forming its spliced variants. Moreover, the ubiquitous mRNA expression of this TrxR ortholog highlights its putative functional importance in fish physiology. Interestingly, the transcriptional response of *RbTrxR-3* in the livers of rock breams under live pathogen stress correlated with the temporal mRNA expression pattern of its putative substrate, *RbTrx-1*, suggesting that it may play an important role in immune or post-immune responses. In addition, the detectable thiol reductase activity of RbTrxR-3 further hints its plausible involvement in the rock bream Trx system. Overall, the findings of this study indicate that RbTrxR-3 plausibly plays a role in defending against oxidative stress.

PART C

Characterization of ferritin H (FerH) subunit from rock bream

1. ABSTRACT

Ferritins are iron binding proteins made out of 24 subunits, involved in iron homeostasis and metabolism in cellular environments. Here, we sought to identify and functionally characterize a one type of subunits of ferritin (ferritin H-like subunit) from rock bream (*Oplegnathus fasciatus*; RbFerH). The complete coding sequence of *RbFerH* was 531 bp in length, encoding a 177-amino acid protein with a predicted molecular mass of 20.8 kD. The deduced protein structure possessed the domain architecture characteristic of known ferritin H subunits, including metal ligands for iron binding, a ferroxidase center, and two iron-binding region signatures. As expected, the 5' untranslated region of the *RbFerH* cDNA sequence contained a putative iron response element region, a characteristic regulatory element involved in its translation. The *RbFerH* gene comprised 5 exons and 4 introns spanning a 4195 bp region. Overexpressed recombinant RbFerH protein demonstrated prominent Fe(II) ion depriving activity, bacteriostatic properties, and protective effects against oxidative double-stranded DNA damage. Using quantitative polymerase chain reaction (qPCR), we found that *RbFerH* was expressed ubiquitously in the majority of physiologically important tissues in rock bream. A greater abundance of the mRNA transcripts were detected in blood and liver tissues. Upon administering different microbial pathogens and pathogen-derived mitogens, *RbFerH* transcription was markedly elevated in the blood of rock bream. Taken together, our findings suggest that RbFerH

acts as a potent iron sequestrator in rock bream and may actively participate in antimicrobial as well as antioxidative defense.

2. MATERIALS AND METHODS

2.1. Identification and sequence analysis of *RbFerH*

To identify the full-length cDNA sequence of *RbFerH*, we analyzed rock bream DNA sequence data from a cDNA library, constructed previously (section 2.1, part A in chapter 2). by using the Basic Local Alignment Search Tool (BLAST) algorithm (<http://blast.ncbi.nlm.nih.gov/Blast.cgi>). The putative complete open reading frame (ORF) of *RbFerH* was identified and the corresponding amino acid sequence was deduced using the DNAsist 2.2 software. Protein domains were predicted using the ExPASy Prosite database (<http://prosite.expasy.org>). Physicochemical properties were determined using the ExPASy ProtParam tool (<http://web.expasy.org/protparam>). Pairwise and multiple sequence comparisons of *RbFerH* with its homologues were performed using the EMBOSS needle (<http://www.Ebi.ac.uk/Tools/emboss/align>) and ClustalW2 (<http://www.Ebi.ac.uk/Tools/clustalw2>) programs, respectively. The phylogenetic reconstruction of *RbFerH* and its orthologs was generated by the neighbor-joining method using Molecular Evolutionary Genetics Analysis version 4.0 (MEGA 4.0) software (Tamura et al., 2007).

The complete gene sequence of *RbFerH* was also identified in a custom constructed rock bream random-shear bacterial artificial chromosome (BAC) genomic DNA library (Lucigen®, USA). The BAC clone bearing the *RbFerH* gene was identified using a two-step polymerase chain reaction (PCR)-based genomic library screening approach using gene specific-primers

(RbFerHqF and RbFerHqR; Table 16). The putative *RbFerH*-containing clone was then sequenced using the GS-FLXTM system (Macrogen, Korea) to obtain full-length genomic sequence. Using the National Center for Biotechnology Information (NCBI) Spidey online server (<http://www.ncbi.nlm.nih.gov/spidey>) and previously identified full-length *RbFerH* cDNA sequences, we annotated the exon-intron arrangement. Annotated sequence information for *RbFerH* was deposited in the NCBI GenBank database (accession number KJ461740).

Table 16. Oligomers used in the study on RbFerH

Name	Purpose	Sequence (5' → 3')
RbFerH-qF	BAC library screening and qPCR of <i>RbFerH</i>	GGATGACCAGGCATTGCACAACCTT
RbFerH-qR	BAC library screening and qPCR of <i>RbFerH</i>	AGGGACTGGTTCACGCTCTTCT
RbFerH-F	ORF amplification (<i>EcoRI</i>)	GAGAGAGaattcATGAGTTCCCAGGTGAGACAGAACTTC
RbFerH-R	ORF amplification (<i>HindIII</i>)	GAGAGAAagcttTTAGCTGCTTTCTTTGCCAGGGT
Rb-βF	qPCR for rock bream β-actin gene	TCATCACCATCGGCAATGAGAGGT
Rb-βR	qPCR for rock bream β-actin gene	TGATGCTGTTGTAGGTGGTCTCGT

2.2. Expression and purification of recombinant RbFerH fusion protein

rRbFerH fused to maltose binding protein (MBP) was expressed and purified as previously described, but with some modifications (section 2.5-Part A in chapter 2). Briefly, the coding sequence of the *RbFerH* gene was amplified using the sequence-specific primers RbFerH-F and RbFerH-R, which contained restriction enzyme sites for *EcoRI* and *HindIII*, respectively (Table 16). PCR was performed in a TaKaRa thermal cycler (TaKaRa, Japan) in a total volume of 50 μL containing 5 U TaKaRa ExTaq polymerase, 5 μL of 10× TaKaRa ExTaq buffer, 8 μL 2.5 mM dNTPs, 80 ng of template, and 20 pmol of each primer. The PCR was performed under the following conditions: initial denaturation at 94°C for 3 min, followed by 35 cycles of 94°C for

30 s, 57°C for 30 s, 72°C for 1 min, with a final extension at 72°C for 5 min. The PCR product (~534 bp) was resolved on a 1% agarose gel, excised, and purified using the Expin™ Gel SV kit (GeneAll., Korea). Digested pMAL-c2X vector (170 ng) and PCR product (40 ng) were ligated using Mighty Mix (5.0 µl; TaKaRa) at 4°C overnight. The ligated pMAL-c2X/RbFerH product was transformed into DH5α cells and sequenced. After sequence validation, the recombinant expression plasmid was transformed into *Escherichia coli* BL21 (DE3) competent cells. Expression of the rRbFerH fusion protein was induced using isopropyl-β-D-galactopyranoside (IPTG, 1 mM). *E. coli* cells were grown in 500 mL Luria broth (LB) supplemented with ampicillin (100 µg/mL) and glucose (0.2%) at 37°C for 3 h. Induced *E. coli* BL21 (DE3) cells were then cooled on ice for 30 min and harvested by centrifugation at 3500 rpm for 30 min at 4°C. Harvested cells were resuspended in 20 mL of column buffer (20 mM Tris-HCl pH 7.4 and 200 mM NaCl) and stored at -20°C. *E. coli* cells were thawed and lysed in column buffer using cold sonication. The protein was then purified using the pMAL™ Protein Fusion and Purification System (New England BioLabs, Ipswich, MA, USA). The purified protein was eluted using an elution buffer (10 mM maltose in column buffer). Its concentration was determined using the Bradford method using bovine serum albumin as the standard (Bradford, 1976). Next, the rRbFerH-MBP fusion product was cleaved using Factor Xa, according to the pMAL™ Protein Fusion and Purification kit protocol. The resultant cleaved protein (rRbFerH) was assayed for its iron(II) depriving, antibacterial, and oxidative DNA damage protection activities. Samples collected at different steps of the rRbFerH purification were analyzed by reducing 12% sodium dodecyl sulfate polyacrylamide gel electrophoresis (SDS-PAGE) using standard protein size markers (Enzyomics, Korea). The gel was stained with 0.05% Coomassie blue R-250, followed by a standard destaining procedure. In addition, to analyze the purified

rRbFerH under native conditions, rRbFerH was analyzed by non-reducing native-PAGE using apoferritin from equine spleen (Sigma – USA) as a marker.

2.3. Iron(II) depriving activity of rRbFerH

The iron(II) depriving activity of rRbFerH was determined using a previously published method with some modifications (De Zoysa and Lee, 2007). Briefly, 20 μ L of 2 mM FeSO₄ was added to 1 mL of the recombinant protein diluted to different concentrations in column buffer. Samples were incubated at room temperature (25°C) for 10 min. To each sample, 5 mM ferrozine (Sigma, USA) was added. Samples were mixed thoroughly and incubated again at room temperature for 15 min. The optical density (OD) of each sample was measured at 562 nm by using a spectrophotometer. To investigate the effect of MBP in the cleaved recombinant fusion protein samples, corresponding concentrations of Factor Xa-cleaved recombinant MBP were used as controls. Each assay was performed in triplicate and the mean OD value was used to calculate the percentage of Fe(II) deprivation. Moreover, in order to determine whether the ferroxidase center in rRbFerH is active, the above assay was repeated in triplicates using 25 μ g of rRbFerH (~ 0.02 μ g/ μ L) under reducing conditions. Therein, reducing medium was produced by the addition of Tin (II) ions (~0.16 M) into the reaction medium as a potent reducing agent of Fe (III) ions possibly formed by the ferroxidase activity of rRbFerH, after the first incubation at room temperature and again incubated for 5 min after the addition of Tin (II) in to the medium, before addition of ferrozine into the final reaction medium. Finally, the OD₅₆₂ values obtained for the Fe(II) – ferrozine complex formed in this reaction setup and that of non-reducing conditions (without tin (II)) were compared with the OD values detected for the control (reaction setups without rRbFerH) to calculate the percentage Fe(II) deprivation.

2.4. Antibacterial activity of rRbFerH

To analyze the effect of RbFerH on *E. coli* (DH5 α) bacterial growth, we measured *E. coli* cell density in liquid culture media at various time points after treating the culture with purified rRbFerH. Bacteria were cultured initially in LB medium at 37°C until they reached the exponential phase. Cultures were then diluted in fresh LB medium to $\sim 10^4$ CFU/mL. Diluted cultures were separated into three aliquots (170 mL each). To one of the three aliquots, rRbFerH (50 μ g/mL), recombinant MBP (50 μ g/mL), or column buffer was added. Aliquots were distributed into the wells of a 96-well cell culture plate. Plates were incubated at 37°C and cell densities were analyzed by measuring OD₆₀₀ at different time points post-incubation. The assay was carried out in triplicate and the mean OD₆₀₀ reading at corresponding time points was used as the net OD value.

2.5. Determination of the effect of rRbFerH on oxidative damage of DNA

We evaluated the effect of rRbFerH on DNA strand breakage under conditions of oxidative stress. The conversion of supercoiled plasmid DNA to nicked (circular) form DNA was measured in solutions containing Fe(II) ions and H₂O₂ in the presence and absence of rRbFerH. Briefly, rRbFerH was added separately into the Fe(II)-containing (0.33 mM) column buffer to achieve a final concentrations of approximately 0.4 and 0.8 μ g/ μ L in a total volume of 45 μ L. The mixtures were then incubated at room temperature for 15 min. Subsequently, pUC19 (2 μ g) and H₂O₂ (final concentration of ~ 2.86 mM) were added. Reactions were incubated at 37°C for 10 min to induce DNA breakage through the formation of hydroxyl radicals from the reaction of Fe(II) and H₂O₂. Factor Xa-treated recombinant MBP (final concentration of 0.8 μ g/ μ L) was used in one parallel assay in place of rRbFerH as a control. Another control assay was performed

using an equal volume of column buffer without protein. Immediately after incubation, DNA in each reaction mixture was purified using the Expin™ PCR SV kit (GeneAll., Korea) according to manufacturer's instructions, thus terminating the DNA cleavage reactions. The purified DNA was eluted using 30 μ L of DNA elution buffer and the total volume was loaded onto a 1% agarose gel and analyzed by electrophoresis. Bands were compared to undigested pure pUC19 vector DNA. The assay was repeated three times to confirm the reliability of results.

2.6 Experimental fish and tissue collection

Healthy rock bream with an average body weight of 50 g were obtained from the Jeju Special Self-Governing Province Ocean and Fisheries Research Institute (Jeju, Republic of Korea). Animals were acclimatized for 1 week prior to the experiment in a controlled environment (34 ± 1 practical salinity units, pH 7.6 ± 0.5 , and $22\text{--}24^\circ\text{C}$). Fish used for tissue collection were maintained in 400 L tanks and fed a commercially available fish feed. Whole blood (1 mL/fish) was collected from the caudal fin by using a sterilized syringe. The samples were immediately centrifuged at $3000 \times g$ for 10 min at 4°C to separate the blood cells from the plasma. The collected cells were snap-frozen in liquid nitrogen. Fish were sacrificed, and the gill, liver, skin, spleen, head kidney, kidney, heart, muscle, brain, and intestine were excised. Tissues were snap-frozen in liquid nitrogen and stored at -80°C until they were used for total RNA extraction.

2.7. Immune challenge experiments

In time-course immune challenge experiments, we investigated the transcriptional regulation of *RbFerH* in response to pathogenic infection by *Edwardsiella tarda* and rock bream Iridovirus (RBIV), and immune stimulation elicited by lipopolysaccharides (LPS) and polyinosinic:polycytidylic acid (Poly I:C). *E. tarda* was obtained from the Department of Aqualife Medicine, Chonnam National University, Korea. The bacteria were incubated at 25°C for 12 h in brain-heart infusion broth (Eiken Chemical Co. Japan) supplemented with 1% sodium chloride. The cultures were resuspended in sterile phosphate-buffered saline (PBS) and diluted to the desired concentration ($1 \times 10^5/\text{mL}$) for injection. For the virus challenge experiment, kidney tissue specimens were obtained from moribund rock bream infected with RBIV and homogenized in 20 volumes of PBS. Tissue samples were centrifuged at $3000 \times g$ for 10 min at 4°C to obtain the RBIV containing supernatants. Supernatants were filtered through a 0.45 μm membrane and injected into the fish. LPS (*E. coli* 055:B5, Sigma) was resuspended in sterilized PBS to reach the desired concentration for injection. The immune challenge experiments were performed as previously described (section 2.9.-part A in chapter 2). Tissues were collected from at least 3 animals from each challenge group at each time point. Tissues were collected as described in Section 2.6.

2.8 Total RNA extraction and cDNA synthesis

Using Tri Reagent™ (Sigma), total RNA was extracted from the blood, gill, liver, spleen, head kidney, kidney, brain, skin, muscle, intestine, and brain tissues from healthy rock breams, as well as from blood cells collected from immune-challenged animals according to the

manufacturer's instructions; subsequently cDNA was synthesized from each total RNA as previously described (section 2.10-part A in chapter 2).

2.9 *RbFerH* transcriptional analysis by quantitative real-time PCR

Quantitative real-time PCR (qPCR) was used to analyze the expression levels of *RbFerH* in the blood, gill, liver, spleen, head kidney, kidney, skin, muscle, brain, and intestine tissues of healthy fish. The temporal expression of *RbFerH* in liver tissues of immune-challenged animals was also measured using qPCR. Total RNA was extracted at different time points following the respective immune challenges, and first-strand cDNA synthesis was performed as described in Section 2.8. qPCR was performed using the Dice™ Real-Time System thermal cycler (TP800; TaKaRa, Japan) in a 15 μ L reaction volume containing 4 μ L of diluted cDNA from each tissue, 7.5 μ L of 2 \times TaKaRa ExTaq™ SYBR premix, 0.6 μ L of each primer (*RbFerH*-qF and *RbFerH*-qR; Table 16), and 2.3 μ L of ddH₂O as per the essential MIQE guidelines (Bustin et al., 2009). qPCR analysis was performed under the following conditions: 95°C for 10 s; 35 cycles of 95°C for 5 s, 58°C for 10 s, and 72°C for 20 s; and a final cycle of 95°C for 15 s, 60°C for 30 s, and 95°C for 15 s. The baseline was set automatically by the Dice™ Real Time System software (version 2.00). *RbFerH* expression was determined using the Livak ($2^{-\Delta\Delta CT}$) method (Livak and Schmittgen, 2001). The same qPCR cycle profile parameters were used for the internal control gene, rock bream β -actin (GenBank ID: FJ975145). The primers used for the control gene are listed in Table 13. No tissue-specific difference in β -actin expression was observed under these experimental conditions. The data are presented as the mean \pm standard deviation (SD) of the relative mRNA expression in experiments performed in triplicate. To determine statistical significance ($P < 0.05$) between the experimental and control groups, two-tailed un-paired Student's *t*-tests were performed. In immune challenge experiments, the expression levels of

RbFerH mRNA relative to that of the rock bream β -actin gene were calculated. Values were further normalized to the corresponding PBS-injected controls at each time point. The relative expression level in the uninjected control at the 0-h time point was used as the baseline reference.

3. RESULTS AND DISCUSSION

3.1. Sequence profiles and homology

The *in silico* analysis of the identified cDNA sequence (1151 bp) showed that *RbFerH* consisted of a 531 bp coding sequence flanked by 307 bp 5' and 313 bp 3' untranslated regions (UTRs). Resembling the typical characteristics of ferritin H subunits, the 5' UTR of *RbFerH* bears an iron response element (IRE - ⁴⁸TTACCTGCTTCAACAGTGCTTGAACGGCAA⁷⁷), which is important to regulate its expression depending on the availability of Fe(II) in the cellular environment (Thomson et al., 1999). The deduced amino acid sequence of RbFerH consisted of 177 amino acids. We calculated the molecular mass to be ~20.8 kD and the theoretical isoelectric point was 5.56. The amino acid sequence of RbFerH possessed the characteristic domain architecture of ferritin H, including two iron-binding region signatures (⁵⁸EEREHAEKLMKLNQRGGR⁷⁶ and ¹²³DPHLCDFIETHYLDEQVK¹⁴⁰) and seven putative amino acid residues that comprise the ferroxidase center (E-24, Y-31, E-58, E-59, H-62, E-104, and Q-138) (Fig.50).

Sea bass	---	MSSQVRQNFHQDCEAAINRQINLELYASYVYLSMAYYFDRDDQALHNFAKFFRNQS	56
Large yellow croaker	---	MSSQVRQNFHQDCEAAVNRQINLELYASYVYLSMAYYFDRDDQALHNFAKFFRNQS	56
Rock bream	---	MSSQVRQNFHQDCEAAINRQINLELYASYVYLSMAYYFDRDDQALHNFAKFFRNQS	56
Orange-spotted grouper	---	MSSQVRQNYHQDCEAAINRQINLELYASYVYLSMGYYFDRDDQALHNFAKFFRHQS	56
Zebrafish	---	MSSQVRQNFEEACEAAVNRQINMELYASYVYLSMSYYFDRDDQALHNFAKFFRHQS	56
Human		MTTASTQVRQNYHQDSEAAINRQINLELYASYVYLSMSYYFDRDDVALKNFAKYFLHQ	60
Mouse		MTTASPSQVRQNYHQDAEAAINRQINLELYASYVYLSMSCYFDRDDVALKNFAKYFLHQ	60
Chicken		MATP-PSQVRQNYHQDCEAAINRQINLELYASYVYLSMSYYFDRDDVALKNFAKYFLHQ	59
Frog	---	MNSQIRQNFHQEACEAAINRQVNMELYASYVYLSMSYYFDRDDVALKNFAKYFLHQ	56
		* *	
Sea bass		QEEREHAEKLMKVQNQRGGRIFLQDIRKPERDEWGSIEALECALQLEKSVNQSLLDLHK	116
Large yellow croaker		QEEREHAEKLMKLNQRGGRIFLQDIRKPERDEWGSIEALECALQLEKSVNQSLLDLHK	116
Rock bream		HEEREHAEKLMKLNQRGGRIFLQDVVKPERDEWGSIEALECALQLEKSVNQSLLDLHK	116
Orange-spotted grouper		HEEREHAEKLMKLNQRGGRIFLQDVKKPERDEWGSIEALECALQLEKSVNQSLLDLHK	116
Zebrafish		HEEREHAEKLMKLFQNRGGRIFLQDVKKPEKDEWGSIEALECALQLEKSVNHSLLELHK	116
Human		HEEREHAEKLMKLNQRGGRIFLQDIKKPCDDWESGLNAMECALHLEKSVNQSLLELHK	120
Mouse		HEEREHAEKLMKLNQRGGRIFLQDIKKPRDDWESGLNAMECALHLEKSVNQSLLELHK	120
Chicken		HEEREHAEKLMKLNQRGGRIFLQDIKKPRDDWENGLTAMECALHLEKSVNQSLLELHK	119
Frog		HEEREHAEKLMKMNQNRGGRIFLQDIKKPERDEWANGLEALECSLQLEKSVNQSLLELHK	116
		* *	
Sea bass		LCS DHNDPHL CDFIETHYLDE QVKS IKELADWV TNLRMGAP QNGMAEYLF DKHTL GKES	176
Large yellow croaker		LCS DHNDPHM CDFIETHYLDE QVKS IKELADWV TNLRMGAP QNGMAEYLF DKHTL GKES	176
Rock bream		LCS DHNDPHL CDFIETHYLDE QVKS IKELADWV TNLRMGAP QNGMAEYLF DKHTL GKES	176
Orange-spotted grouper		LCSEHNDPHL CDFIETHYLDE QVKS IKELADWV TNLRMGAP QNGLAEYLF DKHTMGKES	176
Zebrafish		LASQHNDPHM CDFIETHYLDE QVKS IKELGDHVTNLRMGAP QNGMAEYMF DKHTL GKES	176
Human		LATDKNDPHL CDFIETHYLNE QVKA IKELGDHVTNLRKMGAP ESGLAEYLF DKHTLGSD	180
Mouse		LATDKNDPHL CDFIETYLYSE QVKS IKELGDHVTNLRKMGAP EAGMAEYLF DKHTLGHD	180
Chicken		LATEKNDPHL CDFIETHYLDE QVKA IKELGDHVTNLRKMGAP KYGMAEYLF DKHTLGESD	179
Frog		LSTDHNDPHL CDFLESHYLDE QVKS MKELGDHITNLRMGAP SNGLAEYLF DKHTLGEDH	176
		* *	
Sea bass	S--	177	
Large yellow croaker	S--	177	
Rock bream	S--	177	
Orange-spotted grouper	S--	177	
Zebrafish	S--	177	
Human	NES	183	
Mouse	-ES	182	
Chicken	--S	180	
Frog	E--	177	

Fig. 50. Multiple sequence alignment of vertebrate ferritin H subunit orthologs including rock bream ferritin H (RbFerH). Two putative iron-binding region signatures of RbFerH are indicated by the double underline. Conserved residues involved in iron binding and the formation of the ferroxidase center are shaded in gray. Residues conserved in all the aligned sequences are denoted by asterisks (*).

The sequencing results showed that the *RbFerH* gene was 4195 nucleotides in length and split into 5 exons separated by 4 introns (Fig. 51). As shown in Fig. 51, orthologs from the other teleosts examined had five exons, suggesting they had similar genomic architecture. The size of the internal exons 2–4 (flanked by the first and last introns) and the coding region of the last exon were found to be highly conserved. Notably, the 5' UTR of *RbFerH* was split between two exons, a feature common to the genomic gene architectures of the other teleost species examined. The genomic organizations of teleost ferritin H genes were dramatically different compared to that of the higher vertebrates (mammals and birds). In this regard ferritin H genes belonging to mammals (human and mouse) and birds (chicken) contained only 4 exons, with the coding region starting on the first exon, while the teleost genes consisted of 5 exons. Therefore, we speculate that one intron was lost from the ferritin H genes of teleosts or single intron was acquired by teleostan counterparts at the divergence of the lower and higher vertebrates. Nevertheless, a loss of an intron likely trim down the functional diversity of ferritin H through reducing the number of variants generated by alternative splicing, while potentially increasing the rate of the gene evolution (Parmley et al., 2007; Keren et al., 2010) or *vice versa*. However, further studies on molecular evolutionary aspects of ferritin H should be carried out to draw clear conclusions on this observation. The sizes of exons 2 and 3 of the higher vertebrate ferritin H orthologs were observed to be identical to that of exons 3 and 4 of the teleost orthologs including *RbFerH*. These conserved exons may represent functionally important regions in the coding sequence of ferritins.

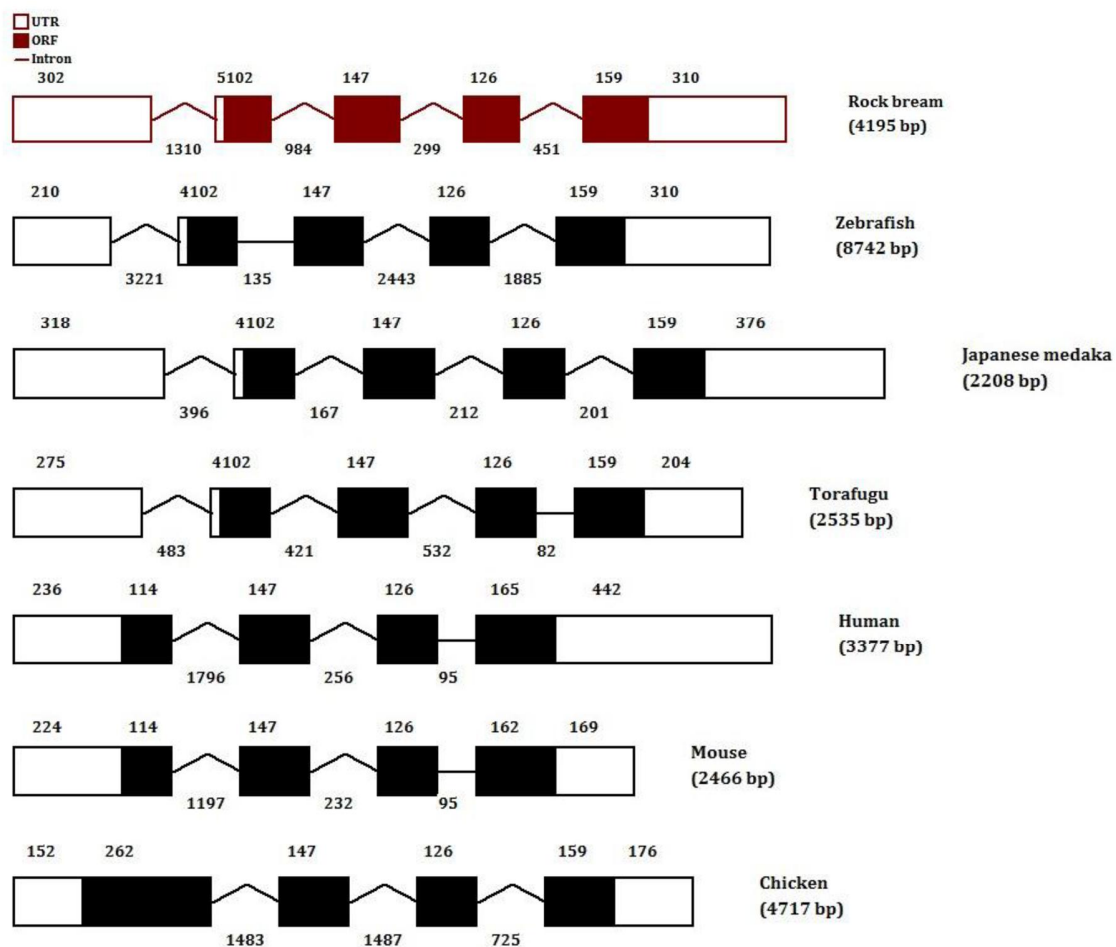


Fig. 51. Exon-intron arrangement of the RbFerH gene and its orthologs from other vertebrate species. Introns greater than 150 bp are indicated by peaked lines. The intron and exon lengths are indicated above and below each structure, respectively. The genomic DNA sequence information for each ortholog was obtained from the National Center for Biotechnology Information (NCBI) GenBank database. The NCBI gene ID numbers as follows: zebrafish, 18858718; Japanese medaka, 101169025; torafugu, 101064331; human, 2495; mouse, 14391; and chicken, 395970.

Identity and similarity analysis of RbFerH with its homologues was performed using pairwise sequence alignments. RbFerH shared clear homology with vertebrate ferritin H orthologs and substantial homology with ferritin M orthologs, which are known to possess properties similar to ferritin H subunits (Table 17). The ferritin H subunit of the European sea bass (*D. labrax*) showed the greatest percent sequence similarity and identity to RbFerH. On the other hand, RbFerH shared relatively low sequence similarity to the ferritin L orthologs included in the analysis, affirming the distant relationship between two subunit genes. Multiple sequence alignment of RbFerH with its vertebrate orthologs revealed that the seven amino acid residues of RbFerH that bind iron and form the ferroxidase center are conserved among all the orthologs examined. These data can partially validate that RbFerH is a homolog of the vertebrate ferritin H subunit (Fig. 50).

Table 17. Percentage similarity and identity values of RbFerH with its orthologs

Species name	Subunit type	NCBI accession number	Amino acids	Identity	Similarity
1. European seabass (<i>Dicentrarchus labrax</i>)	H	ACN80998	177	97.7	99.4
2. <i>Larimichthys crocea</i> (Large yellow croaker)	H	ACY75475	177	97.2	99.4
3. <i>Anoplopoma fimbria</i> (Sablefish)	H	ACQ59065	177	97.2	98.9
4. <i>Epinephelus coioides</i> (Orange-spotted grouper)	H	AEG78374	177	95.5	99.4
5. <i>Salmo salar</i> (Atlantic salmon)	H	NP001117129	177	92.7	98.9
6. <i>Danio rerio</i> (Zebrafish)	H	NP571660	177	88.7	94.9
7. <i>Xenopus laevis</i> (Frog)	H	NP001083072	182	80.2	94.4
8. <i>Taeniopygia guttata</i> (Zebra finch)	H	NP001232211	180	79.4	89.4
9. <i>Gallus gallus</i> (Chicken)	H	NP990417	180	78.9	90.0
10. <i>Mus musculus</i> (Mouse)	H	NP034369	182	78.7	86.9
11. <i>Cavia porcellus</i> (Guinea pig)	H	NP001166318	182	78.6	87.9
12. <i>Canis lupus familiaris</i> (Dog)	H	NP001003080	183	78.1	88.0
13. <i>Anas platyrhynchos</i> (Mallard)	H	AGD91914	181	77.9	88.4
14. <i>Homo sapiens</i> (Human)	H	NP002023	183	76.5	88.0
15. <i>Chionodraco rastrispinosus</i> (Ice fish)	M	CC075659	176	71.3	84.8
16. <i>Sciaenops ocellatus</i> (Red drum)	M	ADF80517	176	70.6	86.4
17. <i>Homo sapiens</i> (Human)	L	AAA52439	175	55.4	73.4
18. <i>Mus musculus</i> (Mouse)	L	NP034370	183	53.0	71.4
19. <i>Drosophila melanogaster</i> (Fruit fly)	H	NP524873	205	29.2	40.6

3.2. Phylogenetic relationship of RbFerH

A Phylogenetic reconstruction of RbFerH and its homologs showed that the three ferritin subunits, H, L and M, formed three distinct clusters which grouped closely and independently (Fig. 52). The ferritin H subunit cluster was further divided into mammalian, avian, and piscine clades. The orthologs belonging to the marine teleosts were diverged from their fresh water teleost counterparts, represented by zebrafish ferritin H. With strong bootstrapping support (86), RbFerH was grouped within the ferritin H sub-clade formed by the orthologs of sea bass and large yellow croaker, supporting its homology to teleost ferritin H orthologs. RbFerH was observed to have a distant evolutionary relationship with vertebrate L and M subunits, as evidenced by their distinctive clustering patterns. Moreover, our tree predicts that teleosts possess H and M ferritin subunits, whereas mammals are more likely have H and L subunits. These data suggest that ferritin H is likely to be the common ancestral type of ferritin subunits. In addition, the H subunit of the fruit fly, the sole invertebrate ortholog included in the tree construction, was clearly separated from the main vertebrate cluster, forming an out-group. Taken together, the overall clustering pattern of our phylogenetic reconstruction suggests that RbFerH shares a common ancestral origin with the ferritin subunits of vertebrates, and more specifically with teleosts.

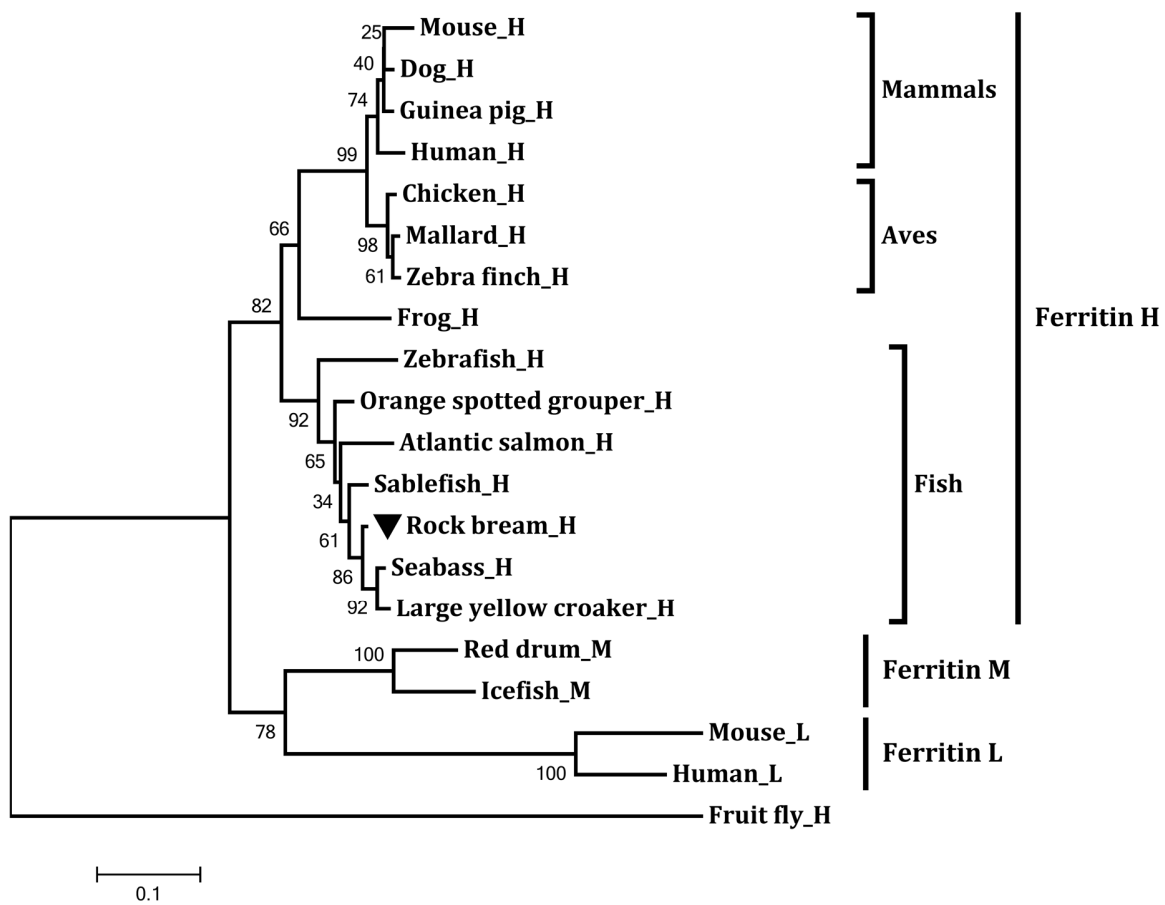


Fig. 52. Phylogenetic reconstruction of RbFerH and its orthologs. The evolutionary relationship of the different ferritin subunits was analyzed based on ClustalW alignments of the respective amino acid sequences by using the neighbor-joining function of the MEGA 4.0 software. Corresponding bootstrap values are indicated on nodes of the tree. NCBI GenBank accession numbers of the ferritin H subunit amino acid sequences used in the construction are listed in Table 17.

3.3. Integrity, purity and degree of ferritin complex formation of rRbFerH

SDS-PAGE analysis showed that the rRbFerH fusion protein was successfully produced using IPTG induction under the experimental conditions (Fig. 53A). A single band was resolved from the sample collected after the protein purification process (lane 4), suggesting that our fusion protein was eluted with high purity and was intact (Fig. 53A). The fusion protein was approximately 63 kD in size, correlating with the predicted molecular mass of RbFerH (20.8 kD) and MBP (42.5 kD). After treatment with Factor Xa, the fusion protein was successfully cleaved into rRbFerH and MBP, as evidenced by the two bands with corresponding molecular masses that resolved in lane 5. Our native-PAGE analysis affirmed that rRbFerH monomers have adequately assembled into ferritin protein complex to form apoferritin (protein nano cage), as detected by the band resolved on the gel (Fig. 53B; lane 2) aligning with the band observed corresponding to the equine apoferritin (Fig. 53B; lane 1). In addition, rest of the bands present in the gel (lane 2) may reflect the monomers as well as oligomers of rRbFerH and cleaved MBP.

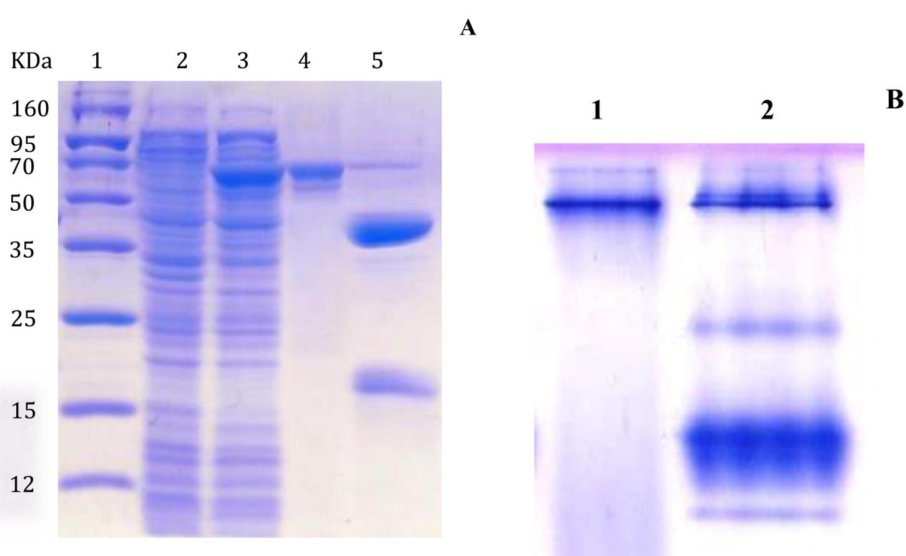


Fig. 53. (A), SDS-PAGE analysis of the purified recombinant RbFerH (rRbFerH)-maltose binding protein (MBP) fusion protein and its cleaved products after treatment with Factor Xa. Lane 1, protein size marker; lane 2, total cellular extract from *E. coli* BL21 (DE3) carrying the rRbFerH-MBP expression vector prior to IPTG induction; lane 3, crude extract of rRbFerH after IPTG induction; lane 4, purified recombinant fusion protein (rRbFerH-MBP) after IPTG induction (1 mM); lane 5, cleaved products (MBP and rRbFerH) of the rRbFerH fusion protein after treatment with Factor Xa; (B), Non reducing, native PAGE analysis of Factor Xa cleaved rRbFerH. Lane 1, apoferritin from equine spleen (Sigma) as a marker and lane 2, Factor Xa cleaved rRbFerH.

3.4. Iron(II) depriving activity of rRbFerH

The iron(II) depriving activity of rRbFerH was analyzed using an assay that is based on the principle of OD reduction of the Fe(II)-ferrozine chromogenic complex at 562 nm, due to the binding of free Fe(II) ions by iron binding proteins like ferritins. According to the observed results, rRbFerH was detected to deprive Fe(II) in the medium in a concentration-dependent manner (Fig. 54A). At an rRbFerH concentration of 0.025 g/ L, the percentage of deprived iron(II) reached its maximum level (~90 %). The dose-response curve plateaued at higher concentrations of rRbFerH, suggesting the optimal conditions for the reaction had been attained. However, under reducing conditions, iron(II) deprivation in the final reaction medium was significantly lower (~23 %) than that of non-reducing conditions (~87 %) with the presence of rRbFerH (Fig. 54B). In general, H subunits of ferritins can demonstrate ferroxidase activity by converting Fe(II) ions into Fe(III) ions in the medium (Lawson et al., 1989), which could be further prefigured regarding rRbFerH, due to the presence of residues for the ferroxidase center,

as per our *in-silico* prediction. Thus, according to our observation, reducing conditions could compensate the iron(II) deprivation by rRbFerH to a significant extend, suggesting that detectable ferroxidase activity can be demonstrated by rRbFerH, via active ferroxidase center. Notably, the MBP control did not show any significant Fe(II) deprivation at any concentration tested, suggesting that it does not contribute to the prominent ferroxidase activity of rRbFerH.

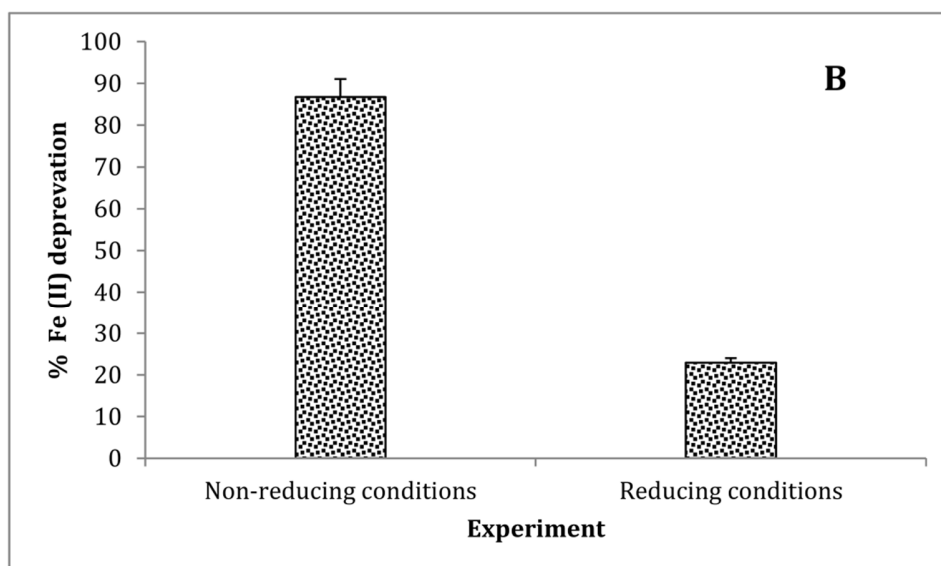
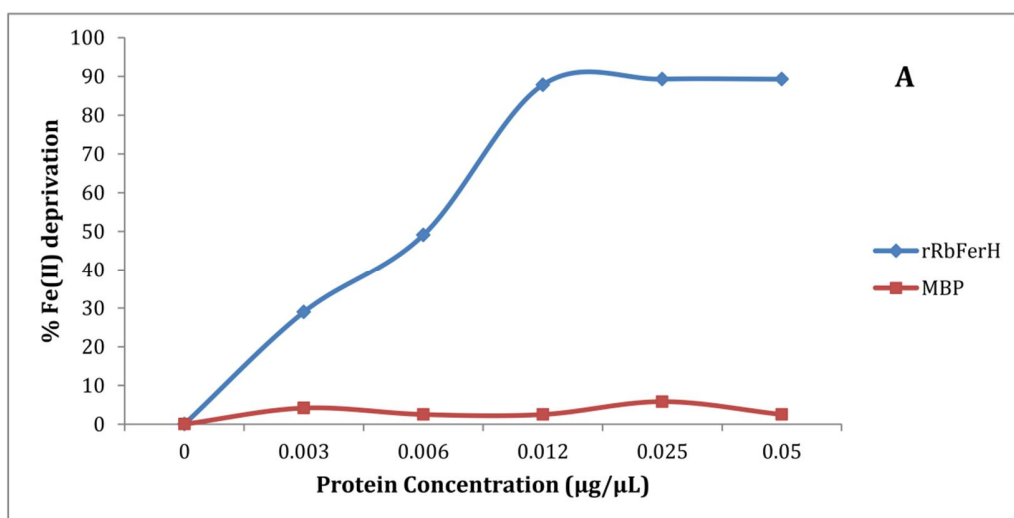


Fig. 54 (A), *In vitro* iron(II) deprivation by rRbFerH. The percentage of Fe(II) deprivation is shown for different concentrations of rRbFerH. Error bars represent standard deviation (SD; n = 3). The percentage of Fe(II) deprivation was calculated from OD₅₆₂ values measured 10 min after adding ferrozine to the mixture of FeSO₄ containing different concentrations of rRbFerH. **(B)**, The percentage Fe(II) deprivation for 0.2 g/ L of rRbFerH under reducing (with Tin(II) ions) and non-reducing (without Tin(II) ions) conditions. Error bars represent standard deviation (SD; n = 3).

3.5. Antibacterial activity of rRbFerH

Since rRbFerH demonstrated a substantial iron(II) depriving activity (section 3.4), we evaluated its bacteriostatic activity towards the growth of *E. coli* (DH5 α) potentially mediated by iron(II) binding and conversion to the less-soluble and less biologically available form of iron; iron(III) at its ferroxidase center (Krewulak and Vogel, 2008). As shown in Fig. 55, rRbFerH restricted bacterial growth. Bacterial cell density, measured by OD₆₀₀ started to decline 6 h post-rRbFerH treatment compared to that of control culture samples at same time point. In contrast, the bacterial cell density (OD₆₀₀) of MBP-treated cultures elevated gradually, in a manner similar to the control culture sample. Therefore, we could infer that MBP in the rRbFerH solution does not have any detectable antibacterial effect on *E. coli*. The bacteriostatic activity of rRbFerH was likely mediated through the deprivation of Fe(II) ions in the culture medium, reducing the free iron (Fe(II) ions) available for bacterial growth. This may probably due to binding of free Fe(II) ions to the ferroxidase center of rRbFerH apoferritin complex to convert them into less biologically available Fe III (section 3.4). Moreover, to a lesser extend *E.coli* growth reduction

may depends on the depletion of dissolved oxygen in the culture medium, as a result of iron(II) oxidation process at its ferroxidase center.

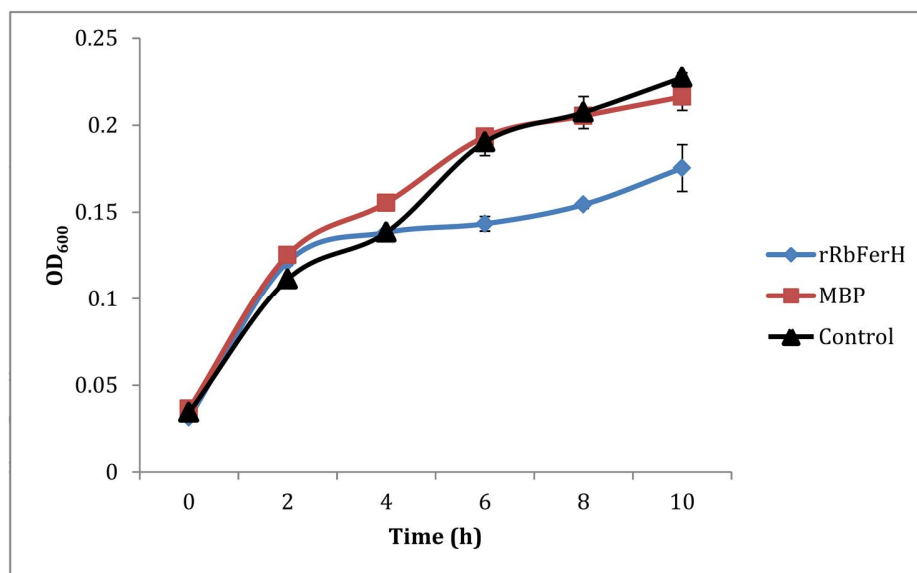


Fig. 55. Bacteriostatic activity of rRbFerH, as measured by the effect of rRbFerH (50 $\mu\text{g/mL}$) on *E. coli* in LB medium. OD₆₀₀ was measured to determine the cell density of *E. coli* in the presence of rRbFerH or MBP, or in the absence of both proteins at different time points. Error bars represent SD (n = 3).

3.6. Protective effect of rRbFerH in oxidative DNA damage

Fe(II) ions are catalysts for the Fenton-type reactions that can damage DNA in cells through the production of radicals using substrates such as H_2O_2 (Luo et al., 1996)(Luo et al., 1996). However, iron binding proteins like ferritins can help to prevent these reactions by reducing the availability of free Fe(II) in cells, in turn preventing oxidative DNA damage. We tested the ability of rRbFerH to protect DNA against the radical formation caused by the reaction between Fe(II) and H_2O_2 *in vitro*. In reaction solutions containing Fe(II) and H_2O_2 , rRbFerH protected pUC19

plasmid DNA from strand breakage, as indicated by the significant reduction in the conversion of supercoiled to nicked DNA (Fig. 56, lanes 4 and 5) relative to the untreated control (Fig. 56, lane 2). The intensity of the DNA band corresponding to the nicked DNA decreased with increasing concentrations of rRbFerH, suggesting its protective effect on DNA breakage was concentration-dependent (Fig. 56, lanes 5 to 4). MBP-treated controls did not show any detectable protection against Fe(II) and H₂O₂-mediated DNA damage. In these controls, the majority of the supercoiled DNA was converted into the nicked form, suggesting MBP is inert in the rRbFerH solution. Based on these observations, we speculate that RbFerH prevents the DNA damage induced by Fenton-type reactions, probably due to the binding of Fe(II) ions to the active ferroxidase center of RbFerH apoferritin complex (section 3.4), thereby restricting free iron(II) availability. Therefore, RbFerH may play an indirect role in cellular antioxidative defense.

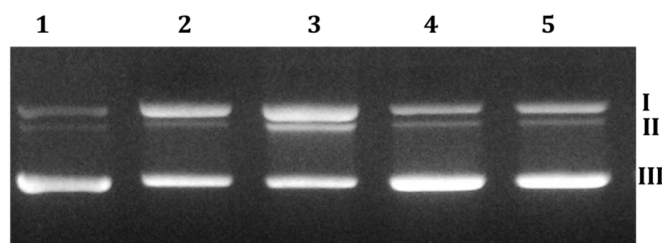


Fig. 57. Protective effect of rRbFerH on oxidative damage to dsDNA. Supercoiled pUC19 DNA was converted into a nicked form due to H₂O₂ and Fe(II)-mediated radical formation. The effect of rRbFerH on this process was assessed. The reaction mixtures were analyzed by agarose gel electrophoresis to determine the degree of DNA breakage. Lane 1, pUC19 plasmid DNA alone; lane 2, reaction mixture without the addition of rRbFerH (untreated); lane 3, reaction mixture treated with 50 µg of MBP; lane 4, reaction mixture treated with 50 µg of rRbFerH; and lane 5, reaction mixture treated with 25 µg of rRbFerH.

3.7. Spatial expression pattern of *RbFerH*

RbFerH was found to be expressed ubiquitously in the tissues examined, indicating its vital function in rock bream physiology. From the tissues examined, the liver and blood tissues showed the highest level of expression (Fig. 57). Interestingly, these data are consistent with previous studies reporting high-level expression of ferritin H in the livers of the Atlantic salmon (*S. salar*) (Andersen et al., 1995), Antarctic notothenioids (Scudiero et al., 2007), catfish (Liu et al., 2010), and sea bass (Neves et al., 2009). The ferritin H ortholog identified in turbot, on the other hand, is highly expressed in muscle tissue and moderately expressed in liver tissues (Zheng et al., 2010b). In contrast to teleost ferritin H expression, mammalian orthologs of ferritin H are expressed predominantly in the heart and brain.

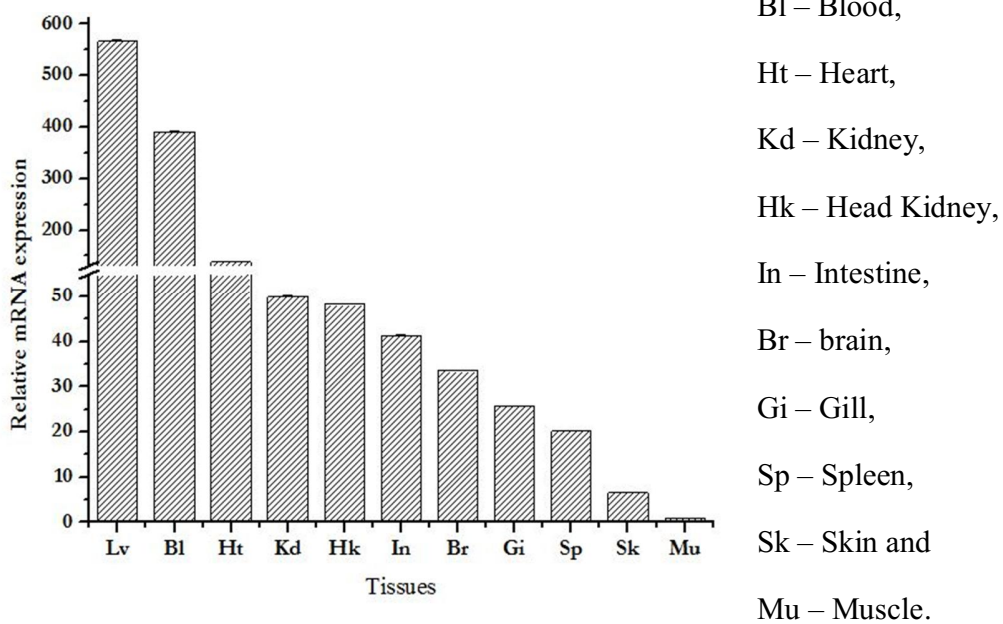


Fig. 57. Tissue-specific distribution of *RbFerH* expression in rock bream measured using quantitative real-time polymerase chain reaction (qPCR). Fold-changes in expression are shown relative to the mRNA expression level in muscle tissue. Error bars represent SD (n = 3).

The liver acts as a key mediator of iron metabolism and iron storage (Anderson and Frazer, 2005; Graham et al., 2007). Moreover, the liver functions in the first line host defense because it houses different immune-related cell types including Kupffer and natural killer cells (Seki et al., 2000). Thus, we anticipated the prominent expression of RbFerH-like subunits of ferritin important in formation of its apoferritin-complex in the liver because of the involvement of ferritins in iron metabolism, storage (Watt, 2011), and acute phase inflammatory reactions (Worwood, 1990). The liver is an organ in which a wide array of metabolic reactions occurs. In turn, these metabolic reactions generate ROS such as peroxides. In Section 3.6, we demonstrated that RbFerH reduced the production of radicals generated by Fenton-type reactions using peroxides as the substrate. This may also explain the pronounced expression of *RbFerH* in liver tissues. Because blood cells are involved in first line host defense against invading pathogens, the prominent expression of *RbFerH* in the blood can be attributed to the involvement of ferritins in acute-phase reactions (Worwood, 1990) and its potent antimicrobial activity (Ong et al., 2006). Blood cells such as macrophages store iron after erythrophagocytosis and this iron is then liberated in response to regulation by proteins involved in iron metabolism, including ferritins (Hausmann et al., 1976; Knutson et al., 2005). Therefore, the abundant expression of prominent ferritin constituents, such as *RbFerH*, in rock bream blood tissue is not unexpected.

3.8. Transcriptional modulation of *RbFerH* expression upon immune stimulation

To decipher the potential role of RbFerH in host immune defense under conditions of pathogenic stress, we analyzed the temporal transcriptional regulation of *RbFerH* in blood tissue after stimulating healthy fish with live pathogens (*E. tarda*, RBIV) and pathogen-derived mitogens (Poly I:C and LPS). As expected, upon stimulation with bacterial stimulants (LPS and

E. tarda), a significant ($P < 0.05$) increase in *RbFerH* transcription was detected, albeit with a relatively low fold-difference (Fig. 58A). Under conditions of LPS stimulation, *RbFerH* basal transcription was significantly elevated during the early phase (3 h and 6 h) post-stimulation (p.s). In contrast, *E. tarda*, a common Gram-negative bacterial pathogen of fish induced transcription at a slightly later time point (6 h and 12 h p.s.). However, both stimulants triggered a similar pattern of transcriptional response. In both groups, the *RbFerH* transcript returned to basal levels, suggesting that LPS and *E. tarda* exerted the same immunogenic effects irrespective to their strength of induction. Notably, LPS is a well-known endotoxin of Gram-negative bacteria such as *E. tarda*. Ultimately, this immune stimulation might have elevated *RbFerH* expression to form its apoprotein, in turn suppressing bacterial proliferation in cellular environments through an iron-sequestering strategy (Ong et al., 2006). On the other hand, the observed inductive transcriptional responses of *RbFerH* may also be a secondary response to control the production of reactive oxygen or nitrogen intermediates triggered by the bacterial invasion or LPS stimulation by the host first line immune defense system (Wink et al., 2011), by elevating the ferritin complex formation to withhold iron(II) (Ong et al., 2006), in turn regulating the oxidative stress of the cells elicited by Fenton type reactions (Crichton et al., 2002).

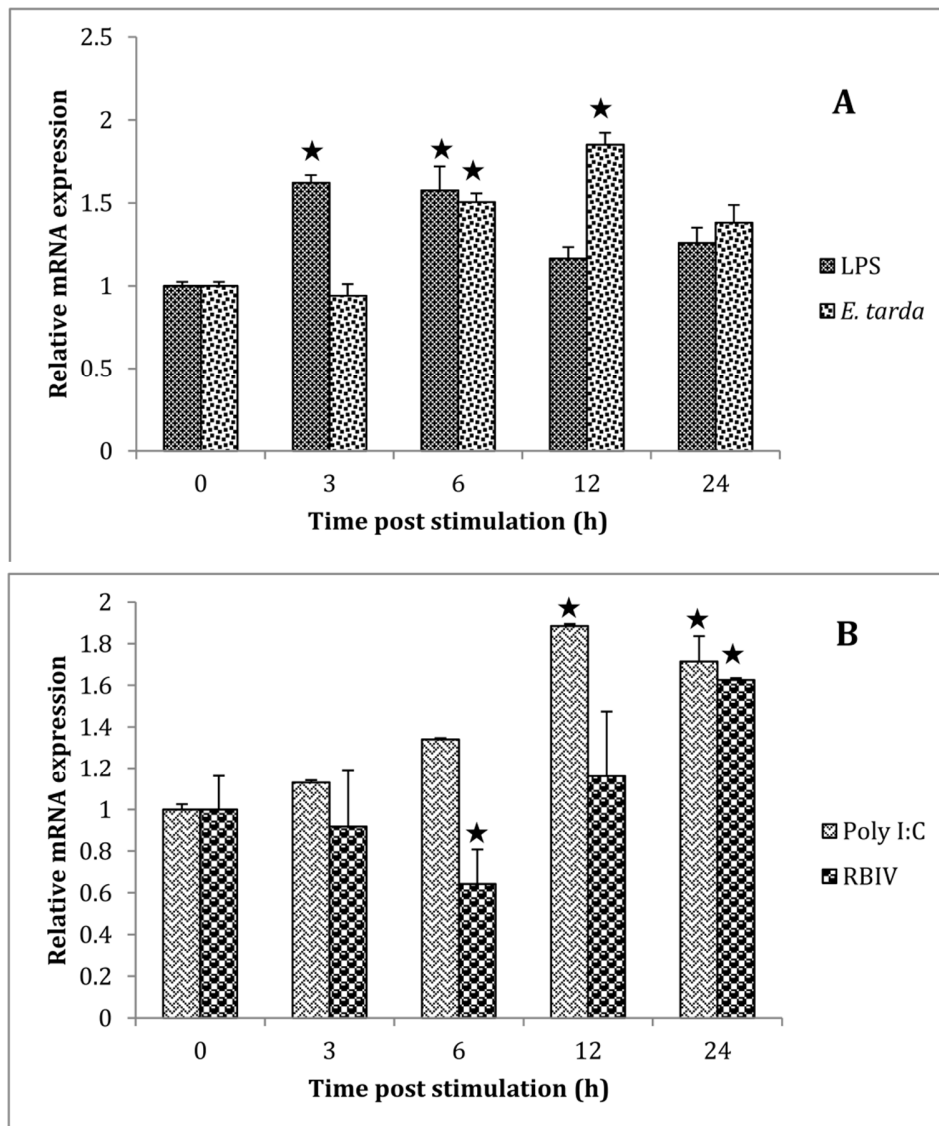


Fig. 58. Temporal regulation of *RbFerH* transcription in blood tissue upon immune stimulation with (A) lipopolysaccharides (LPS) and *E. tarda*, and (B) polyinosinic:polycytidylic acid (poly I:C) and rock bream Iridovirus (RBIV), as measured using qPCR. The relative expression was calculated using the $2^{-\Delta\Delta CT}$ method. Rock bream β -actin was used as the reference gene in the corresponding PBS-injected controls at each time point. The relative fold-change in expression at 0 h post-injection was used as the baseline. Error bars represent SD (n = 3); ★ $P < 0.05$.

Transcriptional upregulation of the ferritin H subunit gene upon bacterial invasion was also detected in other fish species including catfish (Liu et al., 2010), sea bass (Neves et al., 2009), and turbot (Zheng et al., 2010b). In the case of catfish, treatment with *Edwardsiella ictaluri* and iron dextran elevates the transcriptional level of ferritin H at 4 h and 7 d post-treatment in liver tissues. The late-phase elevation (7 d) was presumed to be the response induced by the bacterial pathogen. On the other hand, a bacterium known as *Photobacterium damsela* triggers a significant transcriptional induction of the ferritin H subunit gene in the liver and brain tissues of sea bass at two time points (72 h and 96 h) and three time points (48 h, 72 h, and 96 h) p.s., respectively. Upon the exposure to *Listonella anguillarum*, *E. tarda*, or *Streptococcus iniae*, the transcript levels of turbot ferritin H are positively regulated at several time points post-exposure, showing prominent fold-changes compared to its basal level of transcription.

Providing the first insights into the transcriptional regulation of the ferritin H subunit in fish upon live viral infection, we showed that the expression of *RbFerH* was significantly ($P < 0.05$) induced by RBIV invasion in blood cells during the late phase p.s. (24 h p.s.; Fig. 58B). ROS are reportedly generated to induce apoptosis in cells as a host antiviral defense strategy (Skulachev, 1998). To regulate the excessive ROS produced by Fenton-type reactions (Crichton et al., 2002), ferritin may have an indispensable role in binding free Fe(II) ions. This is in accordance with our observation that the transcriptional response of *RbFerH* is induced upon RBIV infection. At 6 h p.s., *RbFerH* transcript levels were diminished, probably due to an immune evasion mechanism orchestrated by RBIV. Immune evasion mechanisms are typical of other viral pathogens of vertebrate host species (Iannello et al., 2006). Plausibly, this stimulates ROS production in host blood cells. A number of viral pathogens are known to maintain their

presence by promoting the spread of virions through destroying host cells by using virus-induced ROS generation(Yang et al., 2010). Treatment with poly I:C, a well-known double-stranded viral RNA analog significantly ($P < 0.05$) increased the basal transcription of *RbFerH* during the late phase of the experiment (12 h and 24 h p.s.). This result is consistent with that of a previous report in turbot (Zheng et al., 2010b). Poly I:C treatment in turbot also triggers an inductive transcriptional response during the late phase post-treatment and relatively high fold-changes. The distinct patterns of the transcriptional responses elicited by two different viral stimuli may be attributed to the induction of two different immune pathways that ultimately regulate the expression of *RbFerH*. Taken together, the transcriptional regulation of *RbFerH* under conditions of pathogenic stress suggests that RbFerH plays an important role in the host antimicrobial defense system. This is supported by the prominent antibacterial activity of RbFerH *in vitro* (Section 3.5).

4. CONCLUSION

The results of this study revealed that RbFerH shared significant features of typical vertebrate H ferritins and it is transcribed in tissue-specific manner, with prominent expression levels in blood and liver tissues. Moreover, *RbFerH* expression in blood tissue is regulated by pathogen infection. Analyses of RbFerH functionality indicated its potential participation in antibacterial and antioxidative defense, probably through its iron-sequestering properties. Based on these data, we identify RbFerH as a major factor involved in multiple biological functions, including regulatory functions related to rock bream physiology.

PART D

Characterization of ferritin M (FerM) subunit from rock bream

1. ABSTRACT

Ferritins are biological iron withholders that can sequester excess iron to maintain iron homeostasis in the body. Ferritins basically consist of 2 types of subunits, designated as H and L. However, another new subunit, ferritin “M” which possesses characteristic features of both the H and L subunits, was recently identified in lower vertebrates, mostly in fish. In this study, a ferritin M-like subunit from rock bream (*Oplegnathus fasciatus*) (RbFerM) was characterized at the molecular level, and its transcriptional profile was analyzed in healthy fish, as well as in pathogen- and mitogen-stimulated fish. Furthermore, its functional properties were evaluated using a recombinant protein. The complete coding sequence of RbFerM was 528 bp in length, encoding a 176-amino acid peptide with a calculated molecular mass of 20 kD. *In silico* analysis of RbFerM revealed that it has features similar to both the mammalian ferritin subunits, H and L. Phylogenetic analysis depicted the higher evolutionary proximity of RbFerM with its fish counterparts. Quantitative real time polymerase chain reaction (PCR) analysis detected a ubiquitous transcriptional profile of RbFerM in selected tissues of rock bream, in which more pronounced expression was observed in blood and liver tissues. Significant transcriptional inductions of RbFerM were detected in liver tissues upon lipopolysaccharides (LPS), *Edwardsiella tarda*, *Streptococcus iniae*, and rock bream irido virus (RBIV) exposures in time-course immune-challenge experiments. The purified recombinant protein of RbFerM demonstrated detectable iron binding activity that varied with the temperature. Moreover, the

recombinant RbFerM rendered a detectable protection effect against iron (II) and H₂O₂-mediated DNA damage.

2. MATERIALS AND METHODS

2.1 Identification and sequence profiling

The complete cDNA sequence of RbFerM was identified from our sequence database of the previously constructed rock bream cDNA library (Whang et al., 2011a) using the Basic Local Alignment Tool (BLAST) algorithm (<http://blast.ncbi.nlm.nih.gov/Blast.cgi>). Subsequently, the identified sequence was characterized using different bioinformatics tools. Prediction of protein domains was carried out using the ExPASy-prosite database (<http://prosite.expasy.org>) and the MotifScan scanning algorithm (http://myhits.isb-sib.ch/cgi-bin/motif_scan), whereas other properties of RbFerM were determined using the ExPASy Prot-Param tool (<http://web.expasy.org/protparam>). Pairwise sequence alignment and multiple sequence alignment with orthologous sequences were performed using the EMBOSS needle program (<http://www.Ebi.ac.uk/Tools/emboss/align>) and the ClustalW2 program (<http://www.Ebi.ac.uk/Tools/clustalw2>), respectively. The phylogenetic relationship of RbFerM was determined using the neighbor-joining method and the Molecular Evolutionary Genetics Analysis (MEGA) software version 4 (Tamura et al., 2007). The reliability of the resultant phylogenetic reconstruction was tested using 1000 bootstrap replications.

2.2 Overexpression and purification of the recombinant RbFerM fusion protein

Recombinant RbFerM was expressed as a fusion protein with the maltose binding protein (MBP), and purified as described previously (section 2.2 in Part C, chapter 2) with some

modifications. Briefly, the coding sequence of the RbFerM gene was amplified using the sequence-specific primers RbFer-F and RbFer-R, which contained restriction enzyme sites for *EcoRI* and *HindIII*, respectively (Table 18). Polymerase chain reaction (PCR) was performed in a TaKaRa thermal cycler in a total volume of 50 μ L with 5 U of ExTaq polymerase (TaKaRa, Japan), 5 μ L of 10X ExTaq buffer, 8 μ L of 2.5 mM dNTPs, 80 ng of template, and 20 pmol of each primer. The reaction was carried out at 94 °C for 30 s, 55 °C for 30 s, 72 °C for 1 min, followed by a final extension at 72°C for 5 min. The PCR product (~530 bp) was resolved in 1% agarose gel, excised, and purified using the Accuprep™ gel purification kit (Bioneer Co., Korea). The digested pMAL-c2X vector (150 ng) and the PCR product (60 ng) were ligated using Mighty Mix (7.5 μ l; TaKaRa) at 4 °C overnight. The ligated pMAL-c2X/RbFerM product was transformed into DH5 α cells and sequenced. After sequence confirmation, the recombinant expression plasmid was transformed into *Escherichia coli* BL21 (DE3) competent cells. The recombinant RbFerM protein was then overexpressed using isopropyl- β -D-galactopyranoside (IPTG, 1 mM final concentration) induction in *E. coli* cells, grown in a 500 mL Luria broth (LB) medium supplemented with ampicillin (100 μ g/mL) and glucose (0.2 % final concentration) at 37 °C for 3 h. After the incubation at 37 °C, induced *E. coli* BL21 (DE3) cells were cooled on ice for 30 min and harvested by centrifugation at 3500 rpm for 30 min at 4 °C. Harvested cells were resuspended in 20 mL of column buffer (20 mM Tris-HCL, pH 7.4, 200 mM NaCl) and stored at -20 °C. Subsequently, the protein was purified using the pMAL™ protein fusion and purification system (New England Biolabs, Ipswich, MA). Briefly, the cells were thawed in an ice water bath and lysed by cold sonication. The lysate was then centrifuged at 13,000 x g for 30 min at 4 °C and resultant supernatant (crude extract) was subsequently mixed with 1 mL of amylose resin and placed on ice for 2 hs while mixing within every 10 min to facilitate affinity binding.

Thereafter, the settled resin-extract mixture was loaded onto a 1 cm x 5 cm column and washed with 12 x volume of the column buffer. Finally, the rRbFerM –MBP fusion protein was eluted using an elution buffer (10 mM maltose), and its concentration was determined by the Bradford method by using bovine serum albumin as the standard (Bradford, 1976). Next, the recombinant RbFerM–MBP fusion product was cleaved using factor Xa, according to the pMAL™ protein fusion and purification protocol (New England Biolabs, Ipswich, MA). The resultant non-fused RbFerM (rRbFerM) was assayed for its iron binding and DNA protection activities. The RbFerM samples that were collected at different purification steps followed by cleavage with factor Xa were analyzed by 12% sodium dodecyl sulfate polyacrylamide gel electrophoresis (SDS-PAGE) under reduced conditions by using standard protein size markers (Enzyomics, Korea). The gel was stained with 0.05% Coomassie blue R-250, followed by a standard de-staining procedure.

Table 18. Oligomers used in the study on RbFerM

Name	Purpose	Sequence (5' →3')
RbFerM-qF	BAC library screening and qPCR of <i>RbFerM</i>	TCAACATGGAGCTGTTTGCCTCTTACT
RbFerM-qR	BAC library screening and qPCR of <i>RbFerM</i>	ACAACCTTCAGAGCTGACATCAGCTTCT
RbFerM-F	ORF amplification (<i>EcoRI</i>)	GAGAGAGaattcATGGAGTCCCAAGTGCATCAG
RbFerM-R	ORF amplification (<i>HindIII</i>)	GAGAGAAagcttTTAGCT CTT GCC CCC CAGG
Rb-βF	qPCR for rock bream β-actin gene	TCATCACCATCGGCAATGAGAGGT
Rb-βR	qPCR for rock bream β-actin gene	TGATGCTGTTGTAGGTGGTCTCGT

2.3 Effect of rRbFerM protein concentration on the iron binding activity

The iron binding activity of rRbFerM was determined using a previously published method with some modifications (De Zoysa and Lee, 2007). Briefly, 20 μ L of 2 mM FeSO₄ was added to different concentrations of the recombinant protein in 1 mL of column buffer (20 mM Tris-HCl and 200 mM NaCl) and was incubated at room temperature (27 °C) for 10 min. Thereafter, 5 mM ferrozine (Sigma, USA) was added to each mixture, mixed thoroughly, and then incubated again at the same temperature for 15 min. Finally, the optical density (OD) of each mixture was measured using a spectrophotometer at 562 nm. Corresponding concentrations of MBP were used as controls in each assay to investigate the effect of MBP in the cleaved recombinant fusion protein sample. Each assay was performed in triplicate, and the mean OD value was used for the calculation of the percentage iron (II) binding.

2.4. Effect of temperature on the iron binding activity of rRbFerM

The iron binding activity of rRbFerM was measured at increasing temperatures by using 50 μ g/mL of the recombinant protein. The methods described in section 2.3 were followed, except that the temperature of first incubation was changed. Each assay proceeded in parallel with factor Xa-treated MBP and equal volume of elution buffer, instead of the recombinant protein, as controls. Assays were performed in triplicate to obtain the mean OD₅₆₂ value. This mean value was used in the final calculation of the percentage of bound Fe (II) ions: $(OD_{562} \text{ of the negative control} - OD_{562} \text{ of the assay mixture}) / OD_{562} \text{ of the negative control} \times 100$.

2.5. Determination of the DNA protection effect of rRbFerM under oxidative stress

In order to investigate the DNA protection activity of rRbFerM from strand breakage under oxidative stress, the conversion of supercoiled plasmid DNA to linear form DNA was measured with and without the addition of rRbFerM in the reaction mixture of iron (II) ions and H₂O₂, as previously described (Kang, 2010), with some modifications. Briefly, rRbFerM was added to the iron (II) solutions (0.4 mM) in column buffer to achieve final concentrations of 0.5, 1, and 2 µg/µL in a total volume of 45 µL and the mixtures were then incubated at 37 °C for 15 min. Subsequently, the mixtures were treated with pUC19 (2 µg) and H₂O₂ (final concentration of 4 mM in the reaction mixture). Mixtures were incubated at 37 °C for 15 min in order to elicit DNA breakage through the formation of hydroxyl radicals from the reaction of iron (II) and H₂O₂. A factor Xa-treated MBP (at a final concentration of 2 µg/µL) assay was conducted in parallel without the addition of rRbFerM as a control. Immediately after incubation, DNA in each reaction mixture was purified separately by using the AccuPrep® PCR purification kit (Bioneer, Korea) according to manufacturer's instructions, thus terminating the DNA cleavage reactions. Thereafter, the purified DNA was eluted into 25 µL of DNA elution buffer, and the total volume was loaded and analyzed by electrophoresis on 1% agarose gel with undigested, pure pUC19 vector DNA to observe the respective bands.

2.6. Experimental fish and tissue collection

Healthy Rock bream with an average body weight of 50 g were obtained from the Jeju Special Self-Governing Province Ocean and Fisheries Research Institute (Jeju, Republic of Korea). Animals acclimatized for 1 week prior to the experiment in a controlled environment (salinity 34 ± 1 psu, pH 7.6 ± 0.5, at 22°C–24°C) in 400 L tanks and fed with commercially available fish

feed were used for tissue collection. Whole blood (1 mL/fish) was collected from the caudal fin by using a sterilized syringe, and the sample was immediately centrifuged at $3000 \times g$ for 10 min at 4 °C to separate the blood cells from the plasma. The collected cells were snap-frozen in liquid nitrogen. Meanwhile, the sampled fish was sacrificed, and the gill, liver, skin, spleen, head kidney, kidney, heart, muscle, brain, and intestine were excised, which were immediately snap-frozen in liquid nitrogen and stored at -80 °C until use for total RNA extraction.

2.7. Immune challenge experiments

In order to determine the transcriptional modulation of RbFerM upon pathogen infections, *Streptococcus iniae*, *Edwardsiella tarda*, rock bream iridovirus (RBIV), and lipopolysaccharides (LPS) served as immune-stimulants in time-course immune challenge experiments. Two bacterial pathogens were obtained from the Department of Aqualife Medicine, Chonnam National University, Korea. The bacteria were incubated at 25 °C for 12 h using a brain heart infusion (BHI) broth (Eiken Chemical Co. Japan) supplemented with 1 % sodium chloride. The cultures were resuspended in sterile phosphate buffered saline (PBS) and subsequently diluted to a desired concentration to inject fish. For the virus challenge experiment, kidney tissue specimens obtained from the moribund rock bream infected with RBIV were homogenized in 20 volumes of PBS and then centrifuged at $3000 \times g$ for 10 min at 4 °C to obtain the supernatant of RBIV sample. Subsequently, the obtained supernatant was filtered through a 0.45 µm membrane and used to inject fish. The immune challenge experiments were carried out as previously described, sacrificing at least 3 animals for tissue collection from each challenge group at each time point (Whang et al., 2011b). Thereafter, tissues were collected as described in section 2.6.

2.8 Total RNA extraction and cDNA synthesis

Total RNA was extracted by Tri Reagent™ (Sigma-USA) from blood, gill, liver, spleen, head kidney, kidney, skin, muscle, intestine, and brain tissues from healthy rock breams, as well as from liver tissues collected from immune-challenged animals according to the manufacturer's instructions. Subsequently, cDNAs were synthesized from each set of RNA, as instructed in vendor's protocol.

2.9 RbFerM transcriptional analysis by quantitative real time PCR (qPCR)

qPCR was used to analyze the expression levels of RbFerM in blood, gill, liver, spleen, head kidney, kidney, skin, muscle, brain, and intestine tissues of healthy fish, and the temporal expression of RbFerM in liver tissues of immune-challenged animals. Total RNA was extracted at different time points following the respective immune challenges, and first-strand cDNA synthesis was carried out as described in section 2.8. qPCR was carried out using the thermal cycler Dice™ Real Time System (TP800; TaKaRa, Japan) in a 15 µL reaction volume containing 4 µL of diluted cDNA from each tissue, 7.5 µL of 2X TaKaRa ExTaq™ SYBR premix, 0.6 µL of each primer (RbFer-qF and RbFer-qR; Table 18), and 2.3 µL of ddH₂O. qPCR analysis was performed under the following conditions: 95 °C for 10 s, followed by 35 cycles of 95 °C for 5 s, 58 °C for 10 s, and 72 °C for 20 s, and a final cycle of 95 °C for 15 s, 60 °C for 30 s, and 95 °C for 15 s. The baseline was set automatically by Dice™ Real Time System software (version 2.00). Moreover, no template control experiments were carried out to affirm that the PCR reagents were not contaminated with templates. Since we have designed the qPCR oligomers flanking two exon-intron boundaries, affirmed by two different sized bands (~200 bp with respect to cDNA template and ~700 bp with respect to genomic DNA template) observed in

agarose gel electrophoresis after the PCR amplification of the target DNA fragments using both synthesized cDNA and genomic DNA as templates, undetectable effect of potential genomic DNA contamination in total RNA samples was ascertained by the signal peaked melting curves of the amplicon of each qPCR experiment. In order to confirm the specific amplification of the target using respective oligomers, corresponding melting curve analysis was carried out and product size (~200 bp) was affirmed by agarose gel electrophoresis. RbFerM expression was determined by the Livak ($2^{-\Delta\Delta CT}$) method (Livak and Schmittgen, 2001). The same qPCR cycle profile was used for the internal control gene, rock bream β -actin (Genbank ID:FJ975145) by using respective oligomers (Table 18), which did not show any significant expressional variation within each tissue under provided experimental conditions. All data are presented as means \pm standard deviation (SD) of the relative mRNA expression of 3 replicates. To determine statistical significance ($P < 0.05$) between the experimental and control groups, two-tailed unpaired student *t*-tests were carried out. In all qPCR analyses regarding immune challenge experiments, expression levels of RbFerM mRNA relative to the corresponding fold-change in expression of the rock bream β -actin gene were detected, and these were further normalized to the corresponding phosphate-buffered saline (PBS)-injected controls at each time point. The relative expression level at the 0-h time point (uninjected control) was used as the baseline reference

3. RESULTS AND DISCUSSION

3.1. Sequence characterization of RbFerM

The complete cDNA sequence of RbFerM consisted of 1056 bp, in which the coding sequence comprised 528 bp, whereas the 5' and 3' untranslated region (UTR) sequences contained 205 and 323 bp, respectively. Interestingly, a regulatory element that modulates ferritin expression upon iron load, designated as the iron response element (IRE) (Thomson et al., 1999), was identified within the 5' UTR of the RbFerM cDNA sequence (Fig. 59). With respect to the predicted protein sequence, the molecular mass of RbFerM was determined to be approximately 20 kD, and the theoretical isoelectric point was 5.58, as predicted by the ExPASy Prot-Param tool. Bioinformatics analysis revealed that RbFerM contained featured characteristics of both ferritin H and L subunits, affirming that the derived protein sequence was indeed an ortholog of the ferritin M subunit. Two ferritin iron-binding signatures (IBRS; residues 58–76 and 123–143), 7 metal ligands important in iron binding and ferroxidation in mammalian ferritin H subunits (E-24, Y-31, E-58, E-59, H-62, E-104, and Q-138), as well as residues involved in iron nucleation in the mammalian ferritin L subunit were identified in the deduced peptide sequence of RbFerM (Fig. 59).

GACACCAGGG AAGAAAACCTTAAGG AGTTCCTGCTTCAAC AGTGTTTGAACGGAA -205

CTTCTCCTTCGTCC CGCTTTGTTTATCAA CTAATCTGCATTCCG GAAGACGAACAACCT TTTTCTAATTGAACA -150

CTACTGATAAAGTCG TCGTGAAGCTCTATT TTTGTACCGTTTTGT TAAAGAAAAGCACAA GAACCGCCAGCCAAG -75

ATGGAGTCCCAAGTG CGTCAGAACTACCAC CGCGACTGCGAGGCC GCCATCAACCGAATG GTCAACATGGAGCTG 75

M E S Q V R Q N Y H R D C E A A I N R M V N M E L 25

TTTGCCCTTACTCC TACACTTCAATGGCC TTTTACTTCTCCCGT GACGATGTGGCCCTT CCAGGCTTCTCCCAT 150

F A S Y S Y T S M A F Y F S R D D V A L P G F S H 50

TTCTTCAAGGAGAAC AGCGAGGAGGAGAGG GAGCACGCCGAGAAG CTGCTGTCCTTCCAG AACAAAAGAGGAGGA 225

F F K E N S E E E R E H A E K L L S F Q N K R G G 75

CGCATCTTCTCCAG GACATCAAGAAACCG GAGCGTGATGAGTGG GGGAGTGGGCTGGAG GCCATGCAGTGCGCC 300

R I F L Q D I K K P E R D E W G S G L E A M Q C A 100

CTGCAGCTGGAGAAG AACGTCAACCAGGCT CTGCTGGACCTGCAC AAACGGCCTCCGAG CACGGAGACCCTCAT 375

L Q L E K N V N Q A L L D L H K L A S E H G D P H 125

CTGTGTGACTTCTCG GAGACCCACTACCTG AACGAGCAGGTGGAG GCCATCAAGAAGCTG GCGACTACATTTCC 450

L C D F L E T H Y L N E Q V E A I K K L G D Y I S 150

AACCTCAGCCGCATG GACGCCACACCAAC AAGATGGCGGAGTAC CTGTTTGACAAGCAT TCCCTGGGGGGCAAG 525

N L S R M D A H T N K M A E Y L F D K H S L G G K 175

AGCTAAACGCAAAGT CCCATGATGGAGCCT GGAGTGAAAATCTTA ATGACACACAGGCTT TAACTAAACACGCG 600

S

TTTCTGCTTTGGCTG CTCATTCAGTGGCG CAATATATCTAATCT GCTTAACCTATGAAG TTGACAAGTTCTGGT 675

ATGTCGTGGTGGTGT CGCTGTTTTTAAATG TCATATGGAAGGATG GATATTAATCAGGTT ACGGCTTTGCCCTCA 750

TTACCTATAAGCCTC CTTGTGACATTTTA ACAATGATTGTGACT GAATGTTTCTGATCT GTTCTTAATCTGAAT 825

AAACATTTTTGAGCT AGGAAAAAAA 851

Fig. 59. Nucleotides and deduced amino acid sequence of RbFerM. Start codon (ATG), stop codon (TAA), and poly A signal (AATAA) are underlined. The iron response element (IRE) at the 5' UTR is underlined, and the 2 putative iron binding region signatures (IBRS) are depicted with gray shading. Seven metal ligands responsible for iron binding and ferroxidation are shown in boxes, whereas residues (E) involved in iron nucleation are represented in red color font.

Pairwise sequence alignment of RbFerM with its homologs reflected substantial compatibility with its vertebrate counterparts, especially with fish, and the highest percent identity (96.6%) and similarity (99.4%) was observed with the ferritin M subunit of the red drum, *Sciaenops ocellatus* (Table 19).

Table 19. Percentage similarity and identity values of RbFerM and its orthologs

Name	NCBI- GenBank accession No.	Amino acids	% identity	% similarity
1. <i>Sciaenops ocellatus</i> (red drum)	ADF80517	176	96.6	99.4
2. <i>Larimichthys crocea</i> (large yellow croaker)	ACY75476	176	95.5	99.4
3. <i>Scophthalmus maximus</i> (turbot)	ADI24354	176	92.6	97.7
4. <i>Anoplopoma fimbria</i> (sablefish)	ACQ57862	176	90.9	97.7
5. <i>Salmo salar</i> (Atlantic salmon)	ACI67714	176	88.1	96.6
6. <i>Oncorhynchus mykiss</i> (rainbow trout)	ACO08179	176	86.9	96.6
7. <i>Ictalurus punctatus</i> (catfish)	ADO29006	177	70.1	87.0
8. <i>Osmerus mordax</i> (rainbow smelt)	ACO09242	173	84.1	93.8

Moreover, multiple sequence alignment demonstrated that the residues responsible for iron binding and ferroxidation in RbFerM were highly conserved among the ferritin H and M subunits of other vertebrates, whereas anticipated residues in the iron nucleation center showed conservation among ferritin L and M subunits of other vertebrate species, thereby validating our ferritin subunit as an ortholog of the M subunit (Fig. 60).

```

Human-H             MTTASTS-QVRQNYHQDSEAAINRQINLELYASYVYLSMSYYFDRDDVALKNFAKYFLHQ 59
Mouse-H            MTTASPS-QVRQNYHQDAEAAINRQINLELYASYVYLSMSCYFDRDDVALKNFAKYFLHQ 59
Catfish-H         ----MSS-QVRQNFHQDCEAAINRQINLELYASYVYLSMSYYFDRDDQALHNFAKFFRKQ 55
Atlantic salmon-M ----MES-QIRQNYHHDCAAINRMINMEMFASYTYTSMAFYFSRDDVALPGFAHFFKEN 55
Rainbow trout-M   ----MES-QIRQNYHHDCAAINRMINLEMFASYTYTSMAFYFSRDDVALSGFAHFFKEN 55
Red drum-M        ----MES-QVRQNYHRDCEAAINRMVNMELFASYTYTSMAFYFSRDDVALPGFSHFFKEN 55
Large yellow croaker-M ----MES-QVRQNYHRDCEAAINRNMVNMELFASYTYTSMAFYFSRDDVALPGFSHFFKEN 55
Rock bream-M    ----MES-QVRQNYHRDCEAAINRNMVNMELFASYSYTSMAFYFSRDDVALPGFSHFFKEN 55
Turbot-M          ----MES-QVRQNYNRDCEAAVNRMVNMELFASYTYTSMAFYFSRDDVALPGFSHFFKEN 55
Catfish-M        ----METSQIRQNYHRDCEAAINKMINMELYASYTYTSMAYFTRDDVALEGFHFFKEN 56
Mouse-L           ----MTS-QIRQNYSTEVEAAVNRLVNLHLRASytyLSLGGFFDRDDVALEGVGHFFRDL 55
Human-L           ----MSS-QIRQNYSTDVEAAVNSLVNLYLQASytyLSLGFYFDRDDVALEGVSHFFRDL 55
: *::**:: : ***:* :*: : ** * *:* : * ** * ..::* .

Human-H           SHEEREHAEKLMKLQNRGGRI FLQDIKEPCDDWESGQNAMECALHLEKNNVQSLELH 119
Mouse-H           SHEEREHAEKLMKLQNRGGRI FLQDIKKPDRDDWESGLNAMECALHLEKSVNQSLLELH 119
Catfish-H         SHEEREHAEKLMKVNQRGGRI FLQDIKKPERDEWGSMEALECALQLEKNNVQSLLDLH 115
Atlantic salmon-M SEEEERHADKLLSFQNKRGGRI LLQDIKKPERDEWNGLEAMQCALQLEKNNVQALLDLH 115
Rainbow trout-M   SDEEERHADKLLSFQNKRGGRI FLQDIKKPERDEWNGLEAMQCALQLEKNNVQALLDLH 115
Red drum-M        SDEEERHADKLLSFQNKRGGRI FLQDVKKPERDEWGSLEAMQCALQLEKNNVQALLDLH 115
Large yellow croaker-M SDEEERHADKLLSFQNKRGGRI FLQDVKKPERDEWGSLEAMQCALQLEKNNVQALLDLH 115
Rock bream-M   SEEEERHADKLLSFQNKRGGRI FLQDIKKPERDEWGSLEAMQCALQLEKNNVQALLDLH 115
Turbot-M          SEEEERHADKLLSFQNNRGGRI FLQDVKKPEKDEWGSLEAMQCALQLEKNNVQALLDLH 115
Catfish-M         SHEEREHAEKFMSFQNKRGGRI FLQDVKKPKRDEWGSLEAMQCALQLEKTVNQALLDLH 116
Mouse-L           AEEKREGAERLLEFQNDRGGRALFQDVQKPSQDEWGKTQEAMEAALAMEKNNLQALLDLH 115
Human-L           AEEKREGYERLLKMQNRGGRALFQDIKKPAEDEWGKTPDAMKAAMALEKKNLQALLDLH 115
:.::* *  ::::..**.* **  :*:::* * *  .  :*:::.. : **::**:* **

Human-H           KLATDKNDPHLCDFIETHYLNQVKA IKELGDHVTNLRKMGAPE-----SGLAEYLF 171
Mouse-H           KLATDKNDPHLCDFIETYYLSEQVKS IKELGDHVTNLRKMGAPE-----AGMAEYLF 171
Catfish-H         KVATDHNDPHMCD FIEAHYLDEQVKS IKELSDWVTNLRMGAPQ-----NGMAEYLF 167
Atlantic salmon-M KIADKVDPHLCDFLETHYLNQVEAIKKLGDHITNLTKMDAVK-----NKMAEYLF 167
Rainbow trout-M   KIADKVDPHLCDFLETHYLNQVEAIKKLGDHITNLTKMDAVK-----NKMAEYLF 167
Red drum-M        KLASEHVDPHLCDFLETHYLNQVEAIKKLGDYISNLSRMDANT-----NKMAEYLF 167
Large yellow croaker-M KLASEHVDPHLCDFLESHYLNQVEAIKKLGDYISNLTMRDAHT-----NKMAEYLF 167
Rock bream-M   KLASEHVDPHLCDFLETHYLNQVEAIKKLGDYISNLSRMDAHT-----NKMAEYLF 167
Turbot-M          KLASDHVDPHMCD FLETHYLNQVEAIKKLGDYISNLTMRDAKN-----NKMAEYLF 167
Catfish-M         KLASDKADPHLCDFLETHYLNQVEAIKKLGDHISNLTKMDAAS-----NRMAEYLF 168
Mouse-L           ALGSARADPHLCDFLESHYLDEKVKLIKMGNHLTNLRRVAGPPAQTGAPQSGLYEYLF 175
Human-L           ALGSARTDPHLCDFLETHFLDEEVKLIKMGDHLTNLHRLGGPE-----AGLGEYLF 167
.: : * * : * * : * * : * * : * * : * * : * * : * * : .       .:****

Human-H           DKHTLGSDSNES 183
Mouse-H           DKHTLGHD-ES 182
Catfish-H         DKHTLGSES--S 177
Atlantic salmon-M DKHTLGGQS--- 176
Rainbow trout-M   DKHTLGGQS--- 176
Red drum-M        DKHSLGGKS--- 176
Large yellow croaker-M DKHTLGGKS--- 176
Rock bream-M   DKHSLGGKS--- 176
Turbot-M          DKHSLGGKS--- 176
Catfish-M         DKHTLGGKS--- 177
Mouse-L           ERLTLKHD---- 183
Human-L           ERLTLKHD---- 175
.: : *

```

Fig. 60. Multiple sequence alignment of different vertebrate ferritin subunits. Sequence alignments were obtained using the ClustalW method. Conserved residues important in metal binding and ferroxidation among H and M subunits are shaded in gray, whereas residues involved in iron nucleation, showing high conservation among different M and L subunits, are indicated by green shading.

3.2. Evolutionary proximity of RbFerM with its orthologs

The phylogenetic analysis of RbFerM using different counterparts of ferritin subunits resulted a tree construct indicating three main clusters of ferritin subunits, M, H and L. As expected, members of respective fish and mammalian ferritin subunits were clustered closely and independently where ferritin M cluster represented exclusively a piscine origin, convincing its restricted distribution among lower vertebrates (Fig. 61).

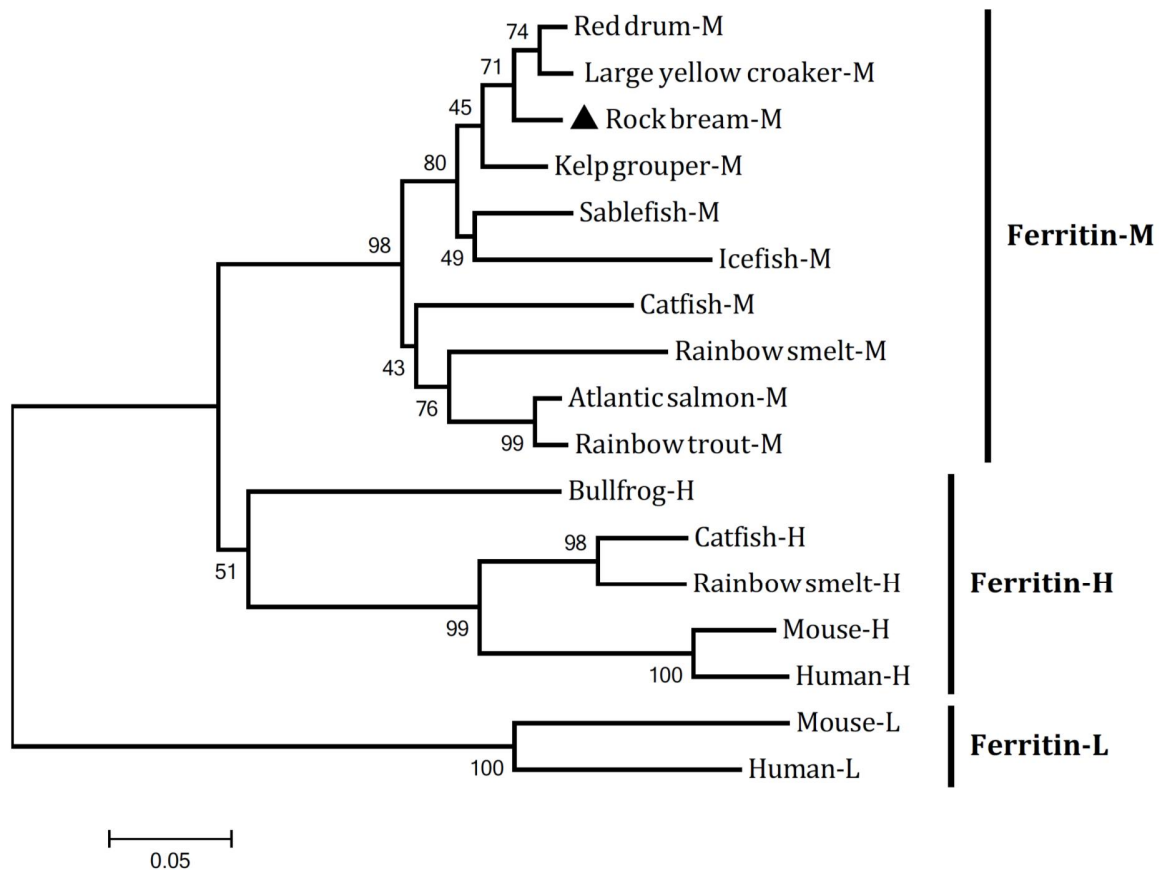


Fig. 61. Phylogenetic relationship of RbFerM and its orthologs. Evolutionary proximity of different ferritin subunits of their vertebrate counterparts was analyzed on the basis of ClustalW alignments of the respective protein sequences by using the neighbor-joining method of MEGA 4.0 software. Corresponding bootstrap values are indicated on the lineages of the tree. NCBI-GenBank accession numbers of the protein sequences of ferritin M subunits are listed in Table 19 except icefish (CCO75659) and kelp grouper (AEI87383). Gen bank accession numbers for H and L ferritin subunits are as follows: Bullfrog-H: AAA49532, catfish-H: NP001187267, rainbow smelt-H: ACO09727, mouse-H: AAH12314, human-H: AAH66341, mouse-L: NP034370, and human-L: AAA52439.

It is also intriguing to note that the cluster of all ferritin M counterparts was supported by a prominent bootstrapping value (98) where RbFerM was clustered with a subgroup of red drum and large yellow croaker ferritin M subunits which was also supported by a fairly high bootstrapping value (71), reflecting a close evolutionary relationship with its teleostan counterparts. In contrast, compared to ferritin M subunits, RbFerM showed a distant relationship with L and H subunits of vertebrate species, which formed separate clades with its orthologs, affirming its evolutionary deviation from H and L subunits. Therefore, these observations affirmed that RbFerM has evolved from a common ancestor indicating that it is indeed an ortholog of vertebrate ferritin M subunits.

3.3. Integrity and purity of overexpressed recombinant RbFerM (rRbFerM)

The SDS-PAGE analysis reflected the successful overexpression of rRbFerM in *E.coli* cells further revealing the significant purity and integrity of the finally eluted fusion product through the appearance of signal band on corresponding lane of the purified recombinant fusion protein

(Fig. 62). Moreover, the molecular mass of the protein was observed to be approximately 60 kD, which conformed to the molecular mass of the predicted RbFerM (~20 kD), because the molecular mass of MBP is ~42.5 kD. In addition, the products obtained after cleavage of the fusion protein resolved as 2 bands, affirming the complete cleavage of the rRbFerM-MBP fusion product into MBP and rRbFerM, as evident by the corresponding band sizes in the gel.

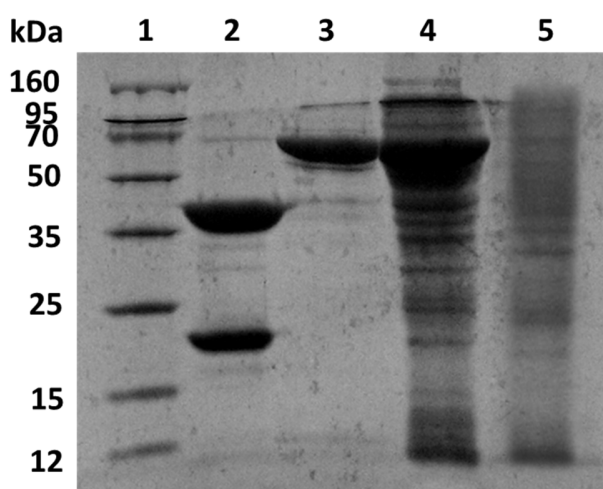


Fig. 62. SDS-PAGE analysis of the overexpressed and purified recombinant RbFerM fusion protein and cleaved products after treatment of the fusion protein with factor Xa. Lane 1, protein marker (Enzymomics, Korea); Lane 2, resultant cleaved products (MBP and rRbFerM) of the rRbFerM fusion protein after treatment with factor Xa; Lane 3, purified recombinant fusion protein (rRbFerM-MBP) after IPTG induction (1 mM); Lane 4, crude extract of rRbFerM after IPTG induction; Lane 5, total cellular extract from *E. coli* BL21 (DE3) carrying the rRbFerM-MBP expression vector prior to IPTG induction.

3.4. Iron binding activity for different concentrations of rRbFerM

The iron binding activity of the rRbFerM protein was demonstrated using an assay system based on the OD reduction of the iron (II)-ferrozine chromogenic complex at 562 nm, which occurs upon binding of Fe (II) ions by ferritin. As shown in Fig. 63, even under the lowest concentration of rRbFerM (0.006 $\mu\text{g}/\mu\text{L}$), percentage iron binding was found to be significantly high, compared to the control (without the protein), further validating its structural predictions and similarities with the known ferritin M and H subunits of other species. However, subsequent increases of rRbFerM concentration resulted in stable iron binding of rRbFerM, as evidenced by the plateau shape of the curve (Fig. 63).

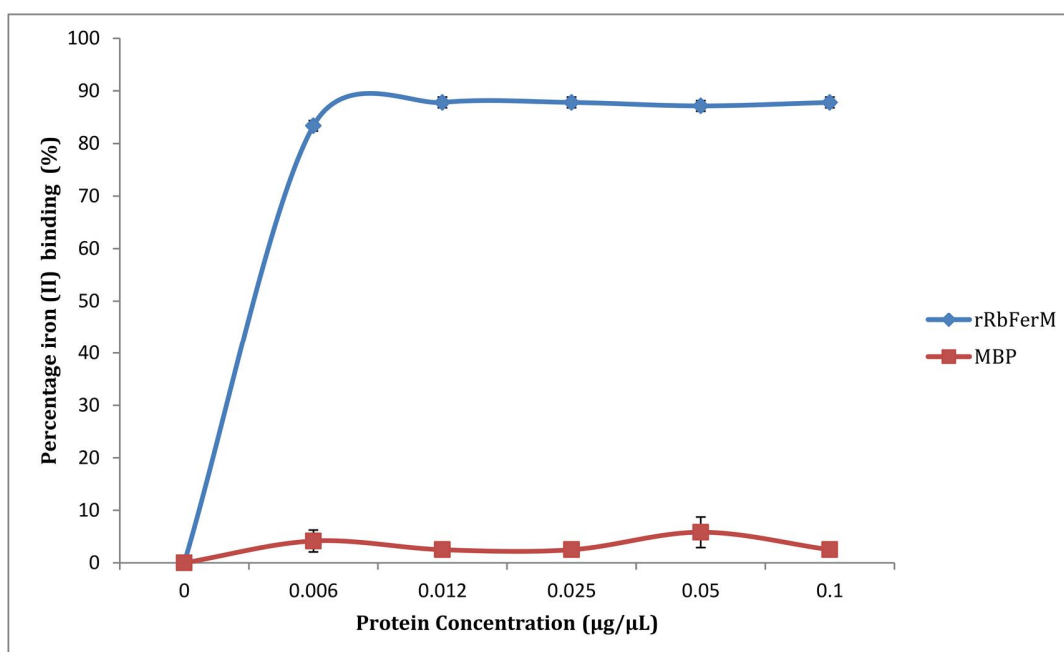


Fig. 63. *In vitro* iron binding activity at different concentrations of rRbFerM. Error bars represent SDs ($n = 3$). Ferrozine was added and OD_{562} was measured after mixing FeSO_4 with different concentrations of rRbFerM, followed by incubation at room temperature for 10 min.

Furthermore, the initial protein concentration (0.012 $\mu\text{g}/\mu\text{L}$) of the plateau may also represent the optimal concentrations for iron binding at the given conditions. The control experiment with MBP did not show any significant iron binding at any concentration used in the assays, demonstrating the dormant behavior of MBP in the factor Xa-cleaved rRbFerM fusion protein product.

3.5. Iron binding activity of rRbFerM as a function of temperature

Temperature dependence of the iron binding activity of rRbFerM was investigated using 100 μg of the recombinant protein, following the same assay protocol implemented in the concentration-dependent experiment. The percentage of iron binding drastically declined as a result of increasing the temperature from 20 $^{\circ}\text{C}$ to 100 $^{\circ}\text{C}$ (Fig. 64), suggesting that heat may damage the three-dimensional folding of the protein, thereby alter the structure of its iron-binding sites. Interestingly, the reduction in iron binding of rRbFerM with increasing temperature was found to be comparable with results of a previous study on the ferritin M subunit from *Scophthalmus maximus*, in which the heat-denatured recombinant protein did not show any detectable iron binding at any protein concentration used in the experiment (Zheng et al., 2010a). Collectively, our observations with rRbFerM suggest that it can actively bind Fe (II) at lower temperatures, which are compatible with the natural environmental conditions of rock bream. MBP did not show any considerable iron binding at any temperature, affirming its negligible interference with the iron-withholding function of rRbFerM.

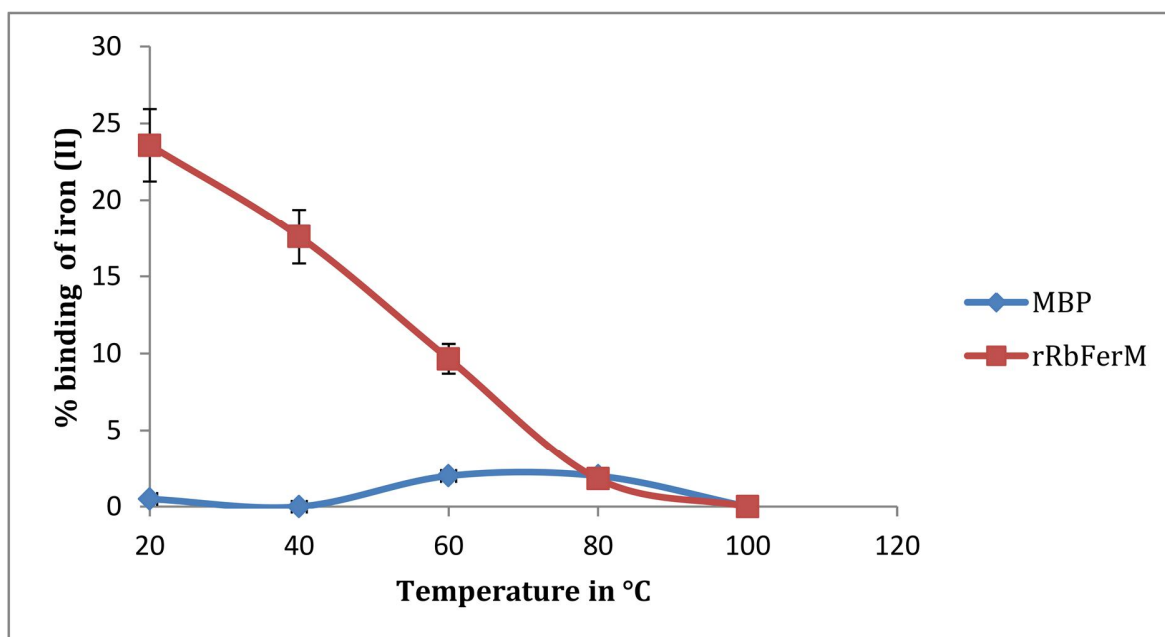


Fig. 64. Variation of *in vitro* iron binding activity of rRbFerM with temperature. Error bars represent SDs (n = 3). Each assay was carried out with 0.05 $\mu\text{g}/\mu\text{L}$ of rRbFerM.

3.6. DNA protection effect of rRbFerM under oxidative stress

Iron (II) ions can form hydroxyl radicals through Fenton-type reactions as a result of interactions with the H_2O_2 yielded in cellular metabolic processes, which render DNA damage in cells (Luo et al., 1996). However, ferritins can potentially deprive these ions and can thus prevent the occurrence of Fenton-type reactions while protecting DNA from oxidative damage. Accordingly, rRbFerM demonstrated detectable protection against iron (II)- and H_2O_2 -mediated DNA damage. As shown in Fig. 65, strand cleavage of pUC19 DNA was significantly inhibited in rRbFerM-treated reaction mixtures. Furthermore, as expected, the suppression of DNA breakage was detected to be more prominent with increasing concentrations of rRbFerM. In contrast, untreated and MBP-treated controls did not show any significant protection effect on pUC19 DNA

cleavage rendered by iron (II) and the H₂O₂ system, as evidenced by a prominent band in the gel corresponding with the nicked form of the vector. However, compared to the untreated control, the DNA band corresponding to the nicked form of the vector in MBP treated control was appeared to be less intense, probably due to the potential physical interference of MBP on the radical generating reaction between iron (II) and H₂O₂, since addition of MBP (~42.5 kD) like bulk protein into the reaction medium can reduce the mobility as well as the probability of collision of the reactants while bringing down the reaction rate within a given period of time. Collectively, our observations affirm that RbFerM can act as an inhibitor of cellular DNA damage probably due to its iron sequestrating function, further providing indirect evidence of its potent antioxidant properties.

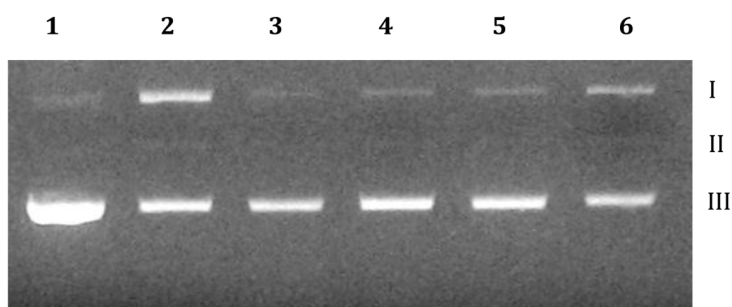


Fig. 65. The effect of rRbFerM on DNA cleavage by reaction of H₂O₂ with iron (II) ions, as analyzed using agarose gel electrophoresis. I, II, III represent the circular, linear and supercoiled plasmid conformations, respectively. Lane 1, pUC19 plasmid DNA alone; Lane 2, reaction mixture without the addition of rRbFerM (untreated); Lane 3, reaction mixture treated with 100 µg of rRbFerM; Lane 4, reaction mixture treated with 50 µg of rRbFerM; Lane 5, reaction mixture treated with 25 µg of rRbFerM; Lane 6, reaction mixture treated with 100 µg of MBP.

3.7. Transcriptional distribution of RbFerM in selected tissues

The qPCR analysis revealed that RbFerM was ubiquitously transcribed in tissues of healthy fish. The most prominent mRNA expression level was detected in blood cells, and moderately high expression levels were observed in liver, heart, and brain tissues, compared to the level in the head kidney (Fig. 66).

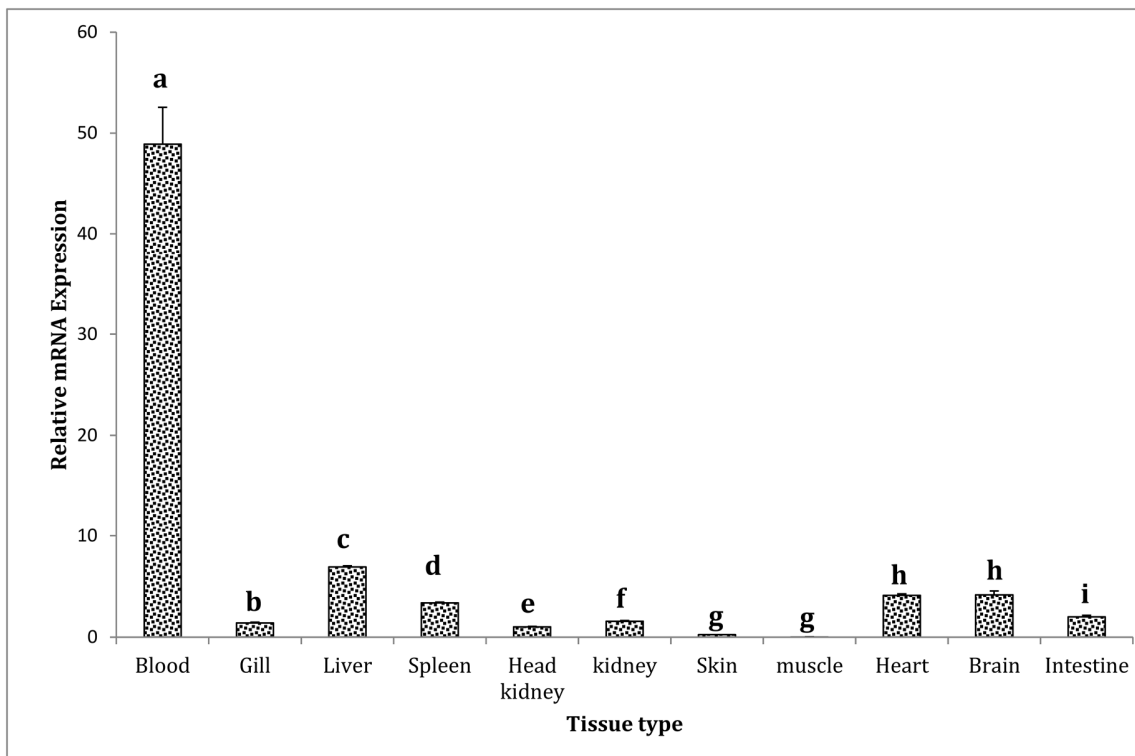


Fig. 66. The transcriptional distribution of RbFerM among different tissues of rock bream determined by qPCR. Fold changes in expression are shown relative to the mRNA expression level in the head kidney. Error bars represent SDs ($n = 3$). Bars with different letters are significantly different ($P < 0.05$) from each other.

Ferritins are considered as iron storing molecules owing to the iron nucleation function of their L subunits (Thompson et al., 2002), and they are known to act as acute phase proteins that are involved in several inflammatory reactions (Worwood, 1990). Furthermore, through its iron withholding strategy, ferritin functions as an antimicrobial protein by suppressing bacterial proliferation in host cells and reducing the free iron ion availability for bacterial growth (Ong et al., 2006). These properties likely explain the fact that the most pronounced transcript level of RbFerM was observed in the blood, which is another characteristic feature of L and H subunits; this is because blood cells, especially macrophages, can store iron after erythrophagocytosis and release it under thorough regulation of proteins involved in iron metabolism, such as ferritins (Hausmann et al., 1976; Knutson et al., 2005). Moreover, blood cells are involved in the innate immune system and play a key role in forming an organism's first line of defense against infection. Severe susceptibility to invading pathogens requires frequent immune responses against foreign invaders, thereby enhancing the basal metabolism of the blood cells involved in the immune response. As a consequence, generation of reactive oxygen species (ROS) such as H_2O_2 increases, which in turn induces the basal expression of ferritin-like iron sequestering molecules to suppress Fenton-type reactions and prevent further free radical generation (Orino et al., 2001). The liver is considered to be a long term iron reservoir (Harrison and Arosio, 1996), probably because of its substantial composition of L ferritins. The brain and heart are known to be enriched with H ferritins (Harrison and Arosio, 1996), which may be directly involved in iron metabolism through their ferroxidase activities. Accordingly, we observed moderately high transcript levels in the liver, brain, and heart. On the other hand, liver, brain and heart are known to be highly vascularized organs, there by prominent ferritin M expression in tissues in those organs are likely to be expected due to its most pronounced expression in blood.

3.8. Transcriptional behavior of RbFerM upon immune stimulation

In order to anticipate the immunological behavior of RbFerM in rock bream upon pathogen infection, its temporal transcriptional modulation in the liver was investigated under pathological conditions by using 3 live pathogens, *E. tarda*, *S. iniae*, and RBIV, along with the well-characterized bacterial endotoxin LPS for immune stimulation. The results showed that bacterial and viral stimuli significantly enhanced RbFerM transcription ($P < 0.05$) in liver tissues, suggesting its potential involvement in host immune defense and confirming documented evidence of its expressional modulation upon microbial infection (Orino and Watanabe, 2008; Knovich et al., 2009). As shown in Fig. 67A, upon LPS stimulation, the RbFerM transcript level was significantly elevated ($P < 0.05$), exhibiting an approximately 5-fold increase compared to the basal level. However, the expression level subsequently dropped down to the basal level at 6 h post-injection (p.i) and did not show any detectable upregulation throughout the remainder of the experiment. Similarly, pathogenic stress due to *E. tarda* also significantly upregulated RbFerM transcription levels ($P < 0.05$), demonstrating the highest fold expression (~2.5-fold) at 3 h p.i (Fig. 67B), and even further augmenting the expression level at 6 h p.i. Because LPS is a well-characterized endotoxin of Gram-negative bacteria such as *E. tarda*, the compatible transcriptional modulation patterns detected in LPS and *E. tarda* challenges at the early phase of the experiment might be attributed to the activation of the same immune signaling pathway. Nevertheless, upon *E. tarda* exposure, RbFerM transcription was significantly downregulated at the late phase of the experiment (12 h and 24 h p.i; $P < 0.05$), showing a deviation in the expressional profile compared to that under LPS exposure. This observation can be attributed to the nature of the stimulant in these challenge experiments because, as a live pathogen, *E. tarda*

may exert different and specific evasion mechanisms in rock bream against host immune mechanisms, as has been demonstrated in several bacterial species (Pieters, 2001).

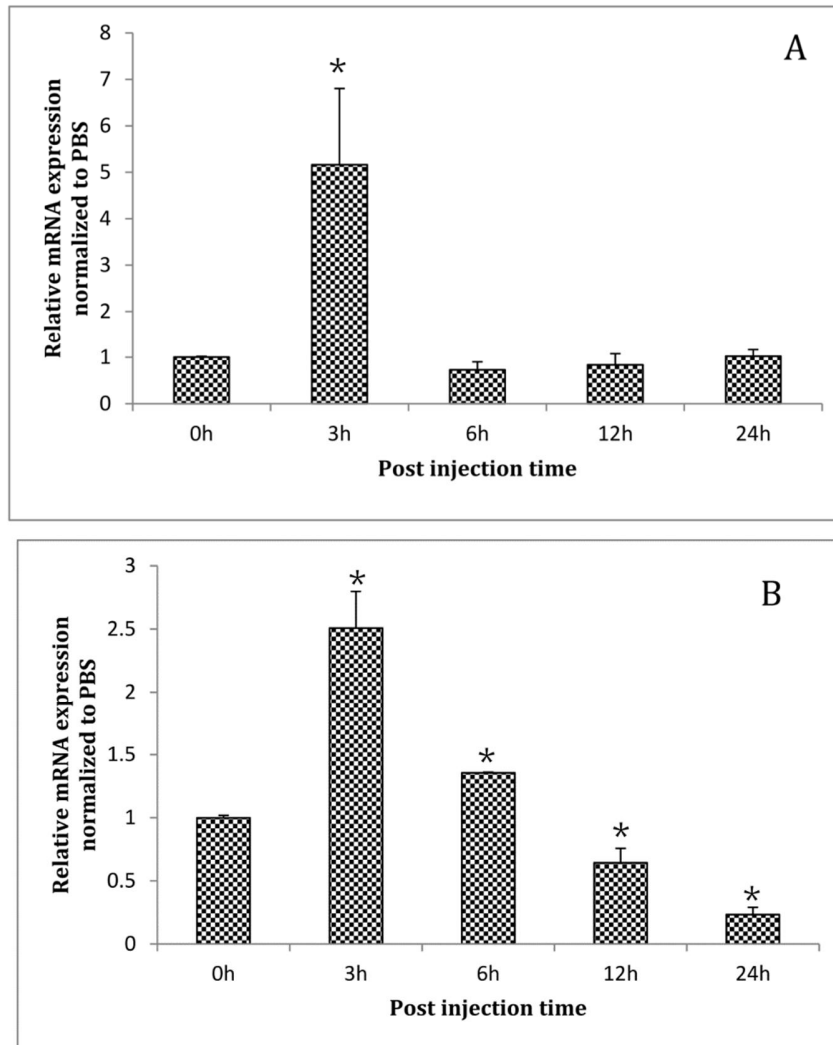


Fig. 67. Expression profile of RbFerM mRNA in liver tissues upon immune stimulation with (A) LPS, (B) *E. tarda*, as determined by qPCR. The relative expression was calculated by the $2^{-\Delta\Delta CT}$ method by using rock bream β -actin as the reference gene with respect to corresponding PBS-injected controls at each time point. The relative fold-change in expression at 0 h post-injection was used as the basal line. Error bars represent SDs (n = 3); * $P < 0.05$.

As previously reported, the mRNA expression level of the *Sciaenops ocellatus* ferritin M subunit in the liver was found to be upregulated by *E. tarda* infection from 4 to 48 h p.i, eliciting both early- and late-phase inductions (Hu et al., 2010). However, upon stimulation of Gram-negative bacteria such as *Listonella anguillarum*, ferritin M transcription was induced at the late phase of the experiment (12 h, 24 h, and 48 h) in the liver and spleen tissues of *Scophthalmus maximus* (Zheng et al., 2010a), whereas in *Cynoglossus semilaevis*, this induction occurred only at the early phase of the experiment in the liver (1 h and 4 h) and spleen (4 h), but in both phases of the experiment in the kidney (1 h, 4 h, 24 h, 48 h) (Wang et al., 2011). Moreover, in *Pseudosciaena crocea*, the ferritin M transcript level in the kidney was markedly elevated 5 days after stimulation, whereas it reached its maximum expression at 12 h p.i in both the spleen and liver (Zhang et al., 2010).

Under the pathogenic stress evoked by the Gram-positive bacteria *S. iniae*, RbFerM transcription was also significantly upregulated in the liver at both 3 h (~2.5 fold) and 6 h (~4 fold) p.i, which resembled the early-phase response upon *E. tarda* exposure (Fig. 68). However, at 12 h p.i, the RbFerM transcript level was detected to be almost equal to the basal level, where it was maintained throughout the rest of the experiment.

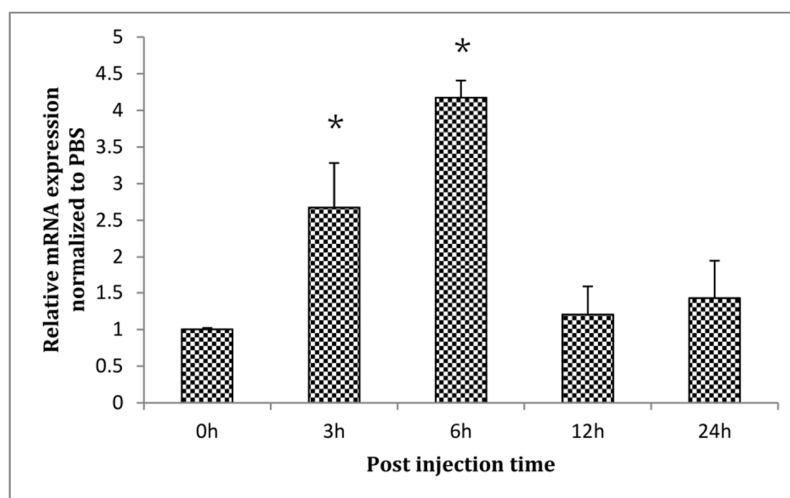


Fig. 68. Expression profile of RbFerM mRNA in liver tissues upon immune stimulation with *S.iniae*, as determined by qPCR. Error bars represent SDs (n = 3); * $P < 0.05$.

As mentioned earlier, ferritins are known to involve in acute phase reactions through its intracellular iron sequestering and storage abilities triggering immune responses (Weiss and Goodnough, 2005). They play crucial roles in protecting the organisms against microbial proliferation in host cells and oxidative damage (Orino et al., 2001; Ong et al., 2006). Therefore, the detected inductive expression of RbFerM upon the stimulation of *S.iniae* may reflect its potential acute phase engagement in bacteriostatic strategy of host defense. On the other hand it possibly arose in order to counterbalance the production of ROS upon bacterial invasion, through sequestering the Fe (II) ions, since pathogen infections prompt the ROS production as a primary defensive mechanism functioning in host phagocytic cells (Babior, 1984). According to the transcriptional profile observed in liver and kidney tissues of *Cynoglossus semilaevis* after challenge with *S. iniae*, ferritin M transcription was elevated at the early phase (4 h) and the late phase (24 h), while inductive responses were observed exclusively at the late phase (24 h and 48

h p.i) in kidney tissues (Wang et al., 2011). Furthermore, the same stimulant significantly upregulated the mRNA expression level of the *Sciaenops ocellatus* ferritin M subunit from 4 to 48 h p.i in the liver tissues ($P < 0.05$ and $P < 0.01$), while elevating M ferritin transcription in the liver and spleen from 12 to 48 h and from 8 to 48 h, respectively.

This study provides the first report of transcriptional modulation of the ferritin M subunit upon live virus infection in a teleost species, rock bream. qPCR analysis revealed that the RbFerM transcript level was significantly induced by RBIV exposure at the early phase of the experiment (3 h and 6 h p.i; $P < 0.05$), reaching the highest expression level (~2-fold) at 6 h p.i (Fig. 69).

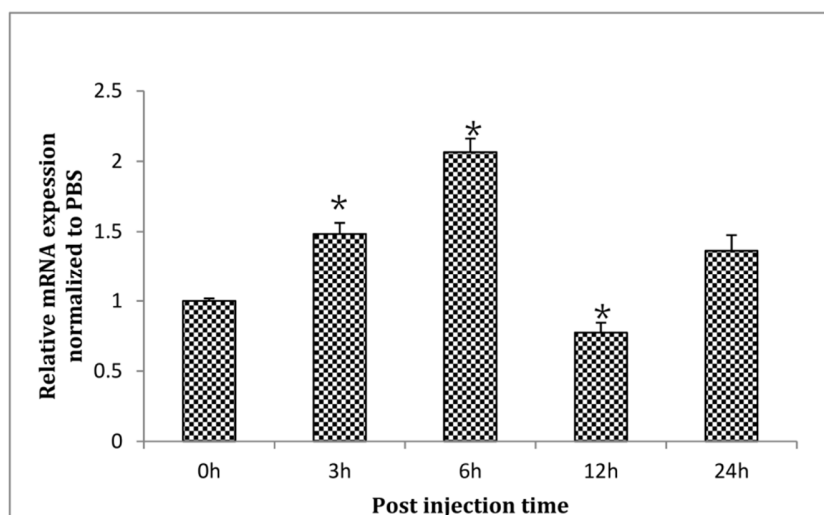


Fig. 69. Expression profile of RbFerM mRNA in liver tissues upon immune stimulation with RBIV, as determined by qPCR. Error bars represent SDs ($n = 3$); $*P < 0.05$.

However, at 12 h p.i, significant downregulation of RbFerM expression was observed ($P < 0.05$), either as a response to viral evasion mechanisms orchestrated against the host immune defense (Iannello et al., 2006) or because of the influence of the virus' induction of ROS production in host cells in order to propagate its infection into other cells (Spooner and Yilmaz, 2011) because

ferritins can suppress ROS production through inhibition of Fenton-type reactions by sequestering free iron in cellular environments (Berberat et al., 2003). Even though, to our knowledge, no studies have addressed expressional inductions of ferritin M subunits upon live pathogen infections in teleosts, one study on *Scophthalmus maximus* provides some evidence about this process, in which a viral mitogen, poly I:C, was used to stimulate fish instead of a live virus, and it was found to substantially enhance transcription of the ferritin M subunit in the liver and spleen tissues compared to controls (Zheng et al., 2010a). The overall inductive response of RbFerM upon different pathogen and mitogen stimuli observed in the present study suggests its potential role in host immune defense, which further confirms the results of a previous study on the antimicrobial behavior of ferritins through its iron depriving function (Ong et al., 2006).

4. CONCLUSION

Overall molecular insight into RbFerM provides strong evidence pointing to its importance as a subunit of the rock bream ferritin protein complex, which resembles structural features of ferritin H and L subunits, especially those involved in iron binding. Moreover, through its iron depriving properties, RbFerM can provide a protective effect against potential DNA damage, which is most likely induced by hydroxyl radicals generated through Fenton-type reactions. Iron binding properties of RbFerM can vary as a function of temperature, and it exhibits optimal activity under the physiological temperature of rock bream. Phylogenetic analysis confirmed that RbFerM evolved from a common ancestor origin of vertebrates. According to the modulated transcriptional profile upon pathogen stimulation, RbFerM expression appears to be promoted under viral and bacterial stress, further demonstrating its potential role in the host immune

defense, which is likely based on the reduction of free iron availability resulting from its iron withholding effect.

GENERAL CONCLUSION

This thesis presents several studies on identification and molecular characterization of putative acute phase proteins and molecular antioxidants from a teleostan origin. In first phase of the studies (described in first chapter) we evidence for the existence of three different APP homologues (CRP, SAA and Hp) from black rock fish which is a highly demanded fish delicacy in Asia Pacific region, deciphering their expressional modulation under experimentally induced septic conditions. Moreover, we have also provided some insights into the plausible functional roles of one APP (RfCRP) in host antimicrobial defense, using its recombinant protein. Taken together, we can suggest that aforementioned three APPs potentially play an indispensable role of the acute phase of an infection, in turn hinting on their candidature to be targeted for induction against pathogenic infections to develop disease resistance in black rock fish.

Second phase (described in second chapter) of the thesis describes the studied devoted for the identification and characterization of four distinct role players from rock bream in its antioxidative defense. First two molecules (RbCat and RbTrxR3) were evidence for their agreement to the functional roles of known counterparts, as direct partakers in host antioxidant system. On the other hand, indirect antioxidant behavior exerting through depriving the catalysts (Fe^{2+}) of oxidative reactions were affirmed for the next two molecules (RbFerM and RbFerH). However, all four molecules were found to be modulated by pathogen stress and particularly RbFerH was shown to involve in host antibacterial defense. Collectively, the data gathered in

second phase of the studies suggests their importance in host antioxidant defense and immune responses, in turn indicating their potential importance in survival of fish under stress conditions.

References

- Adams, E.C. and Weiss, M.R., 1969. Calorimetric studies of the haemoglobin-haptoglobin reaction. *Biochem J* 115, 441-7.
- Aebi, H., 1984. Catalase in vitro. *Methods Enzymol* 105, 121-6.
- Agrawal, A., Shrive, A.K., Greenhough, T.J. and Volanakis, J.E., 2001. Topology and structure of the C1q-binding site on C-reactive protein. *J Immunol* 166, 3998-4004.
- Agrawal, A., Singh, P.P., Bottazzi, B., Garlanda, C. and Mantovani, A., 2009. Pattern recognition by pentraxins. *Adv Exp Med Biol* 653, 98-116.
- Agrawal, A. and Volanakis, J.E., 1994. Probing the C1q-binding site on human C-reactive protein by site-directed mutagenesis. *J Immunol* 152, 5404-10.
- Alderman, D.J. and Hastings, T.S., 1998. Antibiotic use in aquaculture: development of antibiotic resistance – potential for consumer health risks. *J. Food Sci. Technol.* 33, 139-155.
- Alkhateeb, A.A. and Connor, J.R., 2010. Nuclear ferritin: A new role for ferritin in cell biology. *Biochim Biophys Acta* 1800, 793-7.
- Andersen, O., Dehli, A., Standal, H., Giskegjerde, T.A., Karstensen, R. and Rorvik, K.A., 1995. Two ferritin subunits of Atlantic salmon (*Salmo salar*): cloning of the liver cDNAs and antibody preparation. *Mol Mar Biol Biotechnol* 4, 164-70.
- Anderson, A.D., Nelson, J.M., Rossiter, S. and Angulo, F.J., 2003. Public health consequences of use of antimicrobial agents in food animals in the United States". *Microb. Drug Resist* 9, 373-379.
- Anderson, G.J. and Frazer, D.M., 2005. Hepatic iron metabolism. *Semin Liver Dis* 25, 420-32.
- Andersson, M., Holmgren, A. and Spyrou, G., 1996. NK-lysin, a disulfide-containing effector peptide of T-lymphocytes, is reduced and inactivated by human thioredoxin reductase. Implication for a protective mechanism against NK-lysin cytotoxicity. *J Biol Chem* 271, 10116-20.
- Andrews, S.C., Arosio, P., Bottke, W., Briat, J.F., von Darl, M., Harrison, P.M., Laulhere, J.P., Levi, S., Lobreaux, S. and Yewdall, S.J., 1992. Structure, function, and evolution of ferritins. *J Inorg Biochem* 47, 161-74.
- Arias, D.G., Regner, E.L., Iglesias, A.A. and Guerrero, S.A., 2012. *Entamoeba histolytica* thioredoxin reductase: molecular and functional characterization of its atypical properties. *Biochim Biophys Acta* 1820, 1859-66.
- Armstrong, P.B. and Quigley, J.P., 1999. Alpha2-macroglobulin: an evolutionarily conserved arm of the innate immune system. *Dev Comp Immunol* 23, 375-90.
- Arner, E.S., Nordberg, J. and Holmgren, A., 1996. Efficient reduction of lipoamide and lipoic acid by mammalian thioredoxin reductase. *Biochem Biophys Res Commun* 225, 268-74.
- Arnoult, D., Soares, F., Tattoli, I., Castanier, C., Philpott, D.J. and Girardin, S.E., 2009. An N-terminal addressing sequence targets NLRX1 to the mitochondrial matrix. *J Cell Sci* 122, 3161-8.
- Arockiaraj, J., Easwvaran, S., Vanaraja, P., Singh, A., Othman, R.Y. and Bhassu, S., 2012. Molecular cloning, characterization and gene expression of an antioxidant enzyme catalase (MrCat) from *Macrobrachium rosenbergii*. *Fish Shellfish Immunol* 32, 670-82.

- Arosio, P., Ingrassia, R. and Cavadini, P., 2009. Ferritins: a family of molecules for iron storage, antioxidation and more. *Biochim Biophys Acta* 1790, 589-99.
- Arosio, P., Yokota, M. and Drysdale, J.W., 1976. Structural and immunological relationships of iso-ferritins in normal and malignant cells. *Cancer Res* 36, 1735-9.
- Aydemir, T. and Kuru, K., 2003. Purification and Partial Characterization of Catalase from Chicken Erythrocytes and the Effect of Various Inhibitors on Enzyme Activity. *Turk. J. Chem* 27, 85-98.
- Babior, B.M., 1984. The respiratory burst of phagocytes. *J Clin Invest* 73, 599-601.
- Badolato, R., Wang, J.M., Murphy, W.J., Lloyd, A.R., Michiel, D.F., Bausserman, L.L., Kelvin, D.J. and Oppenheim, J.J., 1994. Serum amyloid A is a chemoattractant: induction of migration, adhesion, and tissue infiltration of monocytes and polymorphonuclear leukocytes. *J Exp Med* 180, 203-9.
- Baker, A., Payne, C.M., Briehl, M.M. and Powis, G., 1997. Thioredoxin, a gene found overexpressed in human cancer, inhibits apoptosis in vitro and in vivo. *Cancer Res* 57, 5162-7.
- Baldo, E.A. and Fletcher, T.C., 1973. C-reactive protein like Precipitins in plaice. *Nature* 16, 145-146.
- Bausserman, L.L., Saritelli, A.L., Van Zuiden, P., Gollaher, C.J. and Herbert, P.N., 1987. Degradation of serum amyloid A by isolated perfused rat liver. *J Biol Chem* 262, 1583-9.
- Bayne, C.J. and Gerwick, L., 2001. The acute phase response and innate immunity of fish. *Dev Comp Immunol* 25, 725-43.
- Bayne, C.J., Gerwick, L., Fujiki, K., Nakao, M. and Yano, T., 2001. Immune-relevant (including acute phase) genes identified in the livers of rainbow trout, *Oncorhynchus mykiss*, by means of suppression subtractive hybridization. *Dev Comp Immunol* 25, 205-17.
- Berberat, P.O., Katori, M., Kaczmarek, E., Anselmo, D., Lassman, C., Ke, B., Shen, X., Busuttill, R.W., Yamashita, K., Csizmadia, E., Tyagi, S., Otterbein, L.E., Brouard, S., Tobiasch, E., Bach, F.H., Kupiec-Weglinski, J.W. and Soares, M.P., 2003. Heavy chain ferritin acts as an antiapoptotic gene that protects livers from ischemia reperfusion injury. *FASEB J* 17, 1724-6.
- Bjornstedt, M., Hamberg, M., Kumar, S., Xue, J. and Holmgren, A., 1995. Human thioredoxin reductase directly reduces lipid hydroperoxides by NADPH and selenocystine strongly stimulates the reaction via catalytically generated selenols. *J Biol Chem* 270, 11761-4.
- Black, D.L., 2000. Protein diversity from alternative splicing: a challenge for bioinformatics and post-genome biology. *Cell* 103, 367-70.
- Black, S., Kushner, I. and Samols, D., 2004. C-reactive Protein. *J Biol Chem* 279, 48487-90.
- Borjesson, D.L., Kobayashi, S.D., Whitney, A.R., Voyich, J.M., Argue, C.M. and Deleo, F.R., 2005. Insights into pathogen immune evasion mechanisms: *Anaplasma phagocytophilum* fails to induce an apoptosis differentiation program in human neutrophils. *J Immunol* 174, 6364-72.
- Bracken, C., 2001. NMR spin relaxation methods for characterization of disorder and folding in proteins. *J Mol Graph Model* 19, 3-12.
- Bradford, M.M., 1976. A rapid and sensitive method for the quantitation of microgram quantities of protein utilizing the principle of protein-dye binding. *Anal Biochem* 72, 248-54.
- Brown, D.M., Upcroft, J.A. and Upcroft, P., 1996. A thioredoxin reductase-class of disulphide reductase in the protozoan parasite *Giardia duodenalis*. *Mol Biochem Parasitol* 83, 211-20.

- Bruchhaus, I. and Tannich, E., 1995. Identification of an *Entamoeba histolytica* gene encoding a protein homologous to prokaryotic disulphide oxidoreductases. *Mol Biochem Parasitol* 70, 187-91.
- Bryant, D.D. and Wilson, G.N., 1995. Differential evolution and expression of murine peroxisomal membrane protein genes. *Biochem Mol Med* 55, 22-30.
- Buettner, G.R. and Jurkiewicz, B.A., 1993. Ascorbate free radical as a marker of oxidative stress: an EPR study. *Free Radic Biol Med* 14, 49-55.
- Buonocore, G., Perrone, S. and Tataranno, M.L., 2010. Oxygen toxicity: chemistry and biology of reactive oxygen species. *Semin Fetal Neonatal Med* 15, 186-90.
- Bustin, S.A., Benes, V., Garson, J.A., Hellems, J., Huggett, J., Kubista, M., et al. The MIQE guidelines: minimum information for publication of quantitative real-time PCR experiments. *Clin Chem* 55, 611-22.
- Campanella, J.J., Bitincka, L. and Smalley, J., 2003. MatGAT: an application that generates similarity/identity matrices using protein or DNA sequences. *BMC Bioinformatics* 4, 29.
- Caskey, J.H., Jones, C., Miller, Y.E. and Seligman, P.A., 1983. Human ferritin gene is assigned to chromosome 19. *Proc Natl Acad Sci U S A* 80, 482-6.
- Casso, D. and Beach, D., 1996. A mutation in a thioredoxin reductase homolog suppresses p53-induced growth inhibition in the fission yeast *Schizosaccharomyces pombe*. *Mol Gen Genet* 252, 518-29.
- Ceron, J.J., Eckersall, P.D. and Martynez-Subiela, S., 2005. Acute phase proteins in dogs and cats: current knowledge and future perspectives. *Vet Clin Pathol* 34, 85-99.
- Chae, H.Z., Chung, S.J. and Rhee, S.G., 1994. Thioredoxin-dependent peroxide reductase from yeast. *J Biol Chem* 269, 27670-8.
- Chang, M.K., Binder, C.J., Torzewski, M. and Witztum, J.L., 2002. C-reactive protein binds to both oxidized LDL and apoptotic cells through recognition of a common ligand: Phosphorylcholine of oxidized phospholipids. *Proc Natl Acad Sci U S A* 99, 13043-8.
- Chelikani, P., Fita, I. and Loewen, P.C., 2004. Diversity of structures and properties among catalases. *Cell Mol Life Sci* 61, 192-208.
- Circu, M.L. and Aw, T.Y., 2010. Reactive oxygen species, cellular redox systems, and apoptosis. *Free Radic Biol Med* 48, 749-62.
- Coffman, L.G., Brown, J.C., Johnson, D.A., Parthasarathy, N., D'Agostino, R.B., Jr., Lively, M.O., et al., 2008. Cleavage of high-molecular-weight kininogen by elastase and tryptase is inhibited by ferritin. *Am J Physiol Lung Cell Mol Physiol* 294, L505-15.
- Colon, W. and Kelly, J.W., 1992. Partial denaturation of transthyretin is sufficient for amyloid fibril formation in vitro. *Biochemistry* 31, 8654-60.
- Crane, D., Holmes, R. and Masters, C., 1982. Proteolytic modification of mouse liver catalase. *Biochem Biophys Res Commun* 104, 1567-72.
- Cray, C., Zaias, J. and Altman, N.H., 2009. Acute phase response in animals: a review. *Comp Med* 59, 517-26.
- Crichton, R.R. and Declercq, J.P., 2010. X-ray structures of ferritins and related proteins. *Biochim Biophys Acta* 1800, 706-18.
- Crichton, R.R., Wilmet, S., Leggsyter, R. and Ward, R.J., 2002. Molecular and cellular mechanisms of iron homeostasis and toxicity in mammalian cells. *J Inorg Biochem* 91, 9-18.
- D'Armiento, J., Dalal, S.S. and Chada, K., 1997. Tissue, temporal and inducible expression pattern of haptoglobin in mice. *Gene* 195, 19-27.

- Dai, S., Saarinen, M., Ramaswamy, S., Meyer, Y., Jacquot, J.P. and Eklund, H., 1996. Crystal structure of *Arabidopsis thaliana* NADPH dependent thioredoxin reductase at 2.5 Å resolution. *J Mol Biol* 264, 1044-57.
- Dancygier, H., 2010. *Clinical Hepatology: Principles and practice of hepatobiliary diseases*, Springer, New York.
- Danielsen, B., Sorensen, I.J., Nybo, M., Nielsen, E.H., Kaplan, B. and Svehag, S.E., 1997. Calcium-dependent and -independent binding of the pentraxin serum amyloid P component to glycosaminoglycans and amyloid proteins: enhanced binding at slightly acid pH. *Biochim Biophys Acta* 1339, 73-8.
- De Zoysa, M. and Lee, J., 2007. Two ferritin subunits from disk abalone (*Haliotis discus discus*): cloning, characterization and expression analysis. *Fish Shellfish Immunol* 23, 624-35.
- Dennis, C., 2001. Haemoglobin scavenger. *Nature* 409, 141.
- Dickey, L.F., Sreedharan, S., Theil, E.C., Didsbury, J.R., Wang, Y.H. and Kaufman, R.E., 1987. Differences in the regulation of messenger RNA for housekeeping and specialized-cell ferritin. A comparison of three distinct ferritin complementary DNAs, the corresponding subunits, and identification of the first processed in amphibia. *J Biol Chem* 262, 7901-7.
- Droege, M. and Hill, B., 2008. The Genome Sequencer FLX System--longer reads, more applications, straight forward bioinformatics and more complete data sets. *J Biotechnol* 136, 3-10.
- Earle, D.P., Taggart, J.V. and Shannon, J.A., 1944. Glomerulonephritis. A Survey of the Functional Organization of the Kidney in Various Stages of Diffuse Glomerulonephritis. *J Clin Invest* 23, 119-37.
- Eckersall, P.D. and Bell, R., 2010. Acute phase proteins: Biomarkers of infection and inflammation in veterinary medicine. *Vet J* 185, 23-7.
- Edagawa, T., Murata, M., Hattori, M., Onuma, M. and Kodama, H., 1993. Cell surface C-reactive protein of rainbow trout lymphocytes. *Dev Comp Immunol* 17, 119-27.
- Ekanayake, P.M., De Zoysa, M., Kang, H.S., Wan, Q., Jee, Y., Lee, Y.H., Kim, S.J. and Lee, J., 2008. Cloning, characterization and tissue expression of disk abalone (*Haliotis discus discus*) catalase. *Fish Shellfish Immunol* 24, 267-78.
- Ellis, J.E., Yarlett, N., Cole, D., Humphreys, M.J. and Lloyd, D., 1994. Antioxidant defences in the microaerophilic protozoan *Trichomonas vaginalis*: comparison of metronidazole-resistant and sensitive strains. *Microbiology* 140 (Pt 9), 2489-94.
- Ellison, R.T., 3rd and Giehl, T.J., 1991. Killing of gram-negative bacteria by lactoferrin and lysozyme. *J Clin Invest* 88, 1080-91.
- Elvitigala, D.A., Premachandra, H.K., Whang, I., Priyathilaka, T.T., Kim, E., Lim, B.S., et al., 2013. Marine teleost ortholog of catalase from rock bream (*Oplegnathus fasciatus*): molecular perspectives from genomic organization to enzymatic behavior with respect to its potent antioxidant properties. *Fish Shellfish Immunol* 35, 1086-96.
- Elvitigala, D.A., Priyathilaka, T.T., Whang, I., Nam, B.H. and Lee, J., 2015. A teleostan homolog of catalase from black rockfish (*Sebastes schlegelii*): Insights into functional roles in host antioxidant defense and expressional responses to septic conditions. *Fish Shellfish Immunol* 44, 321-31.
- Engstad, R.E., Robertsen, B. and Frivold, E., 1992. Yeast glucan induces increase in lysozyme and complement-mediated haemolytic activity in Atlantic salmon blood. *Fish & shellfish immunology* 3, 267-277.

- Falco, A., Cartwright, J.R., Wiegertjes, G.F. and Hoole, D., 2012. Molecular characterization and expression analysis of two new C-reactive protein genes from common carp (*Cyprinus carpio*). *Dev Comp Immunol* 37, 127-38.
- Fan, H. and Cook, J.A., 2004. Molecular mechanisms of endotoxin tolerance. *J Endotoxin Res* 10, 71-84.
- Forman, H.J., Maiorino, M. and Ursini, F., 2010. Signaling functions of reactive oxygen species. *Biochemistry* 49, 835-42.
- Fujiki, K., Shin, D.H., Nakao, M. and Yano, T., 2000. Molecular cloning and expression analysis of carp (*Cyprinus carpio*) interleukin-1 beta, high affinity immunoglobulin E Fc receptor gamma subunit and serum amyloid A. *Fish Shellfish Immunol* 10, 229-42.
- Gabay, C. and Kushner, I., 1999. Acute-phase proteins and other systemic responses to inflammation. *N Engl J Med* 340, 448-54.
- Gasdaska, J.R., Berggren, M. and Powis, G., 1995. Cell growth stimulation by the redox protein thioredoxin occurs by a novel helper mechanism. *Cell Growth Differ* 6, 1643-50.
- Gerhard, G.S., Kauffman, E.J. and Grundy, M.A., 2000. Molecular cloning and sequence analysis of the Danio rerio catalase gene. *Comp Biochem Physiol B Biochem Mol Biol* 127, 447-57.
- Goodsell, D.S., 2005. Representing structural information with RasMol. *Curr Protoc Bioinformatics* Chapter 5, Unit 5 4.
- Gordon, S., 2002. Pattern recognition receptors: doubling up for the innate immune response. *Cell* 111, 927-30.
- Govind, K., Bakshi, A. and Savithri, H.S., 2014. Interaction of Sesbania mosaic virus (SeMV) RNA-dependent RNA polymerase (RdRp) with the p10 domain of polyprotein 2a and its implications in SeMV replication. *FEBS Open Bio* 4, 362-9.
- Goyal, M.M. and Basak, A., 2010. Human catalase: looking for complete identity. *Protein Cell* 1, 888-97.
- Graham, R.M., Chua, A.C., Herbison, C.E., Olynyk, J.K. and Trinder, D., 2007. Liver iron transport. *World J Gastroenterol* 13, 4725-36.
- Groeger, G., Quiney, C. and Cotter, T.G., 2009. Hydrogen peroxide as a cell-survival signaling molecule. *Antioxid Redox Signal* 11, 2655-71.
- Guo, H., Zhang, D., Cui, S., Chen, M., Wu, K., Li, Y., et al., 2011. Molecular characterization and mRNA expression of catalase from pearl oyster *Pinctada fucata*. *Mar Genomics* 4, 245-51.
- Ha, E.M., Oh, C.T., Ryu, J.H., Bae, Y.S., Kang, S.W., Jang, I.H., et al., 2005. An antioxidant system required for host protection against gut infection in *Drosophila*. *Dev Cell* 8, 125-32.
- Han, H.J., Kim, D.Y., Kim, W.S., Kim, C.S., Jung, S.J., Oh, M.J. and Kim, D.H., 2011. Atypical *Aeromonas salmonicida* infection in the black rockfish, *Sebastes schlegeli* Hilgendorf, in Korea. *J Fish Dis* 34, 47-55.
- Harrison, P.M. and Arosio, P., 1996. The ferritins: molecular properties, iron storage function and cellular regulation. *Biochim Biophys Acta* 1275, 161-203.
- Hatfield, D.L. and Gladyshev, V.N., 2002. How selenium has altered our understanding of the genetic code. *Mol Cell Biol* 22, 3565-76.
- Hausmann, K., Wulfhekel, U., Dullmann, J. and Kuse, R., 1976. Iron storage in macrophages and endothelial cells. Histochemistry, ultrastructure, and clinical significance. *Blut* 32, 289-95.

- Hayden, M.S., West, A.P. and Ghosh, S., 2006. NF-kappaB and the immune response. *Oncogene* 25, 6758-80.
- Heinrich, P.C., Castell, J.V. and Andus, T., 1990. Interleukin-6 and the acute phase response. *Biochem J* 265, 621-36.
- Hess, J., Angel, P. and Schorpp-Kistner, M., 2004. AP-1 subunits: quarrel and harmony among siblings. *J Cell Sci* 117, 5965-73.
- Holmgren, A., 1979. Reduction of disulfides by thioredoxin. Exceptional reactivity of insulin and suggested functions of thioredoxin in mechanism of hormone action. *J Biol Chem* 254, 9113-9.
- Hu, Y.H., Zheng, W.J. and Sun, L., 2010. Identification and molecular analysis of a ferritin subunit from red drum (*Sciaenops ocellatus*). *Fish Shellfish Immunol* 28, 678-86.
- Huong Giang, D.T., Van Driessche, E., Vandenberghe, I., Devreese, B. and Beeckmans, S., 2010. Isolation and characterization of SAP and CRP, two pentraxins from *Pangasianodon* (*Pangasius*) *hypophthalmus*. *Fish Shellfish Immunol* 28, 743-53.
- Iannello, A., Debbeche, O., Martin, E., Attalah, L.H., Samarani, S. and Ahmad, A., 2006. Viral strategies for evading antiviral cellular immune responses of the host. *J Leukoc Biol* 79, 16-35.
- Jacob, R.A., 1995. The Integrated Antioxidant Nutr Res 15, 755-766.
- Jang, H.H., Lee, K.O., Chi, Y.H., Jung, B.G., Park, S.K., Park, J.H., et al., 2004. Two enzymes in one; two yeast peroxiredoxins display oxidative stress-dependent switching from a peroxidase to a molecular chaperone function. *Cell* 117, 625-35.
- Jensen, L.E., Hiney, M.P., Shields, D.C., Uhlar, C.M., Lindsay, A.J. and Whitehead, A.S., 1997. Acute phase proteins in salmonids: evolutionary analyses and acute phase response. *J Immunol* 158, 384-92.
- Johnson, H.L., Chiou, C.C. and Cho, C.T., 1999. Applications of acute phase reactants in infectious diseases. *J Microbiol Immunol Infect* 32, 73-82.
- Jorgensen, J.B., Lunde, H., Jensen, L., Whitehead, A.S. and Robertsen, B., 2000. Serum amyloid A transcription in Atlantic salmon (*Salmo salar* L.) hepatocytes is enhanced by stimulation with macrophage factors, recombinant human IL-1 beta, IL-6 and TNF alpha or bacterial lipopolysaccharide. *Dev Comp Immunol* 24, 553-63.
- Jorgensen, J.B., Sharp, G.J.E., Secombes, C.J. and Robertsen, B., 1993. Effect of a yeast cell wall glucan on the bacteriocidal activity of rainbow trout macrophages. *Fish Shellfish Immunol* 3, 267-277.
- Kamata, H., Honda, S., Maeda, S., Chang, L., Hirata, H. and Karin, M., 2005. Reactive oxygen species promote TNFalpha-induced death and sustained JNK activation by inhibiting MAP kinase phosphatases. *Cell* 120, 649-61.
- Kaneko, J.J., 1997. Serum proteins and the dysproteinemias, in: Kaneko, J.J., Harvey, J.W. and Bruss, M.L. (Eds.), *Clinical biochemistry of domestic animals*. San Diego (CA) Academic Press, pp. 117-138.
- Kang, J.H., 2010. Oxidative Damage of DNA induced by Ferritin and Hydrogen Peroxide. *Bulletin of Korean Chemical Society* 31, 2873-2876.
- Kang, S.W., Rhee, S.G., Chang, T.S., Jeong, W. and Choi, M.H., 2005. 2-Cys peroxiredoxin function in intracellular signal transduction: therapeutic implications. *Trends Mol Med* 11, 571-8.

- Kashiwagi, A., Kashiwagi, K., Takase, M., Hanada, H. and Nakamura, M., 1997. Comparison of catalase in diploid and haploid *Rana rugosa* using heat and chemical inactivation techniques. *Comp Biochem Physiol B Biochem Mol Biol* 118, 499-503.
- Ken, C.F., Lin, C.T., Wu, J.L. and Shaw, J.F., 2000. Cloning and expression of a cDNA coding for catalase from zebrafish (*Danio rerio*). *J Agric Food Chem* 48, 2092-6.
- Keren, H., Lev-Maor, G. and Ast, G., 2010. Alternative splicing and evolution: diversification, exon definition and function. *Nat Rev Genet* 11, 345-55.
- Kim, J.H., Rhee, J.S., Lee, J.S., Dahms, H.U., Lee, J., Han, K.N. and Lee, J.S., 2010. Effect of cadmium exposure on expression of antioxidant gene transcripts in the river pufferfish, *Takifugu obscurus* (Tetraodontiformes). *Comp Biochem Physiol C Toxicol Pharmacol* 152, 473-9.
- Kimura, T., Yoshimizu, M., Oseko, N. and Nishizawa, T., 1989. Rhabdovirus Olivaceus (Hirame Rhabdovirus), in: Winfried, A. and Edouard, K. (Eds.), *Viruses of Lower Vertebrates*. Springer-Verlag Berlin Heidelberg, pp. 388-395.
- Klotz, M.G., Klassen, G.R. and Loewen, P.C., 1997. Phylogenetic relationships among prokaryotic and eukaryotic catalases. *Mol Biol Evol* 14, 951-8.
- Knovich, M.A., Storey, J.A., Coffman, L.G., Torti, S.V. and Torti, F.M., 2009. Ferritin for the clinician. *Blood Rev* 23, 95-104.
- Knutson, M.D., Oukka, M., Koss, L.M., Aydemir, F. and Wessling-Resnick, M., 2005. Iron release from macrophages after erythrophagocytosis is up-regulated by ferroportin 1 overexpression and down-regulated by hepcidin. *Proc Natl Acad Sci U S A* 102, 1324-8.
- Kodama, H., Arimitsu, H., Mukamoto, M. and Sugimoto, C., 1999. Enhancement of phagocytic and chemokinetic activities of rainbow trout head kidney cells by C-reactive protein. *Am J Vet Res* 60, 240-4.
- Kodama, H., Yamada, F., Murai, T., Nakanishi, Y., Mikami, T. and Izawa, H., 1989. Activation of trout macrophages and production of CRP after immunization with *Vibrio anguillarum*. *Dev Comp Immunol* 13, 123-32.
- Kohchi, C., Inagawa, H., Nishizawa, T. and Soma, G., 2009. ROS and innate immunity. *Anticancer Res* 29, 817-21.
- Kottgen, E., Hell, B., Kage, A. and Tauber, R., 1992. Lectin specificity and binding characteristics of human C-reactive protein. *J Immunol* 149, 445-53.
- Kowaltowski, A.J., de Souza-Pinto, N.C., Castilho, R.F. and Vercesi, A.E., 2009. Mitochondria and reactive oxygen species. *Free Radic Biol Med* 47, 333-43.
- Krem, M.M. and Di Cera, E., 2002. Evolution of enzyme cascades from embryonic development to blood coagulation. *Trends Biochem Sci* 27, 67-74.
- Krewulak, K.D. and Vogel, H.J., 2008. Structural biology of bacterial iron uptake. *Biochim Biophys Acta* 1778, 1781-804.
- Kushner, I., 1982. The phenomenon of the acute phase response. *Ann N Y Acad Sci* 389, 39-48.
- Kushner, I. and Mackiewicz, A., 1993. *Acute phase proteins: molecular biology, biochemistry, and clinical applications*, CRC press, Inc., Florida.
- Lacey, B.M. and Hondal, R.J., 2006. Characterization of mitochondrial thioredoxin reductase from *C. elegans*. *Biochem Biophys Res Commun* 346, 629-36.
- Lacroix, I., Lipcey, C., Imbert, J. and Kahn-Perles, B., 2002. Sp1 transcriptional activity is up-regulated by phosphatase 2A in dividing T lymphocytes. *J Biol Chem* 277, 9598-605.

- Laurent, T.C., Moore, E.C. and Reichard, P., 1964. Enzymatic Synthesis of Deoxyribonucleotides. Iv. Isolation and Characterization of Thioredoxin, the Hydrogen Donor from *Escherichia Coli* B. J Biol Chem 239, 3436-44.
- Lavie, G., Zucker-Franklin, D. and Franklin, E.C., 1978. Degradation of serum amyloid A protein by surface-associated enzymes of human blood monocytes. J Exp Med 148, 1020-31.
- Lawson, D.M., Artymiuk, P.J., Yewdall, S.J., Smith, J.M., Livingstone, J.C., Treffry, A., et al., 1991. Solving the structure of human H ferritin by genetically engineering intermolecular crystal contacts. Nature 349, 541-4.
- Lawson, D.M., Treffry, A., Artymiuk, P.J., Harrison, P.M., Yewdall, S.J., Luzzago, A., et al., 1989. Identification of the ferroxidase centre in ferritin. FEBS Lett 254, 207-10.
- Lee, S.R., Kim, J.R., Kwon, K.S., Yoon, H.W., Levine, R.L., Ginsburg, A. and Rhee, S.G., 1999. Molecular cloning and characterization of a mitochondrial selenocysteine-containing thioredoxin reductase from rat liver. J Biol Chem 274, 4722-34.
- Leto, T.L., Morand, S., Hurt, D. and Ueyama, T., 2009. Targeting and regulation of reactive oxygen species generation by Nox family NADPH oxidases. Antioxid Redox Signal 11, 2607-19.
- Li, C., Ni, D., Song, L., Zhao, J., Zhang, H. and Li, L., 2008. Molecular cloning and characterization of a catalase gene from Zhikong scallop *Chlamys farreri*. Fish Shellfish Immunol 24, 26-34.
- Li, M.F., Chen, C., Li, J. and Sun, L., 2013. The C-reactive protein of tongue sole *Cynoglossus semilaevis* is an acute phase protein that interacts with bacterial pathogens and stimulates the antibacterial activity of peripheral blood leukocytes. Fish Shellfish Immunol 34, 623-31.
- Lim, S.K., Ferraro, B., Moore, K. and Halliwell, B., 2001. Role of haptoglobin in free hemoglobin metabolism. Redox Rep 6, 219-27.
- Liman, M., Wenji, W., Conghui, L., Haiyang, Y., Zhigang, W., Xubo, W., et al., 2013. Selection of reference genes for reverse transcription quantitative real-time PCR normalization in black rockfish (*Sebastes schlegeli*). Mar Genomics 11, 67-73.
- Ling, S.H., Wang, X.H., Xie, L., Lim, T.M. and Leung, K.Y., 2000. Use of green fluorescent protein (GFP) to study the invasion pathways of *Edwardsiella tarda* in in vivo and in vitro fish models. Microbiology 146 (Pt 1), 7-19.
- Liu, H., Takano, T., Peatman, E., Abernathy, J., Wang, S., Sha, Z., Kucuktas, H., Xu, D.H., Klesius, P. and Liu, Z., 2010. Molecular characterization and gene expression of the channel catfish ferritin H subunit after bacterial infection and iron treatment. J Exp Zool A Ecol Genet Physiol 313, 359-68.
- Livak, K.J. and Schmittgen, T.D., 2001. Analysis of relative gene expression data using real-time quantitative PCR and the 2(-Delta Delta C(T)) Method. Methods 25, 402-8.
- Lu, J. and Holmgren, A., 2012. Thioredoxin system in cell death progression. Antioxid Redox Signal 17, 1738-47.
- Lund, V. and Olafsen, J.A., 1999. Changes in serum concentration of a serum amyloid P-like pentraxin in Atlantic salmon, *Salmo salar* L., during infection and inflammation. Dev Comp Immunol 23, 61-70.
- Luo, Y., Henle, E.S. and Linn, S., 1996. Oxidative damage to DNA constituents by iron-mediated fenton reactions. The deoxycytidine family. J Biol Chem 271, 21167-76.

- Mackay, W.J. and Bewley, G.C., 1989. The genetics of catalase in *Drosophila melanogaster*: isolation and characterization of acatalasemic mutants. *Genetics* 122, 643-52.
- Malle, E., Steinmetz, A. and Raynes, J.G., 1993. Serum amyloid A (SAA): an acute phase protein and apolipoprotein. *Atherosclerosis* 102, 131-46.
- Marchler-Bauer, A., Anderson, J.B., Chitsaz, F., Derbyshire, M.K., DeWeese-Scott, C., Fong, J.H., et al., 2009. CDD: specific functional annotation with the Conserved Domain Database. *Nucleic Acids Res* 37, D205-10.
- Martin, R., Fitzl, G., Mozet, C., Martin, H., Welt, K. and Wieland, E., 2002. Effect of age and hypoxia/reoxygenation on mRNA expression of antioxidative enzymes in rat liver and kidneys. *Exp Gerontol* 37, 1481-7.
- Massad, G., Arceneaux, J.E. and Byers, B.R., 1992. Novel heme-binding component in the serum of the channel catfish (*Ictalurus punctatus*). *Biometals* 5, 57-62.
- Mathew, S., Kumar, K.A., Anandan, R., Viswanathan Nair, P.G. and Devadasan, K., 2007. Changes in tissue defence system in white spot syndrome virus (WSSV) infected *Penaeus monodon*. *Comp Biochem Physiol C Toxicol Pharmacol* 145, 315-20.
- Matsuyama, H., Mangindaan, R.E.P. and Yano, T., 1992. Protective effect of schizophyllan and scleroglucan against *Streptococcus* sp. infection in yellow tail (*Seriola quinqueradiata*). *Aquaculture* 101, 197-203.
- May, J.M., Cobb, C.E., Mendiratta, S., Hill, K.E. and Burk, R.F., 1998. Reduction of the ascorbyl free radical to ascorbate by thioredoxin reductase. *J Biol Chem* 273, 23039-45.
- May, J.M., Mendiratta, S., Hill, K.E. and Burk, R.F., 1997. Reduction of dehydroascorbate to ascorbate by the selenoenzyme thioredoxin reductase. *J Biol Chem* 272, 22607-10.
- McClung, C.R., 1997. Regulation of catalases in *Arabidopsis*. *Free Radic Biol Med* 23, 489-96.
- Migita, K., Kawabe, Y., Tominaga, M., Origuchi, T., Aoyagi, T. and Eguchi, K., 1998. Serum amyloid A protein induces production of matrix metalloproteinases by human synovial fibroblasts. *Lab Invest* 78, 535-9.
- Missirlis, F., Holmberg, S., Georgieva, T., Dunkov, B.C., Rouault, T.A. and Law, J.H., 2006. Characterization of mitochondrial ferritin in *Drosophila*. *Proc Natl Acad Sci U S A* 103, 5893-8.
- Mitchell, P. and Tollervey, D., 2001. mRNA turnover. *Curr Opin Cell Biol* 13, 320-5.
- Mitchell, T.I., Coon, C.I. and Brinckerhoff, C.E., 1991. Serum amyloid A (SAA3) produced by rabbit synovial fibroblasts treated with phorbol esters or interleukin 1 induces synthesis of collagenase and is neutralized with specific antiserum. *J Clin Invest* 87, 1177-85.
- Modrek, B. and Lee, C., 2002. A genomic view of alternative splicing. *Nat Genet* 30, 13-9.
- Mohankumar, K. and Ramasamy, P., 2006. White spot syndrome virus infection decreases the activity of antioxidant enzymes in *Fenneropenaeus indicus*. *Virus Res* 115, 69-75.
- Mohomad-Jawad, L.A.H., Rabu, A., Mohomad, R. and Mohd-Adnad, A., 2012. Phylogenetic characterization and the expression of recombinant C-reactive protein from the Asian seabass (*Lates calcarifer*). *Aquaculture* 338, 13-22.
- Moore, C.B., Bergstralh, D.T., Duncan, J.A., Lei, Y., Morrison, T.E., Zimmermann, A.G., et al., 2008. NLRX1 is a regulator of mitochondrial antiviral immunity. *Nature* 451, 573-7.
- Moreira, S.F., Bailao, A.M., Barbosa, M.S., Jesuino, R.S., Felipe, M.S., Pereira, M. and de Almeida Soares, C.M., 2004. Monofunctional catalase P of *Paracoccidioides brasiliensis*: identification, characterization, molecular cloning and expression analysis. *Yeast* 21, 173-82.

- Morey, M., Serras, F., Baguna, J., Hafen, E. and Corominas, M., 2001. Modulation of the Ras/MAPK signalling pathway by the redox function of selenoproteins in *Drosophila melanogaster*. *Dev Biol* 238, 145-56.
- Muller, H.E., 1985. Detection of hydrogen peroxide produced by microorganisms on an ABTS peroxidase medium. *Zentralbl Bakteriol Mikrobiol Hyg A* 259, 151-4.
- Murata, M., Kodama, H. and Onuma, M., 1995. Characterization of rainbow trout C-polysaccharide binding proteins. *J Vet Med Sci* 57, 419-25.
- Murthy, M.R., Reid, T.J., 3rd, Sicignano, A., Tanaka, N. and Rossmann, M.G., 1981. Structure of beef liver catalase. *J Mol Biol* 152, 465-99.
- Mustacich, D. and Powis, G., 2000. Thioredoxin reductase. *Biochem J* 346 Pt 1, 1-8.
- Nakano, H., Nakajima, A., Sakon-Komazawa, S., Piao, J.H., Xue, X. and Okumura, K., 2006. Reactive oxygen species mediate crosstalk between NF-kappaB and JNK. *Cell Death Differ* 13, 730-7.
- Nakayama, T., Sonoda, S., Urano, T., Yamada, T. and Okada, M., 1993. Monitoring both serum amyloid protein A and C-reactive protein as inflammatory markers in infectious diseases. *Clin Chem* 39, 293-7.
- Nam, Y.K., Cho, Y.S., Choi, B.N., Kim, K.H., Kim, S.K. and Kim, D.S., 2005. Alteration of antioxidant enzymes at the mRNA level during short-term starvation of rockbream *Oplegnathus fasciatus*. *Fisheries science* 71, 1385-1387.
- Nauta, A.J., Daha, M.R., van Kooten, C. and Roos, A., 2003. Recognition and clearance of apoptotic cells: a role for complement and pentraxins. *Trends Immunol* 24, 148-54.
- Nenoi, M., Ichimura, S., Mita, K., Yukawa, O. and Cartwright, I.L., 2001. Regulation of the catalase gene promoter by Sp1, CCAAT-recognizing factors, and a WT1/Egr-related factor in hydrogen peroxide-resistant HP100 cells. *Cancer Res* 61, 5885-94.
- Neves, J.V., Wilson, J.M. and Rodrigues, P.N., 2009. Transferrin and ferritin response to bacterial infection: the role of the liver and brain in fish. *Dev Comp Immunol* 33, 848-57.
- Nicholls, P., Fita, I. and Loewen, P.C., 2000. Enzymology and structure of catalases. *Adv Inorg Chem* 51, 51-106.
- Nielsen, M.J. and Moestrup, S.K., 2009. Receptor targeting of hemoglobin mediated by the haptoglobins: roles beyond heme scavenging. *Blood* 114, 764-71.
- Nishiyama, A., Masutani, H., Nakamura, H., Nishinaka, Y. and Yodoi, J., 2001. Redox regulation by thioredoxin and thioredoxin-binding proteins. *IUBMB Life* 52, 29-33.
- Nordberg, J. and Arner, E.S., 2001. Reactive oxygen species, antioxidants, and the mammalian thioredoxin system. *Free Radic Biol Med* 31, 1287-312.
- Nunomura, W., 1991. C-reactive protein in eel: purification and agglutinating activity. *Biochim Biophys Acta* 1076, 191-6.
- Ong, S.T., Ho, J.Z., Ho, B. and Ding, J.L., 2006. Iron-withholding strategy in innate immunity. *Immunobiology* 211, 295-314.
- Orino, K., Lehman, L., Tsuji, Y., Ayaki, H., Torti, S.V. and Torti, F.M., 2001. Ferritin and the response to oxidative stress. *Biochem J* 357, 241-7.
- Orino, K. and Watanabe, K., 2008. Molecular, physiological and clinical aspects of the iron storage protein ferritin. *Vet J* 178, 191-201.
- Oshino, N., Chance, B., Sies, H. and Bucher, T., 1973. The role of H₂O₂ generation in perfused rat liver and the reaction of catalase compound I and hydrogen donors. *Arch Biochem Biophys* 154, 117-31.

- Pacitti, D., Wang, T., Martin, S.A., Sweetman, J. and Secombes, C.J., 2014. Insights into the fish thioredoxin system: expression profile of thioredoxin and thioredoxin reductase in rainbow trout (*Oncorhynchus mykiss*) during infection and in vitro stimulation. *Dev Comp Immunol* 42, 261-77.
- Park, S.I., 2009. Disease Control in Korean Aquaculture. . *Fish Pathology* 44, 19-23.
- Parmley, J.L., Urrutia, A.O., Potrzebowski, L., Kaessmann, H. and Hurst, L.D., 2007. Splicing and the evolution of proteins in mammals. *PLoS Biol* 5, e14.
- Parrott, C., Seidner, T., Duh, E., Leonard, J., Theodore, T.S., Buckler-White, A., Martin, M.A. and Rabson, A.B., 1991. Variable role of the long terminal repeat Sp1-binding sites in human immunodeficiency virus replication in T lymphocytes. *J Virol* 65, 1414-9.
- Patel, H., Fellowes, R., Coade, S. and Woo, P., 1998. Human serum amyloid A has cytokine-like properties. *Scand J Immunol* 48, 410-8.
- Pepys, M.B., Baltz, M., Gomer, K., Davies, A.J. and Doenhoff, M., 1979. Serum amyloid P-component is an acute-phase reactant in the mouse. *Nature* 278, 259-61.
- Pepys, M.B. and Hirschfield, G.M., 2003. C-reactive protein: a critical update. *J Clin Invest* 111, 1805-12.
- Petersen, H.H., Nielsen, J.P. and Heegaard, P.M., 2004. Application of acute phase protein measurements in veterinary clinical chemistry. *Vet Res* 35, 163-87.
- Pieters, J., 2001. Evasion of host cell defense mechanisms by pathogenic bacteria. *Curr Opin Immunol* 13, 37-44.
- Polticelli, F., Bocedi, A., Minervini, G. and Ascenzi, P., 2008. Human haptoglobin structure and function--a molecular modelling study. *FEBS J* 275, 5648-56.
- Press, C.M. and Evensen, O., 1999. The morphology of the immune system in teleost fishes. *Fish Shellfish Immunol* 4, 309-318.
- Prilusky, J., Felder, C.E., Zeev-Ben-Mordehai, T., Rydberg, E.H., Man, O., Beckmann, J.S., Silman, I. and Sussman, J.L., 2005. FoldIndex: a simple tool to predict whether a given protein sequence is intrinsically unfolded. *Bioinformatics* 21, 3435-8.
- Putnam, C.D., Arvai, A.S., Bourne, Y. and Tainer, J.A., 2000. Active and inhibited human catalase structures: ligand and NADPH binding and catalytic mechanism. *J Mol Biol* 296, 295-309.
- Quan, X., Lim, S.O. and Jung, G., 2011. Reactive oxygen species downregulate catalase expression via methylation of a CpG island in the Oct-1 promoter. *FEBS Lett* 585, 3436-41.
- Quiniou, S.M., Katagiri, T., Miller, N.W., Wilson, M., Wolters, W.R. and Waldbieser, G.C., 2003. Construction and characterization of a BAC library from a gynogenetic channel catfish *Ictalurus punctatus*. *Genet Sel Evol* 35, 673-83.
- Raida, M.K. and Buchmann, K., 2009. Innate immune response in rainbow trout (*Oncorhynchus mykiss*) against primary and secondary infections with *Yersinia ruckeri* O1. *Dev Comp Immunol* 33, 35-45.
- Ramos, F. and Smith, A.C., 1978. The c-reactive protein (CRP) test for the detection of early disease in fishes. *Aquaculture* 14, 261-266.
- Rawlings, N.D. and Barrett, A.J., 1993. Evolutionary families of peptidases. *Biochem J* 290 (Pt 1), 205-18.
- Reese, M.G., 2001. Application of a time-delay neural network to promoter annotation in the *Drosophila melanogaster* genome. *Comput Chem* 26, 51-6.

- Rhodes, B., Furnrohr, B.G. and Vyse, T.J., 2011. C-reactive protein in rheumatology: biology and genetics. *Nat Rev Rheumatol* 7, 282-9.
- Rismstad, E., 2011. Examples of emerging virus diseases in salmonid aquaculture. *Aquaculture Research* 42, 86-89.
- Rombout, J.H., Huttenhuis, H.B., Picchiatti, S. and Scapigliati, G., 2005. Phylogeny and ontogeny of fish leucocytes. *Fish Shellfish Immunol* 19, 441-55.
- Rose, A.B., 2008. Intron-mediated regulation of gene expression. *Curr Top Microbiol Immunol* 326, 277-90.
- Roy, A., Kucukural, A. and Zhang, Y., 2010. I-TASSER: a unified platform for automated protein structure and function prediction. *Nat Protoc* 5, 725-38.
- Santambrogio, P., Levi, S., Cozzi, A., Corsi, B. and Arosio, P., 1996. Evidence that the specificity of iron incorporation into homopolymers of human ferritin L- and H-chains is conferred by the nucleation and ferroxidase centres. *Biochem J* 314 (Pt 1), 139-44.
- Santarem, M., Novoa, B. and Figueras, A., 1997. Effects of beta-glucans on the non-specific immune response of turbot (*Scophthalmus maximus* L.). *Fish Shellfish Immunol* 7, 429-437.
- Saranya Revathy, K., Umasuthan, N., Whang, I., Lee, Y., Lee, S., Oh, M.J., Jung, S.J., Choi, C.Y., Park, C.J., Park, H.C. and Lee, J., 2012. A novel acute phase reactant, serum amyloid A-like 1, from *Oplegnathus fasciatus*: genomic and molecular characterization and transcriptional expression analysis. *Dev Comp Immunol* 37, 294-305.
- Scheer, M., Grote, A., Chang, A., Schomburg, I., Munaretto, C., Rother, M., Sohngen, C., Stelzer, M., Thiele, J. and Schomburg, D., 2011. BRENDA, the enzyme information system in 2011. *Nucleic Acids Res* 39, D670-6.
- Schroedl, W., Fuerll, B., Reinhold, P., Krueger, M. and Schuett, C., 2001. A novel acute phase marker in cattle: lipopolysaccharide binding protein (LBP). *J Endotoxin Res* 7, 49-52.
- Scibior, D. and Czczot, H., 2006. [Catalase: structure, properties, functions]. *Postepy Hig Med Dosw (Online)* 60, 170-80.
- Scudiero, R., Trinchella, F., Riggio, M. and Parisi, E., 2007. Structure and expression of genes involved in transport and storage of iron in red-blooded and hemoglobin-less antarctic notothenioids. *Gene* 397, 1-11.
- Segawa, T., Amatsuji, H., Suzuki, K., Suzuki, M., Yanagisawa, M., Itou, T., Sakai, T. and Nakanishi, T., 2013. Molecular characterization and validation of commercially available methods for haptoglobin measurement in bottlenose dolphin. *Results Immunol* 3, 57-63.
- Seki, S., Habu, Y., Kawamura, T., Takeda, K., Dobashi, H., Ohkawa, T. and Hiraide, H., 2000. The liver as a crucial organ in the first line of host defense: the roles of Kupffer cells, natural killer (NK) cells and NK1.1 Ag⁺ T cells in T helper 1 immune responses. *Immunol Rev* 174, 35-46.
- Sheth, K. and Bankey, P., 2001. The liver as an immune organ. *Curr Opin Crit Care* 7, 99-104.
- Shrive, A.K., Cheetham, G.M., Holden, D., Myles, D.A., Turnell, W.G., Volanakis, J.E., Pepys, M.B., Bloomer, A.C. and Greenhough, T.J., 1996. Three dimensional structure of human C-reactive protein. *Nat Struct Biol* 3, 346-54.
- Skulachev, V.P., 1998. Possible role of reactive oxygen species in antiviral defense. *Biochemistry (Mosc)* 63, 1438-40.
- Spooner, R. and Yilmaz, O., 2011. The role of reactive-oxygen-species in microbial persistence and inflammation. *Int J Mol Sci* 12, 334-52.

- Stewart, C., Johnson, J.W.T., Sandra, B., Nagasawa, K. and Kabata, Z., 2004. A Review of the Impact of Parasitic Copepods on Marine Aquaculture. *Zoological Studies* 43, 229-243.
- Storz, G. and Tartaglia, L.A., 1992. OxyR: a regulator of antioxidant genes. *J Nutr* 122, 627-30.
- Strissel, K.J., Girard, M.T., West-Mays, J.A., Rinehart, W.B., Cook, J.R., Brinckerhoff, C.E. and Fini, M.E., 1997. Role of serum amyloid A as an intermediate in the IL-1 and PMA-stimulated signaling pathways regulating expression of rabbit fibroblast collagenase. *Exp Cell Res* 237, 275-87.
- Sun, Y., 1997. Multiplicity of antioxidant enzyme catalase in mouse liver cells. *Free Radic Res* 26, 343-50.
- Suresh, M.V., Singh, S.K., Ferguson, D.A., Jr. and Agrawal, A., 2006. Role of the property of C-reactive protein to activate the classical pathway of complement in protecting mice from pneumococcal infection. *J Immunol* 176, 4369-74.
- Szalai, A.J., 2002. The antimicrobial activity of C-reactive protein. *Microbes Infect* 4, 201-5.
- Szalai, A.J., Norcum, M.T., Bly, J.E. and Clem, L.W., 1992. Isolation of an acute-phase phosphorylcholine-reactive pentraxin from channel catfish (*Ictalurus punctatus*). *Comp Biochem Physiol B* 102, 535-43.
- Tamura, K., Dudley, J., Nei, M. and Kumar, S., 2007. MEGA4: Molecular Evolutionary Genetics Analysis (MEGA) software version 4.0. *Mol Biol Evol* 24, 1596-9.
- Tan, S.S., Ng, P.M., Ho, B. and Ding, J.L., 2005. The antimicrobial properties of C-reactive protein (CRP). *J Endotoxin Res* 11, 249-56.
- Taniguchi, M., Hashimoto, M., Hori, N. and Sato, K., 2005. CCAAT/enhancer binding protein-beta (C/EBP-beta), a pivotal regulator of the TATA-less promoter in the rat catalase gene. *FEBS Lett* 579, 5785-90.
- Tavares-Sanchez, O.L., Gomez-Anduro, G.A., Felipe-Ortega, X., Islas-Osuna, M.A., Sotelo-Mundo, R.R., Barillas-Mury, C. and Yepiz-Plascencia, G., 2004. Catalase from the white shrimp *Penaeus (Litopenaeus) vannamei*: molecular cloning and protein detection. *Comp Biochem Physiol B Biochem Mol Biol* 138, 331-7.
- Theil, E.C., 1987. Ferritin: structure, gene regulation, and cellular function in animals, plants, and microorganisms. *Annu Rev Biochem* 56, 289-315.
- Thompson, K.J., Fried, M.G., Ye, Z., Boyer, P. and Connor, J.R., 2002. Regulation, mechanisms and proposed function of ferritin translocation to cell nuclei. *J Cell Sci* 115, 2165-77.
- Thomson, A.M., Rogers, J.T. and Leedman, P.J., 1999. Iron-regulatory proteins, iron-responsive elements and ferritin mRNA translation. *Int J Biochem Cell Biol* 31, 1139-52.
- Tian, B. and Brasier, A.R., 2003. Identification of a nuclear factor kappa B-dependent gene network. *Recent Prog Horm Res* 58, 95-130.
- Tiron, A. and Vasilescu, C., 2008. [Role of the spleen in immunity. Immunologic consequences of splenectomy]. *Chirurgia (Bucur)* 103, 255-63.
- Toranzo, A.E., Magariños, B. and Romalde, J.L., 2005. A review of the main bacterial fish diseases in mariculture systems. *Aquaculture Research* 246, 37-61.
- Tort, L., 2011. Stress and immune modulation in fish. *Dev Comp Immunol* 35, 1366-75.
- Tripathi, P., 2007. Nitric oxide and immune response. *Indian J Biochem Biophys* 44, 310-9.
- Turnell, W., Sarra, R., Glover, I.D., Baum, J.O., Caspi, D., Baltz, M.L. and Pepys, M.B., 1986. Secondary structure prediction of human SAA1. Presumptive identification of calcium and lipid binding sites. *Mol Biol Med* 3, 387-407.
- Uribe, C., Folch, H., Enriquez, R. and Moran, G., 2011. Innate and adaptive immunity in teleost fish: a review. *Veterinari Medicina* 56, 486-503.

- Urig, S. and Becker, K., 2006. On the potential of thioredoxin reductase inhibitors for cancer therapy. *Semin Cancer Biol* 16, 452-65.
- Vatansever, F., de Melo, W.C., Avci, P., Vecchio, D., Sadasivam, M., Gupta, A., Chandran, R., Karimi, M., Parizotto, N.A., Yin, R., Tegos, G.P. and Hamblin, M.R., 2013. Antimicrobial strategies centered around reactive oxygen species--bactericidal antibiotics, photodynamic therapy, and beyond. *FEMS Microbiol Rev* 37, 955-89.
- Vigneshkumar, B., Pandian, S.K. and Balamurugan, K., 2013. Catalase activity and innate immune response of *Caenorhabditis elegans* against the heavy metal toxin lead. *Environ Toxicol* 28, 313-21.
- Vinayagam, A., Konig, R., Moormann, J., Schubert, F., Eils, R., Glatting, K.H. and Suhai, S., 2004. Applying Support Vector Machines for Gene Ontology based gene function prediction. *BMC Bioinformatics* 5, 116.
- Wang, C., Yue, X., Lu, X. and Liu, B., 2013. The role of catalase in the immune response to oxidative stress and pathogen challenge in the clam *Meretrix meretrix*. *Fish Shellfish Immunol* 34, 91-9.
- Wang, W., Knovich, M.A., Coffman, L.G., Torti, F.M. and Torti, S.V., 2010. Serum ferritin: Past, present and future. *Biochim Biophys Acta* 1800, 760-9.
- Wang, W., Zhang, M. and Sun, L., 2011. Ferritin M of *Cynoglossus semilaevis*: an iron-binding protein and a broad-spectrum antimicrobial that depends on the integrity of the ferroxidase center and nucleation center for biological activity. *Fish Shellfish Immunol* 31, 269-74.
- Wang, Y., Kinzie, E., Berger, F.G., Lim, S.K. and Baumann, H., 2001. Haptoglobin, an inflammation-inducible plasma protein. *Redox Rep* 6, 379-85.
- Watt, R.K., 2011. The many faces of the octahedral ferritin protein. *Biomaterials* 24, 489-500.
- Weiss, G. and Goodnough, L.T., 2005. Anemia of chronic disease. *N Engl J Med* 352, 1011-23.
- Whang, I., Lee, Y., Kim, H., Jung, S.J., Oh, M.J., Choi, C.Y., et al., 2011a. Characterization and expression analysis of the myeloid differentiation factor 88 (MyD88) in rock bream *Oplegnathus fasciatus*. *Mol Biol Rep* 38, 3911-20.
- Whang, I., Lee, Y., Lee, S., Oh, M.J., Jung, S.J., Choi, C.Y., et al., 2011b. Characterization and expression analysis of a goose-type lysozyme from the rock bream *Oplegnathus fasciatus*, and antimicrobial activity of its recombinant protein. *Fish Shellfish Immunol* 30, 532-42.
- Whyte, S.K., 2007. The innate immune response of finfish--a review of current knowledge. *Fish Shellfish Immunol* 23, 1127-51.
- Wink, D.A., Hines, H.B., Cheng, R.Y., Switzer, C.H., Flores-Santana, W., Vitek, M.P., Ridnour, L.A. and Colton, C.A., 2011. Nitric oxide and redox mechanisms in the immune response. *J Leukoc Biol* 89, 873-91.
- Winkelhake, J.L. and Chang, R.J., 1982. Acute phase (C-reactive) protein-like macromolecules from rainbow trout (*Salmo gairdneri*). *Dev Comp Immunol* 6, 481-9.
- Worwood, M., 1990. Ferritin. *Blood Rev* 4, 259-69.
- Worwood, M., Brook, J.D., Cragg, S.J., Hellkuhl, B., Jones, B.M., Perera, P., Roberts, S.H. and Shaw, D.J., 1985. Assignment of human ferritin genes to chromosomes 11 and 19q13.3---19qter. *Hum Genet* 69, 371-4.
- Yamada, T., 1999. Serum amyloid A (SAA): a concise review of biology, assay methods and clinical usefulness. *Clin Chem Lab Med* 37, 381-8.

- Yamada, T., Liepnieks, J.J., Kluge-Beckerman, B. and Benson, M.D., 1995. Cathepsin B generates the most common form of amyloid A (76 residues) as a degradation product from serum amyloid A. *Scand J Immunol* 41, 94-7.
- Yamamoto, K., Banno, Y., Fujii, H., Miake, F., Kashige, N. and Aso, Y., 2005. Catalase from the silkworm, *Bombyx mori*: gene sequence, distribution, and overexpression. *Insect Biochem Mol Biol* 35, 277-83.
- Yamamoto, M., Katoh, N. and Adachi, Y., 1998. The presence of two low molecular mass proteins immunologically related to 14 kilodalton serum amyloid A in the lipoprotein fraction and their decreased serum concentrations in calves with experimentally induced pneumonia. *J Vet Med Sci* 60, 181-7.
- Yang, T.C., Lai, C.C., Shiu, S.L., Chuang, P.H., Tzou, B.C., Lin, Y.Y., Tsai, F.J. and Lin, C.W., 2010. Japanese encephalitis virus down-regulates thioredoxin and induces ROS-mediated ASK1-ERK/p38 MAPK activation in human promonocyte cells. *Microbes Infect* 12, 643-51.
- Zhang, Q., Li, F., Zhang, X., Dong, B., Zhang, J., Xie, Y. and Xiang, J., 2008. cDNA cloning, characterization and expression analysis of the antioxidant enzyme gene, catalase, of Chinese shrimp *Fenneropenaeus chinensis*. *Fish Shellfish Immunol* 24, 584-91.
- Zhang, X., Wei, W., Wu, H., Xu, H., Chang, K. and Zhang, Y., 2010. Gene cloning and characterization of ferritin H and M subunits from large yellow croaker (*Pseudosciaena crocea*). *Fish Shellfish Immunol* 28, 735-42.
- Zhang, Y., 2008. I-TASSER server for protein 3D structure prediction. *BMC Bioinformatics* 9, 40.
- Zheng, W.J., Hu, Y.H. and Sun, L., 2010a. Identification and analysis of a *Scophthalmus maximus* ferritin that is regulated at transcription level by oxidative stress and bacterial infection. *Comp Biochem Physiol B Biochem Mol Biol* 156, 222-8.
- Zheng, W.J., Hu, Y.H., Xiao, Z.Z. and Sun, L., 2010b. Cloning and analysis of a ferritin subunit from turbot (*Scophthalmus maximus*). *Fish Shellfish Immunol* 28, 829-36.
- Zhou, J., Wang, W., Ma, G., Wang, A., He, W. and Wang, P., 2008. Gene expression of ferritin in tissue of the Pacific white shrimp, *Litopenaeus vannamei* after exposure to pH stress. *Aquaculture* 275, 356-360.